UNIVERSITY OF CRETE
DEPARTMENT OF CHEMISTRY

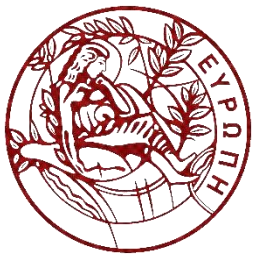

DOCTORAL THESIS

POLYMER DYNAMICS IN NANOHYBRID MATERIALS

EFFECTS OF THE POLYMER ARCHITECTURE AND THE ADDITIVE GEOMETRY

KRYSTALENIA ANDROULAKI

SUPERVISOR: SPIROS H. ANASTASIADIS

HERAKLION 2019

To my colleagues,

Committee Members (alphabetical order)

Prof. Spiros H. Anastasiadis (supervisor)

Prof. Dimitrios N. Bikiaris

Dr. Kiriaki Chrissopoulou

Prof. George E. Froudakis

Prof. George Petekidis

Prof. Konstantinos S. Triantafyllidis

Prof. Dimitris Vlassopoulos

Acknowledgements

The present research, performed in Hybrid Nanostructures laboratory of the Institute of Electronic Structure and Laser at FORTH, was supervised by Prof. Spiros H. Anastasiadis to whom I am grateful for his support and for believing in me throughout the years of my postgraduate studies.

My sincere thanks to Dr. Kiriaki Chrissopoulou, the co-supervisor of this work, who stood by me from the beginning till the end and taught me to work in a systematic manner and to focus on the important things as required in research.

I owe many thanks to everyone in the research group of Prof. Simone Capaccioli in the Physics Department of the University of Pisa in Italy, where the dielectric spectroscopy measurements were performed. Special thanks to Dr. Massimiliano Labardi for the help, the excellent collaboration and for the hospitality.

I would like to also thank all my colleagues, the current and former members of our research group, not only, for making a significant contribution to my work with their advice, experience, creative thinking but mostly for the relationships we have developed. In particular I want to thank Melina Frysali, Hellen Papananou, Stavros Bollas, Lampros Papoutsakis, Nikos Vassilakis, George Papadakis, Aleka Manousaki, the researchers Manos Glynos, Georgina Kaklamani, George Deligeorgis, George Kenanakis, Kostas Vassilopoulos and Maria Kaliva, the master and undergraduate students of our group, Dimitris, Socrates, Georgia, Antigonos, Tasos, Liana, Irini, Evi, Niki, Argyro, Elena, Chrissa and Stefan.

I would also like to acknowledge the rest of the members of the advisory committee and the seven-membered examination committee for their time and for the evaluation of the present dissertation.

Last but certainly not least, I would like to express my gratitude to the people supporting me in numerous and various ways throughout the years, my parents and my brother for being proud of whom I have become, Tasos for being by my side, my comrades during the major and minor struggles we have given in the past difficult years.

Ευχαριστίες

Η παρούσα διδακτορική εργασία εκπονήθηκε στο εργαστήριο Υβριδικών Νανοδομών του Ινστιτούτου Ηλεκτρονικής δομής και Λέιζερ του Ι.Τ.Ε. υπό την επίβλεψη του Καθ. Σπύρου Χ. Αναστασιάδη τον οποίο και ευχαριστώ για την υποστήριξη και εμπιστοσύνη που μου έδειξε καθ' όλη την διάρκεια των μεταπτυχιακών μου σπουδών.

Θα ήθελα ιδιαίτερα να ευχαριστήσω την Δρ. Κυριακή Χρυσοπούλου η οποία ανέλαβε την επίβλεψη της συγκεκριμένης εργασίας και ήταν δίπλα μου σε κάθε βήμα της ερευνητικής μου δουλειάς. Μέσα από την συνεργασία μας με έμαθε να εμβαθύνω και να δουλεύω συστηματικά όπως απαιτείται στην έρευνα.

Ξεχωριστά θα ήθελα να εκφράσω τις ευχαριστίες μου στην ερευνητική ομάδα του Prof. Simone Capaccioli στο τμήμα Φυσικής του Πανεπιστημίου της Πίζα στην Ιταλία, όπου και διεξήχθησαν οι μετρήσεις διηλεκτρικής φασματοσκοπίας. Ιδιαίτερα ευχαριστώ τον Dr. Massimiliano Labardi για την βοήθεια, την άριστη συνεργασία και την φιλοξενία του.

Ακόμη θα ήθελα να ευχαριστήσω όλους τους συναδέλφους μου, τα μέλη της ερευνητικής ομάδας και όχι μόνο, που συνέβαλαν σημαντικά στην πραγματοποίηση της εργασίας μου με συμβουλές, με εμπειρία, με δημιουργικό προβληματισμό αλλά και με τις σχέσεις που αναπτύξαμε. Συγκεκριμένα θέλω να ευχαριστήσω τους Μελίνα Φρυσάλη, Ελένη Παπανάνου, Σταύρο Μπόλα, Λάμπρο Παπουτσάκη, Νίκο Βασιλάκη, τον Γιώργο Παπαδάκη και την Αλέκα Μανουσάκη, τους ερευνητές Μάνο Γλυνό, Τζωρτζίνα Κακλαμάνη, Γιώργο Δεληγιώργη, Γιώργο Κενανάκη, Κώστα Βασιλόπουλο και Μαρία Καλύβα αλλά και τους μεταπτυχιακούς και προπτυχιακούς φοιτητές της ομάδας, Δημήτρη, Σωκράτη, Γεωργία, Αντίγονο, Τάσο, Λιάνα, Ειρήνη, Εύη, Νίκη, Αργυρώ, Έλενα, Χρύσα και Στέφανο.

Ευχαριστώ επίσης τα υπόλοιπα μέλη της τριμελούς συμβουλευτικής επιτροπής και της επταμελούς εξεταστικής επιτροπής για τον χρόνο και την αξιολόγηση της παρούσας διατριβής.

Τέλος θέλω να ευχαριστήσω ιδιαίτερα τους ανθρώπους που είχα δίπλα μου που με στήριζαν και με βοήθησαν με τον δικό τους τρόπο ο καθένας, τους γονείς μου και τον αδερφό μου που είναι περήφανοι για εμένα, τον Τάσο που είμαστε πάντα δίπλα ο ένας στον άλλο και αυτό μας κάνει καλύτερους, τους συντρόφους μου στους μικρούς και μεγάλους αγώνες που δώσαμε τα δύσκολα αυτά χρόνια.

Curriculum Vitae

Krystalenia (Lina) Androulaki was born in Heraklion, Crete. She graduated from the 4th High School of Heraklion in 2004 and was accepted in the Chemistry Department, Aristotle University of Thessaloniki with the best scores of the year 2004. Following her graduation, she returned to Heraklion in order to continue her studies and in 2013 she acquired her Masters Diploma from the Chemistry Department, University of Crete. Her master thesis entitled "Polymer Structure and Dynamics in Hyperbranched Polymer/Layered Silicate Nanocomposites" was performed under the supervision of Prof. Spiros H. Anastasiadis and Dr. Kiriaki Chrissopoulou. Since 2011 she is a member of the Hybrid Nanostructures Group of the Institute of Electronic Structure and Laser in FORTH. During her PhD studies, she investigated polymer dynamics in nanocomposite materials. Her research was presented in numerous conferences and a part of her work is published in reviewed scientific journals.

Publications:

- Krystalenia Androulaki, Kiriaki Chrissopoulou, Daniele Prevosto, Massimiliano Labardi and Spiros H. Anastasiadis
  "Dynamics of Hyperbranched Polymers under Confinement: A Dielectric Relaxation Study"
  ACS Applied Materials & Interfaces 2015, 7, 12387−12398
- Krystalenia Androulaki, Kiriaki Chrissopoulou, Daniele Prevosto, Massimiliano Labardi and Spiros H Anastasiadis
  "Structure and Dynamics of Biobased Polyester Nanocomposites"
  Biomacromolecules 2019, 20, 164–176

Βιογραφικό Σημείωμα

Η Κρυσταλένια (Λίνα) Ανδρουλάκη γεννήθηκε στο Ηράκλειο Κρήτης. Το 2004 αποφοίτησε από το 4ο Ενιαίο Λύκειο Ηρακλείου και εισήλθε στο τμήμα Χημείας της Σχολής Θετικών Επιστημών του Αριστοτελείου Πανεπιστημίου Θεσσαλονίκης, με την καλύτερη βαθμολογία στο έτος της. Μετά την αποφοίτηση της επέστρεψε στην Κρήτη και συνέχισε τις σπουδές της στο γενικό πρόγραμμα μεταπτυχιακών σπουδών του τμήματος Χημείας της Σχολής Θετικών και Τεχνολογικών Σπουδών του Πανεπιστημίου Κρήτης. Το 2013 παρουσίασε με επιτυχία την μεταπτυχιακή της διατριβή με θέμα «*Δομή και Δυναμική Νανοσύνθετων Υλικών Βασισμένων σε Υπερδιακλαδισμένα Πολυμερή*» υπό την επίβλεψη του Καθ. Σπύρου Χ. Αναστασιάδη και της Δρ. Κυριακής Χρυσοπούλου. Από το 2011 είναι μέλος της ομάδας υβριδικών νανοδομών του Ινστιτούτου Ηλεκτρονικής Δομής και Λέιζερ του Ι.Τ.Ε. Τα αποτελέσματα της διδακτορικής της διατριβής με ελληνικό τίτλο «*Δυναμική πολυμερών σε νανοσύνθετα υλικά: Επίδραση της αρχιτεκτονικής των πολυμερικών αλυσίδων και της γεωμετρίας του ανόργανου*» παρουσιάστηκαν σε πληθώρα συνεδρίων ενώ μέρος της εργασίας έχει ήδη δημοσιευτεί σε έγκριτα διεθνή επιστημονικά περιοδικά.

Δημοσιεύσεις:

- Krystalenia Androulaki, Kiriaki Chrissopoulou, Daniele Prevosto, Massimiliano Labardi and Spiros H. Anastasiadis
  “Dynamics of Hyperbranched Polymers under Confinement: A Dielectric Relaxation Study”
  ACS Applied Materials & Interfaces 2015, 7, 12387−12398
- Krystalenia Androulaki, Kiriaki Chrissopoulou, Daniele Prevosto, Massimiliano Labardi and Spiros H Anastasiadis
  “Structure and Dynamics of Biobased Polyester Nanocomposites”
  Biomacromolecules 2019, 20, 164–176

Abstract

The investigation of polymer dynamics is an intriguing scientific problem, as it influences the structure to property relationship because of the complexity it exhibits over many length- and time-scales. Polymer dynamics includes vibrational motions, rotations of side groups, the segmental α-process as well as the overall chain dynamics, thus covering a very broad time regime of more than ten decades from the pico-second (ps) to the second (s) regime.

In recent years novel classes of polymers have emerged such as the biobased and biodegradable aliphatic polyesters, due to the combination of biodegradability and physicochemical properties comparable to those of conventional polymers, and the hyperbranched polymers, which show the unique features of dendrimers like low viscosity at high molecular weight, high solubility, miscibility, and reactivity influenced by the end groups, together with a cost-effective synthesis. Moreover, polymer nanocomposites, comprising a polymer matrix and nanoscale additives (e.g., nanoparticles, clays, nanotubes, graphene, etc.), possess improved and often innovative physicochemical properties compared to the bulk polymer or conventionally filled systems.

In the present thesis polymer dynamics is investigated in nanocomposites comprising of polymers with different architecture and various additives. The polymers examined were three linear polyesters with hydroxyl end groups and different repeating units, three hyperbranched polyester polyols of different generations and a hyperbranched poly (ester amide). Nanocomposites based on these polymers and three different additives, silica nanoparticles of spherical geometry, a multi-layer graphite oxide and a layered silicate, sodium montmorillonite, were prepared by solution mixing.

The structural and thermal characterization shows favorable polymer-additive interactions with dispersed nanoparticles within the polymeric matrix and with intercalated structures formed in the case of the layered additives. By increasing the concentration of the additive in all nanocomposites the thermal properties of the polymer are gradually suppressed as a result of a thin polymer layer formed close to the interface of the additive. Additionally strong confinement effect was observed depending on the system.

Polymer dynamics investigated by Broadband Dielectric Spectroscopy reveals multiple relaxation processes, observed in both the bulk polymer and the nanocomposites. Nevertheless, significant

differences are observed due to the interactions with the additive and the effect of confinement. The local motions, attributed to the rotation of hydroxyls and the reorientation of carbonyls, possess lower activation energy in most of the nanocomposite cases in comparison to the bulk, because they are less constrained due to the reduced hydrogen bonding in nanohybrids. For the linear polyesters the segmental relaxation in nanocomposites retains its VFT temperature dependence whereas for the hyperbranched polymer nanocomposites, the segmental relaxation appears below the glass transition temperature of the respective bulk polymer with an Arrhenius temperature dependence. The confinement strongly affects the segmental dynamics of the hyperbranched polymers in both GO and clay nanocomposites. On the contrary, the segmental dynamics for the linear polyesters is similar to the bulk, not only in silica nanohybrids of lower confinement but in clay nanocomposites as well, due to their low molecular weight.

Keywords: polymer dynamics, dielectric spectroscopy, nanocomposites, biobased/biodegradable polyesters, hyperbranched polymers

Περίληψη

Η μελέτη της δυναμικής των πολυμερών είναι ένα ενδιαφέρον επιστημονικό πρόβλημα καθώς επηρεάζει την σχέση δομής-ιδιοτήτων λόγω της πολυπλοκότητας που εμφανίζει σε χωρική αλλά και χρονική κλίμακα. Περιλαμβάνει δονητικές κινήσεις, περιστροφές πλευρικών ομάδων, την τμηματική α-κίνηση και την συνολική διάχυση της αλυσίδας καλύπτοντας μία χρονική κλίμακα από την περιοχή των ps έως την περιοχή των sec.

Τα τελευταία χρόνια ιδιαίτερο ερευνητικό ενδιαφέρον παρουσιάζουν τα αποικοδομήσιμα πολυμερή και πιο συγκεκριμένα οι αλειφατικοί πολυεστέρες καθώς είναι «φιλικά για το περιβάλλον» και λόγω των ιδιοτήτων τους μπορούν να χρησιμοποιηθούν ως εναλλακτικές λύσεις στα συμβατικά μη-διασπώμενα πολυμερή. Επίσης μια άλλη κατηγορία πολυμερών με ερευνητικό ενδιαφέρον είναι τα υπερδιακλαδισμένα πολυμερή τα οποία διαθέτουν χαμηλό ιξώδες ακόμη και για μεγάλα μοριακά βάρη, υψηλή διαλυτότητα, συμβατότητα και δραστικότητα που οφείλεται στον εξαιρετικά μεγάλο αριθμό δραστικών τους ομάδων, σε συνδυασμό με τη χαμηλού κόστους σύνθεση τους συγκριτικά με τα δενδριμερή. Ταυτόχρονα τα τελευταία χρόνια, τα νανοσύνθετα υλικά που αποτελούνται από πολυμερή και πρόσθετα που διαθέτουν μια ή περισσότερες διαστάσεις στη νανοκλίμακα, έχουν μελετηθεί ιδιαίτερα λόγω της επίδρασης του πρόσθετου στις ιδιότητες του πολυμερούς που συχνά προσδίδει βελτιωμένες ιδιότητες όπως η αυξημένη αντοχή, η μεγάλη θερμική αντίσταση, η μειωμένη διαπερατότητα από αέρια, η μειωμένη αναφλεξιμότητα κ.ά.

Στην παρούσα εργασία μελετάται η επίδραση προσθέτων διαφορετικής γεωμετρίας στην δυναμική πολυμερών που διαθέτουν παραπλήσιες λειτουργικές ομάδες και διαφορετική αρχιτεκτονική. Πιο συγκεκριμένα μελετήθηκαν τρεις γραμμικοί πολυεστέρες με διαφορετική επαναλαμβανόμενη μονάδα, υπερδιακλαδισμένοι πολυεστέρες τριών διαφορετικών γενεών (βαθμός διακλάδωσης) και ένα υπερδιακλαδισμένο πολυεστερικό αμίδιο, τα οποία διαθέτουν διαφορετικό αριθμό ακραίων υδροξυλικών ομάδων. Τα παραπάνω πολυμερή αναμίχθηκαν με νανοσωματίδια πυριτίας σφαιρικής γεωμετρίας, με οξείδιο του γραφίτη φυλλώδους δομής και με τον φυλλώδη αργιλοπυριτικό πηλό, μοντμοριλλονίτη νατρίου, για την παρασκευή νανοσύνθετων υλικών.

Νανοσύνθετα υλικά διαφορετικών συστάσεων σε πολυμερές παρασκευάστηκαν με ανάμιξη από διάλυμα σε απιονισμένο νερό και για όλα τα δείγματα ακολούθησε θερμική ανόπτηση ώστε να

επιτευχθούν δομές ισορροπίας. Η μελέτη της δομής εξετάστηκε με περίθλαση ακτίνων Χ (XRD) ενώ οι θερμικές ιδιότητες με διαφορική θερμιδομετρία σάρωσης (DSC) και θερμοσταθμική ανάλυση (TGA). Επίσης για τη μελέτη της δυναμικής των πολυεστέρων τόσο για το ελεύθερο πολυμερές όσο και για τα νανοσύνθετα, πραγματοποιήθηκαν μετρήσεις διηλεκτρικής φασματοσκοπίας ευρέος φάσματος (BDS).

Από τη μελέτη της δομής και των θερμικών ιδιοτήτων διαπιστώνονται ευνοϊκές αλληλεπιδράσεις πολυμερούς – ανοργάνου, με σφαιρικά σωματίδια διεσπαρμένα στην πολυμερική μήτρα και σχηματισμό δομών παρεμβολής για τα φυλλώδη πρόσθετα. Οι θερμικές μεταβάσεις των πολυμερών μειώνονται στα νανοσύνθετα υλικά όπου οι πολυμερικές αλυσίδες αλληλεπιδρούν με την διεπιφάνεια του προσθέτου ή βρίσκονται υπό ισχυρό χωρικό περιορισμό.

Μέσω της μελέτης της δυναμικής των πολυμερών παρατηρούνται πολλαπλές διεργασίες χαλάρωσης στην περίπτωση του καθαρού πολυμερούς ενώ οι ίδιες διεργασίες παρατηρούνται και στα νανοσύνθετα με σημαντικές διαφοροποιήσεις ανά περίπτωση.

Οι διεργασίες που παρατηρούνται σε θερμοκρασίες κάτω από το T_g αποδίδονται στις κινήσεις μικρών πολικών ομάδων, όπως στην περιστροφή των υδροξυλίων και στον αναπροσανατολισμό των καρβονυλίων. Υπό ισχυρό χωρικό περιορισμό οι διεργασίες αυτές έχουν μικρότερες ενέργειες ενεργοποίησης καθώς μειώνονται οι σχηματιζόμενοι δεσμοί υδρογόνου μεταξύ των ομάδων αυτών. Οι α διεργασίες χαλάρωσης εμφανίζουν εξάρτηση από τη θερμοκρασία υαλώδους μετάβασης του εκάστοτε πολυμερούς για το καθαρό υλικό, ενώ για τα νανοσύνθετα μπορεί να αλλάζει σημαντικά ή όχι ανάλογα με το σύστημα. Για τους γραμμικούς πολυεστέρες η α διεργασία χαλάρωσης διατηρεί την VFT θερμοκρασιακή εξάρτηση ενώ για τους υπερδιακλαδισμένους πολυεστέρες διαφορετικών γενεών η α διεργασία χαλάρωσης, εμφανίζει εξάρτηση από τη γενεά και αλλάζει η θερμοκρασιακή εξάρτηση σε γραμμική. Ο ισχυρός χωρικός περιορισμός των υπερδιακλαδισμένων πολυεστέρων στα νανοσύνθετα με δομές παρεμβολής επιδρά στην δυναμική τους ενώ στην περίπτωση των γραμμικών πολυεστέρων δεν εμφανίζεται σημαντική επίδραση όχι μόνο στα νανοσύνθετα με σφαιρικά σωματίδια πυριτίας αλλά και με πολυστρωματικούς πηλούς λόγω του χαμηλού μοριακού τους βάρους.

Λέξεις κλειδιά: δυναμική πολυμερών, νανοσύνθετα υλικά, αποικοδομήσιμοι πολυεστέρες, υπερδιακλαδισμένα πολυμερή

Table of Contents

Introduction and Background

In recent years the development of various innovative materials possessing the appropriate physical and chemical properties depending on the desired application is investigated. More specifically, polymer-based materials gained great interest during the past decades, due to the capability of controlling their properties by altering their “chemistry”; different functional groups, repeating units, molecular weight, polymer architecture, even block copolymers can be utilized to obtain different materials adjusted to the end-use. Moreover, polymers can be synthesized at low cost, combining ease of processing and light weight. One drawback, though, is the environmental pollution caused by their long degradation times and their petroleum origin. Recently, biobased and biodegradable polymers are rising as a new class of materials to substitute conventional polymers; nevertheless further research is required in order to improve their performance for a wide range of applications.

Polymer dynamics is investigated in an attempt to further understand the structure to properties relationship because of the complexity it exhibits over many length and time scales. In spite of the already developed theories on polymer dynamics, certain debates remain over basic concepts in polymer physics, such as the segmental dynamics related to the glass transition temperature (T_g), the dynamic relaxations of polymer chains and their temperature dependence, polymer dynamics in ultra-thin films and the effect of the additives in nanocomposite materials. Many of these concepts were introduced as macroscopic properties, whose definitions, characterizations or relation with local properties are not clear on the nanoscale.

Polymers involve much richer and more complicated interactions, compared to inorganic compounds or small molecules, due to the abundance of chemical structures that result in different chemical and physical properties. Many techniques are developed in order to examine polymer dynamics, such as neutron scattering, dynamic light scattering, dielectric relaxation spectroscopy etc. Molecular simulations are also complementary in polymer dynamics investigation but with limitations on the number of the examined molecules and the approximations, that most often differ from experimental results. Polymers with different functional groups, molecular weight or architecture are investigated with the intent of understanding the effect on their macroscopic properties.

A bright research field in material science is the “composite materials”, consisting of organic and inorganic matter in the micro-scale, combining the very different properties of both materials. By investigating composite materials, optimized properties may emerge due to the weighted average properties of the constituents as well as due to the interactions at the interface of the ingredients. These interactions and thus the new properties are enhanced by increasing the amount of interfaces utilizing fillers of one or more dimensions in the nanoscale. Especially polymer nanohybrids comprising a polymer matrix and inorganic additives (e.g., nanoparticles, nanorods, nanofibers, clays, graphene etc.) as the nanofiller, possess improved properties compared to micro-composite materials.

Polymer dynamics is investigated in nanohybrids in order to comprehend the microscopic mechanisms that result in the different macroscopic properties. Recent studies reveal the effect of the different polymer-additive interactions on the segmental relaxation of the polymer with either faster or slower dynamics observed. Additionally, the strong effect of the interfacial interactions on the polymer properties is observed in thin films below few tens of nanometers. This strong confinement effect is reported to alter the temperature dependence of the segmental motion resulting in a stronger glass behavior.

In both systems (polymer nanohybrids and thin films) the structure, the thermal properties and the dynamics of the polymer are affected. The next step is to tune material properties as needed, through established methods such as adjusting functionalities, polymer architecture, composition, molecular weight and by including the proper additives.

Introduction in this Work

In the current work we contribute to the investigation of polymer dynamics in a systematic manner in order to further understand the effect of the different functional groups, polymer architecture and of the nature and geometry of the inorganic additive, on the properties of the nanohybrid materials.

The present thesis consists of seven chapters:

The first chapter shortly introduces polymer dynamics and focuses on biobased and biodegradable polymers, as well as, on a new class of polymers obtaining different architecture, the hyperbranched polymers. Moreover, the benefits of nanocomposite materials are presented, especially nanocomposites based on additives like silica nanoparticles, graphite oxide and layered silicates. The effect of the polymer / additive interactions on polymer dynamics according to the current knowledge is discussed.

In the second chapter the materials (polymers and additives) utilized in the current study are reported. Moreover the methods and the basic principles of the experimental techniques used, i.e. X-ray diffraction (XRD), differential scanning calorimetry (DSC), thermogravimetric analysis (TGA) and broadband dielectric spectroscopy (BDS), are briefly presented.

Chapter three focuses on the effect of the different functional groups and polymer architecture on bulk polymer properties and dynamics. The structural and thermal properties of the two series of the bulk polymers (the linear polyesters and the hyperbranched polymers) are presented. Furthermore, polymer dynamics is investigated by BDS for two linear polyesters and for the hyperbranched polymers in a wide temperature regime. Both local and segmental relaxations are observed and the origin of the respective motions is discussed extensively.

In the fourth chapter, nanocomposites of silica nanoparticles and linear polyesters are prepared, by dispersion in water, in different compositions. Polymer structure, thermal properties and dynamics are more or less affected by the additive and presented herein.

Chapter five describes the properties of hyperbranched polymer / graphite oxide nanocomposites. In these systems due to the polymer-additive interactions, the formation of thin polymer films between the layers of the GO is evident. This strong confinement of the polymer results in a significant effect on both local and segmental dynamics. Additionally, the effect of the thermal reduction of GO in the different nanocomposites is discussed.

The sixth chapter, focuses on the severe confinement of both the linear and the hyperbranched polymers in polymer / layered silicate nanocomposites. The effect on the structural and the thermal properties of both semi-crystalline and amorphous polymers, as

well as, the polymer dynamics in nanocomposites, when all polymer chains are under confinement, are presented.

The final seventh chapter summarizes the main results obtained in the current study and focuses on the effect of both the additive geometry and the polymer architecture on the polymer properties in nanocomposites.

1 Polymer Dynamics

The investigation of polymer dynamics has been a continuous and intriguing scientific problem throughout the years with many theories trying to predict the various motions. [1]–[5] Polymer dynamics reveals the structure to properties relationship with the complexity it exhibits over many length- and time- scales. [6]–[8] Polymer dynamics includes vibrational motions, rotations of side groups, the segmental α-process as well as the overall chain diffusion, thus, covering a very broad time regime of more than ten decades from the pico-second (ps) to the second (s) regime. This necessitates the use of different experimental techniques with complementary spatial and temporal capabilities (**Figure 1.1**), like, for example, light and neutron scattering [9] and/or dielectric relaxation spectroscopy. [10], [11]

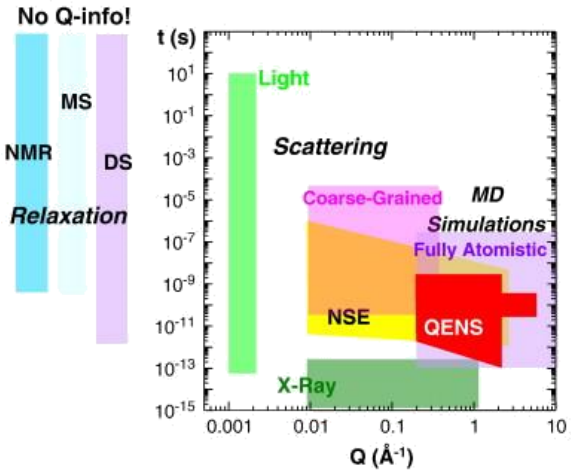

Figure 1.1: Map of the different techniques utilized to investigate polymer dynamics. [6]

In **Figure 1.2** the dynamic modulus as it may be observed on an amorphous polymer melt is related with the length and time scales of molecular motion underlying the rheological behavior. [12] As displayed in **Figure 1.3** this behavior can be observed in a typical relaxation map for a polymer and the following regimes can be distinguished:

- At low temperatures the material is in the glassy state and only motions of small amplitude like vibrations, fluctuations, short range rotations or secondary relaxations are possible. These relaxations cause the first small step in the dynamic modulus of such a polymer system. Below the glass transition temperature, T_g, the relaxations observed are denoted by the Greek letters β, γ etc. The relaxation times, τ, for the secondary processes usually exhibit a temperature dependence that follows the Arrhenius law:

$$\tau(T) = \tau_0 \exp\left(\frac{E_\alpha}{k_B T}\right) \quad (1.1)$$

where E_α is the activation energy and k_B is the Boltzmann' s constant.

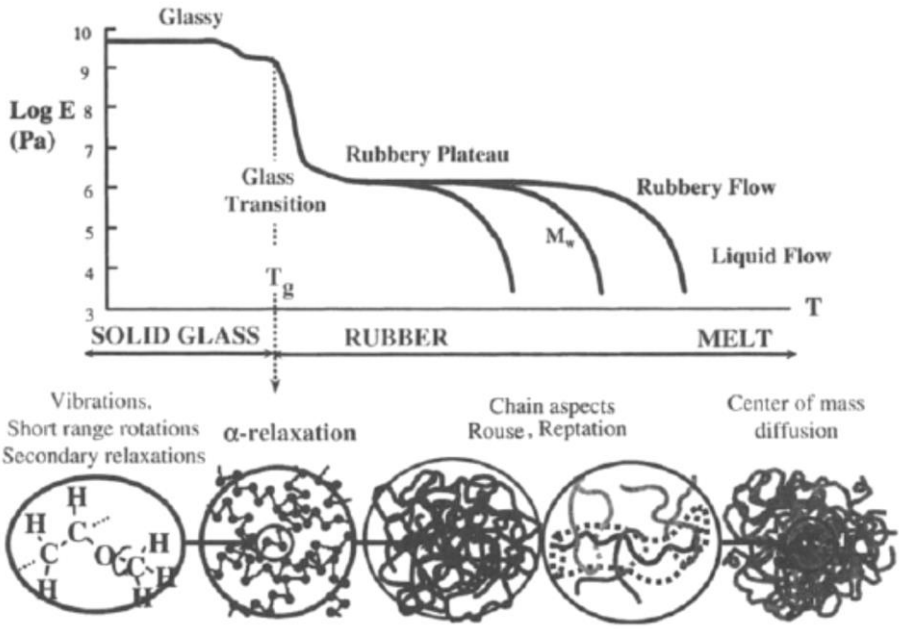

Figure 1.2: Richness of dynamic modulus in a bulk polymer and its molecular origin. [12]

- At the glass transition temperature, T_g, the primary relaxation (α-process) is probed due to the cooperative motion of chain segments, allowing the polymer chains to move. In the dynamic modulus, the α-relaxation causes a significant step of typically three orders of magnitude in strength. The temperature dependence of its characteristic relaxation time is displayed in **Figure 1.3**. The relaxation time of the α-process increases rapidly near T_g; for every 3-5 K of temperature drop the relaxation time increases by nearly one order of magnitude and the behavior is analyzed with the Vogel−Fulcher−Tammann equation [6], [8], [9]

$$\tau(T) = \tau_0 \exp\left(\frac{B}{T - T_0}\right) \quad (1.2)$$

where τ_0 represents the limit of relaxation times at high temperatures (usually the value of $\tau_0 = 10^{-12}$ to 10^{-14} s), T_0 the "ideal" glass point that corresponds to the "Vogel temperature" (usually 30 – 50 K below the T_g) and B is a parameter correlated to the fragility parameter $D = B/T_0$. When temperature, T, tends to 0 K the VFT behavior becomes more Arrhenius-like. [13]

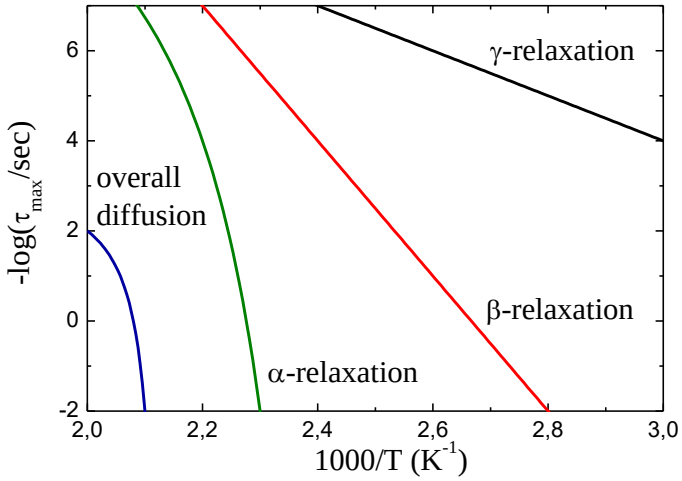

Figure 1.3: Arrhenius representation of relaxation times.

- The rubbery plateau in the modulus relates to large scale motions within a polymer chain. Two aspects stand out. The first is the entropy-driven relaxation of fluctuations out of equilibrium. Secondly, these relaxations are limited by confinement effects caused by the mutually interpenetrating chains. This confinement is modelled most successfully in terms of the reptation model by de Gennes and Doi & Edwards. [3], [4] In the framework of this model, confinement effects are described in terms of a tube following the coarse grained chain profile. Motion is only allowed along the tube profile leading to the reptation "snake-like" motion of a polymer chain.
- When a chain has lost the memory of its initial state, rubbery flow sets in. The associated characteristic relaxation time is displayed in **Figure 1.3** denoted as the overall diffusion of the polymer chain. This relaxation of the end-to-end vector of a given chain can be measured by dielectric spectroscopy only for polymers with an electric dipole moment in the direction of the chain. The rubbery flow passes over to liquid flow, which is characterized by the translational diffusion coefficient of the chain. Depending on the molecular weight, the characteristic length scales from the motion of a single bond to the overall chain diffusion may cover about three orders of magnitude, while the associated time scales easily may be stretched over ten or more orders.

In dielectric spectroscopy of inhomogeneous materials like suspensions or colloids, biological materials, phase separated polymers, blends, and crystalline or liquid crystalline polymers, Maxwell-Wagner polarization processes appear as well. The MWS occurs either at inner dielectric boundary layers on a mesoscopic scale, or at the external electrode-

sample interface on a macroscopic scale; in both cases this leads to a separation of charges. The charges are often separated over a considerable distance (relative to the atomic and molecular sizes), and the contribution to dielectric loss can therefore be orders of magnitude larger than the dielectric response due to molecular fluctuations. [11]

1.1 Novel Classes of Polymers

1.1.1 Biobased and biodegradable polymers

During the past century the polymer industry has been developed completely relying on petroleum-derived chemistry, refinery, and engineering processes. The negative impacts on the environment, though, led to the rise of a new class of polymers, the biobased and biodegradable polymers. Biobased polymers (renewable polymers) i.e. polymers derived mostly or entirely from biomass, contribute to the reduction of the dependence on petrochemical resources, help in minimizing toxicity due to volatile organic compounds or solvents and lead to lower CO_2 emissions. The development of biodegradable polymers is recognized as one of the most successful innovations in the polymer industry to address environmental issues. Over the last three decades, a number of industries tend to substitute petroleum-based with bio-based intermediate materials in order to reduce the environmental footprint of their products. The evolving research on this field is promising in order to expand the potential applications in the future. [14], [15]

The importance of biobased polymers is well known, and much research and development activities concern the use of biobased polymers in science, engineering, and industry. Generally, biobased polymers are classified into three classes:

- 1st class; naturally derived biomass polymers: direct use of biomass as polymeric material including chemically modified ones such as cellulose, cellulose acetate, starches, chitin, modified starch, etc.
- 2nd class; bio-engineered polymers: bio-synthesized by using microorganisms and plants such as polyhydroxyalkanoates (PHAs), poly (glutamic acid), etc.
- 3rd class; synthetic polymers such as polylactide (PLA), poly (butylene succinate) (PBS), bio-polyolefins, bio-poly (ethylene terephthalic acid) (bio-PET), etc.

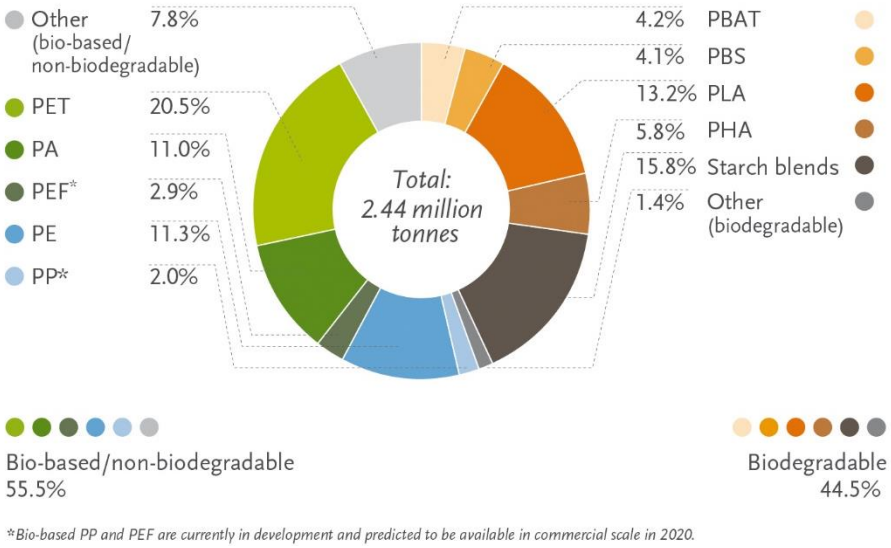

Figure 1.4: Global production of bioplastics in 2022 (by material type). Prediction by European Bioplastics, nova-Institute (2017).

Usually, polymers of the 1st class are directly used without any purification and of the 2nd class are directly produced from naturally derived polymers without any breakdown and they play an important role in situations that require biodegradability. Direct usage of 1st and 2nd class polymers allows more efficient production, leading to materials with desired functionalities and physical properties, but chemical structure designs have still limited flexibility. In the 3rd class, it is the monomers that are produced from naturally derived molecules or by the breakdown of naturally derived macromolecules through the combination of chemical and biochemical processes. As breakdown processes allow monomers to have versatile chemical structures, polymers comprised of these monomers have extremely versatile chemical structures as well. It is practically possible to introduce monomers in 3rd class polymers into the existing production system of petroleum-derived polymers. For the above reasons, the 3rd class of biobased polymers is the most promising. Although some of these polymers are not supposed to enter natural biological cycles after use, the contribution for reducing environmental impact is mainly derived from reducing the carbon footprint. [15]

In recent years the research on biobased polymers has grown and a wide range of polymers are included, polyurethanes, polyolefins, polyesters, and vinyl polymers suitable for wide-range applications, such as commodity items (e.g., plasticware, electronics casings, synthetic fabrics, cushioning, adhesives) and tailored materials (e.g., compact discs, screen protectors, biomedical devices, separation membranes). Biobased polymers can be synthesized by

utilizing glassy blocks derived from plant sugars and starch, lignocellulosic biomass, pine resin and rubbery blocks derived from fatty acids and essential oils. As reviewed by Holmberg et al. alternative synthesis methods are needed for renewable biobased polymers because controlled chain-growth polymerizations often require high monomer purity or are limited by the types of monomers or sequence of monomers that can be polymerized. These shortcomings can be circumvented through the implementation of non-"living" or non-controlled approaches. Most notably, polymers prepared by bacterial polymerizations or step-growth techniques (e.g., polycondensation and ADMET polymerization) can be chain-extended from or coupled to various end-group functionalized polymers. [14]

Due to the lower performance, but great potential, of the biobased compared to the conventional polymers, recent studies focus on the enhancement of their properties and their use in innovative applications. For example, citric acid was utilized as a functionality-enhancing monomer in biobased polyesters suitable for coating applications, [16] improved oxygen barrier performance of biobased and biodegradable polylactide (PLA) was achieved through constructing parallel-aligned shish-kebab-like crystals, [17] thermal annealing was utilized to modulate the shape memory behavior of a biobased and biocompatible triblock copolymer scaffold in the human body temperature range. [18]

Poly (alkylene dicarboxylate)s

Among biobased polymers, poly (alkylene dicarboxylate)s constitute a family of biodegradable polymers with increasing interest since typical limitations associated to the molecular weight have been overcomed by different attempts to improve the synthetic procedures. [19], [20] In general, these polymers have an additional interest since they can be prepared from biobased monomers such as diols like 1,4 butylene diol, fatty acids and other dicarboxylic acids like succinic acid and carbohydrates. The availability of different monomers allows getting materials with a wide range of properties and applications. [21]

Biobased aliphatic polyesters have attracted considerable attention due to the combination of biodegradability, biocompatibility, and their physicochemical properties, which, in many cases, are comparable to those of more common and widely utilized polymers. [20], [22]–[24] In these materials, the correlation between the chemical composition and the final properties is very complex; for example, the number of methylene groups in their repeating unit and the

chain length may affect the thermal properties, whereas they may induce important differences in the crystalline structure and morphology. [25], [26]

Moreover their significant biodegradability is crucial for the reduction of the so-called “white pollution” to be enforced during the following decades whereas their biocompatibility renders them suitable for biomedical applications as well. [27], [28] The rate of biodegradation can be influenced by many factors like macromolecular characteristics (chemical structure, stereoregularity, molecular weight, and molecular weight distribution), surface properties (surface area, hydrophilicity/ hydrophobicity), as well as thermal and mechanical properties (glass transition temperature, melting temperature, modulus of elasticity). The crystalline structure, the total crystallinity as well as the size of the spherulites and the lamellae significantly affect not only the material properties, but the mechanism and the rate of biodegradation as well. [29] Crystallinity is generally accepted to hinder biodegradability, which starts from the amorphous regions with much higher erosion rates than those of the crystalline regions. Subsequently, during biodegradation, holes are formed in the center of the spherulites with their size increasing with time; this indicates that the spherulite centers are composed of less ordered lamellae that can degrade more easily. [30] In order to influence the surface properties as well as the crystallinity and crystalline properties of a polymeric material, blending with another polymer is reported in the literature. [31]–[34]

Dynamics of biobased polymers

An area that has attracted less attention from the scientific community regarding biobased polymers is the investigation of their dynamics, although understanding their relaxation processes is crucial in order to derive the optimum processing conditions and, thus, expand the application range of such materials. Some of the most utilized polymers like polylactides and poly (alkylene dicarboxylates) have been investigated by dielectric spectroscopy.

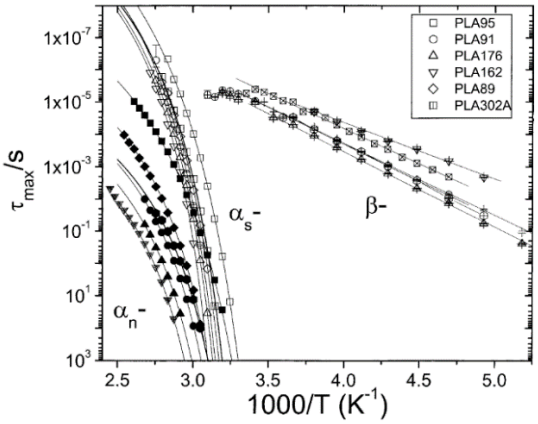

Figure 1.5: Arrhenius representation of the relaxation times for PLA samples. [35]

Amorphous polylactides (PLA) of different molecular weights were investigated by Mierzwa et al., and finite size effects have been observed for both the segmental and the β-process that become slower with increasing molecular weight. Additionally, in PLA which has components of the dipole moment both perpendicular and parallel to the polymer backbone, the overall diffusion of the polymer chain can be observed, denoted as the longest normal mode, α_n; the segmental, α_s, and the longest normal mode, α_n, display different shift factors with the former having a steeper temperature dependence in accordance with earlier studies on different polymers (**Figure 1.5**). [35]

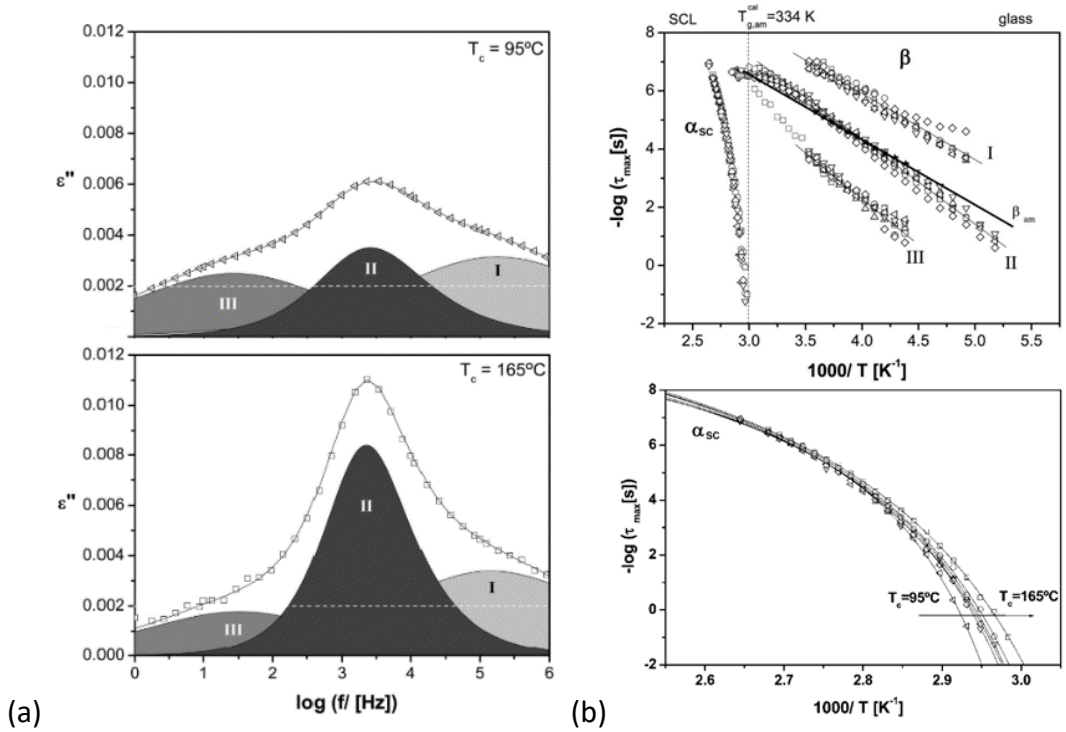

Figure 1.6: Representative fitting with three Havrilliak-Negami functions for PLLA cold-crystallized at -25 °C at two temperatures (a). Relaxation map for semi-crystalline PLLAs (b). [36]

On the other hand, polymer dynamics was investigated in semi-crystalline poly (L-lactic acid)s with different degrees of crystallinity (**Figure 1.6**). In that case the secondary relaxation process showed multicomponent character that varied with crystallinity and turned out to be a probe of the morphology attained. The mobility of the α-relaxation associated with the dynamic glass transition becomes enhanced with the increase of crystallinity attributed to the thicker rigid amorphous phase that decreases the influence of the rigid crystalline wall on the cooperative motions of the main relaxation process and the less dense mobile amorphous phase. [36]

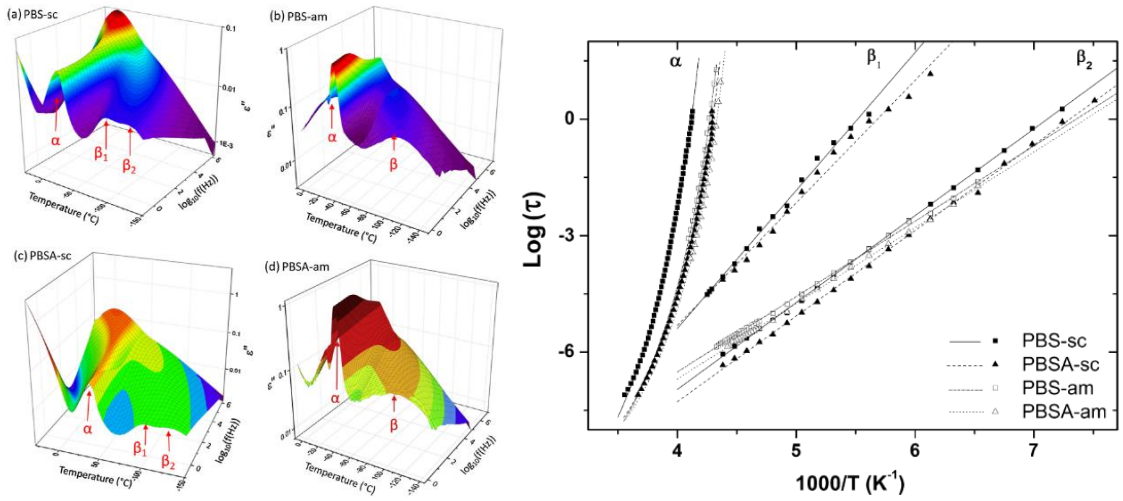

Figure 1.7: Relaxation processes of the amorphous and semi-crystalline poly (butylene succinate), PBS, and the copolymer poly [(butylene succinate)-co-(butylene adipate)], PBSA. [37]

Charlon et al. have investigated the effect of crystallinity on polymer dynamics for poly (butylene succinate), PBS. In order to vary the degree of crystallinity four samples were examined: an amorphous PBS, a semi-crystalline PBS and a poly [(butylene succinate)-co-(butylene adipate)] (PBSA) copolymer; butylene adipate group decreases drastically the degree of crystallinity and the size of the crystal lamellae of the PBSA. The glass transition temperature determined from DSC and BDS is only impacted by the crystallization of PBS (ΔT_g = +9 °C). We can conclude that the decoupling between phase is not complete and the crystalline phase of PBS is sufficient (χ_c = 57%) to induce confinement and modifications of the glass transition of the mobile amorphous fraction. For PBSA, the lower degree of crystallinity (χ_c = 37%) and the smaller crystal lamellae induce a higher decoupling between phases (**Figure 1.7**).

Fragility indexes of the main dielectric relaxation are identical for semi-crystalline polymers showing similar segmental dynamics of amorphous phase. Concerning local motions, BDS reveals complex relaxations for semi-crystalline polymers with a new process observed in more constrained amorphous environments. This extra relaxation mode is attributed to the rigid amorphous fraction. [37]

Both local and segmental dynamics need to be investigated in order to comprehend the structure to properties relationship for a plethora of biobased and biodegradable polymers which are rapidly introduced in several applications.

1.1.2 Hyperbranched polymers

Polymer architecture is of great importance in polymer science since it affects the physical properties including solution viscosity, melt viscosity, solubility in various solvents, glass transition temperature and the size of individual polymer coils in solution. Each of the three main macromolecular architectural classes, i.e. linear, cross-linked, and branched, has spawned rich polymer science. [5] The development of innovative polymers with different architectures has been achieved via the emergence of new synthetic routes and advanced characterization of the obtained structures, phenomena and properties. A relatively new class of non-linear polymers that have attracted the scientific interest are the dendritic polymers because of their unique features like high density, low viscosity, and multiplicity of functional end-groups that make them favorite candidates for numerous applications. [38], [39] They can be separated (**Figure 1.8**) into two broad categories:

- Dendrimers that have symmetric, well-ordered, treelike structure, branches arranged into perfect layers or generations and specified molecular weight.
- Hyperbranched polymers, HBPs, which have many branch points, asymmetric structure and polydispersity.

The HBPs show the same unique features of the dendritic macromolecules like low viscosity at high molecular weight, high solubility, miscibility, and reactivity influenced by the end groups, having the additional advantage of a cost-effective synthesis, as compared to dendrimers, because of their one-pot synthetic method and the lack of need for tedious purification procedures. Numerous synthetic methods have been reported in the past decades

in an attempt to develop various HBPs which can be utilized in industrial applications. [40]–[43]

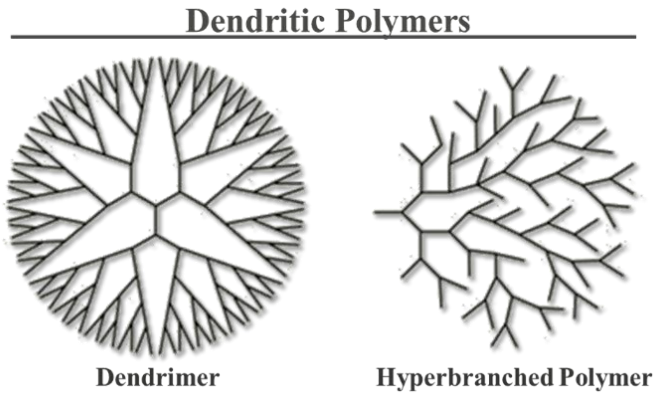

Figure 1.8: Architectures of dendritic polymers.

Hyperbranched polyesters

Hyperbranched polyesters are extensively utilized in polymer blends as additives; e.g. blends with high molecular weight polystyrenes were investigated by Mulkern et al. The processability and compatibility in the blends have revealed that hyperbranched polyesters are extremely effective processing aids with a significant drop in the blend viscosity immediately on addition of HBPs. [44] The gelation and vitrification of various epoxy systems and their blends with dendritic hyperbranched polymers were studied as well; the hydroxyl-functionalized HBP reduced the gel time of the blends because of the accelerating effect of –OH groups to the epoxy curing reaction and gel time was found to increase with increasing functionality. [45]

Hyperbranched polyesters can be modified to achieve enhanced physical, chemical and mechanical properties. Moreover, they can be tailored and further designed to affect several properties simultaneously; e.g. in alkyds they contribute to low viscosities combined with excellent drying; in polyurethanes and radcure, where rapid curing can be obtained by proper molecular design; and in amine-cured epoxies, where a hyperbranched epoxy demonstrates dramatically increased toughening without affecting other properties. [42] Many applications of HBPs are proposed with promising results in membranes, [46] batteries, [47] self-healing materials [48] and nanoscale catalysts. [49]

At the same time many biodegradable and biocompatible HBPs find applications in the pharmaceutical industry and medicine for the encapsulation of substances, targeted delivery of drugs, as therapeutic agents, as in vitro diagnostics for cardiac testing, contrast agents for magnetic resonance imaging (MRI), etc. [50]–[52]

Dynamics of hyperbranched polymers

Up to now, the majority of the experimental studies have addressed issues related to the synthesis and the molecular characterization of hyperbranched polymers, [53]–[55] but only few to their detailed characterization, their ability to form a hydrogen-bond network, and their structure to properties relationship. [56] Dendritic polymer dynamics, investigated by molecular dynamics simulations, in order to explain the characteristics of local environment and its association with the manifestation of glass transition phenomena, revealed that connectivity constraints inherent to this topology impose a strong dynamic contrast within the dendritic structure which increases with molecular size. [57]

Atomistic molecular dynamics simulations have been recently performed, to examine the static and dynamic properties of HBPs in the melt over many length and time scales and to investigate the formation and lifetime of both intra- and intermolecular hydrogen bonds. [58], [59] At the same time, quasielastic neutron scattering was used to investigate experimentally the relaxation processes of a HBP showing a significant influence of the hydrogen bonds on the dynamics as compared to linear polymers. [60]

Moreover, the dynamics of hyperbranched polymers is investigated in thin films of hyperbranched aromatic polyesters, [61] in novel hyperbranched polyamide amines [62] and hyperbranched polyglycerols of three different molecular weights. In the latter, three relaxation processes are observed by dielectric spectroscopy (**Figure 1.9**), one related to glass transition (α-relaxation) and two sub-glass processes (β- and γ-relaxations) with no significant dependence on the M_w. In contrast with the case of glycerol, hyperbranched polyglycerols show two secondary processes, suggesting important interactions between the applied electric field and the associated dipoles of the branched polyglycerol. In particular, the β-relaxation is attributed to the motions of the secondary, whereas the γ-relaxation to the terminal hydroxyl groups. [63]

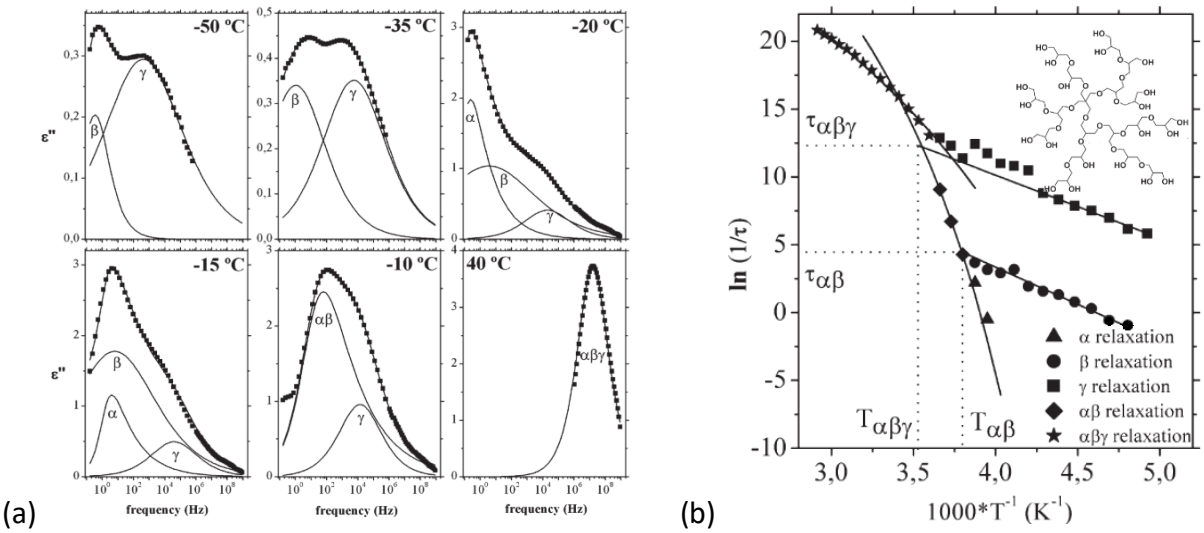

Figure 1.9: Deconvolution of the dielectric relaxations at different temperatures (a) and relaxation map for the hyperbranched polyglycerol (b). [63]

Hyperbranched polyesters with hydroxyl end groups are of great interest due to their functionality but they constitute a complex system with an extended network of H-bonds affecting their properties. Polymer dynamics has been investigated for different generations, by dielectric relaxation spectroscopy, mainly at temperatures below the glass transition due to the strong conductivity. [64]–[66] According to Turky et al. the generation affects strongly the dielectric properties and two local relaxations, the γ-process at lower temperatures and the β-process at higher ones, were observed with too high apparent activation energies, attributed to the complicated structure of such polymers.[67]

Nevertheless, the hyperbranched polymers because of their significant advantages and potential applications, need to be further investigated aiming at understanding the microscopic mechanisms responsible for the manifestation of their macroscopic properties.

1.2 Polymer Nanohybrid Materials

For decades the scientific community was dealing with composite materials where the polymer matrix is reinforced by fillers in the scale of micrometers, possessing the advantages of the inorganic material (e.g. rigidity, thermal stability) and of the organic polymer (e.g. flexibility, dielectric properties, ductility and processability); nevertheless certain problems like reduction of transparency or reduced toughness frequently emerged. [68]

On the other hand in polymer nanocomposites, where the length scale of the additive is in the nanometer scale, the interfacial area per volume is extremely enlarged. Polymer coils are in the same order of magnitude with the nanofiller, thus, molecular interactions between the polymer and the nanoparticles leads to polymer nanocomposites with improved and often innovative physicochemical properties compared to conventionally filled systems. [69]–[75] A plethora of additives are utilized as the nanofiller (some of the most common: silica nanoparticles, clays and graphitic additives) leading to superior properties, that are different from those in the bulk even at small loadings. [76], [77] The unique properties and improved performance of nanohybrids are determined mainly by the existence of many interfaces as well as the polymer-additive interactions.

There are three main methods which are mostly used to obtain the inorganic/polymer nanocomposites: solution blending, melt compounding and in situ polymerization. In solution blending method, a suspension of the additive is mixed with the desired polymer by simple stirring or shear mixing. Melt compounding method involves the mixing of a polymer melt and filler (in a dried powdery form) with or without shear. In situ polymerization method involves the mixing of the additive with the neat monomer, or in a solution of the monomer, followed by polymerization in the presence of the dispersed nanofiller.

1.2.1 Nanocomposites based on additives of different geometry

Various inorganic materials with different geometries can be utilized as nanofillers like:

- Nanoparticles with three dimensions in the nanoscale, e.g. carbon black, silica, gold, titanium oxide nanoparticles etc.
- Nanorods and nanotubes with two nanoscale dimensions, e.g. zinc oxide nanorods, carbon nanotubes, titanium oxide nanotubes etc.
- Nanolayered materials with only one dimension in the nanoscale, e.g. clays, graphene etc.
- Nanoporous materials with cavities in the nanometers range, e.g. zeolites, nanoporous alumina etc.

Polymer/nanoparticle hybrids

Use of spherical nanoparticles with maximum surface area and increased interfacial interactions led to nanocomposites with enhanced properties attributed to the polymer-additive interactions. Metal (e.g., Au, Ag), [78] metal oxide (e.g., SiO_2, TiO_2, Al_2O_3), [68]

semiconductor (e.g., PbS, CdS) nanoparticles, [79] and so forth [80] have been widely used as additives.

In nanocomposites where the nanoparticles are dispersed in the polymer matrix, a part of the polymer chain is adsorbed on the particle surface forming a thin polymer layer. The polymer properties in the interface differ from those in the bulk. In previous studies of our group this polymer confinement between spherical nanoparticles revealed strong effect on both polymer structure and thermal properties. [81]

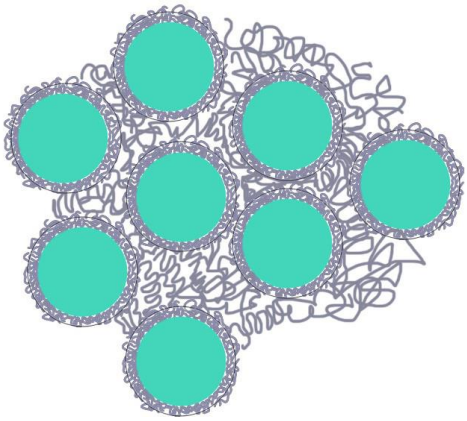

Figure 1.10: Nanoparticles dispersed in a polymer matrix. An interfacial layer is easily observable. [81]

In a recent research, Papananou et al. showed that it is possible to tune the degree of crystallinity of poly (ethylene oxide), PEO, by adding silica nanoparticles of different sizes. In order to profoundly examine this behavior attenuated total reflectance Fourier transform infrared spectroscopy (ATR-FTIR) measurements and molecular dynamics simulations were performed to reveal how the polymer – silica interactions affect the conformations of polymer chains. [75], [82]

Polymer/nanoparticle hybrids have been referred to exhibit high antimicrobial properties, [83] high transparency and UV-absorption characteristics, [84] decreased proton conductivity, water swelling and methanol permeability which could be applied in fuel cells, [85] photo-degradable properties, [86] as well as UV protection properties. Due to those properties there are already commercial products containing nanoparticles such as sunscreens, cosmetics, sports equipment and supplements. Additional advantages obtained are the high flame retardation capacity, [87] the excellent optical transparency utilized in optical devices, [88],

[89] electrical properties suitable for use in organic batteries, [90] for oxygen scavenging [91] and many others.

Polymer / layered silicate nanohybrids

Among the different nanocomposites, the ones consisting of polymers and layered inorganic materials are considered as a new generation of composite materials because they exhibit unique properties such as enhanced strength and thermal resistance, reduced gas permeability, reduced flammability, etc., which render them candidates for a range of various applications such as membranes for fuel cells or separation devices, food packaging, photovoltaic devices, chemical or biochemical sensors, flame retardants, and so forth. [92]–[94]

These systems can exhibit three different types of structure (**Figure 1.11**), depending on the interactions between the constituents. [95]–[97]

- The phase separated structure, where the polymer and the inorganic layers are immiscible in the nanoscale; this is considered to be a microcomposite material.
- In the intercalated systems, where a 0.8−2.5 nm polymer film resides within the galleries formed by the adjacent parallel inorganic layers forming a well-ordered multilayer with a repeat distance of a few nanometers. These hybrids are scientifically interesting for the extra reason that they allow the investigation of the structure, conformation, and dynamics of polymers under confinement utilizing, conventional analytical techniques and macroscopic samples.
- The exfoliated structure that consists of dispersed layers of the additive within the polymer matrix. In this case the polymer/surface interactions are the most favorable. For most applications, where a layered inorganic material is utilized as nanofiller, the exfoliated structure is considered to be the one that ensures enhanced properties and a uniform composition in the material.

Clays are layered nanomaterials, which are usually hydrophilic and, thus, hydrophilic polymers interact favorably with the silicate surfaces leading mostly to intercalated nanocomposites. [98], [99] On the other hand, hydrophobic polymers can lead to intercalated [100], [101] or exfoliated [102], [103] structures when mixed with organophilized clays, i.e., with materials where a cation exchange reaction is utilized to

replace the hydrated cations within the galleries by proper cationic surfactants (e.g., alkylammonium). For polyolefins, which are even less polar polymers, appropriate compatibilizers are required in order to achieve exfoliation by controlling the interactions. [95]–[97]

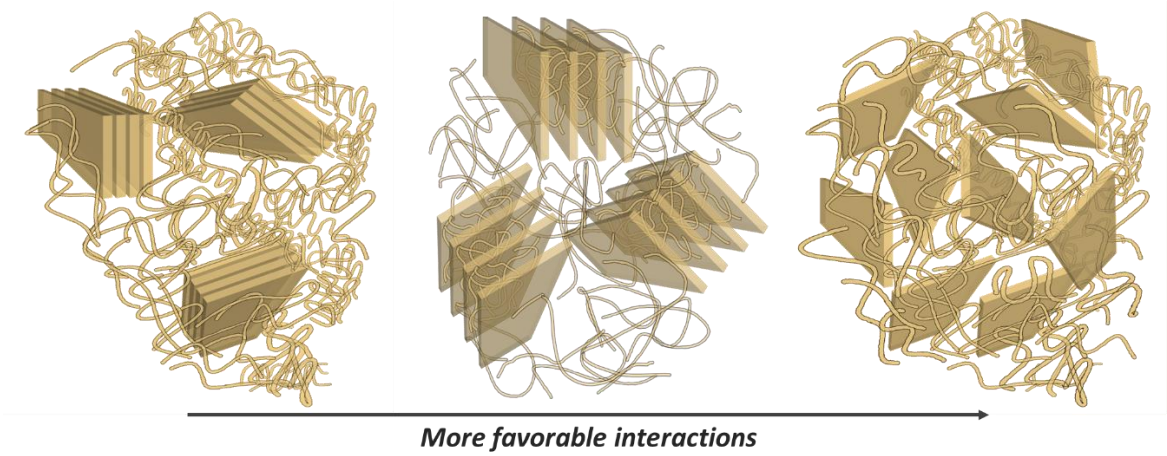

Figure 1.11: Schematic illustration of the different composite structures arising from the interactions of layered nanomaterials and polymers; from left to right: phase-separated; intercalated and exfoliated.

Recent studies on polymer structure and properties close to surfaces, in thin films and in nanocomposites, reveal strong effects. The way polymers crystallize under confinement and / or close to surfaces is a fundamental problem and, at the same time, it is of significant importance for technological applications. [82], [98], [99], [104]

Polymer / graphitic material nanohybrids

Many graphitic materials are also layered such as graphene and graphene oxide. In recent years the graphitic materials are of great interest due to their unique structural and morphological features, relatively easy chemical modification, as well as excellent electrical, mechanical, and thermal properties. Especially polymer/graphitic material nanocomposites obtain plethora of applications in drug delivery, energy materials, solar cells, water splitting, biosensing, bioimaging, environmental, catalytic, photocatalytic, and biomedical technologies. [74], [105]–[108]

Graphene is the flat monolayer of carbon atoms tightly packed into a two-dimensional (2D) honeycomb lattice, and is a basic building block for graphitic materials of all other dimensionalities, shown in **Figure 1.12**; it can be wrapped up into 0D fullerenes, rolled into 1D nanotubes or stacked into 3D graphite. [109]

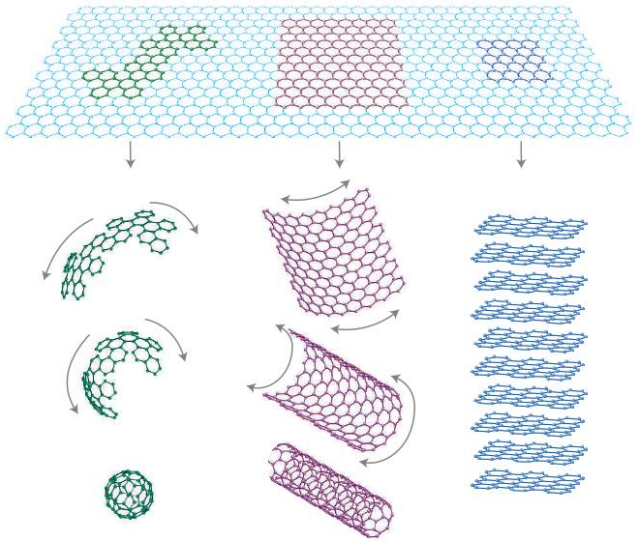

Figure 1.12: Mother of all graphitic forms. Graphene is a 2D building material for carbon materials of all other dimensionalities. It can be wrapped up into 0D buckyballs, rolled into 1D nanotubes or stacked into 3D graphite.[109]

The last decade an extensive research on the preparation and properties of graphene oxide is in progress, although graphite oxide was synthesized many decades ago by the oxidation of graphite. [110]–[112] The obvious difference between graphene and graphene oxide is the addition of oxygen atoms bound with the carbon scaffold as shown in **Figure 1.13**. [113] Graphene oxide can be easily reduced at high yields to reduced graphene oxide that is not graphene due to structural defects created during the oxidation [114] or could be partially reduced. [115], [116]

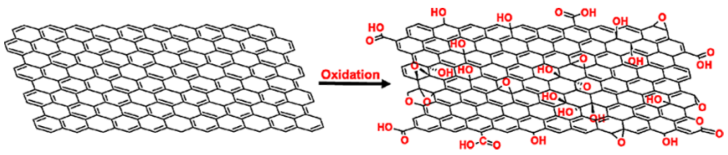

Figure 1.13: Oxidation of graphene sheet to form graphene oxide. [107]

Graphene is hydrophobic in nature whereas graphene oxide is hydrophilic, that is, easily dispersible in water and with favorable interactions with hydrophilic polymers. [105] In addition, graphene oxide contains both aromatic (sp^2) and aliphatic (sp^3) domains, which further expands the types of interactions that can occur with the surface. The oxidation of graphite provides a new additive, graphite oxide, which can obtain tailored surface properties by functionalization. Graphite oxide can be mixed with hydrophilic polymers in order to obtain nanocomposites with either exfoliated or intercalated structures.

1.2.2 Improved properties of biobased and biocompatible nanohybrids

Nanohybrid materials composed of biobased polymers, especially biodegradable ones, and different additives (generally in small concentrations) have attracted scientific interest in recent years. [117], [118] The development of biobased polymers driven by renewability, low carbon footprint and biodegradability is prohibited by some inherent drawbacks of the biobased plastics themselves; thus in many applications the narrow processing window, low heat deflection temperatures, hydrophilicity, inferior biocompatibility, poor barrier and conductivity of biobased polymers must be improved by the use of bionanocomposites. A plethora of nanofillers have been utilized and mixed with biobased polymers, according to their shape, properties, and functionalization routes.

For example PLA is a well-known biobased polymer with good mechanical properties, having tensile strength and elastic modulus comparable to those of PET, but it is very brittle, with less than 10% elongation at break and low toughness. On the other hand PLA exhibits low glass transition temperature that is a disadvantage, especially for certain applications (e.g., hot packaging) requiring resistance at high temperature whereas its gas permeability coefficients to CO_2, O_2, N_2 and $H_2O_{(g)}$ are higher than PET. Therefore, these properties can be improved by additives such as talc, carbon nanotubes, layered silicates, hydroxyapatite, calcium carbonate or metal oxides depending on the end-use. [119]

Nanohybrids that consist of layered silicates and biodegradable polymers from renewable resources like PLA, poly (3-hydroxybutyrate) (PHB), thermoplastic starch (TPS), plant oils, cellulose, gelatin, chitosan and biodegradable polymers from petroleum sources like poly (butylene succinate) (PBS), aliphatic polyesters, poly (ε-caprolactone) (PCL), poly (vinyl alcohol) (PVA), show enhanced mechanical properties, thermal stability, gas barrier and heat distortion temperature.[120]

Moreover graphitic based additives can be combined with biobased polymers. The development of double crystalline biobased blends of PCL and PBS with carbon nanotubes in low loadings, e.g., 0.5 wt%, was sufficient to enhance the thermal and mechanical properties, and thermal and electrical conductivities, of the nanocomposites. [121]

As mentioned before a crucial property of biodegradable polymers is the rate of degradation influenced by the surface properties and the crystallinity of the polymer. [122] One way to

influence the surface properties as well as the crystallinity and crystalline properties of a polymeric material is by blending it with another polymer [31]–[34] or by the incorporation of nanometric additives like hydrophilic or organophilic layered silicates,[120], [123] silica nanoparticles, [124] or graphene derivatives [125] that will be dispersed in the polymer matrix forming a nanocomposite.

In the case of the nanocomposites of aliphatic polyesters, biodegradation due to the enzymatic hydrolysis is a complex process involving different phenomena, namely, water absorption from the polyesters, enzymatic attack to the polyester surface, ester cleavage, formation of oligomer fragments due to endo or exo type hydrolysis, solubilization of oligomer fragments in the surrounding environment, diffusion of soluble oligomers by bacteria and finally consumption of the oligomers and formation of CO_2 and H_2O. Depending on the nanofiller and the existing interactions the degradation could be substantially enhanced due to the catalyzing effect of the existed reactive groups, to the crystallinity decrease, to the higher hydrophilicity of nanofillers and thus higher water uptake etc or on the other hand could be delayed due to the barrier effect of nanofillers and the lower available surface for enzymatic hydrolysis.[126]

Nevertheless, despite the fact that there have been reports on aliphatic polyester nanocomposites with improved properties for biomedical applications in tissue engineering [127] as well as nanocomposites with significantly improved mechanical and thermal properties,[128]–[130] research work is still necessary to understand the structure to properties relationship in these systems.

1.2.3 Polymer dynamics in nanocomposites

The static and dynamic behavior of the polymer close to interfaces and / or in very thin films is examined by different techniques because significant differences can emerge when the molecules are confined over distances comparable to their sizes. [131], [132] Especially the effect of the polymer-surface interactions on the glass transition temperature is still a great challenge for the research community to comprehend.[133]–[139]

The equivalence in the behavior between polymer nanocomposites and thin polymer films has been suggested and quantitatively verified in the case of silica / polystyrene nanocomposites. [140] Thus, the studies on the effect of confinement on polymer dynamics and in particular

on the glass transition temperature have been extended to polymer nanocomposites of various additives, [141] in nature and geometry, [142], [143] different functionalities of the polymer, [144], [145] and by altering the polymer architecture. [60], [146]

The investigation of polymer dynamics in intercalated polymer / layered additive nanocomposites provides the opportunity to study the influence of both confinement and of the different polymer – surface interactions utilizing macroscopic techniques. Recent studies on the dynamics of intercalated polymers reveal that the relaxation processes of the bulk polymer are strongly affected by the interaction with the inorganic layers. [147]–[155]

A number of investigations showed [144], [147], [149], [150], [152] that the segmental relaxation process (α-relaxation) of the polymer under severe confinement appears at temperatures far below the glass transition temperature of the bulk polymer. This behavior is observed for both hydrophobic PMPS when intercalated in organophilized clays (**Figure 1.14**a) and for the hydrophilic PEO in sodium montmorillonite nanocomposites (**Figure 1.14**b). The relaxation times of the segmental relaxation under confinement, noted as α'-process, are much faster than those in the bulk, α-process, with an almost Arrhenius temperature dependence. Moreover, according to the same study, the β-relaxation, corresponding to the local motions, is quite similar between the bulk and the confined PEO.

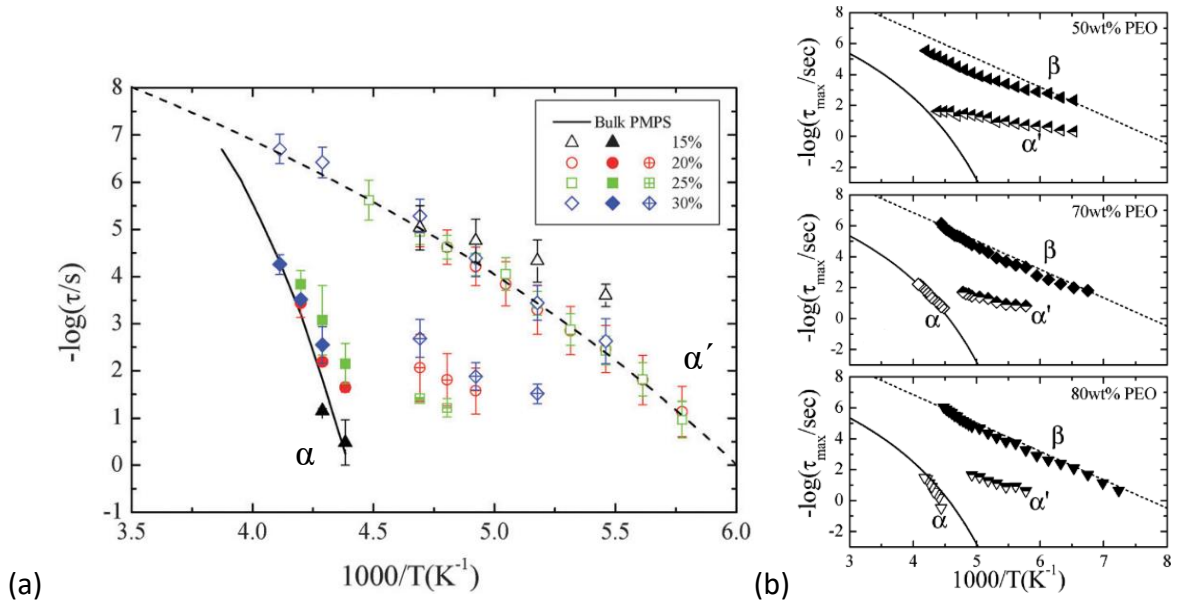

Figure 1.14: Arrhenius plot of the relaxation times for PMPS/clay (a) and PEO/clay (b) nanocomposites. [147], [149]

Nevertheless, in cases where there are more attractive polymer − surface interactions, the probed segmental relaxation shows much slower dynamics than that of the unconfined polymer. [137], [141], [153]–[155] In the case of styrene butadiene rubber (SBR) composites containing nanoclay and silica both the bulk and the interfacial polymer relaxation is observed, as shown in **Figure 1.15**. The glass transition temperature associated with the slower relaxation is used as a way to quantify the interaction strength between the polymer and the surface. [141]

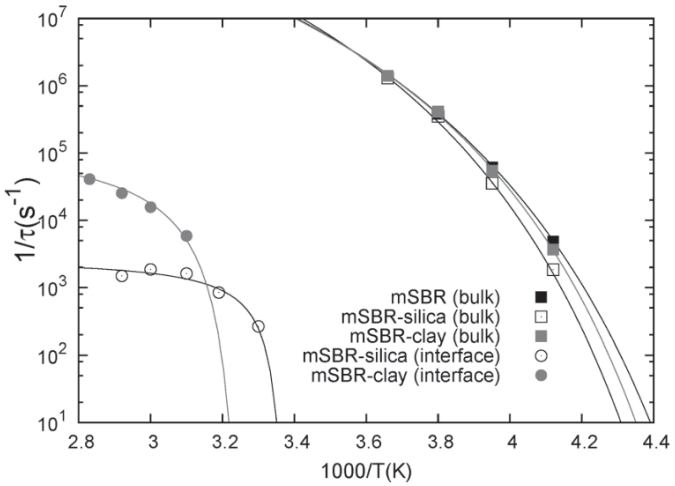

Figure 1.15: Bulk and interfacial relaxation times as a function of temperature for the bulk mSBR and for the mSBR/clay and mSBR/silica nanocomposites. [141]

Although nanocomposites based on novel classes of polymers, such as biobased and hyperbranched polymers, mixed with various additives have been synthesized, it is mainly their structure, properties and potential applications that have been studied. Very few references exist in literature on the investigation of polymer dynamics in those nanohybrids. The need of further understanding the microscopic mechanisms responsible for their macroscopic properties is urgent. In the current work polymer dynamics of novel polymer nanohybrids is investigated.

1.3 Current Work

In the present thesis the polymer structure, properties and dynamics of both linear and hyperbranched polymers are investigated in the bulk and in nanocomposites, with additives of different geometry.

First, two series of polymers with different architecture, three linear polyesters and hyperbranched polymers of different degree of branching and different functional groups, are characterized. The structure is investigated by XRD and the thermal properties by DSC and TGA. Polymer dynamics, obtained by BDS, reveals the origin of both the local and segmental motions.

Three different hydrophilic additives are mixed with the above mentioned polymers in order to examine their interactions and properties in nanocomposite materials. The additives differ either in geometry or in surface groups resulting in different interactions with the polymer.

The nanocomposites are prepared by solution mixing, in various compositions. At first, silica nanoparticles are mixed with linear polyesters to examine the effect of polymer / additive interactions on the hybrids thermal properties and dynamics. Moreover, another system of similar chemistry and molecular weight but of different architecture, i.e. hyperbranched polyester polyols are mixed with a layered graphite oxide additive; another hyperbranched poly (ester amide) is mixed with GO to examine the effect of the different functional groups on the nanohybrid structure and dynamics. Lastly, both linear and hyperbranched polymers are mixed with layered sodium montmorillonite to provide a strongly confined system. For all nanocomposites the same characterization procedure and experimental techniques as for the raw materials are utilized.

Following the nanocomposite characterization, polymer dynamics is investigated in a wide temperature range, in a composition where all the polymer chains are adsorbed on the surface and/or intercalated in the galleries of the additive. The local dynamics attributed to the motions of the small dipoles of the polymer chain (i.e. rotation of hydroxyls, reorientation of carbonyl groups, etc.) is affected by the interfacial interactions with the additive. Moreover, different mechanisms of the segmental relaxation, expressed via a different temperature dependence of the relaxation times, were obtained depending on the additive geometry and the polymer architecture.

1.4 References

[1] P. E. Rouse, “A Theory of the Linear Viscoelastic Properties of Dilute Solutions of Coiling Polymers,” *J. Chem. Phys.*, vol. 21, p. 1272, 1953.

[2] B. H. Zimm, “Dynamics of Polymer Molecules in Dilute Solution: Viscoelasticity, Flow Birefringence and Dielectric Loss,” *J. Chem. Phys.*, vol. 24, p. 269, 1956.

[3] P. G. De Gennes, *Scaling Concepts in Polymer Physics*. Ithaka and London: Cornell University Press, 1979.

[4] M. Doi and S. F. Edward, *The Theory of Polymer Dynamics*. Oxford: Clarendon Press, 1986.

[5] M. Rubinstein and R. H. Colby, *Polymer Physics*. Oxford University Press, 2003.

[6] V. G. Sakai and A. Arbe, “Quasielastic neutron scattering in soft matter,” *Curr. Opin. Colloid Interface Sci.*, vol. 14, no. 6, pp. 381–390, 2009.

[7] K. Chen, E. J. Saltzman, and K. S. Schweizer, “Segmental dynamics in polymers: From cold melts to ageing and stressed glasses,” *J. Phys. Condens. Matter*, vol. 21, no. 50, p. 503101 (20pp), 2009.

[8] B. Frick and D. Richter, “The Microscopic Basis of the Glass-Transition in Polymers from Neutron-scattering Studies,” *Science (80-.).*, vol. 267, pp. 1939–1345, 1995.

[9] J. Colmenero and A. Arbe, “Recent progress on polymer dynamics by neutron scattering: From simple polymers to complex materials,” *J. Polym. Sci. Part B Polym. Phys.*, vol. 51, no. 2, pp. 87–113, 2013.

[10] J. P. Runt and J. J. Fitzgerald, *Dielectric Spectroscopy of Polymeric Materials: Fundamentals and Applications*. Washington: American Chemical Society, 1997.

[11] F. Kremer and A. Schönhals, *Broadband Dielectric Spectroscopy*. Berlin: Springer, 2003.

[12] D. Richter, M. Monkenbusch, A. Arbe, and J. Colmenero, “Neutron Spin Echo in Polymer Systems, Chapter 1,” in *Neutron Spin Echo in Polymer Systems*, 2005, pp. 1–221.

[13] G. P. Johari and M. Goldstein, “Viscous liquids and the glass transition. III. Secondary relaxations in aliphatic alcohols and other nonrigid molecules,” *J. Chem. Phys.*, vol. 55, no. 9, pp. 4245–4252, 1971.

[14] A. L. Holmberg, K. H. Reno, R. P. Wool, and T. H. Epps, “Biobased building blocks for the rational design of renewable block polymers,” *Soft Matter*, vol. 10, no. 38, pp. 7405–7424, 2014.

[15] H. Nakajima, P. Dijkstra, and K. Loos, “The recent developments in biobased polymers toward general and engineering applications: Polymers that are upgraded from biodegradable polymers, analogous to petroleum-derived polymers, and newly developed,” *Polymers (Basel).*, vol. 9, no. 10, pp. 1–26, 2017.

[16] B. A. J. Noordover, R. Duchateau, R. A. T. M. van Benthem, W. Ming, and C. E. Koning, “Enhancing the functionality of biobased polyester coating resins through modification with citric acid,” *Biomacromolecules*, vol. 8, no. 12, pp. 3860–3870, 2007.

[17] H. Bai *et al.*, “Significantly improving oxygen barrier properties of polylactide via constructing parallel-aligned shish-kebab-like crystals with well-interlocked

boundaries," *Biomacromolecules*, vol. 15, no. 4, pp. 1507–1514, 2014.

[18] A. Merlettini *et al.*, "Thermal Annealing to Modulate the Shape Memory Behavior of a Biobased and Biocompatible Triblock Copolymer Scaffold in the Human Body Temperature Range," *Biomacromolecules*, vol. 18, no. 8, pp. 2490–2508, 2017.

[19] D. N. Bikiaris and D. S. Achilias, "Synthesis of poly(alkylene succinate) biodegradable polyesters I. Mathematical modelling of the esterification reaction," *Polymer (Guildf).*, vol. 47, pp. 4851–4860, 2006.

[20] Y. Jiang, G. O. R. A. Van Ekenstein, A. J. J. Woortman, and K. Loos, "Fully biobased unsaturated aliphatic polyesters from renewable resources: Enzymatic synthesis, characterization, and properties," *Macromol. Chem. Phys.*, vol. 215, no. 22, pp. 2185–2197, 2014.

[21] A. Díaz, R. Katsarava, and J. Puiggalí, "Synthesis, properties and applications of biodegradable polymers derived from diols and dicarboxylic Acids: From Polyesters to poly(ester amide)s," *Int. J. Mol. Sci.*, vol. 15, no. 5, pp. 7064–7123, 2014.

[22] T. Fujimaki, "Processability and properties of aliphatic polyesters, 'BIONOLLE', synthesized by polycondensation reaction," *Polym. Degrad. Stab.*, vol. 59, no. 1–3, pp. 209–214, 1998.

[23] D. N. Bikiaris, G. Z. Papageorgiou, and D. S. Achilias, "Synthesis and comparative biodegradability studies of three poly(alkylene succinate)s," *Polym. Degrad. Stab.*, vol. 91, no. 1, pp. 31–43, 2006.

[24] Z. Terzopoulou *et al.*, "Thermal degradation of biobased polyesters: Kinetics and decomposition mechanism of polyesters from 2,5-furandicarboxylic acid and long-chain aliphatic diols," *J. Anal. Appl. Pyrolysis*, vol. 117, pp. 162–175, 2016.

[25] C. Berti *et al.*, "The effect of aliphatic chain length on thermal properties of poly(alkylene dicarboxylate)s," *E-Polymers*, vol. 57, no. 057, pp. 1–18, 2007.

[26] M. Gilbert and F. J. Hybart, "Effect of chemical structure on crystallization rates and melting of polymers: Part 1. Aromatic polyesters," *Polymer (Guildf).*, vol. 13, no. 7, pp. 327–332, 1972.

[27] M. Vert, "Aliphatic polyesters: Great degradable polymers that cannot do everything," *Biomacromolecules*, vol. 6, no. 2, pp. 538–546, 2005.

[28] B. D. Ulery, L. S. Nair, and C. T. Laurencin, "Biomedical applications of biodegradable polymers," *J. Polym. Sci. Part B Polym. Phys.*, vol. 49, no. 12, pp. 832–864, 2011.

[29] Z. Gan, H. Abe, and Y. Doi, "Biodegradable poly(ethylene succinate) (PES). 1. Crystal growth kinetics and morphology," *Biomacromolecules*, vol. 1, no. 4, pp. 704–712, 2000.

[30] Z. Gan, H. Abe, and Y. Doi, "Biodegradable poly(ethylene succinate) (PES). 2. Crystal morphology of melt-crystallized ultrathin film and its change after enzymatic degradation," *Biomacromolecules*, vol. 1, no. 4, pp. 713–720, 2000.

[31] Y. Ichikawa, H. Kondo, Y. Igarashi, K. Noguchi, K. Okuyama, and J. Washiyama, "Crystal structures of α and β forms of poly(tetramethylene succinate)," *Polymer (Guildf).*, vol. 41, no. 12, pp. 4719–4727, 2000.

[32] H. A. Al-Salah, "Crystallization and morphology of poly(ethylene succinate) and poly(β-

hydroxybutyrate) blends," *Polym. Bull.*, vol. 41, no. 5, pp. 593–600, 1998.

[33] H. L. Chen and S. F. Wang, "Crystallization induced microstructure of polymer blends consisting of two crystalline constituents," *Polymer (Guildf).*, vol. 41, no. 14, pp. 5157–5164, 2000.

[34] Z. Qiu, T. Ikehara, and T. Nishi, "Unique morphology of poly(ethylene succinate)/poly(ethylene oxide) blends," *Macromolecules*, vol. 35, no. 22, pp. 8251–8254, 2002.

[35] M. Mierzwa, G. Floudas, J. Dorgan, D. Knauss, and J. Wegner, "Local and global dynamics of polylactides. A dielectric spectroscopy study," *J. Non. Cryst. Solids*, vol. 307–310, pp. 296–303, 2002.

[36] A. R. Bras, P. Malik, M. Dionisio, and J. F. Mano, "Influence of Crystallinity in Molecular Motions of Poly (L -lactic acid) Investigated by Dielectric Relaxation Spectroscopy," *Macromolecules*, vol. 41, pp. 6419–6430, 2008.

[37] S. Charlon, L. Delbreilh, E. Dargent, N. Follain, J. Soulestin, and S. Marais, "Influence of crystallinity on the dielectric relaxations of poly(butylene succinate) and poly[(butylene succinate)-co-(butylene adipate)]," *Eur. Polym. J.*, vol. 84, pp. 366–376, 2016.

[38] D. A. Tomalia, "The dendritic state," *Mater. Today*, vol. 8, no. 3, pp. 34–46, 2005.

[39] C. Gao and D. Yan, *Hyperbranched polymers: synthesis, properties, and applications*. New York: Wiley Series on Polymer Engineering and Technology, 2011.

[40] E. R. Gillies and J. M. J. Fréchet, "Dendrimers and dendritic polymers in drug delivery," *Drug Discov. Today*, vol. 10, no. 1, pp. 35–43, 2005.

[41] B. I. Voit and A. Lederer, "Hyperbranched and Highly Branched Polymer Architectures-Synthetic Strategies and Major Characterization Aspects," *Chem. Rev.*, vol. 109, no. 11, pp. 5924–5973, 2009.

[42] B. Pettersson, "Hyperbranched Polymers: Unique Design Tools for Multi-property Control in Resins and Coatings," *Pigment Resin Technol.*, vol. 25, pp. 4–14, 1996.

[43] P. Froehling, "Development of DSM's Hybrane® Hyperbranched polyesteramides," *J. Polym. Sci. Part A Polym. Chem.*, vol. 42, no. 13, pp. 3110–3115, 2004.

[44] T. J. Mulkern and N. C. B. B. Tan, "Processing and characterization of reactive polystyrene/hyperbranched polyester blends," *Polymer (Guildf).*, vol. 41, no. 9, pp. 3193–3203, 2000.

[45] D. Ratna, R. Varley, and G. P. Simon, "Processing and chemorheology of epoxy resins and their blends with dendritic hyperbranched polymers," *J. Appl. Polym. Sci.*, vol. 92, no. 3, pp. 1604–1610, 2004.

[46] J. Zou, Y. Zhao, and W. Shi, "Preparation and properties of proton conducting organic – inorganic hybrid membranes based on hyperbranched aliphatic polyester and phosphoric acid," *J. Memb. Sci.*, vol. 245, pp. 35–40, 2004.

[47] X. Wang, H. Liu, Y. Jin, and C. Chen, "Polymer-functionalized multiwalled carbon nanotubes as lithium intercalation hosts," *J. Phys. Chem. B*, vol. 110, no. 21, pp. 10236–10240, 2006.

[48] S. J. Garcia, "Effect of polymer architecture on the intrinsic self-healing character of

polymers," *Eur. Polym. J.*, vol. 53, no. 1, pp. 118–125, 2014.

[49] X. Li, J. Le Li, Y. Wang, and T. Cai, "Fabrication of Smart Hybrid Nanoreactors from Platinum Nanodendrites Encapsulating in Hyperbranched Polyglycerol Hollow Shells," *ACS Appl. Nano Mater.*, vol. 1, no. 6, pp. 2559–2566, 2018.

[50] S. Chen, X.-Z. Zhang, S.-X. Cheng, R.-X. Zhuo, and Z.-W. Gu, "Functionalized amphiphilic hyperbranched polymers for targeted drug delivery," *Biomacromolecules*, vol. 9, pp. 2578–2585, 2008.

[51] I. Tanis, K. Karatasos, A. N. Assimopoulou, and V. P. Papageorgiou, "Modeling of hyperbranched polyesters as hosts for the multifunctional bioactive agent shikonin," *Phys. Chem. Chem. Phys.*, vol. 13, no. 22, pp. 10808–10817, 2011.

[52] X. Zeng, Y. Zhang, Z. Wu, P. Lundberg, M. Malkoch, and A. M. Nystrom, "Hyperbranched Copolymer Micelles as Delivery Vehicles of Doxorubicin in Breast Cancer Cells," *J. Polym. Sci. Part A Polym. Chem.*, vol. 50, pp. 280–288, 2012.

[53] E. T. F. Geladé *et al.*, "Molecular structure characterization of hyperbranched polyesteramides," *Macromolecules*, vol. 34, no. 11, pp. 3552–3558, 2001.

[54] E. Zagar and M. Zigon, "Characterization of a Commercial Hyperbranched Aliphatic Polyester Based on 2,2-Bis(methylol) propionic Acid," *Macromolecules*, vol. 35, pp. 9913–9925, 2002.

[55] G. S. Dritsas, K. Karatasos, and C. Panayiotou, "Investigation of thermodynamic properties of hyperbranched aliphatic polyesters by inverse gas chromatography," *J. Chromatogr. A*, vol. 1216, pp. 8979–8985, 2009.

[56] M. Huskic, E. Zagar, M. Zigon, and Z. Ema, "Structure-to-Properties Relationship of Aliphatic Hyperbranched Polyesters," *Macromol. Chem. Phys.*, vol. 208, no. 13, pp. 1379–1387, 2007.

[57] K. Karatasos, "Glass transition in dendrimers," *Macromolecules*, vol. 39, no. 13, pp. 4619–4626, 2006.

[58] I. Tanis and K. Karatasos, "Molecular dynamics simulations of polyamidoamine dendrimers and their complexes with linear poly (ethylene oxide) at different pH conditions: static properties and hydrogen bonding," *Phys. Chem. Chem. Phys.*, vol. 11, pp. 10017–10028, 2009.

[59] I. Tanis and K. Karatasos, "Local Dynamics and Hydrogen Bonding in Hyperbranched Aliphatic Polyesters," *Macromolecules*, vol. 42, no. 24, pp. 9581–9591, 2009.

[60] S. Fotiadou *et al.*, "Structure and Dynamics of Hyperbranched Polymer / Layered Silicate Nanocomposites," *Macromolecules*, vol. 46, pp. 2842–2855, 2013.

[61] A. Serghei, Y. Mikhailova, K.-J. Eichhorn, B. Voit, and F. Kremer, "Discrepancies in the Characterization of the Glass Transition in Thin Films of Hyperbranched Polyesters," *J. Polym. Sci. Part B Polym. Phys.*, vol. 44, pp. 3006–3010, 2006.

[62] J. R. Sangoro *et al.*, "Charge transport and dipolar relaxations in hyperbranched polyamide amines," *Macromolecules*, vol. 42, no. 5, pp. 1648–1651, 2009.

[63] A. Garcia-Bernabé, R. Díaz-Calleja, and R. Haag, "Broadband dielectric spectroscopy studies of hyperbranched polyglycerols," *Macromol. Chem. Phys.*, vol. 207, no. 11, pp.

970–977, 2006.

[64] E. Malmstrom, F. Liu, R. H. Boyd, A. Hult, and U. W. Gedde, “Relaxation processes in hyperbranched polyesters,” *Polym. Bull.*, vol. 32, pp. 679–685, 1994.

[65] E. Malmstrom, A. Hult, U. W. Gedde, F. Liu, and R. H. Boyd, “Relaxation processes in hyperbranched polyesters: influence of terminal groups,” *Polymer (Guildf).*, vol. 38, no. 19, pp. 4873–4879, 1997.

[66] P. W. Zhu, S. Zheng, and G. Simon, “Dielectric Relaxations in a Hyperbranched Polyester with Terminal Hydroxyl Groups : Effects of Generation Number,” *Macromol. Chem. Phys.*, vol. 202, pp. 3008–3017, 2001.

[67] G. Turky, S. S. Shaaban, and A. Schoenhals, “Broadband Dielectric Spectroscopy On the Molecular Dynamics in Different Generations of Hyperbranched Polyester,” *J. Appl. Polym. Sci.*, vol. 113, pp. 2477–2484, 2009.

[68] J. H. Koo, *Polymer Nanocomposites Processing, Characterization and Applications*. McGraw-Hill, 2006.

[69] J. Jancar *et al.*, “Current issues in research on structure-property relationships in polymer nanocomposites,” *Polymer (Guildf).*, vol. 51, no. 15, pp. 3321–3343, 2010.

[70] S. K. Kumar and R. Krishnamoorti, “Nanocomposites: Structure, Phase Behavior, and Properties,” *Annu. Rev. Chem. Biomol. Eng.*, vol. 1, no. 1, pp. 37–58, 2010.

[71] J. Malho, P. Laaksonen, A. Walther, O. Ikkala, and M. B. Linder, “Facile Method for Stiff, Tough, and Strong Nanocomposites by Direct Exfoliation of Multilayered Graphene into Native Nanocellulose Matrix,” *Biomacromolecules*, vol. 13, pp. 1093–1099, 2012.

[72] D. Feldman, “Polymer nanocomposites in medicine,” *J. Macromol. Sci. Part A Pure Appl. Chem.*, vol. 53, no. 1, pp. 55–62, 2016.

[73] R. Mincheva *et al.*, “Binary Mixed Homopolymer Brushes Tethered to Cellulose Nanocrystals: A Step Towards Compatibilized Polyester Blends,” *Biomacromolecules*, vol. 17, no. 9, pp. 3048–3059, 2016.

[74] D. G. Papageorgiou, I. A. Kinloch, and R. J. Young, “Mechanical properties of graphene and graphene-based nanocomposites,” *Prog. Mater. Sci.*, vol. 90, pp. 75–127, 2017.

[75] A. N. Rissanou *et al.*, “Structural and Conformational Properties of Poly(ethylene oxide)/Silica Nanocomposites: Effect of Confinement,” *Macromolecules*, vol. 50, no. 16, pp. 6273–6284, 2017.

[76] K. I. Winey and R. A. Vaia, “Polymer Nanocomposites,” *MRS Bull.*, vol. 32, pp. 314–322, 2007.

[77] A. M. Pourrahimi *et al.*, “Highly Efficient Interfaces in Nanocomposites Based on Polyethylene and ZnO Nano/Hierarchical Particles: A Novel Approach toward Ultralow Electrical Conductivity Insulations,” *Adv. Mater.*, vol. 28, no. 39, pp. 8651–8657, 2016.

[78] T. M. Tolaymat, A. M. El, A. Genaidy, K. G. Scheckel, T. P. Luxton, and M. Suidan, “An evidence-based environmental perspective of manufactured silver nanoparticle in syntheses and applications: A systematic review and critical appraisal of peer-reviewed scientific papers,” *Sci. Total Environ.*, vol. 408, no. 5, pp. 999–1006, 2010.

[79] W. R. Caseri, “Nanocomposites of polymers and inorganic particles : preparation,

structure and properties," *Mater. Sci. Technol.*, vol. 22, no. 7, pp. 807–817, 2006.

[80] T. Hanemann and D. V. Szabó, "Polymer-Nanoparticle Composites: From Synthesis to Modern Applications," *Materials (Basel).*, vol. 3, pp. 3468–3517, 2010.

[81] H. Papananou, "Polymer structure and dynamics under confinement," PhD Thesis, University of Crete, 2017.

[82] H. Papananou *et al.*, "Tuning polymer crystallinity via the appropriate selection of inorganic nanoadditives," *Polymer (Guildf).*, vol. 157, no. September, pp. 111–121, 2018.

[83] M. L. Cerrada *et al.*, "Self-Sterilized EVOH-TiO2 Nanocomposites: Interface Effects on Biocidal Properties," *Adv. Funct. Mater.*, vol. 18, pp. 1949–1960, 2008.

[84] D. Koziej, F. Fischer, N. Kra, W. R. Caseri, and M. Niederberger, "Nonaqueous TiO2 Nanoparticle Synthesis: a UV-Absorbing Composite Films," *ACS Appl. Mater. Interfaces*, vol. 1, no. 5, pp. 1097–1104, 2009.

[85] K. Prashantha and S. G. Park, "Nanosized TiO2-Filled Sulfonated Polyethersulfone Proton Conducting Membranes for Direct Methanol Fuel Cells," *J. Appl. Polym. Sci.*, vol. 98, pp. 1875–1878, 2005.

[86] H. S. Kim, S. Kwak, and T. Suzuki, "Photocatalytic degradation of flexible PVC / TiO2 nanohybrid as an eco-friendly alternative to the current waste landfill and dioxin-emitting incineration of post-use PVC," *Polymer (Guildf).*, vol. 47, pp. 3005–3016, 2006.

[87] T. Kashiwagi *et al.*, "Thermal and Flammability Properties of a Silica–Poly (methylmethacrylate) Nanocomposite," *J. Appl. Polym. Sci.*, vol. 89, pp. 2073–2078, 2003.

[88] Y. Yu, C. Chen, and W. Chen, "Synthesis and characterization of organic – inorganic hybrid thin films from poly (acrylic) and monodispersed colloidal silica," *Polymer (Guildf).*, vol. 44, pp. 593–601, 2003.

[89] C. Chang and W. Chen, "Synthesis and Optical Properties of Polyimide-Silica Hybrid Thin Films," *Chem. Mater.*, vol. 14, no. 10, pp. 4242–4248, 2002.

[90] A. Arya and A. L. Sharma, *Polymer electrolytes for lithium ion batteries : a critical study*. Berlin: Springer-Verlag, 2017.

[91] L. Xiao-e, A. N. M. Green, S. A. Haque, A. Mills, and J. R. Durrant, "Light-driven oxygen scavenging by titania / polymer nanocomposite films," *J. Photochem. Photobiol. A Chem.*, vol. 162, pp. 253–259, 2004.

[92] S. S. Ray and M. Okamoto, "Polymer /layered silicate nanocomposites: a review from preparation to processing," *Prog. Polym. Sci.*, vol. 28, pp. 1539–1641, 2003.

[93] S. C. Tjong, "Structural and mechanical properties of polymer nanocomposites," *Mater. Sci. Eng. R Reports*, vol. 53, no. 3–4, pp. 73–197, 2006.

[94] X. Wang, E. N. Kalali, and D.-Y. Wang, "Two-Dimensional Inorganic Nanomaterials: A Solution to Flame Retardant Polymers," *Nano Adv.*, vol. 1, no. 1, pp. 1–16, 2016.

[95] K. Chrissopoulou, I. Altintzi, S. H. Anastasiadis, E. P. Giannelis, and M. Pitsikalis, "Controlling the miscibility of polyethylene / layered silicate nanocomposites by altering the polymer / surface interactions," *Polymer (Guildf).*, vol. 46, pp. 12440–

12451, 2005.

[96] K. Chrissopoulou *et al.*, “Understanding and Controlling the Structure of Polypropylene/Layered Silicate Nanocomposites,” *J. Polym. Sci. Part B Polym. Phys.*, vol. 46, pp. 2683–2695, 2008.

[97] K. Chrissopoulou and S. H. Anastasiadis, “Polyolefin/layered silicate nanocomposites with functional compatibilizers,” *Eur. Polym. J.*, vol. 47, no. 4, pp. 600–613, 2011.

[98] K. Chrissopoulou *et al.*, “Crystallinity and Chain Conformation in PEO / Layered Silicate Nanocomposites,” *Macromolecules*, vol. 44, pp. 9710–9722, 2011.

[99] S. Bollas, K. Chrissopoulou, K. S. Andrikopoulos, G. A. Voyiatzis, and S. H. Anastasiadis, “Polymer conformation under confinement,” *Polymers (Basel).*, vol. 9, no. 2, pp. 1–14, 2017.

[100] R. A. Vaia, K. D. Jandt, E. J. Kramer, and E. P. Giannelis, “Microstructural Evolution of Melt Intercalated Polymer-Organically Modified Layered Silicates Nanocomposites,” *Chem. Mater.*, vol. 8, no. 11, pp. 2628–2635, 1996.

[101] B. N. Jang and C. A. Wilkie, “The thermal degradation of polystyrene nanocomposite,” *Polymer (Guildf).*, vol. 46, no. 9, pp. 2933–2942, 2005.

[102] U. Arimitsu *et al.*, “Synthesis of Nylon 6-clay hybrid,” *J. Mater. Res.*, vol. 8, no. 5, pp. 1179–1184, 1993.

[103] S. Hotta and D. R. Paul, “Nanocomposites formed from linear low density polyethylene and organoclays,” *Polymer (Guildf).*, vol. 45, no. 22, pp. 7639–7654, 2004.

[104] J. M. Carr, D. S. Langhe, M. T. Ponting, A. Hiltner, and E. Baer, “Confined crystallization in polymer nanolayered films: A review,” *J. Mater. Res.*, vol. 27, no. 10, pp. 1326–1350, 2012.

[105] H. Kim, A. A. Abdala, and C. W. MacOsko, “Graphene/polymer nanocomposites,” *Macromolecules*, vol. 43, no. 16, pp. 6515–6530, 2010.

[106] S. C. Ray, *Applications of Graphene and Graphene-Oxide Based Nanomaterials*. Oxford: Elsevier Inc., 2015.

[107] V. Georgakilas *et al.*, “Noncovalent Functionalization of Graphene and Graphene Oxide for Energy Materials, Biosensing, Catalytic, and Biomedical Applications,” *Chem. Rev.*, vol. 116, no. 9, pp. 5464–5519, 2016.

[108] A. M. Dimiev and S. Eigler, *Graphene Oxide Fundamentals and Applications*. Wiley, 2017.

[109] A. K. Geim and K. S. Novoselov, “The rise of graphene,” *Nat. Mater.*, vol. 6, no. 3, pp. 183–191, 2007.

[110] D. R. Dreyer, S. Park, C. W. Bielawski, and R. S. Ruoff, “The chemistry of graphene oxide,” *Chem. Soc. Rev.*, vol. 39, pp. 228–240, 2010.

[111] D. C. Marcano *et al.*, “Improved Synthesis of Graphene Oxide,” *ACS Nano*, vol. 4, no. 8, pp. 4806–4814, 2010.

[112] J. Zhao, L. Liu, and F. Li, *Graphene Oxide : Physics and Applications*. London: Springer, 2015.

[113] P. Wick *et al.*, "Classification framework for graphene-based materials," *Angew. Chemie - Int. Ed.*, vol. 53, no. 30, pp. 7714–7718, 2014.

[114] B. K. Erickson, R. Erni, Z. Lee, N. Alem, W. Gannett, and A. Zettl, "Determination of the Local Chemical Structure of Graphene Oxide and Reduced Graphene Oxide," *Adv. Mater.*, vol. 22, pp. 4467–4472, 2010.

[115] D. Krishnan *et al.*, "Energetic graphene oxide : Challenges and opportunities," *Nano Today*, vol. 7, no. 2, pp. 137–152, 2012.

[116] S. Eigler, S. Grimm, M. Enzelberger-heim, P. Mu, and A. Hirsch, "Graphene oxide : efficiency of reducing agents," *Chem Commun*, vol. 49, pp. 7391–7393, 2013.

[117] M. M. Reddy, S. Vivekanandhan, M. Misra, S. K. Bhatia, and A. K. Mohanty, "Biobased plastics and bionanocomposites: Current status and future opportunities," *Prog. Polym. Sci.*, vol. 38, no. 10–11, pp. 1653–1689, 2013.

[118] I. Armentano *et al.*, "Nanocomposites based on biodegradable polymers," *Materials (Basel).*, vol. 11, no. 5, 2018.

[119] M. Murariu and P. Dubois, "PLA composites: From production to properties," *Adv. Drug Deliv. Rev.*, vol. 107, pp. 17–46, 2016.

[120] S. S. Ray and M. Bousmina, "Biodegradable polymers and their layered silicate nanocomposites: In greening the 21st century materials world," *Prog. Mater. Sci.*, vol. 50, no. 8, pp. 962–1079, 2005.

[121] T. P. Gumede, A. S. Luyt, and A. J. Müller, "Review on PCL, PBS, AND PCL/PBS blends containing carbon nanotubes," *Express Polym. Lett.*, vol. 12, no. 6, pp. 505–529, 2018.

[122] S. Kumar and P. Maiti, "Controlled biodegradation of polymers using nanoparticles and its application," *RSC Adv.*, vol. 6, no. 72, pp. 67449–67480, 2016.

[123] J. Bandyopadhyay, S. S. Ray, M. Scriba, and T. Malwela, "The impact of nanoclay on the crystal growth kinetics and morphology of biodegradable poly(ethylene succinate) composite," *Polym. (United Kingdom)*, vol. 53, no. 16, pp. 3602–3612, 2012.

[124] A. A. Vasileiou, G. Z. Papageorgiou, M. Kontopoulou, A. Docoslis, and D. Bikiaris, "Covalently bonded poly(ethylene succinate)/SiO2 nanocomposites prepared by in situ polymerisation," *Polym. (United Kingdom)*, vol. 54, no. 3, pp. 1018–1032, 2013.

[125] X. Jing and Z. Qiu, "Influence of thermally reduced graphene low-loadings on the crystallization behavior and morphology of biodegradable poly(ethylene succinate)," *Ind. Eng. Chem. Res.*, vol. 53, no. 1, pp. 498–504, 2014.

[126] D. N. Bikiaris, "Nanocomposites of aliphatic polyesters: An overview of the effect of different nanofillers on enzymatic hydrolysis and biodegradation of polyesters," *Polym. Degrad. Stab.*, vol. 98, no. 9, pp. 1908–1928, 2013.

[127] I. Armentano, M. Dottori, E. Fortunati, S. Mattioli, and J. M. Kenny, "Biodegradable polymer matrix nanocomposites for tissue engineering: A review," *Polym. Degrad. Stab.*, vol. 95, no. 11, pp. 2126–2146, 2010.

[128] S. Sinha Ray and M. E. Makhatha, "Thermal properties of poly(ethylene succinate) nanocomposite," *Polymer (Guildf).*, vol. 50, no. 19, pp. 4635–4643, 2009.

[129] J. Zhao, X. Wang, W. Zhou, E. Zhi, W. Zhang, and J. Ji, "Graphene-reinforced

biodegradable poly(ethylene succinate) nanocomposites prepared by in situ polymerization," *J. Appl. Polym. Sci.*, vol. 130, no. 5, pp. 3212–3220, 2013.

[130] V. Ojijo and S. S. Ray, "Nano-biocomposites based on synthetic aliphatic polyesters and nanoclay," *Prog. Mater. Sci.*, vol. 62, no. 2014, pp. 1–57, 2014.

[131] R. Zorn, "Neutron spectroscopy for confinement studies," *Eur. Phys. J. Spec. Top.*, vol. 189, no. 1, pp. 65–81, 2010.

[132] G. B. McKenna, "Ten (or more) years of dynamics in confinement: Perspectives for 2010," *Eur. Phys. J. Spec. Top.*, vol. 189, no. 1, pp. 285–302, 2010.

[133] J. L. Keddie, R. A. L. Jones, and R. A. Cory, "Size-Dependent Depression of the Glass Transition Temperature in Polymer Films," *Europhys. Lett.*, vol. 27, no. 1, pp. 59–64, 1994.

[134] P. A. O'Connell and G. B. McKenna, "Rheological Measurements of the Thermoviscoelastic Response of Ultrathin Polymer Films," *Science (80-.).*, vol. 307, pp. 1760–1764, 2005.

[135] A. Serghei and F. Kremer, "Molecular Dynamics in Thin Polymer Films," in *Fractals, Diffusion, and Relaxation in Disordered Complex Systems, Part B*, vol. 133, New Jersey: John Wiley & Sons, Inc, 2006, pp. 595–632.

[136] S. Napolitano and M. Wubbenhorst, "The lifetime of the deviations from bulk behaviour in polymers confined at the nanoscale," *Nat. Commun.*, vol. 2, p. 260, 2011.

[137] H. K. Nguyen, M. Labardi, S. Capaccioli, M. Lucchesi, P. Rolla, and D. Prevosto, "Interfacial and Annealing Effects on Primary α -Relaxation of Ultrathin Polymer Films Investigated at Nanoscale," *Macromolecules*, vol. 45, pp. 2138–2144, 2012.

[138] K. L. Ngai, D. Prevosto, and L. Grassia, "Viscoelasticity of nanobubble-inflated ultrathin polymer films: Justification by the coupling model," *J. Polym. Sci. Part B Polym. Phys.*, vol. 51, no. 3, pp. 214–224, 2013.

[139] A. N. Rissanou and V. Harmandaris, "Dynamics of various polymer-graphene interfacial systems through atomistic molecular dynamics simulations," *Soft Matter*, vol. 10, no. 16, pp. 2876–2888, 2014.

[140] A. Bansal *et al.*, "Quantitative equivalence between polymer nanocomposites and thin polymer films," *Nat. Mater.*, vol. 4, no. 9, pp. 693–698, 2005.

[141] L. T. Vo, S. H. Anastasiadis, and E. P. Giannelis, "Dielectric study of Poly(styrene- co -butadiene) Composites with Carbon Black, Silica, and Nanoclay," *Macromolecules*, vol. 44, no. 15, pp. 6162–6171, 2011.

[142] B. J. Ash, R. W. Siegel, and L. S. Schadler, "Glass-transition temperature behavior of alumina/PMMA nanocomposites," *J. Polym. Sci. Part B Polym. Phys.*, vol. 42, no. 23, pp. 4371–4383, 2004.

[143] S. Alexandris, G. Sakellariou, M. Steinhart, and G. Floudas, "Dynamics of unentangled cis -1,4-polyisoprene confined to nanoporous alumina," *Macromolecules*, vol. 47, no. 12, pp. 3895–3900, 2014.

[144] B. Frick *et al.*, "Inelastic neutron scattering for investigating the dynamics of confined glass-forming liquids," *J. Non. Cryst. Solids*, vol. 351, no. 33-36 SPEC. ISS., pp. 2657–

2667, 2005.

[145] P. Rittigstein, R. D. Priestley, L. J. Broadbelt, and J. M. Torkelson, “Model polymer nanocomposites provide an understanding of confinement effects in real nanocomposites,” *Nat. Mater.*, vol. 6, no. 4, pp. 278–282, 2007.

[146] K. Karatasos, “Graphene/hyperbranched polymer Nanocomposites: Insight from molecular dynamics simulations,” *Macromolecules*, vol. 47, no. 24, pp. 8833–8845, 2014.

[147] S. H. Anastasiadis, K. Karatasos, and G. Vlachos, “Nanoscopic-Confinement Effects on Local Dynamics,” *Phys. Rev. Lett.*, vol. 84, no. 5, pp. 915–918, 2000.

[148] K. Chrissopoulou, S. H. Anastasiadis, E. P. Giannelis, and B. Frick, “Quasielastic neutron scattering of poly (methyl phenyl siloxane) in the bulk and under severe confinement,” *J. Chem. Physicshysics*, vol. 127, p. 144910, 2007.

[149] M. M. Elmahdy, K. Chrissopoulou, A. Afratis, G. Floudas, and S. H. Anastasiadis, “Effect of confinement on polymer segmental motion and ion mobility in PEO/layered silicate nanocomposites,” *Macromolecules*, vol. 39, no. 16, pp. 5170–5173, 2006.

[150] K. Chrissopoulou, A. Afratis, S. H. Anastasiadis, M. M. Elmahdy, and G. Floudas, “Structure and dynamics in PEO nanocomposites,” *Eur. Phys. J. Spec. Top.*, vol. 141, pp. 267–271, 2007.

[151] S. H. Anastasiadis, K. Chrissopoulou, and B. Frick, “Structure and dynamics in polymer / layered silicate nanocomposites,” *Mater. Sci. Eng. B*, vol. 152, pp. 33–39, 2008.

[152] S. Fotiadou, K. Chrissopoulou, B. Frick, and S. H. Anastasiadis, “Structure and Dynamics of Polymer Chains in Hydrophilic Nanocomposites,” *J. Polym. Sci. Part B Polym. Phys.*, vol. 48, pp. 1658–1667, 2010.

[153] C. Lorthioir, F. Lauprêtre, J. Soulestin, and J. M. Lefebvre, “Segmental dynamics of poly(ethylene oxide) chains in a model polymer/clay intercalated phase: Solid-state NMR investigation,” *Macromolecules*, vol. 42, no. 1, pp. 218–230, 2009.

[154] D. Prevosto, M. Lucchesi, M. Bertoldo, E. Passaglia, F. Ciardelli, and P. Rolla, “Interfacial effects on the dynamics of ethylene – propylene copolymer nanocomposite with inorganic clays,” *J. Non. Cryst. Solids*, vol. 356, no. 11–17, pp. 568–573, 2010.

[155] M. Labardi, D. Prevosto, H. K. Nguyen, S. Capaccioli, M. Lucchesi, and P. Rolla, “Local dielectric spectroscopy of nanocomposite materials interfaces,” *J. Vac. Sci. Technol.*, vol. 28, no. 3, pp. 11–17, 2010.

2 Materials and Methods

2.1 Linear and Hyperbranched Polymers

The polymers investigated in the current study are briefly presented below. Two series of commercially available hydrophilic polyesters were utilized, one comprise of linear biobased polyesters and the other of hyperbranched polyesters.

Biobased Linear Polyesters

In the present work three different biobased polyester polyols were utilized in order to investigate their structure, their thermal properties as well as their dynamics in the bulk and in nanocomposites. The polyesters were a poly (ethylene succinate), a poly (diethylene succinate) and a poly (1,6-hexylene succinate), with commercial names EG-110, DG-110 and HD-110 respectively, (supplied by Myriant) and their chemical formulae are shown in **Scheme 2.1**.

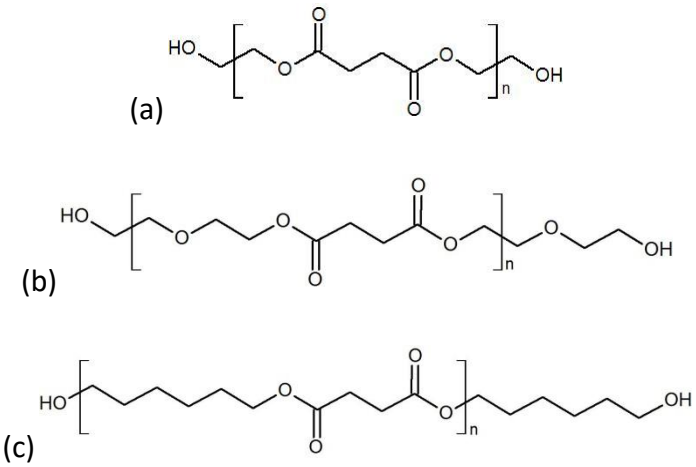

Scheme 2.1: Chemical formulae of poly (ethylene succinate), EG-110, (a), poly (diethylene succinate), DG-110, (b) and poly (1,6-hexylene succinate), HD-110, (c).

All three polymers consist of ester groups in the backbone of the polymer chain, with different number of methylene groups –CH_2– in between and possess hydroxyl end-groups; DG-110 contains an additional ether linkage. Moreover, EG-110 and HD-110 are crystalline polymers, whereas DG-110 is amorphous. The molecular characteristics of the polymers, according to the material data sheets as provided by the supplier, are given in **Table 2.1**. The polyesters are of low molecular weight; the number of the repeating units in each molecule is determined to be ~6 for EG-110 and ~5 for DG-110 and HD-110.

Table 2.1: Characteristics of Myriant biobased polyesters. [1]

Biobased Polyester	Commercial name	OH-number	Acid value	Molecular weight* (g/mol)
Poly (ethylene succinate)	EG-110	107	0.52	1043
Poly (diethylene succinate)	DG-110	113	0.8	986
Poly (1,6 hexalene succinate)	HD-110	108	0.7	1032

*Mw calculated by Mw = [54.1 × 1,000 / (OH number + acid number)] × functionality, according to the data provided by the supplier.

The hydroxyl value is a measure of the content of free hydroxyl groups in a chemical substance. It is defined as the number of milligrams of potassium hydroxide (KOH) required, to neutralize the acetic acid taken up on acetylation of one gram of the substance that contains free hydroxyl groups. The acid value is defined as the mass of potassium hydroxide (KOH) in milligrams that is required to neutralize one gram of the chemical substance.

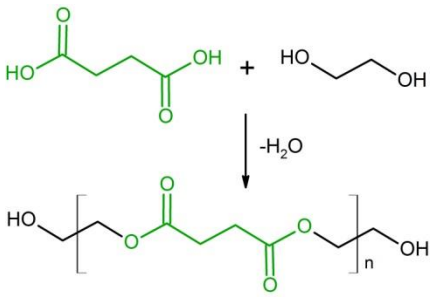

Scheme 2.2: Synthesis of polyester polyol, EG-110, by polycondensation of biobased succinic acid and ethylene glycol. [1]

The polyesters were synthesized by polycondensation of biobased succinic acid with the respective glycol. In **Scheme 2.2** the representative synthesis of EG-110 is shown. Succinic acid that occurs naturally in plant and animal tissues has the same chemical properties as adipic acid, which is regularly utilized for the synthesis of polyester polyols and, thus, it can be introduced without changes to the manufacturing process to increase to a large extend the renewable content.

Hyperbranched Polyesters

The dendritic polymers utilized in this work are the second, third and fourth generation, H20, H30 and H40, of the hyperbranched polyester polyol Boltorn (**Scheme 2.3**), supplied by Polymer Factory, Sweden AB. Their branches consist mainly of ester groups and possess a

number of hydroxyl end-groups depending on the generation. Therefore, these molecules are highly polar and soluble in polar solvents. Moreover, hydrogen bonds are formed between the hydrogens of the hydroxyl groups and the oxygens of either the ester or the hydroxyl groups, within either the same or different molecules. The radii of gyration, R_g, were calculated by atomistic molecular dynamics simulations to be $R_{g,H20} \approx 0.8$ nm and $R_{g,H30} \approx 1.05$ nm at ambient temperature.[2]

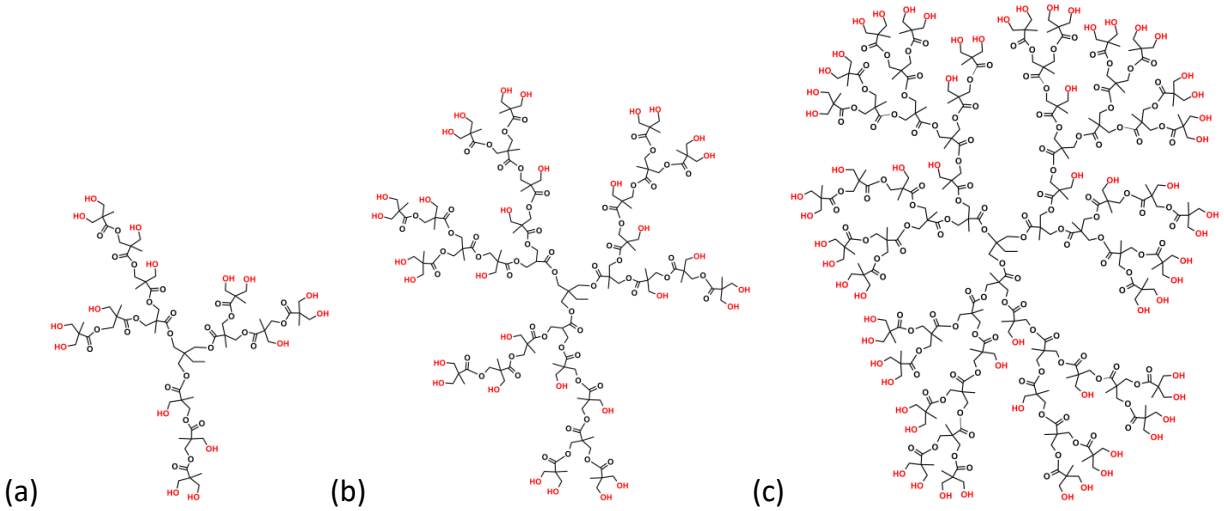

(a) (b) (c)

Scheme 2.3: Chemical formulae of the hyperbranched polyester polyols, Boltorn H20 (a), H30 (b) and H40 (c).

The structure, the thermal properties and the dynamics of the three generations of the hyperbranched polyester polyols, Boltorn, were compared with the respective of another hyperbranched polymer of similar architecture and molecular weight but different functional groups, hyperbranched polyester amide, Hybrane S1200. Hybrane S1200 was supplied by DSM and its chemical formula is shown in **Scheme 2.4**. Its radius of gyration was calculated by molecular dynamics simulations to be , $R_{g\ Hybrane} \approx 0.76$ to 0.80nm in the temperature range 350 to 800 K. [3]

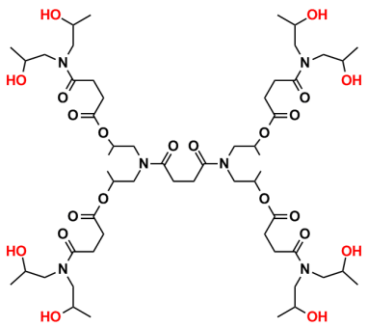

Scheme 2.4: Chemical formulae of the hyperbranched polyester amide, Hybrane S1200.

The hyperbranched polyesters Boltorn and Hybrane are amorphous polymers of low molecular weight. The characteristics of the three generations of Boltorn and the Hybrane S1200 are presented in **Table 2.2**.

Table 2.2: Characteristics of hyperbranched polymers Boltorn H20, H30, H40 and Hybrane S1200. [4]

Hyperbranched polymers	Pseudo-generation	End Groups (-OH)/molecule	Theoretical molecular weight (g/mol)
Boltorn H20	2^{d}	16 (primary)	1750
Boltorn H30	3^{d}	32 (primary)	3608
Boltorn H40	4th	64 (primary)	7323
Hybrane S1200	-	8 (secondary)	1200

2.2 Spherical and Layered Additives

In recent years many different additives have been utilized to improve polymer properties. In particular, polymer nanocomposites are of great scientific and industrial interest due to the unique properties obtained by increasing the interfacial interactions while mixing materials in the nanoscale. The synthesis of new classes of polymers and their combination with different classes of additives is limitless. The additives utilized in the present study are silica nanoparticles, SiO_2, hydrophilic multilayer sodium montmorillonite, Na^+-MMT, and graphite oxide, GO.

SiO_2

Nanoparticles have all dimensions that measure 100 nanometers or less. In nanotechnology, silica-based nanoparticles have a dominant role because of their fundamental characteristics, such as size (generally from 5 to 1000 nm), unique optical properties, high specific surface area, low density, adsorption capacity, capacity for encapsulation, biocompatibility and low toxicity. These features lead to applications in which silica nanoparticles are being widely utilized as an inert solid supporting or entrapping different matrices. [5]

In this work, commercial silica nanoparticles of radius ~7nm were utilized, supplied by Aldrich and noted as Ludox LS. Their surface consists of -OH groups, as shown in **Scheme 2.5**, so that they can interact favorably with hydrophilic polymers.

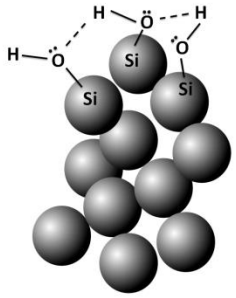

Scheme 2.5: Silica nanoparticles, SiO_2.

The size of the nanoparticles as well as the absence of any aggregation was verified utilizing DLS and TEM in a previous work of our group. [6] **Figure 2.1** shows a TEM image of the nanoparticles to confirm their size.

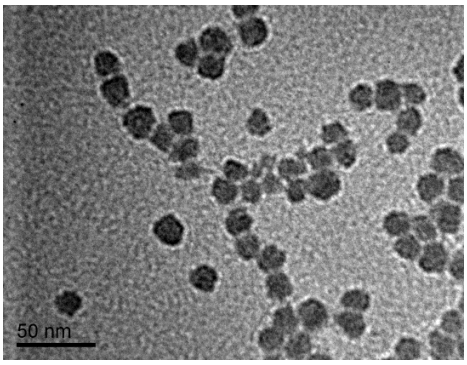

Figure 2.1: TEM image of silica nanoparticles.

Na^+-MMT

Montmorillonite is a 2:1 phyllosilicate mineral, member of the smectite group (two tetrahedral to one octahedral layer). The chemical structure of montmorillonite clays is illustrated in **Scheme 2.6**, showing its sheet structure consisting of layers containing the tetrahedral silicate layer and the octahedral alumina layer. The tetrahedral silicate layer consists of SiO_4 groups linked together to form a hexagonal network of repeating units of composition Si_4O_{10}. The alumina layer consists of two sheets of closely packed oxygens or hydroxyls, between which octahedrally coordinated aluminum atoms are imbedded in such a position that they are equidistant from six oxygens or hydroxyls. The two tetrahedral layers sandwich the octahedral layer, sharing their apex oxygens with the latter. These three layers form one clay sheet that has average lateral dimension around 1 µm and a thickness of 0.96 nm.

The cation exchange capacity of montmorillonite is due to an isomorphous substitution of Mg^{2+} for Al^{3+} in the central alumina plane. The substitution of lower valence cations leaves the

nearby oxygen atoms with a net negative charge that can attract cations. In its natural state Na^+ cation resides on the MMT clay surface. The chemical formula of the montmorillonite clay is $Na_{1/3}(Al_{5/3}\ Mg_{1/3})\ Si_4\ O_{10}\ (OH)_2$. The individual crystals of montmorillonite clay are not tightly bound hence the cations, water or polar polymers can intervene, causing the clay to swell. [7], [8]

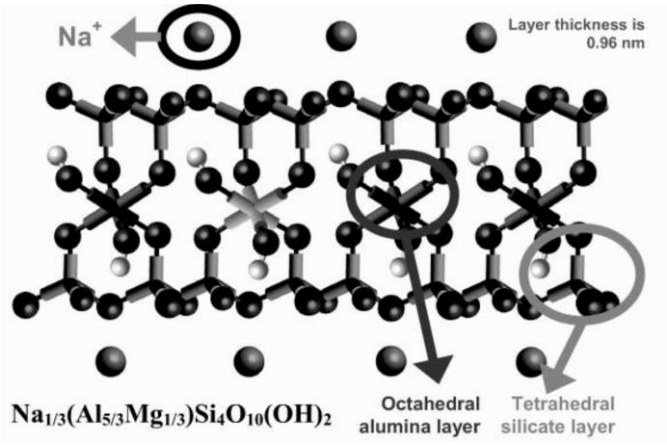

Scheme 2.6: Structure of the natural sodium montmorillonite, Na^+-MMT.

The hydrophilic multilayer sodium montmorillonite, Na^+-MMT, Cloisite Na^+, utilized in the current work, was supplied by Southern Clay. [9] The natural sodium montmorillonite is hydrophilic due to the hydrated cations that exist within its galleries and exhibits a cation exchange capacity, CEC, of 92.6 mmol/100g. Its layered structure is shown in **Figure 2.2** by TEM.

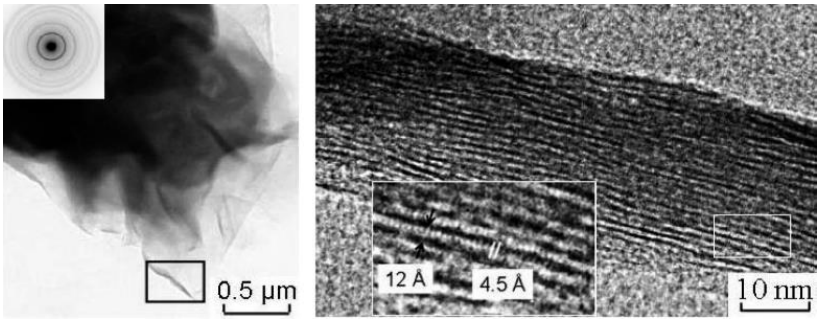

Figure 2.2: TEM image of sodium montmorillonite. [10]

Graphite Oxide

Graphite oxide can be obtained following the oxidation of graphite. The bulk form of graphite oxide is a lamellar paper-like solid material consisting of graphene oxide sheets.

Graphene oxide is derived from the parent two-dimensional graphene backbone by introducing several oxygen functionalities, as shown in **Scheme 2.7**. The oxygen atoms are

covalently bonded to carbon atoms, converting them from the sp^2 -hybridized state in the parent graphene into the sp^3 -hybridized state. In a typical graphene oxide, the number of carbon atoms bonded to oxygen exceeds the number of intact sp^2 -hybridized carbon atoms. This makes graphite oxide very different from the parent graphite. On the one hand, these oxygen functionalities can be considered as defects introduced into the otherwise ideal graphene plane. These defects convert electrically conductive graphite into an insulator. On the other hand, the oxygen functionalities provide graphite oxide with many unique properties. One of these properties is hydrophilicity, i.e. the ability to be dispersed in water and be mixed with polar polymers.

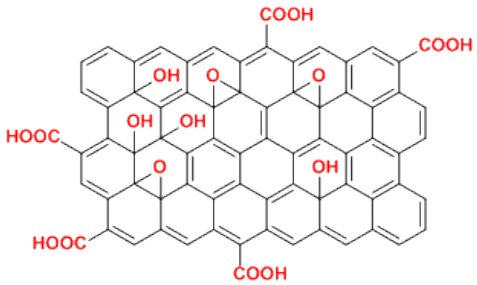

Scheme 2.7: Structure of the Graphite Oxide layer.

The oxygen functionalities decorate the carbon grid from both sides but do not fully cover it. The C/O atomic ratio varies to some extent, and for sufficiently oxidized graphite oxide samples it is approximately 2 : 1. For this reason the graphene oxide flakes are considered to be one atomic layer thick, where the carbon layer is alternated with one layer of oxygen atoms, in the solid graphite oxide.

Graphite oxide has a loosely ordered structure with a repeat distance of 6–9 Å between the constituent graphene oxide layers, depending on the amount of adsorbed water. Despite a weak interaction between the flakes, upon dispersion in water, the graphene oxide flakes easily separate from each other to form a colloidal suspension of single-layer GO sheets. To some extent, the nature of the functional groups of a graphene oxide flake suspended in an aqueous solution is different from that of the same flake placed on a solid substrate, or that sandwiched between neighbors in the form of bulk graphite oxide. This is one of the reasons why the fine chemical structure of graphene oxide is still not fully understood. [11]

Graphite oxide of the present work was purchased by ACS and was produced by Hummer's method. Its edge is ~0.5-5 μm and its thickness 1-3nm according to the supplier. [12] SEM images of the GO show its layered structure in **Figure 2.3**.

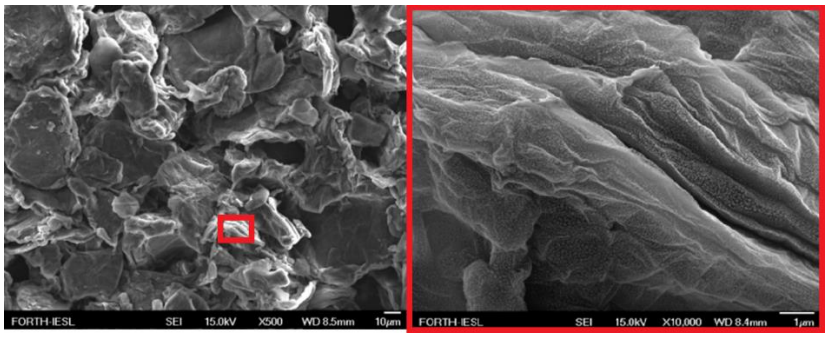

Figure 2.3: SEM images of Graphite oxide.

2.3 Experimental Techniques

The techniques utilized in the current study are presented below. The structure of the bulk polymers, the additives and the nanocomposites was investigated by X-ray diffraction (XRD) while the thermal properties by differential scanning calorimetry (DSC) and thermogravimetric analysis (TGA). Finally polymer dynamics in the bulk and under confinement was studied by broadband dielectric spectroscopy (BDS).

X-Ray diffraction

The crystalline structure of solid materials can be studied at the atomic level by X-rays, since their wavelength is ~10^{-2}-10^{2} Å, which is similar to the distances between atoms and molecules in the organization/ordering of matter. Each crystalline material has its unique characteristic X-ray pattern due to its periodic structure. Except the material identification, X-ray crystallography may be used to determine its structure, i.e. which are the interatomic distances and angles in the crystalline state. Thus X-ray diffraction can be used to determine the size and the shape of the unit cell for any compound.

X-rays are produced by bombarding a metal target (usually Cu or Mo) with a beam of electrons emitted from a hot filament. The incident beam will ionize electrons from the K-shell (1s) of the target atom and X-rays are emitted.

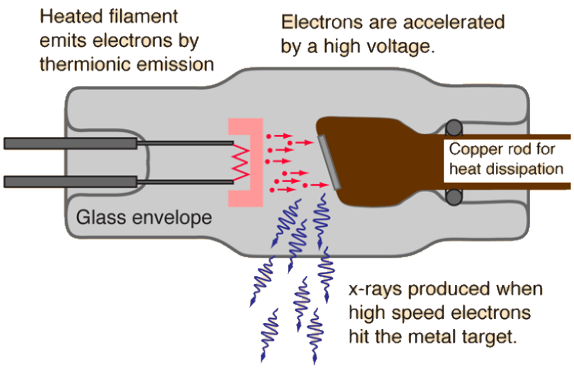

Figure 2.4: X-ray production.

The interaction of the incident rays with the sample causes constructive or destructive interference. Bragg diffraction occurs when radiation is scattered in a specular way by the atoms of a crystalline system, and undergoes constructive interference. For a crystalline solid, the waves are scattered from lattice planes separated by the interplanar distance d. When the scattered waves interfere constructively, they remain in phase since the path length of each wave is equal to an integer multiple of the wavelength. The path difference between two waves undergoing interference is given by 2dsinθ, where θ is the scattering angle (**Figure 2.5**). This leads to Bragg's law, which describes the condition on θ for the maximum constructive interference:

$$2d \sin\theta = n\lambda \qquad 2.1$$

where n is a positive integer and λ is the wavelength of incident wave.

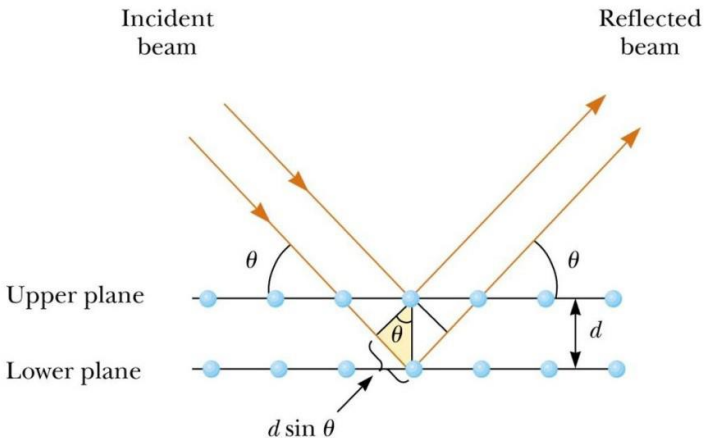

Figure 2.5: Bragg diffraction.

Bragg's law relates the wavelength of electromagnetic radiation to the diffraction angle and the lattice spacing in a crystalline sample. The diffracted X-rays are then detected, processed and counted. By scanning the sample through a range of 2θ angles, all possible diffraction

directions of the lattice should be attained due to the random orientation of the powder material. Conversion of the diffraction peaks to d-spacings allows identification of the crystalline material because each one has a set of unique crystallographic characteristics. Typically, this is achieved by comparison of d-spacings with standard reference patterns. [13]

In the current work the structure of the neat and the nanohybrid materials was examined by X-ray diffraction. A Rigaku RINT 2000 X-ray diffractometer was utilized; the X-rays are produced by a 12 kW rotating anode generator with a Cu anode equipped with a secondary pyrolytic graphite monochromator. The Cu Kα radiation was used with wavelength $\lambda = \lambda_{CuK\alpha}$ = 1.54 Å. All measurements were performed for 2θ from 1.5° to 30° with step of 0.025°.

Differential Scanning Calorimetry

Differential Scanning Calorimetry, DSC, is a technique widely utilized to determine the specific heat during thermal transitions of materials (melting, crystallization and glass transition). It measures the heat flow of the sample in order to keep the same temperature as a reference sample. By DSC all the thermal transitions that take place as a result of chemical or physical changes can be monitored while the sample is cooled or heated.

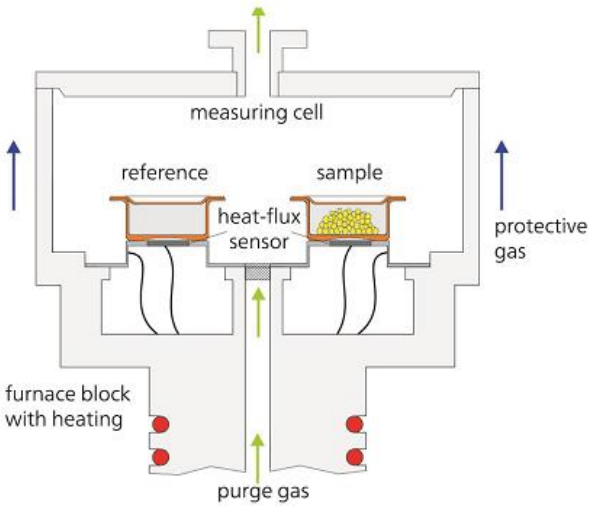

Figure 2.6: DSC basic setup.

The setup, shown in **Figure 2.6**, consists of two individually heated pans connected to heat sensors. One pan is the reference pan and the other is the sample holder. The operating principle is based on maintaining the same temperature in both samples. When the material undergoes a transition, heat is either emitted or absorbed (depending on whether the transition is exothermic or endothermic) leading to a change in the temperature of the sample. Any temperature change results in the resistor to channel more or less heat in order

to maintain the sample temperature similar to that of the reference. This heat difference is equal to the heat of fusion ΔH needed for the sample to make this transition.

DSC is widely used in polymer science in order to investigate the materials thermal properties. The first information that can be extracted is the heat capacity of the sample (C_p). In a DSC diagram the glass transition of a polymer can be observed due to a difference in the heat capacity, as shown in **Figure 2.7**. The glass transition temperature (T_g) is characteristic of amorphous polymers. Below the T_g, an amorphous material is in the glassy state, while above T_g it is an elastomer.

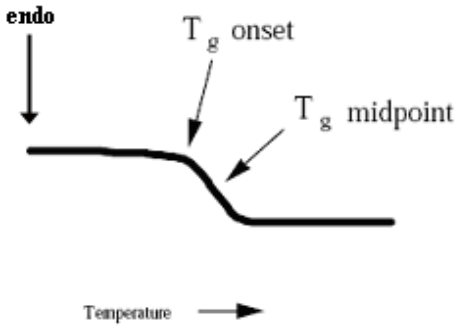

Figure 2.7: Glass transition in a DSC diagram.

Many polymers are not purely amorphous but semi-crystalline. This means that an amorphous and a crystalline phase coexist in the sample. The crystalline phase melts and crystallizes. Above a certain temperature, T_m, the polymer chains absorb energy, increase their mobility and move freely. The melting is an endothermic transition that can be observed in a DSC curve, as presented in **Figure 2.8**a.

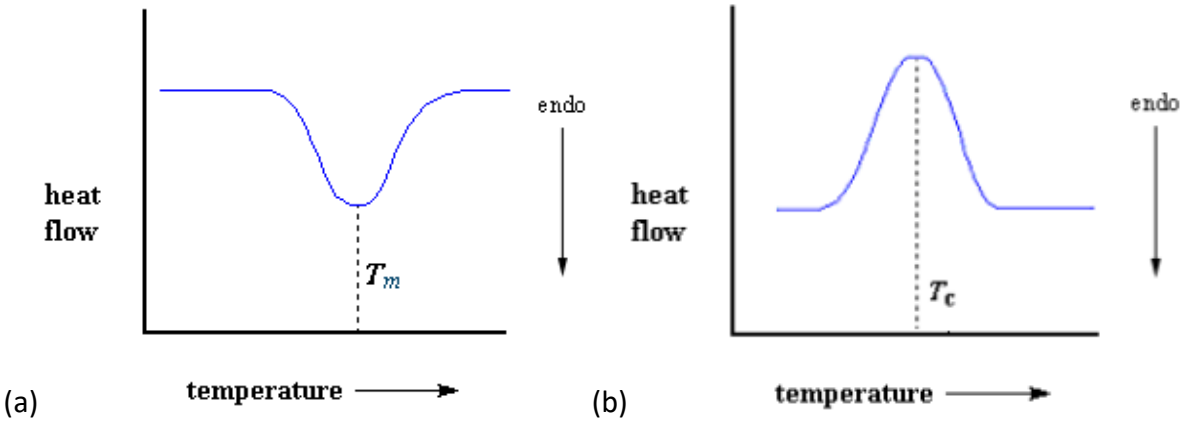

Figure 2.8: Melting curve (a) and crystallization curve (b) in a DSC diagram.

On the other hand, under a certain temperature, T_c, the polymer chains are organized into an ordered state forming crystals and emitting energy by an exothermic transition. The crystallization curve as seen by the DSC is shown in **Figure 2.8**b. [14]–[16]

The DSC measurements of the current work were performed in a Polymer Labs differential scanning calorimeter under a constant nitrogen gas flow and with heating/cooling rate of 10°C/min (except if a different rate is mentioned).

Thermogravimetric Analysis

Thermogravimetric Analysis is a technique in which the mass of a substance is monitored as a function of temperature or time as the sample specimen is subjected to a controlled temperature program in a controlled atmosphere. TGA can provide information about physical phenomena, such as second-order phase transitions, including vaporization, sublimation, absorption, adsorption, and desorption. Likewise, it gives information about chemical phenomena including dehydration, decomposition, and solid-gas reactions (e.g., oxidation or reduction). TGA is commonly used to determine selected characteristics of materials that exhibit either mass loss or gain due to decomposition, oxidation, or loss of volatiles (such as moisture).

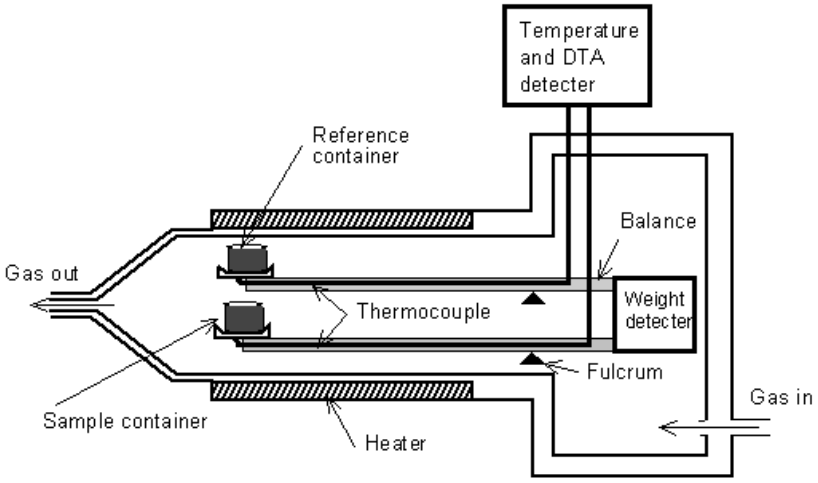

Figure 2.9: Typical TGA experimental setup.

Figure 2.9 shows a typical TGA experimental setup. It consists of a sample and a reference pan supported by a precision balance. The pans reside in a furnace and are heated or cooled during the experiment. The weight detector monitors the mass loss of the sample during the experiment. A sample purge gas, which may be inert or reactive flows over the sample and controls the environment. [16]

In the present work TGA measurements were performed by an SDT600 TGA/DTA apparatus (TA Instruments), to record the decomposition steps and determine the respective decomposition temperatures for the bulk polymers and for all nanohybrids. Heating scans were performed starting from room temperature to 600 °C at a heating rate of 10 °C/min, under constant flow of argon.

Broadband Dielectric Spectroscopy

Dielectric spectroscopy is a very important technique to probe molecular dynamics and to investigate the dielectric properties of materials. Its main advantage over other techniques is the broadband in frequency that covers a range between 10^{-6} to 10^{12} Hz. When an electric field is applied on a parallel plate capacitor containing a dielectric, the atomic and molecular charges in the dielectric are displaced from their equilibrium positions and the material is said to be polarized. There are several different mechanisms that can induce polarization in a dielectric upon the application of a field: 1) polarization due to the propagation of mobile charge carriers 2) separation of charges at interfaces and 3) polarization due to orientation of permanent molecular dipoles.

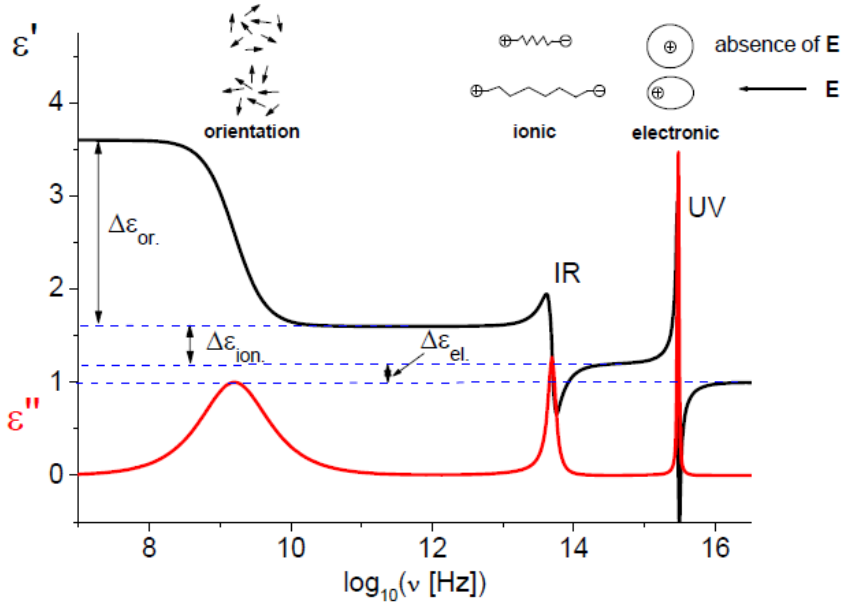

Figure 2.10: Polarization mechanism. Real and imaginary part of the complex dielectric permittivity as a function of frequency.

Migration of charges results in the measured conductivity, which encompasses contributions from both extrinsic (e.g. ionic impurities) and intrinsic (e.g. proton transfers along hydrogen bonds) migrating charges. From the interplay between the extrinsic and intrinsic contributions the measured value of conductivity can display different trends.

The separation of charges can take place at inner dielectric boundary layers (Maxwell-Wagner-Sillars polarization), on a mesoscopic scale and/or at the external electrodes containing the sample (electrode polarization) on a macroscopic scale. Its contribution to dielectric loss can be orders of magnitude larger than the dielectric response due to molecular fluctuations.

The most important polarization mechanism in polymer dynamics is dipole orientation. If a material contains polar molecules, they will be in random orientations when no electric field is applied. When an electric field is applied, the material will be polarized via the orientation of the dipole moments of polar molecules, as shown in **Figure 2.11**, and the effective electric field between the plates will decrease. This orientation (polarization) of permanent dipoles involves cooperative motions of molecular segments in a viscous medium with time scales measurable by dielectric spectroscopy. The time dependent loss of the orientation of the dipoles upon removal of the electric field is called dipole relaxation.

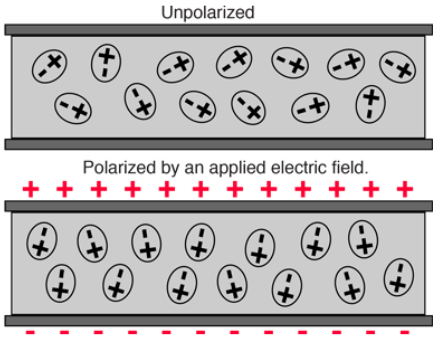

Figure 2.11: Dipolar orientation of materials before and after the application of an electric field.

Dipole relaxation in polymers can be attributed to many different chain motions: the fast local motions, rotations or fluctuations of small dipoles, the cooperative motion of chain segments at longer times, related to the glass transition, and the overall motion of the polymer chain related to the viscoelastic properties of a solution or a melt.

The physical quantity measured by BDS is the complex dielectric permittivity, ε^*, which determines the ability of a material to be polarized as a response to an applied field. The complex dielectric permittivity is measured over frequency at each temperature.

$$\varepsilon^*(\omega) = \varepsilon'(\omega) + i\varepsilon''(\omega) \qquad 2.2$$

where ε' is the real part, ε'' is the imaginary part (or dielectric loss part), $i = \sqrt{-1}$ and $\omega = 2\pi f$ is the angular frequency. Relaxation processes are characterized by a peak in the imaginary

part ε'' and a step-like decrease of the real part ε' of the complex dielectric function with increasing frequency.

The essential quantities that characterize a dielectric relaxation process can be extracted from that behavior. The frequency of maximal loss f_0 is related to a characteristic relaxation time, τ_0, of the dipole motion. From the shape of the loss peak, the distribution of relaxation times can be deduced. The dielectric strength Δε of a relaxation process can be determined either from the area under the loss peak ε'' (ω) or from the step in ε' (ω) by $\Delta\varepsilon = \varepsilon_s - \varepsilon_\infty$ where the ε_∞ is the permittivity at the high frequency limit and the ε_s is the static, low frequency permittivity. [17]

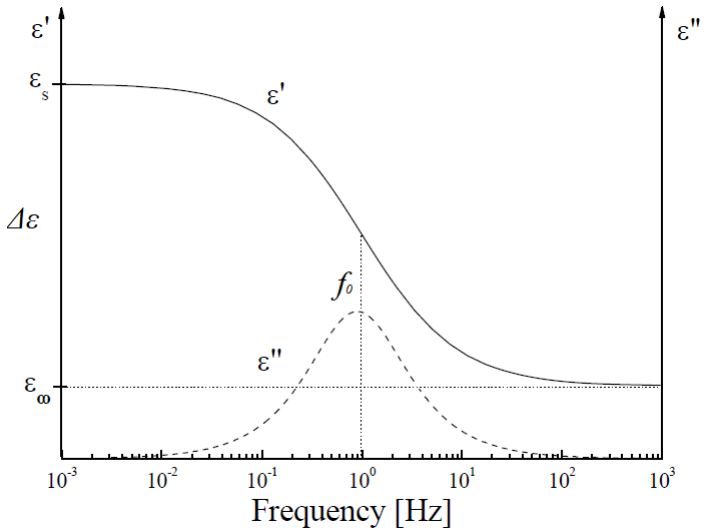

Figure 2.12: Principal behavior of the real and the imaginary part of the dielectric function in the frequency domain.

In the present work, the spectra shown in the following chapters, correspond to the imaginary part of the complex dielectric permittivity, where the relaxation processes appear as a peak.

Dielectric relaxation processes were analyzed through both the real and the imaginary part, by a superposition of the empirical Havriliak - Negami (HN) model functions:

$$\varepsilon^*_{HN}(\omega) = \varepsilon_\infty + \frac{\Delta\varepsilon}{(1+(i\omega\tau_{HN})^\alpha)^\beta} \qquad 2.3$$

where τ_{HN} is the characteristic relaxation time, αand β are the shape parameters describing the symmetric and asymmetric broadening of the complex dielectric function, for which 0 < α, αβ ≤ 1 holds. [18]

The dynamic measurements were performed utilizing a dielectric spectrometer Alpha Analyzer from Novocontrol, in the frequency interval 10^{-2} to 10^{7} Hz. A film (hundreds of micrometers) of the material under study was placed in a stainless steel parallel plate capacitor.

In the case of the bulk polymers, the samples were heated ~10 °C above the melting point or ~50 °C above the T_g and pressed between two plated electrodes with 30 mm diameter. Fused silica fibers with a diameter of 100 μm were used as spacers. The samples were annealed at 130 °C in vacuum for 24 h to remove traces of water.

For the nanocomposites, the powder was pressed to form disks 12 mm in diameter and 0.3−0.6 mm in thickness. In the case of the nanohybrids the pellets were annealed at 120 °C in vacuum for 24 h and adhered between indium foils to improve the electrical contact with the electrodes.

Dielectric spectra of the films were measured isothermally in the range between -140 °C to 150 °C. The temperature was controlled through a heated flow of nitrogen gas, by a Quatro Cryosystem. During measurements, the samples were kept in a pure nitrogen atmosphere.

2.4 References

[1] "Bio-Based Polyurethanes That Work," *GC Innovation America*, 2018. [Online]. Available: https://www.gcinnovationamerica.com/wp-content/uploads/2018/10/Polyols-that-work-2018.pdf.

[2] I. Tanis, K. Karatasos, A. N. Assimopoulou, and V. P. Papageorgiou, "Modeling of hyperbranched polyesters as hosts for the multifunctional bioactive agent shikonin," *Phys. Chem. Chem. Phys.*, vol. 13, no. 22, pp. 10808–10817, 2011.

[3] I. Tanis, D. Tragoudaras, K. Karatasos, and S. H. Anastasiadis, "Molecular dynamics simulations of a hyperbranched poly (ester amide): statics, dynamics, and hydrogen bonding," *J. Phys. Chem. B*, vol. 113, no. 16, pp. 5356–5368, 2009.

[4] "Boltorn - Hybrane," *Polymer Factory*. [Online]. Available: https://www.polymerfactory.com/hyperbranchedpolymers.

[5] A. Bitar, N. N. M. Ahmad, H. Fessi, and A. Elaissari, "Silica-based nanoparticles for biomedical applications," *Drug Discov Today*, vol. 17, no. 19–20, pp. 1147–54, 2012.

[6] H. Papananou, "Polymer structure and dynamics under confinement," PhD Thesis, University of Crete, 2017.

[7] J. H. Koo, *Polymer Nanocomposites Processing, Characterization and Applications*. McGraw-Hill, 2006.

[8] Y. C. Ke and P. Stroeve, *Polymer-Layered Silicate and Silica Nanocomposites*. Elsevier B.V., 2005.

[9] "Cloisite Na+," *Southern Clay Products, Inc*. [Online]. Available: https://gato-docs.its.txstate.edu/jcr:5aba1cec-2a4f-476a-9001-4a95a225fd27/Nanoclay+-+Cloisite+Na%252B.pdf.

[10] V. V. Krupskaya *et al.*, "Experimental Study of Montmorillonite Structure and Transformation of its Properties under the Treatment of Inorganic Acid Solutions," *Minerals*, vol. 7, no. 49, pp. 1–11, 2017.

[11] A. M. Dimiev & S. Eigler, *Graphene Oxide Fundamentals and Applications*. Wiley, 2017.

[12] "Graphite Oxide," *ACS Material*. [Online]. Available: https://www.acsmaterial.com/graphite-oxide.html.

[13] R. J. Roe, *Methods of X-ray and Neutron Scattering in Polymer Science*. Oxford University Press, 2000.

[14] G. Wim, *Characterization of polymers by Thermal Analysis*. 2001.

[15] P. Gallagher, *Handbook of Thermal Analysis and Calorimetry*. 2002.

[16] R. Chartoff and A. Sircar, "Thermal Analysis of Polymers," *Encyclopedia of Polymer Science and technology*. John Wiley & Sons, 2005.

[17] F. Kremer and A. Schönhals, *Broadband Dielectric Spectroscopy*. Berlin: Springer, 2003.

[18] S. Havriliak and S. Negami, "A Complex Plane Representation of Dielectric and Mechanical Relaxation Processes in Some Polymers," *Polymer (Guildf).*, vol. 8, pp. 161–210, 1967.

3 Dynamics and Characterization of the Bulk Polymers

In the present chapter the structure, thermal properties and dynamic behavior of the three linear polyesters (EG-110, DG-110 and HD-110) and the hyperbranched polymers (Boltorn H20, H30, H40 and Hybrane) are discussed. For the linear polymers the different repeating unit in the polymer chain results in different chain conformations so that the final polymer morphology can be either semi-crystalline or amorphous. For the hyperbranched polyesters of the three different generations the effect of branching was observed in their thermal properties resulting in different glass transition temperatures and in the subsequent polymer dynamics. Finally another hyperbranched polyester with an additional amide group in its repeating unit was studied revealing both similarities and differences with the Boltorn polymers.

3.1 Structural and Thermal Characterization of Biobased Linear Polyesters

EG-110

The structure of the bulk poly (ethylene succinate), EG-110, was studied by X-ray diffraction, (XRD) that showed that EG-110 is a semi-crystalline polymer.

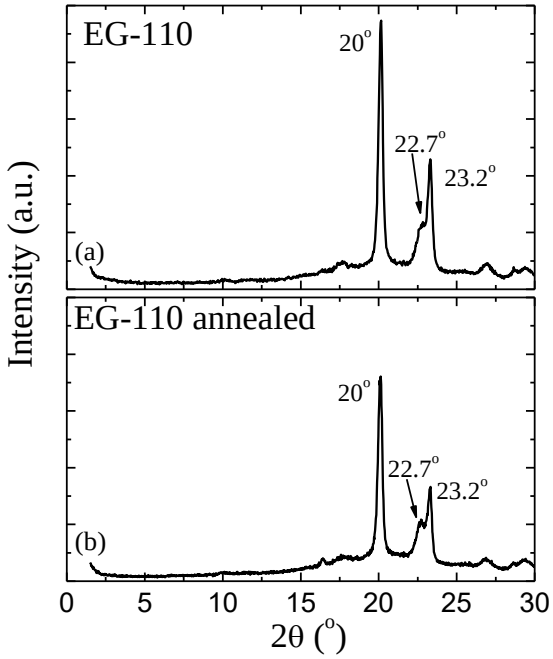

Figure 3.1: X-ray diffractogram of EG-110 (a) and EG-110 after annealing (b).

In Figure 3.1.a its crystalline peaks are observed with a sharp peak at 2θ=20° and a doublet at 2θ=22.7° and 23.2°. These peaks are in good agreement with what is reported in the literature for poly (ethylene succinate) and are assigned to the (021), (121) and (200) planes of its alpha-form, respectively. [1] A second measurement obtained after the annealing of the sample at 200°C for 12 hours, in order to remove any humidity and attain the equilibrium structure, gave the exact same results, as shown in Figure 3.1.b.

The thermal stability of EG-110 was investigated by thermogravimetric analysis (TGA) performed with a heating rate of 10 °C/min. The temperature dependence of the mass loss is shown in Figure 3.2, and the first derivative is calculated (inset) in order to identify the different decomposition temperatures of the sample. From the thermogravimetric curves, it can be seen that EG-110 exhibits a relatively good thermal stability since no significant weight loss occurs until 230 °C.

More specifically, two degradation steps are evident in Figure 3.2; the first is observed between 230 °C and 300 °C with 6 wt % loss of the total mass whereas the second, which is the main mass loss, (corresponding to ~90 wt % of the total mass) is observed above 330 °C. Such an initial low weight loss step was reported before for poly (ethylene succinate) and poly (butylene succinate) and was attributed to the volatilization of small molecules; it was found that succinic acid degrades at temperatures close to 200 °C while ethylene glycol and butylene glycol evaporate at slightly higher temperatures, nevertheless lower than 300 °C. [2]

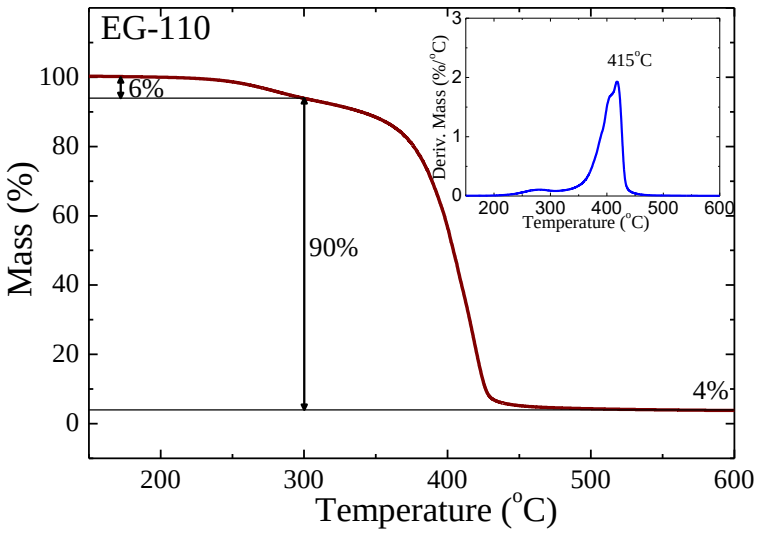

Figure 3.2: Thermal decomposition of EG-110 as measured by TGA. The first derivative is shown in the inset.

At higher temperatures, EG-110 decomposes sharply and loses almost the whole of its weight, (~ 90wt %) until 470 °C whereas a 4 wt % residue remains even after heating of the sample up to 600 °C. The peak of the first derivative of the curve shows the most probable decomposition temperature to be T_d = 415 °C. For polyesters, a random cleavage of the ester bond takes place due to the -CH hydrogen transfer; carboxylic end groups and vinyl groups are formed during this chain scission. [3]

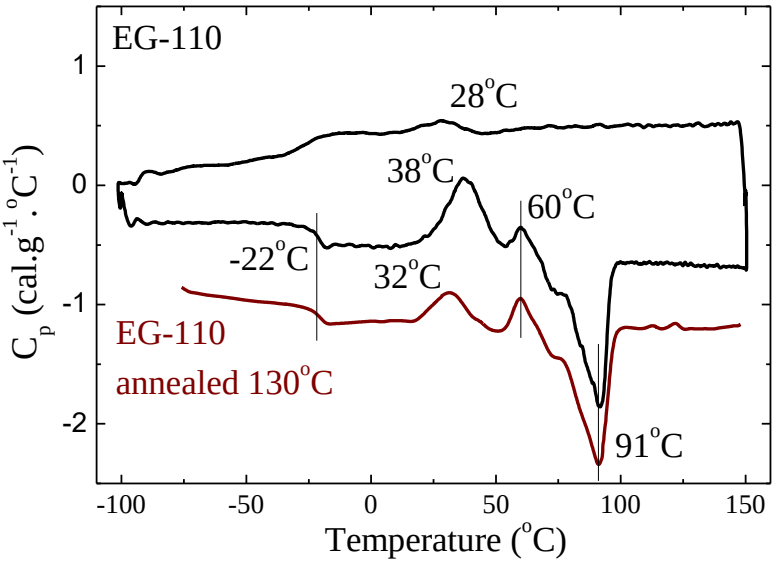

Figure 3.3: DSC measurement expressed as specific heat, C_p, of pure EG-110 before and after the thermal annealing.

The thermal properties of EG-110 are studied by differential scanning calorimetry, DSC, and a full cycle is shown in **Figure 3.3**. This includes the cooling from the melt that followed a first melting from room temperature to 150 °C to erase any previous thermal history (not shown) and the subsequent heating; all runs were performed with a cooling / heating rate of 10 °C/min. A very weak crystallization exotherm at T_c = 28 °C, together with the glass transition at lower temperatures, can be observed during the cooling from the melt. During heating, the glass transition is observed at T_g = -22 °C, whereas, above T_g, a main exothermic peak is observed at T_{c1} = 38 °C and a second weaker one at T_{c2} = 60 °C. Finally, the melting of the material is observed at T_m = 91 °C. After the thermal annealing of the bulk polymer, the thermal transitions are observed at the same temperatures except the cold crystallization which is shifted at lower temperature, T_{c1} = 32 °C. It is noted that the measurement error of the temperatures is ±1°C. The ΔC_p of the glass transition is 0.32 cal/g, whereas, the degree of crystallinity cannot be determined due to the coexistence of two transitions, the crystallization and the melting.

In order to further understand this behavior, the bulk polymer was cooled with a lower rate of 2 °C/min and afterwards heated with 10 °C/min. As shown in **Figure 3.4** the polymer crystallizes during cooling and no cold crystallization is observed. Furthermore, the crystallization appears at a higher temperature, T_c = 43 °C, as expected due to the lower cooling rate. The melting is slightly higher, T_m = 92 °C and seems to coexist with crystallization as above.

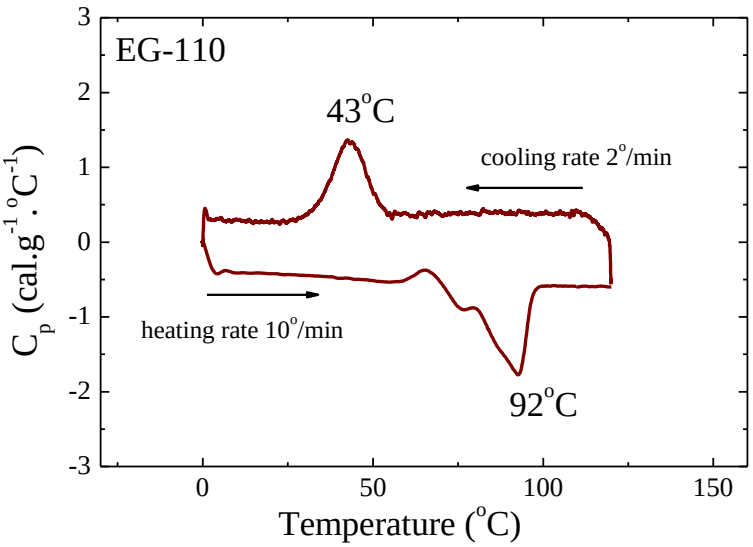

Figure 3.4: DSC measurement expressed as specific heat, C_p, of EG-110 with cooling rate 2°C/min.

This thermal behavior, although not trivial, has been observed before in both isothermal and non-isothermal measurements of EG-110 and its dependence on the cooling rate and on the crystallization temperature was investigated. [4] The two most probable explanations for the behavior involve a dual morphology mechanism and the existence of crystals with different thermal stability [5], [6] on one hand, and a re-organization mechanism of a melting, recrystallization and remelting processes that suggests that the initial crystallization creates crystals of lower degree of perfection or thinner lamellae that melt and recrystallize during heating to produce more perfect crystals on the other hand. [7], [8] Alternatively, the possibility that there are two kinds of polymer chains with different mobility in poly (ethylene succinate), namely, polymer chains with high molecular mobility and polymer chains with low molecular mobility was proposed; nevertheless, temperature modulated DSC experiments showed that the smaller crystallization exotherm was due to melt-recrystallization of the originally existing unstable crystals formed through previous crystallization. [9]

DG-110

The bulk poly (diethylene succinate) is amorphous, as shown in the X-ray diffractogram in **Figure 3.5**.a where there is only a broad peak, the amorphous halo around 20° to 21°, and there are no crystalline peaks. The absence of a crystalline structure for the pure polymer does not change after the thermal annealing of the material at 200°C for 12 hours (**Figure 3.5**.b).

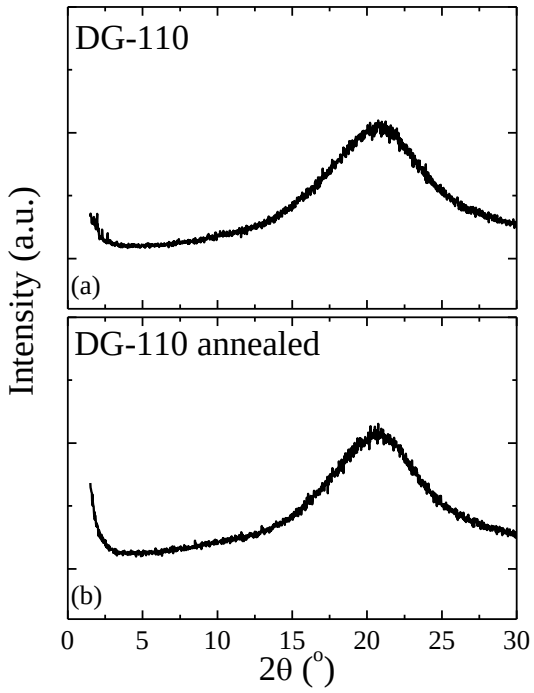

Figure 3.5: X-ray diffractogram of DG-110 (a) and DG-110 after annealing (b).

The thermal stability of DG-110 was investigated by TGA, as shown in **Figure 3.6**, and the first derivative was calculated (inset). The polymer is thermally stable up to 250 °C, where the mass loss is only 1.5 wt%. Its thermal decomposition is observed as a single step above 250 °C, with 100 wt % loss of the total mass. In the first derivative of mass curve, a shoulder can be seen on the main degradation peak due to the volatiles as mentioned in the case of EG-110. The decomposition temperature for the DG-110 is determined to be T_d = 420 °C.

The thermal properties of DG-110 are studied by DSC. The amorphous structure indicated by XRD is confirmed by the DSC measurement, shown in **Figure 3.7**. For the pure polymer before the thermal annealing the glass transition temperature is determined at -36°C and the ΔC_p of the glass transition is 0.20 cal/g, whereas after the annealing the T_g increases at -26°C and the ΔC_p is 0.32 cal/g.

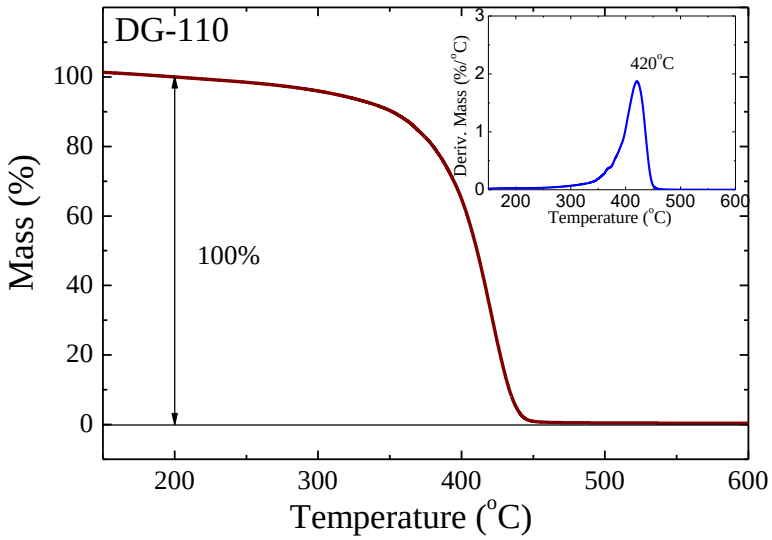

Figure 3.6: DG-110 thermal decomposition as measured by TGA. The first derivative is shown in the inset.

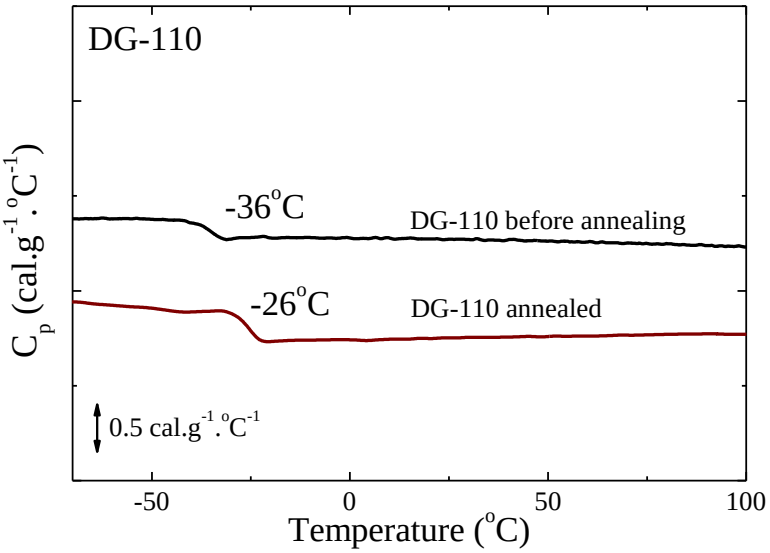

Figure 3.7: DSC measurement expressed as specific heat, C_p, of pure DG-110 before (black line) and after (wine line) the thermal annealing.

HD-110

The structure of the bulk poly (1,6-hexylene succinate) was investigated by XRD and the corresponding measurement is shown in **Figure 3.8**.a and b for the polymer before and after the annealing respectively. Two sharp crystalline peaks are observed at 2θ = 21.4 ° and 2θ = 24.4 °. There is also a wide halo around 20 °. The peaks correspond to 0.41nm and 0.36nm respectively and are assigned to the (220) and (040) planes of its alpha-form. [10] The same results are obtained after the annealing at 200°C for 12 hours.

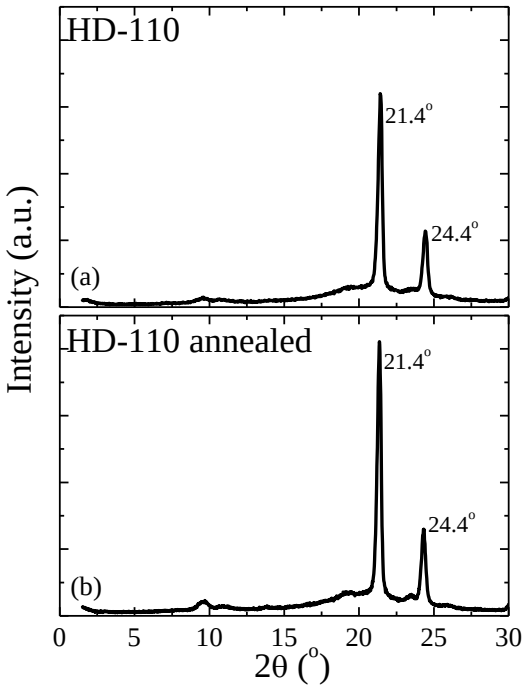

Figure 3.8: X-ray diffractogram of HD-110 (a) and HD-110 after annealing (b).

In **Figure 3.9** the thermal stability of HD-110 is shown investigated by TGA; in this case the first derivative was calculated as well, as shown in the inset. The thermal decomposition is a single process with 100 wt % loss of the total mass. The polymer is thermally stable up to 250 °C where the mass loss is 1.5 wt %.

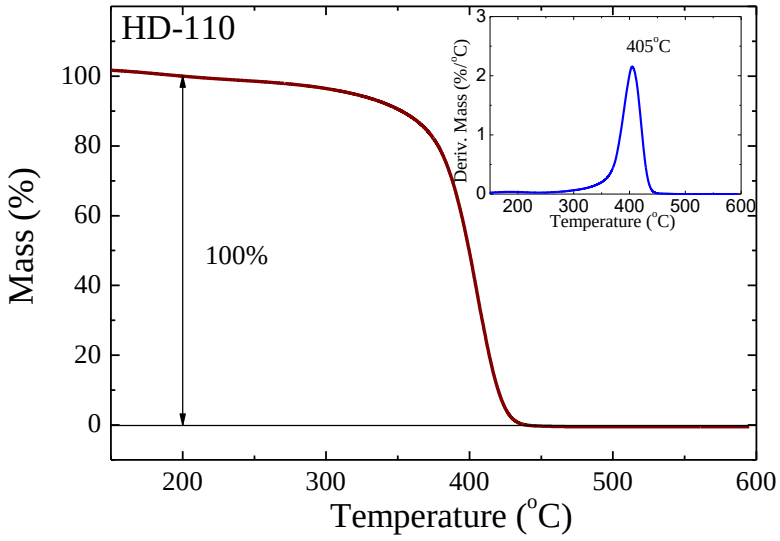

Figure 3.9: HD-110 thermal decomposition as measured by TGA. The first derivative is shown in the inset.

The most probable decomposition temperature at 405 °C reveals a lower degradation temperature for the HD-110 compared to the other two polyesters. As mentioned before, a random cleavage of the ester bond takes place in polyesters due to the -CH hydrogen transfer.

According to the literature, the tendency for chain scission is higher in polyesters which possess monomers with a higher number of methylene groups. [3], [11]

The thermal properties of HD-110 were studied by DSC. The specific heat of the sample during heating and cooling is shown in **Figure 3.10**. During cooling an exothermic peak appears at 18 °C with a small shoulder at high temperatures, whereas, during heating the polymer shows a double melting peak at 43 °C and 49 °C. The glass transition cannot be clearly observed. The double peak can be attributed to different crystallites, of different energy, formed during cooling with 10°C/min. This is a behavior reported in literature for polyesters. [12], [13]

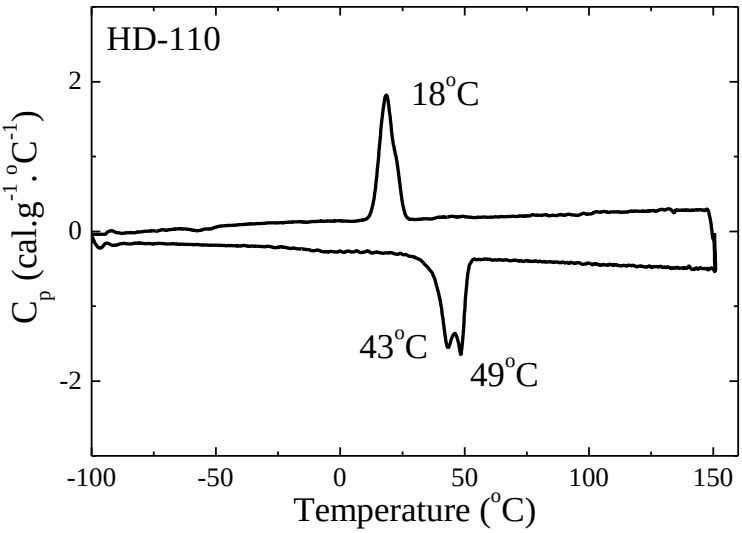

Figure 3.10: DSC measurement expressed as specific heat, C_p, of pure HD-110.

After the thermal annealing of HD-110 (**Figure 3.11**), the melting is observed as a single peak at 51°C with heat of fusion 23.44 cal/g, and the crystallization during the cooling at T_c = 26 °C. Most probably after the annealing and the removal of the water traces in the sample, only one type of crystals is formed. It could be that water molecules benefit a different kind of crystallization in this molecule. The T_g appears as a very broad transition at -45 °C.

In a recent study the crystallization kinetics of poly (1,6-hexthylene succinate), HD-110, was examined by isothermal and non-isothermal measurements from solution, with a constant rate of cooling and quenched. [12] HD-110 appears to exhibit faster crystallization kinetics compared to other polyesters including poly (ethylene succinate), EG-110. [14] The thermal properties of all the linear polymers are summarized in the **Table 3.1**, together with the hyperbranched ones, that will be discussed below.

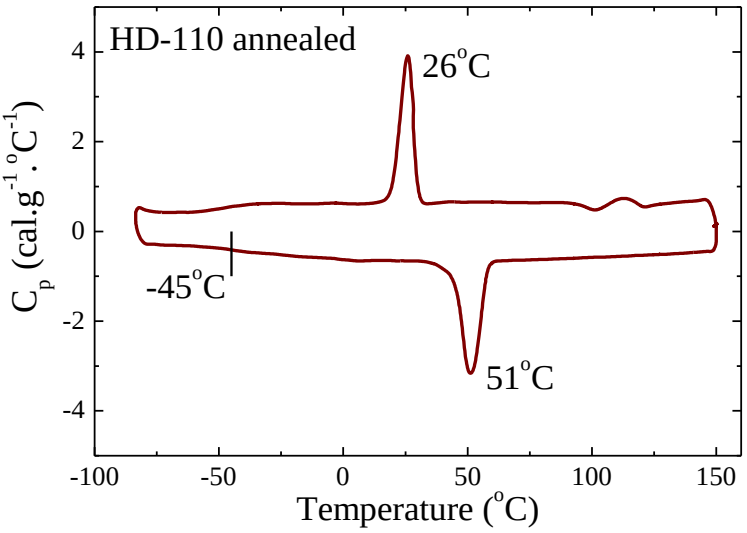

Figure 3.11: DSC measurement expressed as specific heat, C_p, of annealed HD-110.

3.2 Structural and Thermal Characterization of Hyperbranched Polymers

Boltorn

The structure of the three generations of Boltorn H20, H30 and H40 was investigated by X-ray diffraction and the measurements are presented in **Figure 3.12**. All three hyperbranched polyester polyols are amorphous showing only a broad peak with a sharper one at 2θ = 17.3° that corresponds to a distance of ~0.5 nm and indicates a chain packing due to an extensive hydrogen bond network formed mostly between hydroxyl hydrogens and hydroxyl oxygens (OH···OH) and hydroxyl hydrogens and carbonyl oxygens (OH···O=C). [15]–[17]

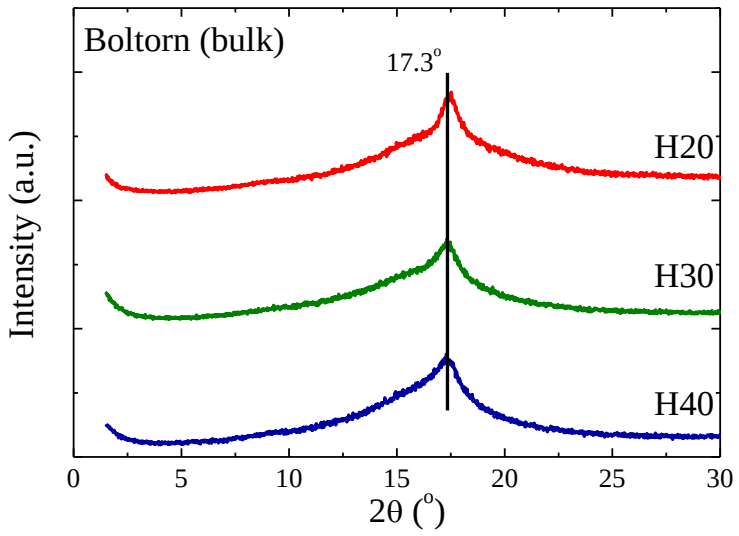

Figure 3.12: X-ray diffractograms of Boltorn H20, H30 and H40.

The thermal stability of the three generations of the Boltorn hyperbranched polyesters were investigated by thermogravimetric analysis, as shown in **Figure 3.13**. The thermal decomposition is observed above 280 °C and results in the complete loss of the mass. The polymers are thermally stable up to 280 °C while their broad decomposition reveal multiple degradation steps. A small step in the first stage of thermal degradation, around 320 °C, is mostly observed for the H40, which could be attributed to water elimination reactions referred in polyols. [18]

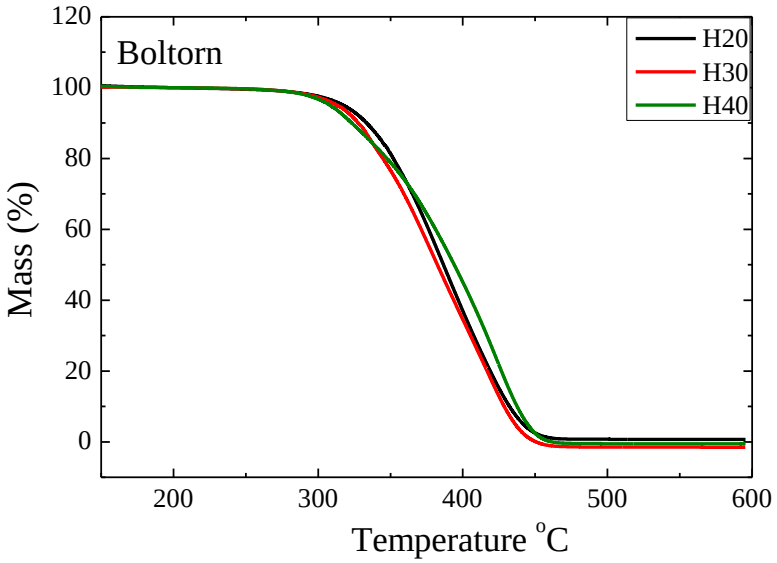

Figure 3.13: TGA measurements of Boltorn H20, H30 and H40

The comparison of the weight loss curves between the three generations shows two main degradation steps with temperatures around 380 °C and 420 °C; the one at lower temperature is mainly obtained for the H20, the H30 exhibits both with similar mass loss, while for the H40 the decomposition at higher temperature is dominant. This complex thermal degradation behavior indicates that through the decomposition mechanism more thermally stable compounds are formed by increasing the generation.

The thermal properties of the neat Boltorn polyester polyols of the three generations were investigated by differential scanning calorimetry. In **Figure 3.14** the DSC thermograms of the annealed H20, H30, and H40 are shown. DSC confirms the amorphous structure of the macromolecules since only one step in the heat capacity is observed and no melting transition is present. The glass transition temperatures of the pure polymers H20, H30 and H40 is obtained at 14°C, 35°C and 46°C respectively.

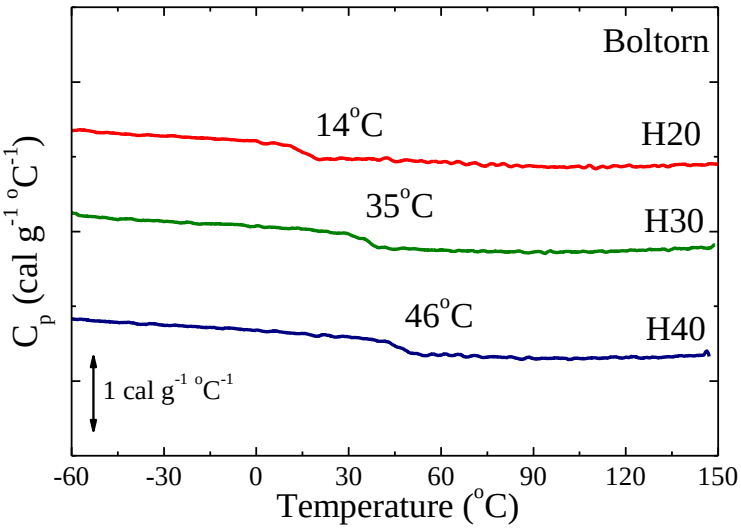

Figure 3.14: DSC measurements of annealed Boltorn H20, H30 and H40 during heating.

A significant dependence of the T_g on the generation is observed as a consequence of the increased molecular weight and the higher degree of branching. Despite the dependence of the T_g on the generation, the heat capacity step at the transition seems to be constant for the three polymers having the value of ΔC_p = 0.11 cal.g^{-1}.°C^{-1}.

Hybrane

The hyperbranched poly (ester amide), Hybrane, is an amorphous polymer, as well, as shown in the X-ray diffractogram, in **Figure 3.15**, showing a weak halo observed and no crystalline peaks. Moreover, in this molecule hydrogen bonds occur between the –OH groups, but no periodicity is observed in the structure of the bulk polymer.

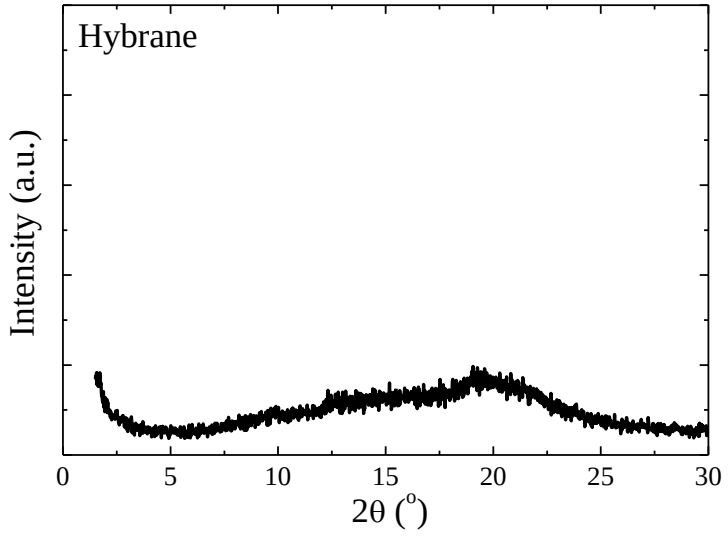

Figure 3.15: X-ray diffractogram of pure Hybrane.

In the case of the hyperbranched poly (ester amide), due to the different functional groups, multiple decomposition steps are revealed in the thermogravimetric analysis measurement, shown in **Figure 3.16**; the first derivative calculated is shown in the inset. The thermal decomposition occurs above 245 °C with 99 wt % loss of the total mass at 600 °C. The polymer mainly degrades at 320 °C, whereas at 435 °C a second degradation is evident.

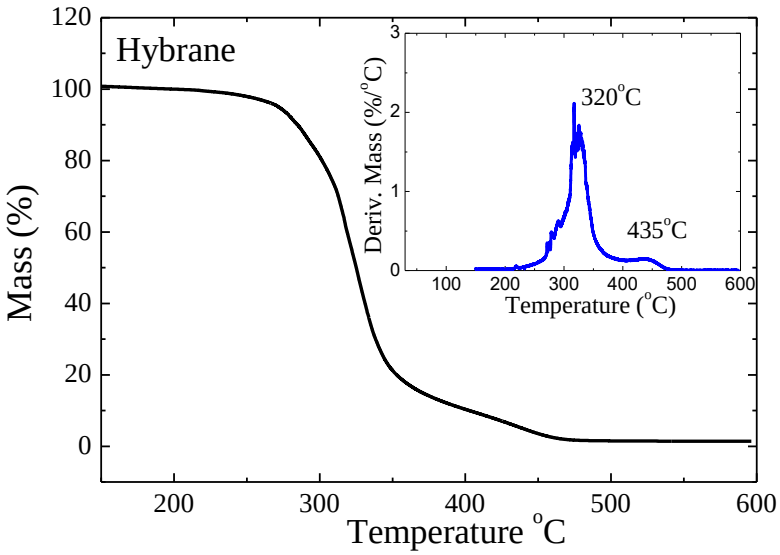

Figure 3.16: TGA measurements of Hybrane. The first derivative is shown in the inset.

The first decomposition step shown at 320 °C, at a lower temperature than the respective of the main step in Boltorn polymers, could be attributed to a different decomposition mechanism involving the amide group. [19] The predominant volatile pyrolysis products of polyamides are reported to be cyclic oligomers and products with nitrile end-groups. Two degradation processes are involved, an intramolecular back-biting process and a hydrogen transfer reaction leading to scission of the C–N bond to the amide group. [20]

The amorphous structure of Hybrane is confirmed by DSC measurements as well (**Figure 3.17**). The glass transition temperature of the pure polymer is 43 °C. Although the Hybrane is a second generation hyperbranched polymer with similar molecular weight to the Boltorn H20, the T_g appears to be at higher temperature. It can be assumed that the amide group of the polymer chain and/or the fewer ester groups in the molecule of the Hybrane, cause this increase of the T_g. The heat capacity step at the transition is ΔC_p = 0.20 cal.g^{-1}.°C^{-1}, which is greater than the respective of the Boltorns.

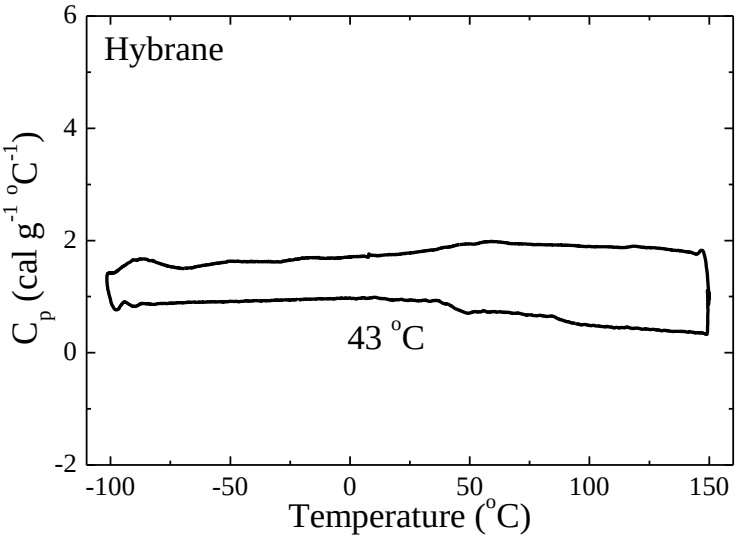

Figure 3.17: DSC measurement of pure Hybrane.

In **Table 3.1** the thermal transition temperatures (glass transition temperatures, crystallization and melting points) as well as the degradation temperatures both for the linear and the hyperbranched polymers discussed above, are presented.

Table 3.1: Thermal characteristics of the linear and the hyperbranched polymers.

Polymer	T_g (°C)	T_c (°C)	T_{c1} (°C)	T_{c2} (°C)	T_m (°C)	Degradation Temperature (°C)
EG-110	-22	28	32	60	91	415
DG-110	-26	No crystallization No melting				420
HD-110	-45	26	No cold crystallization		51	405
Boltorn H20	14	No crystallization No melting				388
Boltorn H30	35					380
Boltorn H40	46					423
Hybrane	43					320 | 423

3.3 Polymer Dynamics in the Bulk

In the present work the dynamics of all polymers is investigated in the bulk by Dielectric Relaxation Spectroscopy (BDS). The effect of the chain architecture on the local motions of

the dipoles, as well as on the segmental motion, is of great interest. The dynamics of the two biobased linear polyesters supplied by Myriant, EG-110 and DG-110 is studied in order to further understand the effect of the different repeating unit on polymer dynamics. Moreover, the effect of the generation for the three hyperbranched polyester polyols Boltorn, H20, H30 and H40 on the various motions is examined together with the hyperbranched poly (ester amide), Hybrane S1200, obtaining different functional groups. Polymer dynamics in hyperbranched polymers is compared to the respective of linear polyesters.

3.3.1 Biobased linear polyesters

EG-110

Polymer dynamics of the bulk poly (ethylene succinate), EG-110, was probed by BDS, over a wide range of frequencies and temperatures, both above and below its glass transition temperature, T_g.

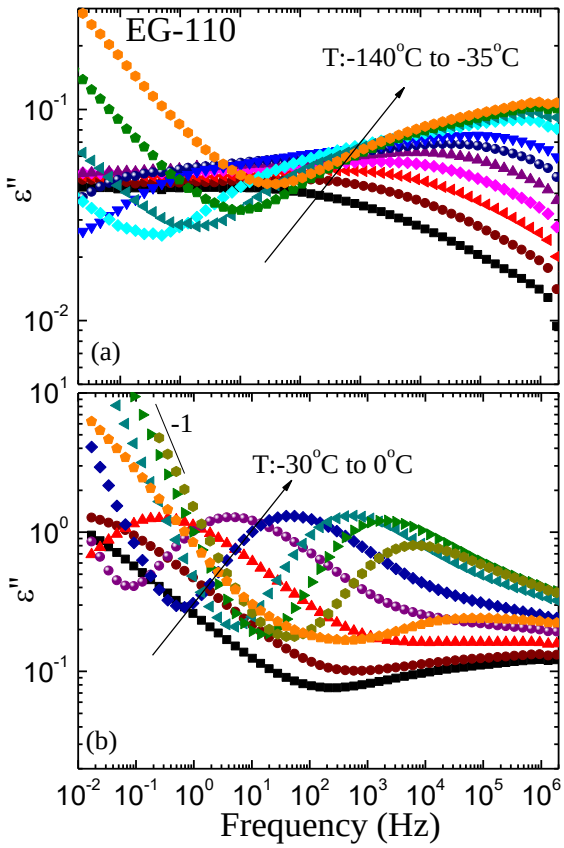

Figure 3.18: Imaginary part of the complex dielectric permittivity, ε'', for the pure EG-110 as a function of frequency, at the low (a) and the high (b) temperature regime.

The polymer was annealed at 130 °C for 30 min and cooled down to -150 °C with a cooling rate of 10 °C/min and, then, the BDS measurements were performed at the temperatures of

interest upon equilibration during heating. With this procedure the polymer at lower temperatures is almost fully amorphous and crystallizes above 0 °C. The raw dielectric data of EG-110 expressed via the imaginary part of the complex dielectric permittivity, ε'', over frequency, is presented in **Figure 3.18** at the low temperature regime from -140 °C to -35 °C (a) and above the bulk polymer T_g from -30 °C to 0 °C (b).

At low temperatures multiple relaxation processes are observed moving towards higher frequencies by increasing temperature as expected. These processes are attributed to the local motions of the small dipoles along the polymer chain. Above -50 °C, (dark cyan left triangles in **Figure 3.18**.a), another process appears in the frequency window. This process can be clearly observed above the T_g of the bulk polymer, at the high temperature regime, in **Figure 3.18**.b, and is attributed to the segmental relaxation (α-process) of the polymer chain. Above -5 °C the amplitude of the segmental relaxation is decreased and at 0 °C (orange hexagons) the process is suppressed due to the cold crystallization of the polymer while heating. At even higher temperatures, the observation of any other relaxation processes is obscured by the conductivity contribution, which is manifested by the ω^{-1} dependence of the ε'' data.

The raw data obtained for the complex dielectric permittivity were analyzed by a superposition of the empirical Havriliak-Negami (HN) functions (Eq. 2.3) and an additional ionic conductivity contribution at low-frequencies and high temperatures.

Figure 3.19 demonstrates the representative analysis of the spectra for two temperatures, below and above the T_g of the bulk EG-110. From the analysis it appears that multiple relaxation processes are necessary to obtain a good fit to the data.

For the fastest process the β parameter is fixed to 1, whereas α (0.2 − 0.3) and $\Delta\varepsilon$ (0.5 − 1) parameters increase with increasing temperature; the values for α (0.2 − 0.3) signify a broad process. The slower sub-T_g process is quite broad with α = 0.3 − 0.45 and $\Delta\varepsilon \approx 0.4$ and it is asymmetric in agreement with the identified γ-process observed in hyperbranched polyesters. [21] At higher temperatures the segmental α-process emerges; this process is asymmetric, whereas the α parameter is determined to be around 0.5 − 0.8 and $\Delta\varepsilon$ is decreasing with increasing temperature taking values from 7 to 5. Moreover, the relaxation strength of the

segmental process decreases around 0 °C due to the cold crystallization and the subsequent decrease of the amorphous polymer content.

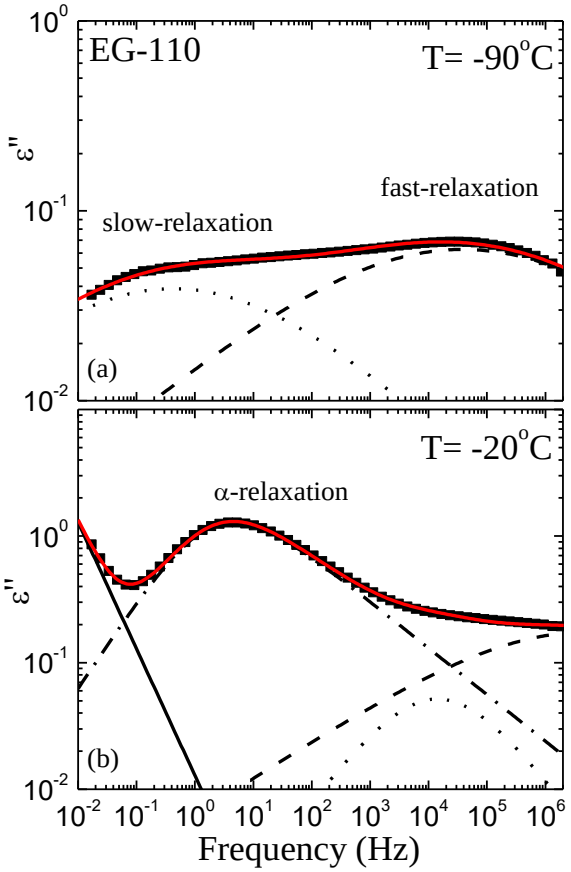

Figure 3.19: Imaginary part of the dielectric permittivity, ε'', for pure EG-110 at T=-90°C (a) and T=-20°C (b) below and above the T_g respectively. The individual Havriliak-Negami functions needed for the deconvolution of the spectra are shown with black lines, whereas the red lines are the total fits.

Figure 3.20 shows the relaxation map of the neat EG-110 in an Arrhenius representation. The relaxation times of the three processes that resulted from the analysis of the dielectric data, show different temperature dependencies. The relaxation times of the two sub-T_g processes follow an Arrhenius temperature dependence, $\tau = \tau_0 \exp[E/RT]$, with activation energy 30 ±1 kJ/mol for the fast process and 59 ±1 kJ/mol for the slow process.

The value obtained for the fast process is in agreement with the activation energy obtained for the β-relaxation process in other systems, as well. [22]–[25] However, in most of those works, a single sub-T_g process was identified. Two sub-T_g processes were observed in an investigation of the dynamics of semi-crystalline poly (butylene succinate) and [poly (butylene succinate)-co-(butylene adipate)], contrary to the case when the same materials were

quenched and, thus, they were amorphous, where a single broad sub-T_g process was obtained; the additional slower process for the semi-crystalline polymers had a higher activation energy and was attributed to the constrained motion of the same groups due to the presence of crystallites. [25]

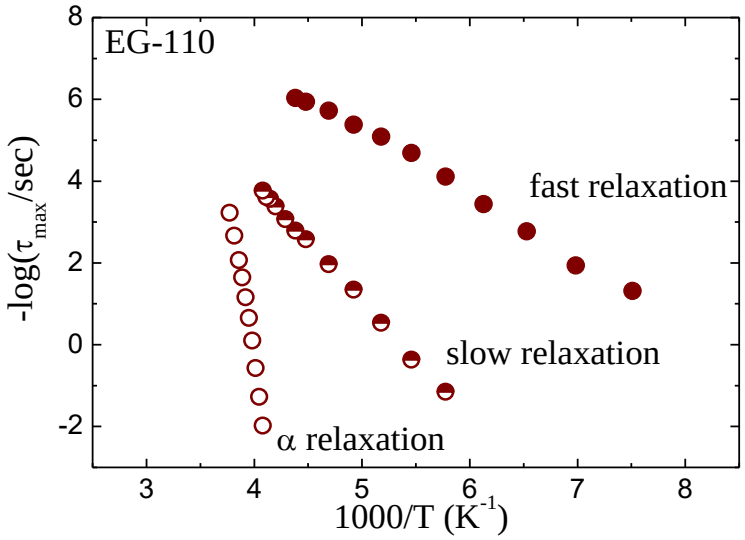

Figure 3.20: Arrhenius relaxation map for the pure EG-110.

At temperatures above the glass transition, the segmental relaxation of the EG-110 is observed, as expected. The temperature dependence of this process appears to follow the Vogel-Fulcher-Tammann (VFT) equation $\tau = \tau_0 \exp[B/(T-T_0)]$. To minimize the error in the fitting of the data with the VFT equation when the range of the experimental data is limited, the value of $\tau_0 = 10^{-13}$ is kept fixed. Fitting of the data resulted in B = 1286 ±5 K and T_0 = 208.0 ±3.0 K. Moreover, the fragility parameter is determined to be $D = B/T_0 \sim 6.2$.

EG-110 quenched

To investigate the effect of the cooling rate on the measured polymer dynamics, BDS measurements were performed for EG-110 following quenching from the melt. The EG-110 specimen was annealed at 130 °C for 30 min, cooled down to -150 °C with liquid nitrogen and BDS measurements were performed at the temperatures of interest upon equilibration during heating. The raw data of the imaginary part of the complex dielectric permittivity over frequency, for the quenched EG-110, are presented in **Figure 3.21**. At the low temperature regime, from -130 °C to -40 °C (**Figure 3.21**.a), two relaxation processes are observed in this case as well. By increasing the temperature from -35 °C to 0 °C (**Figure 3.21**.b), the segmental relaxation occurs, which is suppressed above -10 °C due to the cold crystallization.

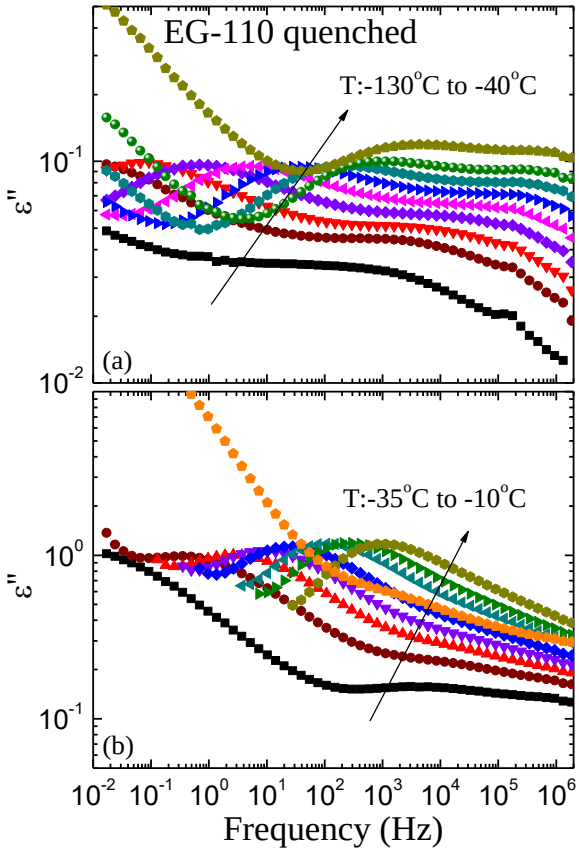

Figure 3.21: Imaginary part of the complex dielectric relaxation for the quenched pure EG-110 as a function of frequency, at the low (a) and the high (b) temperature regime.

Figure 3.22 shows a comparison of the imaginary part of the complex permittivity, ε", for the quenched sample and the one, which was cooled down with a 10 °C/min rate. The comparison is shown for two different temperatures, one below (**Figure 3.22**.a) and one just above (**Figure 3.22**.b) the calorimetric glass transition temperature of the polymer. As shown in the DSC measurement of **Figure 3.3**, this material does not show significant crystallization during cooling with a rate of 10 °C/min; thus, it is anticipated that the two different ways of cooling will not change the morphology of the polymer to a large degree and that they may provide information on the origin of the observed sub-T_g relaxation processes.

It is clear from **Figure 3.22**.a that, for both quenched and slowly cooled samples, two sub-T_g relaxation processes can be observed that have qualitative the same relaxation times. Nevertheless, their dielectric strengths are apparently very different; the fast relaxation process has higher amplitude for the slowly cooled sample, whereas it is the slow one which becomes more intense when the polymer is quenched. This observation may indicate that the two relaxation processes are related with a single relaxation motion, which can be partly free

and partly restricted; the different cooling rates can affect only the relative populations of the fast and slowly moving groups.

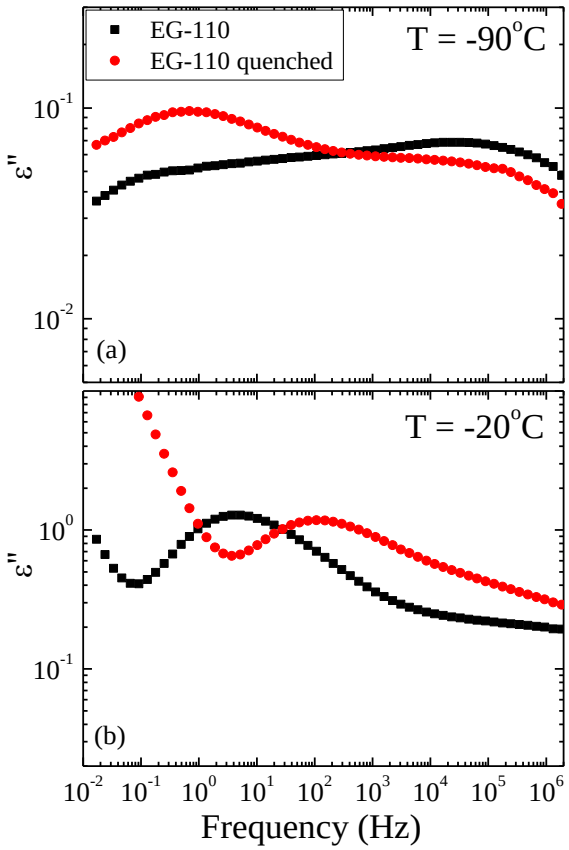

Figure 3.22: Imaginary part of the dielectric permittivity, ε'', for the slowly cooled EG-110 (black squares) and the quenched EG-110 (red circles) at (a) T=-90°C and (b) T=-20°C below and above the T_g respectively.

Above T_g, the segmental mode can be observed in **Figure 3.22**.b, possessing similar amplitude but different relaxation times, being faster for the quenched polymer. This can be attributed to the completely unrestricted motion of the polymer segments when they are quenched compared to the restricted motion of part of them that are tied to the crystallites despite the low degree of crystallinity. Similarly, faster segmental dynamics in initially amorphous poly(L-lactic acid) was observed before, compared to the respective semi-crystalline (annealed) ones.[26], [27]

To be more quantitative, the data were analyzed by the HN functions. In the quenched EG-110, for the fastest process the β parameter is fixed to 1, the α is 0.2 − 0.35 and $\Delta\varepsilon$ is 0.3 − 0.43; the α parameter is very similar to the non-quenched EG-110, whereas the $\Delta\varepsilon$ parameter is significantly lower. The slower sub-T_g process is narrower with $\alpha \approx 0.5$ but more intense with

$\Delta\varepsilon = 0.55 - 0.8$. Also in this case the slower sub-T_g process is asymmetric. The segmental alpha-process, observed at higher temperatures, is asymmetric, with $\alpha = 0.4 - 0.7$ and $\Delta\varepsilon = 7 - 4.5$. This process is more wide that the alpha relaxation of the non-quenched EG-110 but of similar dielectric strength.

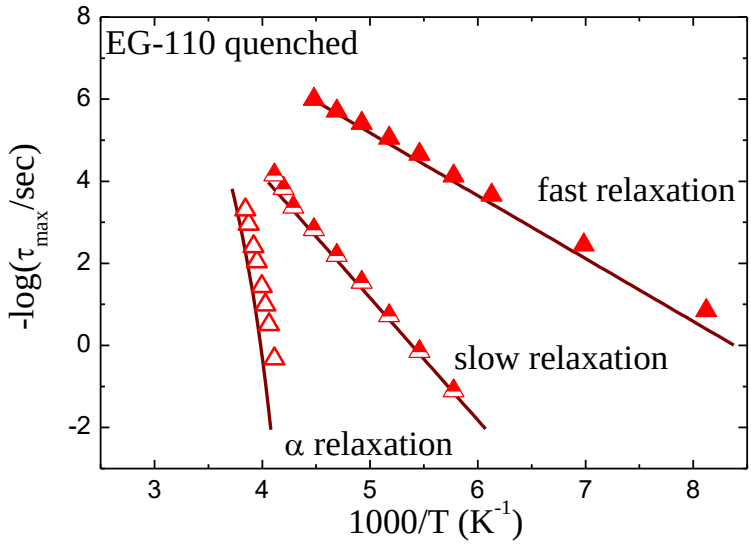

Figure 3.23: Arrhenius relaxation map for the quenched EG-110. Solid lines correspond to the relaxation times of the non-quenched EG-110.

The relaxation times, after the analysis of the BDS measurements, of the quenched EG-110 are illustrated in an Arrhenius relaxation map together with the non-quenched EG-110, in **Figure 3.23**. The two sub-T_g processes possess Arrhenius temperature dependencies. The activation energy for the fast process is 28 ±1 kJ/mol and for the slow process is 58 ±1 kJ/mol, with very similar relaxation times to the non-quenched EG-110, as expected by the data.

At higher temperatures, the segmental relaxation is observed to be faster than the segmental relaxation of the non-quenched EG-110. The temperature dependence of this process also follows the VFT equation. Fitting of the data, with fixed $\tau_0 = 10^{-13}$, resulted in B = 1409 ±9 K and T_0 = 197.2 ±1 K. Moreover, the fragility parameter is determined to be $D = B/T_0 \sim 7.1$ for the quenched EG-110, higher than the EG-110.

DG-110

Polymer dynamics of the amorphous bulk poly (diethylene succinate), DG-110, was studied by BDS over a wide range of frequencies and temperatures as well. In order to prepare the sample, the polymer was annealed at 130 °C for 30 min and cooled down to -150 °C with a cooling rate of 10 °C/min and, then, the BDS measurements were performed at the

temperatures of interest upon equilibration during heating. The imaginary part of the complex dielectric permittivity over frequency for the DG-110, is presented in **Figure 3.24** at both low, from -140 °C to -50 °C, and high, from -40 °C to 10 °C, temperature regime.

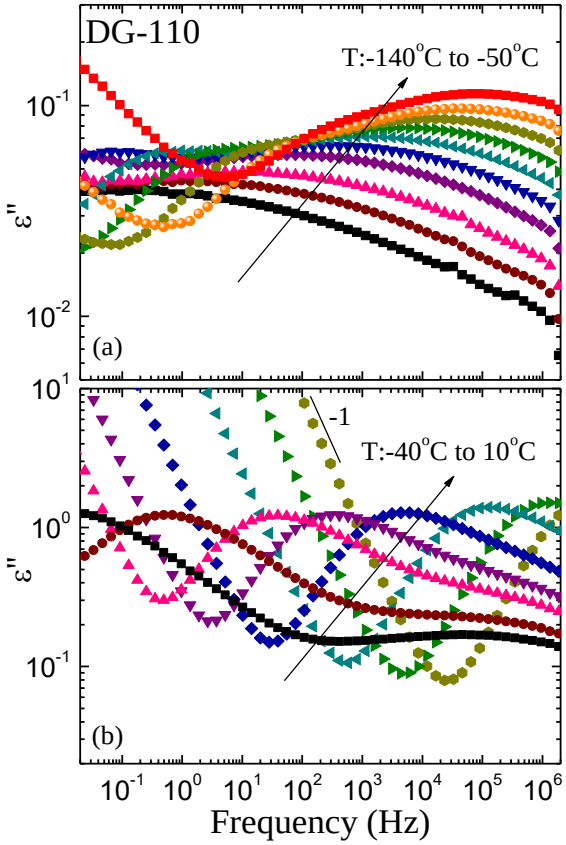

Figure 3.24: Imaginary part of the complex dielectric permittivity, ε'', for the pure DG-110 as a function of frequency, at the low (a) and the high (b) temperature regime.

In the case of the linear biobased polyester DG-110, at the low temperature regime, multiple relaxation processes occur, quite similar to the EG-110 (**Figure 3.24**.a). At the high temperature regime, illustrated in **Figure 3.24**.b, the segmental relaxation is observed above -40 °C, with its peak obtaining a maximum at 10^{-2} Hz for this temperature. The α-process in this case can be observed up to 10 °C in which the peak is out of the frequency range.

The raw data obtained for the complex dielectric permittivity were analyzed by the HN functions and the conductivity contribution. In the following figure, the representative data analysis is illustrated for one low (-90 °C, **Figure 3.25**.a) and one high (-30 °C, **Figure 3.25**.b) temperature. The two sub-T_g relaxation processes and the segmental α-process, are shown.

In the bulk DG-110, for the fastest process the β parameter is fixed to 1 whereas the α (0.2 – 0.3) and Δε (0.5 – 1) parameters increase with increasing temperature. The slower sub-T_g

process possesses lower relaxation strength ($\Delta\varepsilon \approx 0.1$) and appears to be narrower (α = 0.6 - 0.8) as compared to the faster process, but also in comparison with the respective process of the EG-110. The slower sub-T_g process is asymmetric in agreement with the slow sub-T_g process of the EG-110. At higher temperatures, the segmental relaxation emerges; this process is asymmetric for both polymers. The α parameter is determined around 0.5 – 0.8 and $\Delta\varepsilon$ is decreasing with increasing temperature taking values from 7 to 5. All parameters are summarized at the end of the chapter in **Table 3.2**.

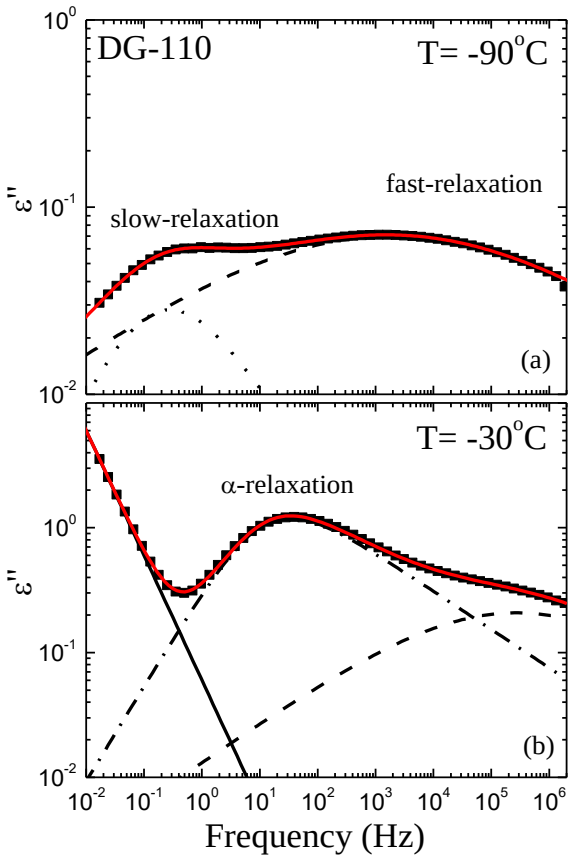

Figure 3.25: Imaginary part of the dielectric permittivity, ε'', for pure DG-110 at (a) T=-90°C and (b) T=-30°C below and above the T_g respectively. The processes needed for the deconvolution of the spectra are shown with black lines, whereas the red lines correspond to the total fits.

The relaxation times obtained by the analysis, are shown in an Arrhenius representation in **Figure 3.26**. For DG-110 the two sub-T_g processes show Arrhenius temperature dependencies; the faster one is slower, whereas the slow process almost coincides with the respective sub-T_g processes of the EG-110. The activation energy for the fast process is 38 ±1 kJ/mol and 60 ±2 kJ/mol for the slow process.

As mentioned before in the discussion on the dynamics of EG-110, two sub-T_g processes were observed for the semi-crystalline poly (butylene succinate) and poly (butylene succinate)-co-(butylene adipate), where the additional slower process of higher activation energy, was attributed to the constrained motion of the same groups due to the presence of crystallites. [25] In the current work, the slower motion indeed possesses higher activation energy; however, it is observed in the case of DG-110 as well, indicating that the constraints are of different origin. Multiple (three) sub-T_g relaxation processes were observed when cold crystallized samples at different crystallization temperatures were investigated; [28] these were attributed to a large variety of environments, whereas the three processes merged in an abnormally broad single process close and below T_g. A single sub-T_g process identified as β-relaxation was observed in the investigation of the dynamics of polylactides. Its shape parameters were $\alpha = 0.3$ and $\beta = 1$, whereas the obtained molecular weight dependence of the relaxation times led to the suggestion that it was not of local character. [22] In that case, the shape parameters of the segmental process were reported as $\alpha = 0.55$ and $\beta = 0.8$.

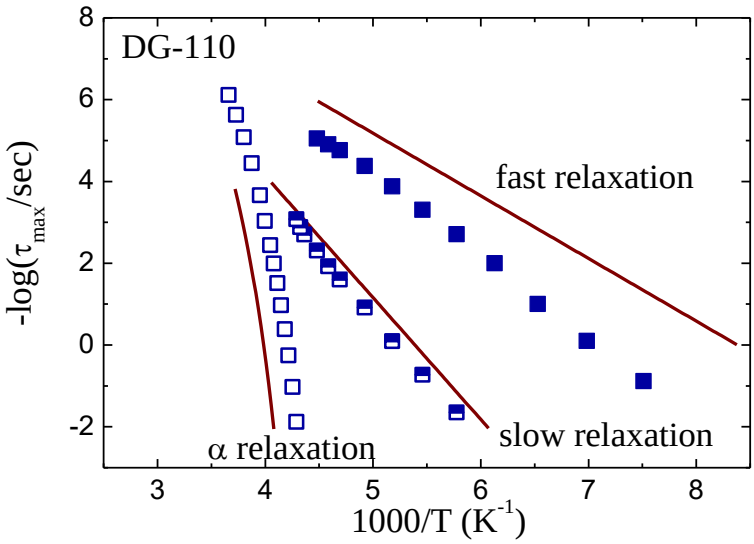

Figure 3.26: Arrhenius relaxation map for the pure DG-110. The solid lines correspond to the relaxation times of the pure EG-110.

The segmental relaxation for DG-110, is observed at temperatures above its calorimetric glass transition, as expected, and it is faster than the respective of EG-110 due to the differences of the T_g between the two polymers.

The relaxation times of the segmental relaxation are fitted with the VFT equation and the value of $\tau_0 = 10^{-13}$ is kept fixed. Fitting of the data resulted in B = 1177 ±5 K and T_0 = 199.0 ±1.0

K. The Vogel temperature, T_0, between the two polymers shows a similar difference as the calorimetric glass transition temperatures, as anticipated. Moreover, the fragility parameter $D = B/T_0 \sim 5.9$ for DG-110, has similar values with that of EG-110 (D = 6.2).

3.3.2 Hyperbranched polyester polyols - Boltorn

Polymer dynamics for the three hyperbranched polyester polyols was probed by dielectric relaxation spectroscopy as well. All samples were kept at the highest starting temperature for 30 min prior to the measurements and were thermally equilibrated at successively decreasing temperatures before the isothermal data collection.

The following figures show the imaginary part of the complex permittivity, ε'', over frequency for the bulk polymers of second, third and fourth generation (H20, H30 and H40), **Figure 3.27**, at low (a, c, e) and high (b, d, f) temperature regime.

The raw dielectric data are very similar for all the three polymers and reveal multiple relaxation processes for the investigated temperature range. At low temperatures a very broad peak, covering almost 7 orders of magnitude in frequency, is observed, which shifts at higher frequencies as temperature increases. This sub-T_g relaxation peak can reflect to the motion of hydroxyl groups and/or the orientation fluctuations of the ester groups, the so called γ- and β-process, respectively, according to the literature. [29]–[32] All three generations of the hyperbranched polyester polyols investigated, exhibit this broad peak at temperatures below 10 °C showing very similar characteristics.

At temperatures around the calorimetric glass transition of each polymer, another peak appears which corresponds to the segmental dynamics (α-process) related to the glass transition as identified by the quantitative analysis which is presented below. At even higher temperatures (60–90°C, depending on the generation) the observation of any relaxation processes is partially obscured by the conductivity contribution in all three polymers.

The dynamics of similar hyperbranched polymers has been studied in the past by dielectric spectroscopy. In those studies, two distinct sub-T_g processes associated with the hydroxyl motion and the ester reorientation were observed, with similar activation energies in the case of hydroxyl-terminated polymers. On the other hand in hyperbranched polyesters with

terminal acetate, benzoate or aliphatic groups only one peak, attributed to the ester group, was observed but with much larger activation energy. [29], [30]

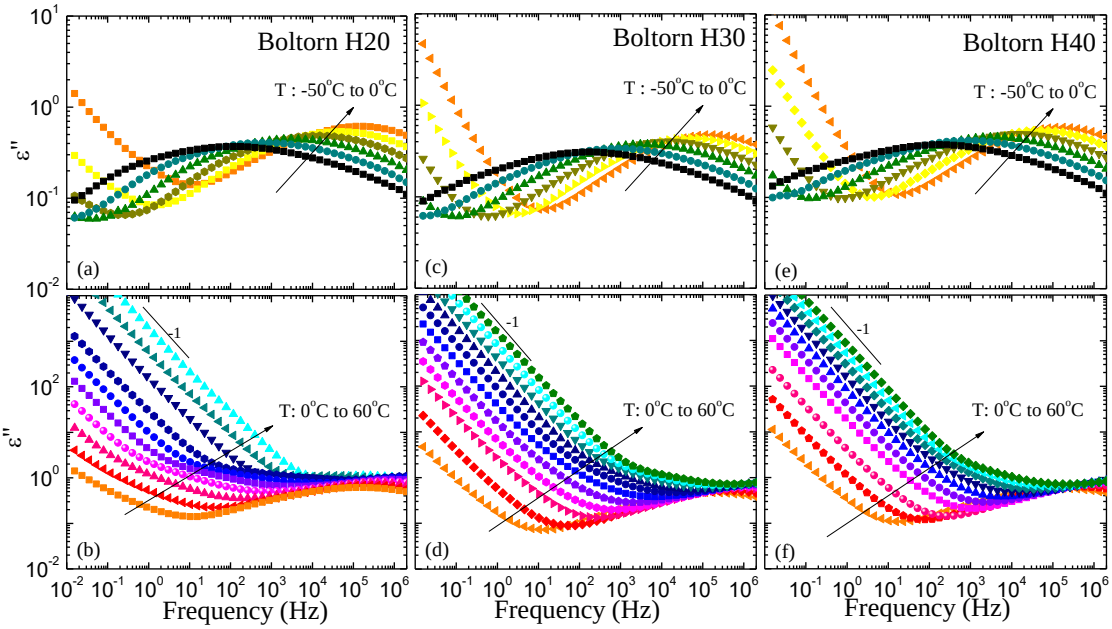

Figure 3.27: Imaginary part of the complex dielectric permittivity, ε'', for the pure Boltorn H20, H30 and H40 as a function of frequency, at the low (a, c, e) and the high (b, d, f) temperature regime.

In another study, where the dynamics of the H20, H30, H40, and H50 hyperbranched polymers was investigated, only one peak was observed, at low temperatures, identified as the γ-process because all other peaks were covered by the effect of conductivity. [31] Finally, the most recent work that investigated the dynamics of the same four generations of hyperbranched polymers resolves the γ- and the β-processes below the glass transition temperature and no other relaxation process above T_g. [32] In general, to the best of our knowledge, there is no investigation up to now that clearly identifies the segmental α-relaxation in the second, third, and fourth generation of hydroxyl terminated hyperbranched polymers.

Figure 3.28 demonstrates the representative analysis of the spectra for three temperatures, below, slightly above and well above the T_g of the second generation hyperbranched polymer, Boltorn H20. From the data at low temperatures, the shape and relaxation strength parameters are determined for the γ- and β-processes. For the γ-process the β parameter is fixed to 0.8 for H20, 0.9 for H30, and 1.0 for H40, whereas the α (0.2 – 0.3) and Δε (2.8 – 6.7) parameters increase with increasing temperature. At higher temperatures, above T_g, the α-

process emerges, as shown for the H20 in **Figure 3.28**.b (dash-dotted line); for this process and for all three polymers, the β parameter is fixed at 1.0, whereas α is determined around 0.36 – 0.45 and Δε is constantly decreasing from 9.3 to 3.7.

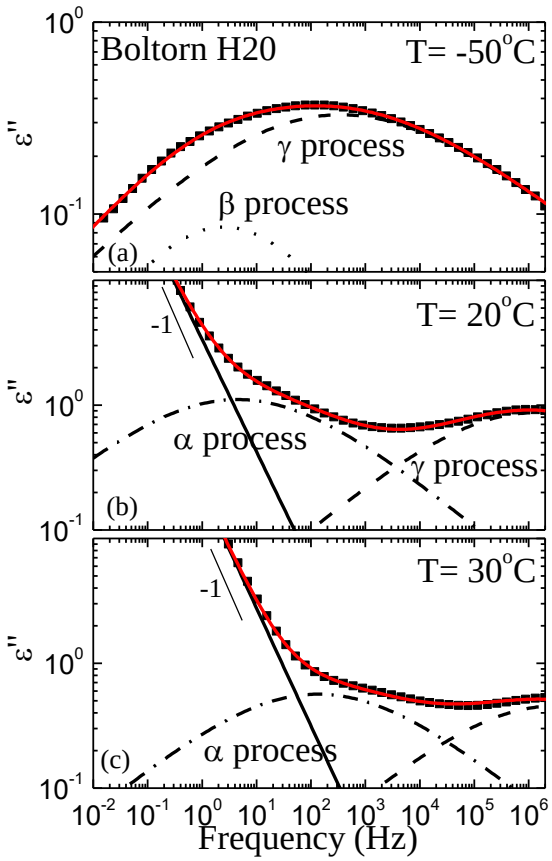

Figure 3.28: Representative analysis of Boltorn H20. Imaginary part of the dielectric permittivity, ε'', at T=-50°C below the T_g (a), T=20°C above and close to the T_g (b), and T=30°C well above the T_g (c). The processes needed for the deconvolution of the spectra are shown with black lines, whereas the red lines are the total fits.

Figure 3.29 shows the results of the above analysis concerning the relaxation times, in an Arrhenius representation. For the three hyperbranched polymers the relaxation times of the γ- and the β-processes coincide and follow an Arrhenius temperature dependence. The activation energies of the γ-process are $E_{\gamma,H20}$ = 65.0 ± 1.5 kJ/ mol, $E_{\gamma,H30}$ = 69.5 ± 1.0 kJ/mol and $E_{\gamma,H40}$ = 66.5 ± 1.5 kJ/mol. This process is due to local fluctuations and rotations of the hydroxyl groups. It is noted that these values of the activation energies are lower than the ones reported in the literature [29], [30], [32] but still high in comparison to local processes of linear polymers. [33]

As far as the intermediate β-process is concerned, there are few temperatures from which we can derive a relaxation time since, as temperature increases, it is in close proximity to the

other two processes. The temperature dependence of its relaxation times seems very similar to the one of the γ-relaxation. The activation energies for the three polymers are $E_{\beta,H20}$ = 70 ± 3 kJ/mol, $E_{\beta,H30}$ = 81 ± 9 kJ/mol, and $E_{\beta,H40}$ = 86 ± 2 kJ/ mol, respectively. For this process, an apparent dependence of the activation energy on the generation is observed probably indicating that the reorientation of the carbonyl groups becomes more difficult as the molecules become denser.

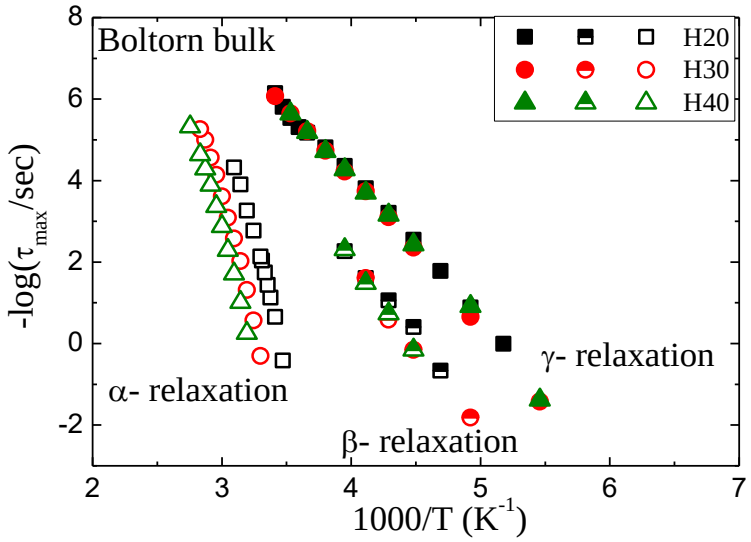

Figure 3.29: Arrhenius relaxation map for the pure Boltorn H20 (black squares), H30 (red circles) and H40 (green triangles).

Around the T_g of each polymer, as determined by DSC, the segmental process appears. This process differs between the three polymers, as expected, due to the differences of the calorimetric glass transition of the three generations. Moreover, the temperature dependence of this process appears to follow the Vogel–Fulcher–Tammann (VFT) equation. The parameters obtained from the fit with VFT expression bare significant error, especially in cases that the range of the experimental data is limited. To minimize the error in the analysis, the value of $\tau_0 = 1 \times 10^{-13}$ is kept fixed for all samples. The resulted parameters are B = 1939 ± 29 K and T_0 = 225.6 ± 1.0 K for H20, B = 2113 ± 24 K, and T_0 = 233.5 ± 1.0 K for H30 and B = 2227 ± 29 K and T_0 = 237.3 ± 1.0 K for H40. The Vogel temperature T_0 increases with generation and shows a similar dependence with that of the calorimetric glass transition temperature, as anticipated. Moreover, the fragility parameter is D = 8.6, 9.0, and 9.4 for H20, H30, and H40, respectively denoting that the increase in the generation results in slightly stronger glasses. [21]

Finally, polymer dynamics in the hyperbranched polyesters Boltorn is compared to the respective linear polyesters of Myriant. Representative relaxation times of the third generation Boltorn H30 are presented in **Figure 3.30** together with the sub-T_g processes of the EG-110 and DG-110. The activation energy of all Arrhenius processes, the B and T_0 determined by the VFT equation for the α-process and the fragility parameters are summarized in **Table 3.3** in the end of the present Chapter.

Concerning the segmental dynamics, the α-process of each polymer depends on its glass transition temperature and appears at a different temperature regime, so it is not discussed here. On the other hand the local dynamics of similar functional groups is compared between polymers of different architecture. The slow processes, discussed for the linear polymer dynamics, coincide with the γ-process of the hyperbranched polyesters, while the fast processes appear at higher frequencies with lower activation energies. As mentioned above, for the EG-110, the fast and the slow processes are related with the same relaxation motion which can be partly free and partly restricted. In the case of the hyperbranched polyesters, the extended H-bonding network discussed earlier, causes this restriction in the motion of hydroxyl groups.

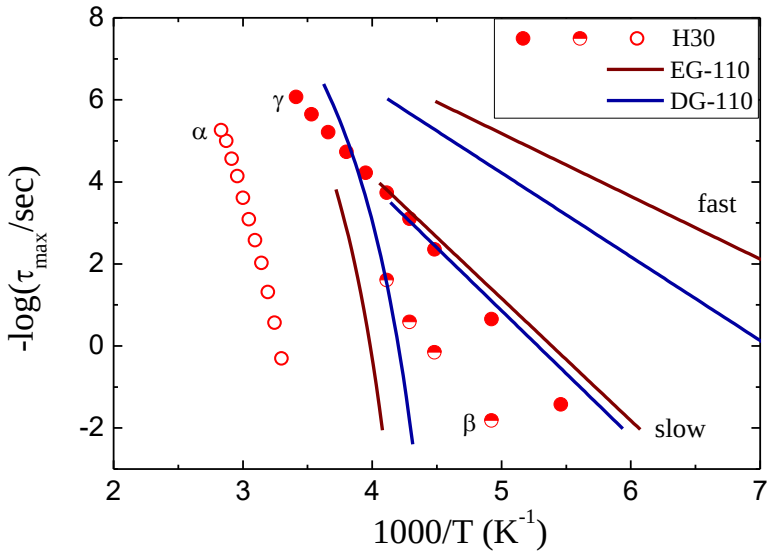

Figure 3.30: Polymer dynamics of the hyperbranched polyester H30 in comparison with the linear polyesters EG-110 and DG-110.

It is noted that in linear polyesters only the motion of the hydroxyl end groups is observed, whereas the ester reorientation observed in hyperbranched polymers is not, probably because its relaxation times are very close to the ones of the segmental mode. The assumption

that both slow and fast processes are attributed to the –OH group motions is supported by the lower dielectric strength of the sub-T_g processes for the linear polymers than the γ-process for the hyperbranched polymers related to the lower number of the hydroxyls (all parameters are shown in **Table 3.2**).

3.3.3 Hyperbranched poly (ester amide) - Hybrane

Polymer dynamics was investigated for another hyperbranched polymer with different functional groups, the hyperbranched poly (ester amide), Hybrane. The sample was annealed at 100 °C for 30 min prior to the measurements and was thermally equilibrated at successively decreasing temperatures before the isothermal data collection.

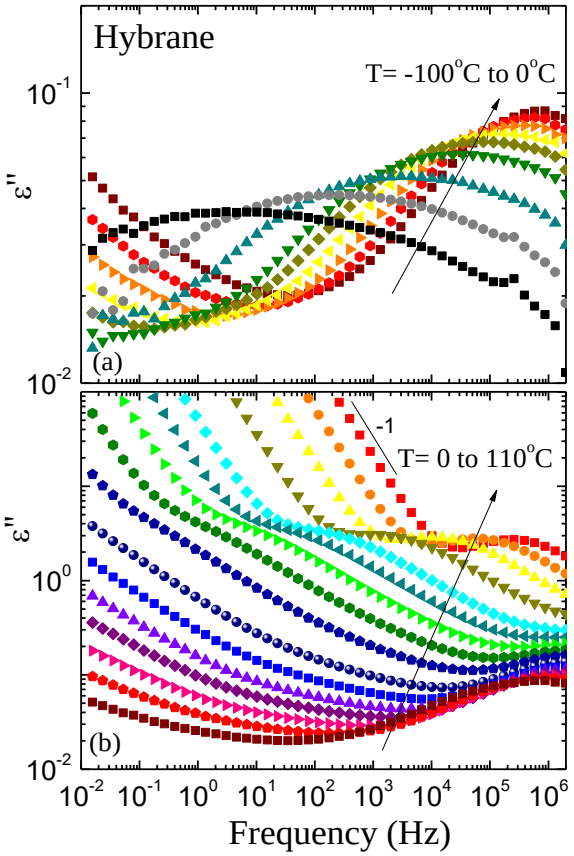

Figure 3.31: Imaginary part of the complex dielectric permittivity, ε'', for the pure Hybrane as a function of frequency, at the low (a) and the high (b) temperature regime.

In **Figure 3.31** the dielectric spectra for a wide range of temperatures are presented. The imaginary part of the complex dielectric permittivity over frequency, at low temperatures (**Figure 3.31**.a), exhibit a very broad peak, similar to the Boltorns, probably due to multiple relaxations. At the high temperature regime the segmental relaxation is clearly observed above the T_g of the bulk polymer, whereas below the T_g another process occur, partly

obscured by the wing of the α-process which enters the frequency window. This intermediate process can be qualitatively observed from 0 °C (wine squares) to 50 °C (blue pentagons).

In **Figure 3.32** the analysis of the spectra is demonstrated at three temperatures, one far below the T_g of the bulk polymer, at -90 °C (**Figure 3.32**.a), one close and below the T_g, at 30 °C (**Figure 3.32**.b) and one above the T_g, at 55 °C (**Figure 3.32**.c). At the low temperature regime the peak is fitted by two HN functions, although it could be fitted by one, because the peak is too broad. The fast process is asymmetric, while the α = 0.2 – 0.46 and Δε = 0.52 – 0.6. The slow process can be discerned only at few temperatures because it is strongly obscured by the broad peak; the β is fixed 1, Δε ≈ 0.05 and α = 0.33 – 0.45.

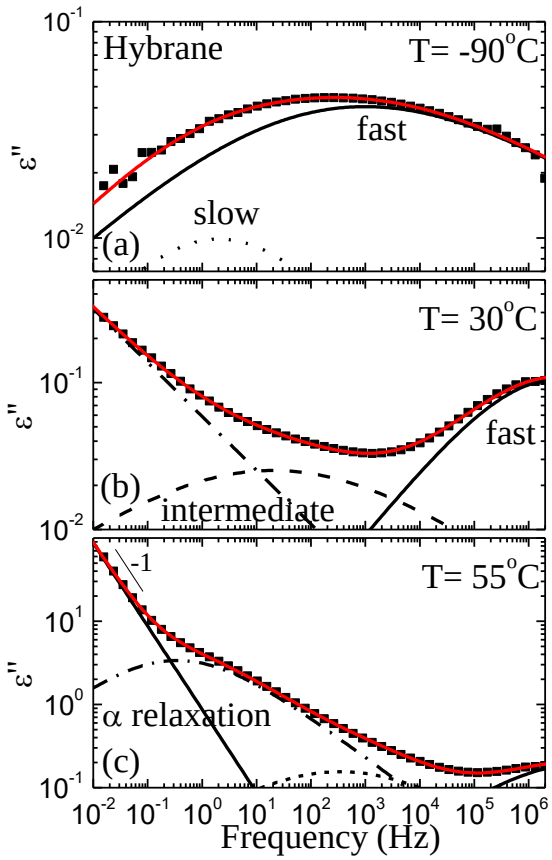

Figure 3.32: Imaginary part of the dielectric permittivity, ε'', for the pure Hybrane at (a) T=-90°C below the T_g (b) T=30°C below and close to the T_g and (c) T=55°C above the T_g. The processes needed for the deconvolution of the spectra are shown with black lines, whereas the red lines are the summations of the processes.

At higher temperatures the intermediate process appears, at -10 °C, with β = 1 and parameters α (0.23 – 0.4) and Δε (0.14 – 0.97) increasing by increasing temperature. This relaxation process is partially obscured by the α-process as shown in **Figure 3.32**.b. Above the T_g of the bulk polymer the segmental relaxation is observed (**Figure 3.32**.c); the β parameter is fixed at

1.0, whereas α is determined around 0.47 – 0.64 and Δε is constantly decreasing from 19.4 to 8.9.

The relaxation times obtained by the analysis are shown in **Figure 3.33** in an Arrhenius representation. The three sub-T_g processes follow an Arrhenius temperature dependence and the activation energies are E_{fast} = 33.0 ± 2 kJ/ mol, E_{slow} = 60 ± 4 kJ/mol and $E_{intrmediate}$ = 83 ± 3 kJ/mol.

Above the glass transition temperature of the bulk Hybrane the segmental relaxation is observed as mentioned before. The temperature dependence of this process follows the Vogel–Fulcher–Tammann (VFT) equation. To obtain parameters from the fit with VFT expression consistent to the other polymers, the value $\tau_0 = 1 \times 10^{-13}$ is kept fixed. The resulted parameters are B = 2127 ± 25 K and T_0 = 259 ± 1.0 K for the Hybrane. Moreover, the fragility parameter is D = 8.2 which is close to the hyperbranched polymers but lower even than the second generation H20, D_{H20} = 8.6 (**Table 3.3**).

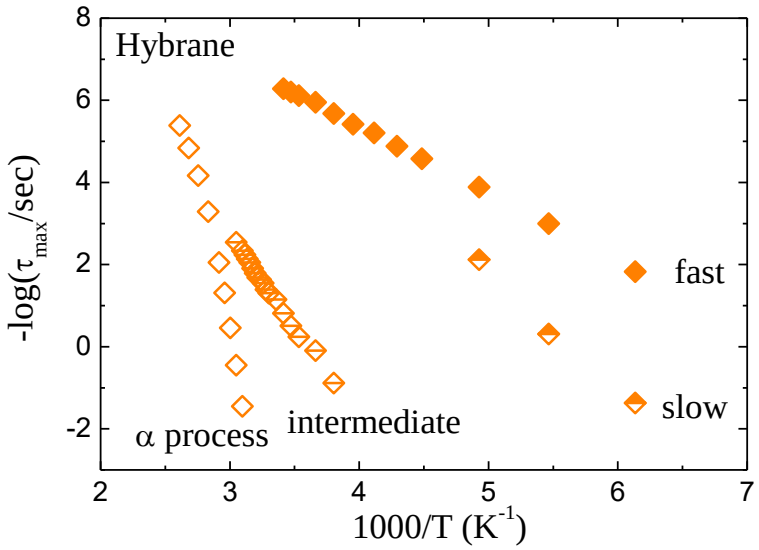

Figure 3.33: Arrhenius relaxation map of pure Hybrane.

In **Figure 3.34** sub-T_g polymer dynamics of the hyperbranched Hybrane is compared with the respective dynamics of both the hyperbranched and the linear polyesters; representative relaxation times of the hyperbranched H30 and the linear DG-110 are presented. In comparison with the other hyperbranched polyesters, the fast process of the Hybrane is faster, with lower activation energy than the γ-process, whereas the slow one resembles both the activation energy and the relaxation times of the γ-process of the Boltorns. The relaxation

times of the fast and the slow processes resemble more the sub-T_g processes of the linear polyesters. The broad peak at low temperatures, deconvoluted in two processes, is attributed to the free and the constrained motion of the hydroxyl groups. The activation energies, for those two processes, are close to the ones reported in literature for a similar cross-linked poly (ester amide) and noted as γ- and β-process. [34] Higher activation energy of the slow process attributed to the hydrogen bonding, observed by molecular simulations, was reported as well. [35]

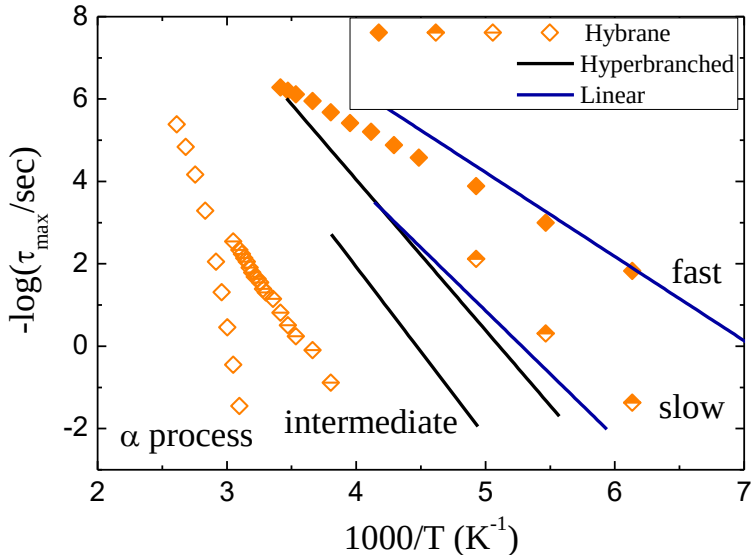

Figure 3.34: Polymer dynamics of the hyperbranched polyester amide Hybrane in comparison with the ones of the H30 hyperbranched polyester Boltorn and the linear polyester DG-110.

The intermediate process is much slower in comparison with the other two sub-T_g processes and obtains very high activation energy. This process can be attributed to the motion of a bigger part of the polymer chain. Molecular dynamics simulations, performed at high temperatures to understand the dynamic behavior of the Hybrane, reveal a process related to a motion involving the polymer branches that is influenced by the intermolecular hydrogen bonding network existing in hyperbranched polymers. [36]

In order to summarize the results obtained by the analysis of the bulk polymers, all parameters of the HN functions utilized to fit the dielectric spectra are presented in **Table 3.2**.

Table 3.2: Parameters of the HN function for each relaxation process.

HN parameters	EG-110	EG-110 quenched	DG-110	BOLTORN	HYBRANE
Fast process – local motions of free –OH groups					
β	1			No process	< 1
α	0.20-0.30	0.20-0.35	0.20-0.30		0.20-0.46
Δε	0.50-1.00	0.30-0.43	0.50-1.00		0.52-0.60
Slow / γ-process – local motions of constrained –OH groups					
β	< 1			≤ 1	1
α	0.30-0.45	0.50	0.60-0.80	0.20-0.30	0.23-0.40
Δε	0.40	0.55-0.80	0.10	2.80-6.70	0.14-0.97
β-process – local motions of ester groups					
β	No process			1	No process
α				0.30-0.45	
Δε				0.4	
Intermediate process – slow motion of a branch					
β	No process				1
α					0.33-0.45
Δε					0.05
α-process – segmental motion					
β	< 1			1	
α	0.50-0.80	0.40-0.70	0.50-0.80	0.36-0.45	0.47-0.64
Δε	7.00-4.50			9.30-3.70	19.40-8.90

The **Table 3.3** reported in the present chapter summarizes the activation energies of all the processes obtaining an Arrhenius temperature dependence, the B and T_0 of the segmental processes and the fragility parameters of all polyesters investigated, both linear and hyperbranched.

Table 3.3: Results of the relaxation processes.

	EG-110	EG-110 quenched	DG-110	BOLTORN H20 | H30 | H40	HYBRANE
Fast process E_a (kJ/mol)	30 ± 1	28 ± 1	38 ± 1	No process	33 ± 2
Slow / γ-process E_a (kJ/mol)	59 ± 1	58 ± 1	60 ± 2	65.0 | 69.5 | 66.5	60 ± 4
β-process E_a (kJ/mol)	No process			70.0 | 81.0 | 86.0	No process
Intermediate process E_a (kJ/mol)				No process	83 ± 3
α-process B (K)	1286 ± 5	1409 ± 9	1177 ± 5	1939 | 2113 | 2227	2127 ± 25
T_0 (K)	208.0 ± 3	197.2 ± 1	199.0 ± 1	225.6|233.5|237.3	259.0 ± 1.0
Fragility parameter	6.2	7.1	5.9	8.6 | 9.0 | 9.4	8.2

3.4 Effect of the Architecture in Polymer Properties and Dynamics

Polymer architecture is of great interest in material science because it strongly affects the polymer chain conformation resulting in different properties of the polymer. In the current chapter the structure and the thermal properties of the bulk linear and hyperbranched polyesters were studied.

For the linear polyesters the difference in their repeating unit results in different properties. EG-110 and HD-110 are semi-crystalline polymers, with a cold crystallization observed for the first one, whereas DG is amorphous. The hyperbranched polymers are amorphous with glass transition temperature depending on the generation of the Boltorns, while the Hybrane obtains a glass transition temperature similar to the fourth generation of much higher molecular weight.

In order to understand the microscopic mechanisms responsible for their properties, polymer dynamics was investigated and the effect of the polymer architecture and the different functional groups was presented.

For the linear polyesters the fast and slow local sub-T_g processes show similar relaxation times and activation energies for the two polymers, with the slower one exhibiting a higher activation energy. The investigation of the dynamics in the quenched EG-110 reveals a correlation between the processes which are related to a single motion that can be either the free (fast process) or the constrained (slow process) motion of the hydroxyl end-groups. The segmental relaxation reveals the effect of the glass transition temperature and faster dynamics for the quenched polyester.

For the hyperbranched polyester polyols, two sub-T_g processes identified as γ and β, i.e., as the local hydroxyl and carbonyl motions, are found with Arrhenius temperature dependencies and large activation energies due to the restrictions imposed by the hydrogen-bond network. The relaxation times of the γ-process, attributed to the hydroxyl motion, coincide with the slow process of the linear polyesters. This observation confirms the origin of those local motions.

On the other hand for the local dynamics of the hyperbranched poly (ester amide), a behavior similar to the linear polymers is observed due to the partial constrained motions of the hydroxyls. In the case of the hyperbranched polyesters in which a large number of hydroxyls are available an extended network is formed resulting in constrained local motions, whereas for the linear polymers and for the hyperbranched poly (ester amide) with fewer hydroxyl groups, both free and constrained hydroxyls are present.

The segmental relaxation reveals the expected dependence on the T_g for all polymers. The fragility parameter D determined by the analysis, is lower for the linear polymers indicating stronger glassy behavior compared to the hyperbranched polymers. Moreover the quenched EG-110 is more fragile in comparison with the slowly cooled polymer. For the Boltorns by increasing the generation the fragility is higher, whereas the hyperbranched poly (ester amide) is a stronger glass.

3.5 References

[1] A. Ueda, Y. Chatani, and H. Tadokoro, “Structural studies of polyesters. IV. Molecular and crystal structures of poly (ethylene succinate) and poly (ethylene oxalate),” *Polym. J.*, vol. 2, no. 3, pp. 387–397, 1971.

[2] K. Chrissafis, K. M. Paraskevopoulos, and D. N. Bikiaris, “Thermal degradation mechanism of poly(ethylene succinate) and poly(butylene succinate): Comparative study,” *Thermochim. Acta*, vol. 435, no. 2, pp. 142–150, 2005.

[3] L. H. Buxbaum, “The Degradation of Poly (ethyene terephthalate),” *Angew. Chemie - Int. Ed.*, vol. 7, no. 3, pp. 182–190, 1968.

[4] G. Z. Papageorgiou and D. N. Bikiaris, “Crystallization and melting behavior of three biodegradable poly(alkylene succinates). A comparative study,” *Polymer (Guildf).*, vol. 46, no. 26, pp. 12081–12092, 2005.

[5] B. S. Hsiao, K. H. Gardner, and D. Q. Wu, “Time-resolved X-ray study of poly (aryl ether ether ketone) crystallization and melting behaviour : 1 . Crystallization,” *Polymer (Guildf).*, vol. 34, no. 19, pp. 3986–3995, 1993.

[6] B. S. Hsiao, K. H. Gardner, and D. Q. Wu, “Time-resolved X-ray study of poly(aryl ether ether ketone) crystallization and melting behaviour: 2. Melting,” *Polymer (Guildf).*, vol. 34, no. 19, pp. 3996–4003, 1993.

[7] D. J. Blundell and B. N. Osborn, “The morphology of poly (aryl-ether-ether- ketone),” *Polymer (Guildf).*, vol. 24, no. 8, pp. 953–958, 1983.

[8] S. Z. D. Cheng and B. Wunderlich, “Glass transition and melting behavior of poly(ethylene 2,6-naphthalenedicarboxylate),” *Macromolecules*, vol. 21, no. 3, pp. 789–797, 1988.

[9] Z. Qiu, T. Ikehara, and T. Nishi, “Crystallization behaviour of biodegradable poly(ethylene succinate) from the amorphous state,” *Polymer (Guildf).*, vol. 44, no. 18, pp. 5429–5437, 2003.

[10] S. Gesti, M. Casas, and J. Puiggalı, “Crystalline structure of poly (hexamethylene succinate) and single crystal degradation studies,” *Polymer (Guildf).*, vol. 48, no. 17, pp. 5088–5097, 2007.

[11] G. Botelho, A. Queiro, S. Liberal, and P. Gijsman, “Studies on thermal and thermo-oxidative degradation of poly (ethylene terephthalate) and poly (butylene terephthalate),” *Polym. Degrad. Stab.*, vol. 74, pp. 39–48, 2001.

[12] L. Franco and J. Puiggali, “Crystallization kinetics of poly (hexamethylene succinate),” *Eur. Polym. J.*, vol. 39, no. 8, pp. 1575–1583, 2003.

[13] M. Yasuniwa and T. Satou, “Multiple Melting Behavior of Poly (butylene succinate). I . Thermal Analysis of Melt-Crystallized Samples,” *J. Polym. Sci. Part B Polym. Phys.*, vol. 40, no. 21, pp. 2411–2420, 2002.

[14] Z. Bai, Y. Liu, T. Su, and Z. Wang, “Effect of Hydroxyl Monomers on the Enzymatic Degradation of Poly (ethylene succinate), Poly(butylene succinate), and Poly(hexylene succinate),” *Polymers (Basel).*, vol. 10, no. 90, pp. 1–13, 2018.

[15] I. Tanis, K. Karatasos, A. N. Assimopoulou, and V. P. Papageorgiou, “Modeling of

hyperbranched polyesters as hosts for the multifunctional bioactive agent shikonin," *Phys. Chem. Chem. Phys.*, vol. 13, no. 22, pp. 10808–10817, 2011.

[16] M. Huskic, E. Zagar, M. Zigon, and Z. Ema, "Structure-to-Properties Relationship of Aliphatic Hyperbranched Polyesters," *Macromol. Chem. Phys.*, vol. 208, no. 13, pp. 1379–1387, 2007.

[17] I. Tanis and K. Karatasos, "Local Dynamics and Hydrogen Bonding in Hyperbranched Aliphatic Polyesters," *Macromolecules*, vol. 42, no. 24, pp. 9581–9591, 2009.

[18] Z. Peng and L. X. Kong, "A thermal degradation mechanism of polyvinyl alcohol/silica nanocomposites," *Polym. Degrad. Stab.*, vol. 92, no. 6, pp. 1061–1071, 2007.

[19] C. L. Beyler and M. M. Hirschler, "Thermal decomposition of polymers," in *SFPE Handbook of Fire Protection Engineering 2*, vol. Section 1, 2002, pp. 111–131.

[20] B. J. Holland and J. N. Hay, "Thermal degradation of nylon polymers," *Polym. Int.*, vol. 49, no. 9, pp. 943–948, 2000.

[21] K. Androulaki, K. Chrissopoulou, D. Prevosto, M. Labardi, and S. H. Anastasiadis, "Dynamics of Hyperbranched Polymers under Confinement: A Dielectric Relaxation Study," *ACS Appl. Mater. Interfaces*, vol. 7, no. 23, pp. 12387–12398, 2015.

[22] M. Mierzwa, G. Floudas, J. Dorgan, D. Knauss, and J. Wegner, "Local and global dynamics of polylactides. A dielectric spectroscopy study," *J. Non. Cryst. Solids*, vol. 307–310, pp. 296–303, 2002.

[23] H.-J. Tai, "Dielectric Spectroscopy of Poly(butylene succinate-co-butylene adipate) Films," *Polym. Eng. Sci.*, vol. 51, pp. 386–390, 2011.

[24] J. J. M. Ramos and H. P. Diogo, "Slow Relaxations in Semicrystalline Poly(butylene succinate) Below and Above Tg," *Polym. Eng. Sci.*, vol. 55, pp. 1873–1880, 2015.

[25] S. Charlon, L. Delbreilh, E. Dargent, N. Follain, J. Soulestin, and S. Marais, "Influence of crystallinity on the dielectric relaxations of poly(butylene succinate) and poly[(butylene succinate)-co-(butylene adipate)]," *Eur. Polym. J.*, vol. 84, pp. 366–376, 2016.

[26] P. Klonos *et al.*, "Glass transition and segmental dynamics in poly (l -lactic acid)/ graphene oxide nanocomposites," *Thermochim. Acta*, vol. 617, pp. 44–53, 2015.

[27] P. Klonos and P. Pissis, "Effects of interfacial interactions and of crystallization on rigid amorphous fraction and molecular dynamics in polylactide / silica nanocomposites : A methodological approach," *Polymer (Guildf).*, vol. 112, pp. 228–243, 2017.

[28] A. R. Bras, P. Malik, M. Dionisio, and J. F. Mano, "Influence of Crystallinity in Molecular Motions of Poly (L -lactic acid) Investigated by Dielectric Relaxation Spectroscopy," *Macromolecules*, vol. 41, pp. 6419–6430, 2008.

[29] E. Malmstrom, F. Liu, R. H. Boyd, A. Hult, and U. W. Gedde, "Relaxation processes in hyperbranched polyesters," *Polym. Bull.*, vol. 32, pp. 679–685, 1994.

[30] E. Malmstrom, A. Hult, U. W. Gedde, F. Liu, and R. H. Boyd, "Relaxation processes in hyperbranched polyesters: influence of terminal groups," *Polymer (Guildf).*, vol. 38, no. 19, pp. 4873–4879, 1997.

[31] P. W. Zhu, S. Zheng, and G. Simon, "Dielectric Relaxations in a Hyperbranched Polyester with Terminal Hydroxyl Groups : Effects of Generation Number," *Macromol. Chem.*

Phys., vol. 202, pp. 3008–3017, 2001.

[32] G. Turky, S. S. Shaaban, and A. Schoenhals, “Broadband Dielectric Spectroscopy On the Molecular Dynamics in Different Generations of Hyperbranched Polyester,” *J. Appl. Polym. Sci.*, vol. 113, pp. 2477–2484, 2009.

[33] M. M. Elmahdy, K. Chrissopoulou, A. Afratis, G. Floudas, and S. H. Anastasiadis, “Effect of confinement on polymer segmental motion and ion mobility in PEO/layered silicate nanocomposites,” *Macromolecules*, vol. 39, no. 16, pp. 5170–5173, 2006.

[34] X. Fernández-Francos *et al.*, “Modification of epoxy-anhydride thermosets with a hyperbranched poly(ester amide). II. Thermal, dynamic mechanical, and dielectric properties and thermal reworkability,” *J. Appl. Polym. Sci.*, vol. 128, no. 6, pp. 4001–4013, 2013.

[35] I. Tanis, D. Tragoudaras, K. Karatasos, and S. H. Anastasiadis, “Molecular dynamics simulations of a hyperbranched poly (ester amide): statics, dynamics, and hydrogen bonding,” *J. Phys. Chem. B*, vol. 113, no. 16, pp. 5356–5368, 2009.

[36] S. Fotiadou *et al.*, “Structure and Dynamics of Hyperbranched Polymer / Layered Silicate Nanocomposites,” *Macromolecules*, vol. 46, pp. 2842–2855, 2013.

4 Polymer / Silica Nanocomposites

The polyesters EG-110, DG-110 and HD-110, the characterization and investigation of properties of which were described in Chapter 3, were mixed with silica nanoparticles, SiO_2, in a large range of compositions, in order to investigate the effect of the additive and of the polymer-surface interactions on their properties. Both structural and thermal characterization of the nanocomposites reveal partly suppressed thermal transitions and reduced crystallinity for the semi-crystalline polymers, by increasing the silica content.

Polymer dynamics in the case of one semi-crystalline, EG-110, and of one amorphous, DG-110, polyester was investigated in nanocomposites with a high amount of silica nanoparticles so that the polymer-additive interactions are dominant and that the polymer chains are under severe confinement. The local dynamics of both polymers, attributed to the motion of the hydroxyl end-groups that could be free or more constrained as discussed in Chapter 3, in the nanocomposites obtains lower activation energies compared to the bulk, while the segmental relaxation reveals similar dynamics to the respective in the bulk for the EG-110 and faster for the DG-110.

4.1 Silica Nanoparticles Characterization

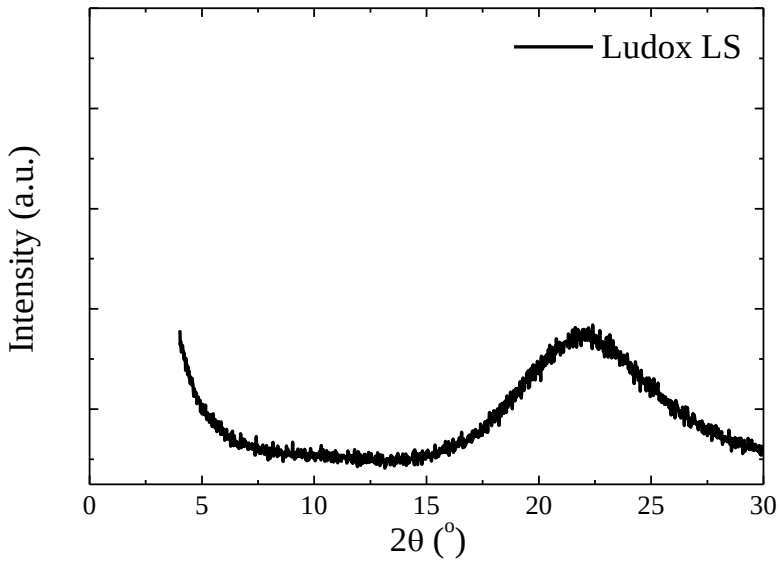

Figure 4.1: X-ray diffractogram of silica nanoparticles.

The Ludox LS silica nanoparticles that were utilized were in aqueous dispersion thus the appropriate amount was dried in a vacuum oven prior the characterization of their structure and properties.

The structural characterization of the nanoparticles was performed by XRD. The nanoparticles were dried under vacuum and annealed at 100 °C for 30 minutes to ensure that no water remained in the sample. **Figure 4.1** shows the X-ray diffractogram of Ludox LS nanoparticles. Only a very broad peak can be observed that is characteristic of amorphous materials.

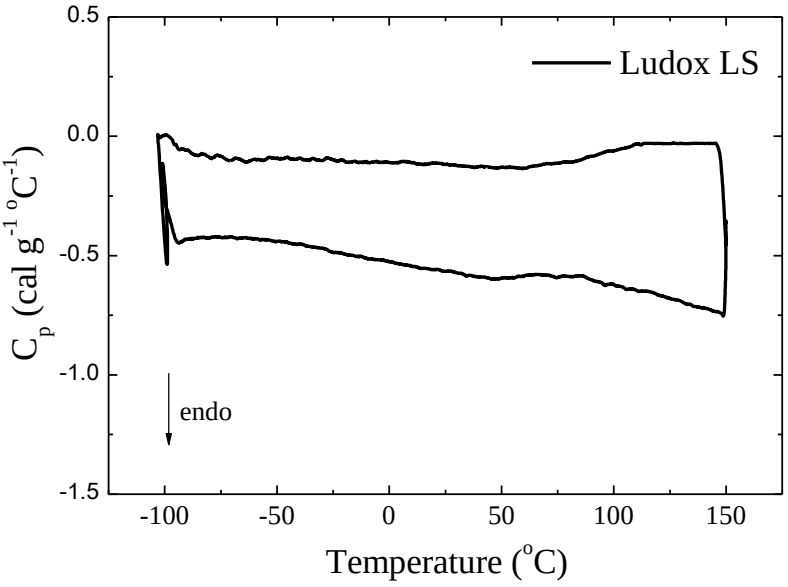

Figure 4.2: DSC measurement of silica nanoparticles.

The amorphous state of the nanoparticles is confirmed by DSC as shown in **Figure 4.2**. The nanoparticles were dried and annealed at 100 °C for 30 minutes and placed in the DSC crucibles in a powder state. The measurement shows no thermal transition, as expected.

Figure 4.3 shows the TGA curve for Ludox LS. The TGA measurement was conducted at a constant heating rate of 10 °C/min. An initial loss of about 6 wt % is attributed to the loss of water in temperatures around 100 °C and an additional weight loss of ~4 wt % in higher temperatures is observed attributed to the loss of absorbed water and dehydration of the residual silanol groups.

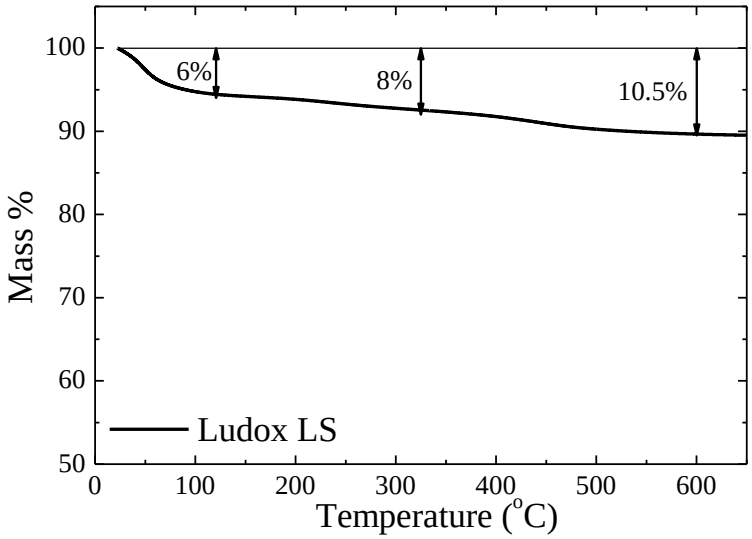

Figure 4.3: TGA measurement of silica nanoparticles.

4.2 Biobased Linear Polyesters / Silica Nanoparticles

In the present work the biobased linear polyesters EG-110, DG-110 and HD-110 were mixed with silica nanoparticles via solution mixing. The polymer was first dissolved in water, the respective amount of nanoparticle dispersion was added in the solution under continuous stirring and then dried under vacuum. Finally, all samples were thermally annealed at 130 °C under vacuum in order to erase any thermal history, and then cooled down to room temperature at a constant rate of 10 °C/min, in order to ensure the same crystallizing conditions (for the semi-crystalline ones). The structure of the synthesized hybrids was examined by XRD, their thermal stability was investigated by TGA, and DSC was utilized to study the effect of the additive on the thermal properties of the three polyesters.

4.2.1 Structural characterization of polyester / silica nanoparticle hybrids

Figure 4.4 shows XRD measurements of the EG-110 / SiO_2 and the HD-110 / SiO_2 nanocomposites, while increasing the amount of inorganic surfaces, together with the diffractogram of the pure amorphous silica and the pure polymers. Since both polymers are semi-crystalline peaks due to their crystalline structure can be observed.

The crystallinity of both polymers is clearly affected in the nanocomposites since the intensity of the crystalline peaks is gradually decreasing upon addition of nanoparticles. For the nanocomposite with 32 wt % EG-110 content, only a wide halo is observed, indicating amorphous structure. At the same concentration HD-110 is mainly but not completely

amorphous; this structure is indicated by the two crystalline peaks of very low intensity observed in Figure 4.4.b. It is noted that the crystalline peaks of the nanocomposites are observed at the same angles to the bulk polymers.

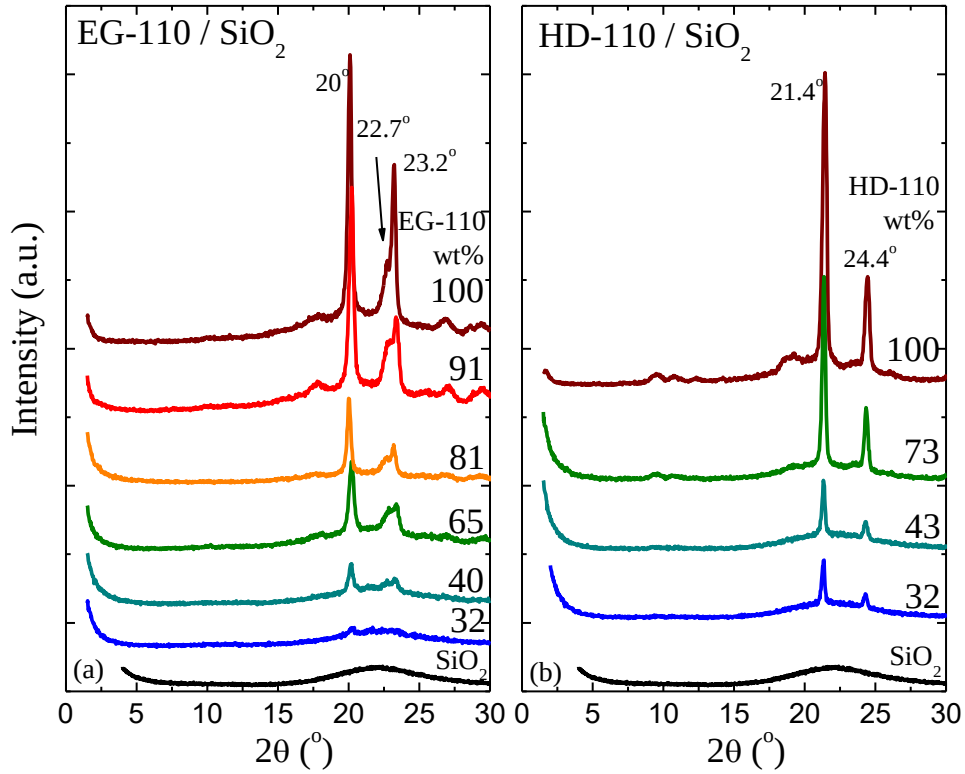

Figure 4.4: X-ray diffractograms of EG-110/ SiO_2 (a) and HD-110/ SiO_2 (b) nanohybrids. The curves have been shifted vertically for clarity.

A similar behavior was observed when another semi-crystalline polymer, poly (ethylene oxide), PEO, was investigated in PEO / silica nanocomposites; in that case polymer chains that were either confined or adsorbed on the surface of the particles could not crystallize; it was only the excess polymer that was able to crystallize, obtaining the same structure of the bulk polymer. [1], [2]

4.2.2 Thermal properties of polyester / silica nanoparticle hybrids

The thermal stability of all nanocomposites was determined by TGA measurements as illustrated in Figure 4.5. As discussed in Chapter 3 for the bulk polyester EG-110 the thermal degradation shows two steps, one due to the volatilization of the residual monomers and the main degradation of the polymer chain. In Figure 4.5.a it can be observed that nanocomposites with low polymer concentration (below 40 wt %) exhibit only the main degradation step, probably due to the lower amount of the volatile substances. The thermal

stability of EG-110 in the nanocomposites is found reduced compared to the bulk since the most probable degradation temperature is decreasing with increasing the amount of inorganic nanoparticles. More specifically, T_d=415, 415, 393, 388, 380 and 375 °C for 100, 91, 81, 65, 40 and 32 wt % respectively.

The same behavior holds for the DG-110 / SiO_2 nanohybrids as well, where T_d= 420, 403, 386 and 385 °C for 100, 56, 41 and 27 wt % respectively, i.e. it is significantly reduced with the increase in the amount of additive. The thermal stability of the HD-110 in nanohybrids is similar to the bulk polymer with its degradation rate maximum T_d=405, 406, 404 and 401 °C for 100, 73, 43 and 32 wt % respectively. This difference in the thermal stability of HD-110 in nanocomposites could be related to the more stable aliphatic character of its polymer chain that is not affected by the silica.

In nanocomposites with high loadings in silica, a continuous weight loss is observed which appears like a step for the HD-110/SiO_2 nanocomposite. This weight loss at temperatures above the polymer degradation and only in high silica loadings must be related to the dehydration of the residual silanol groups discussed above.

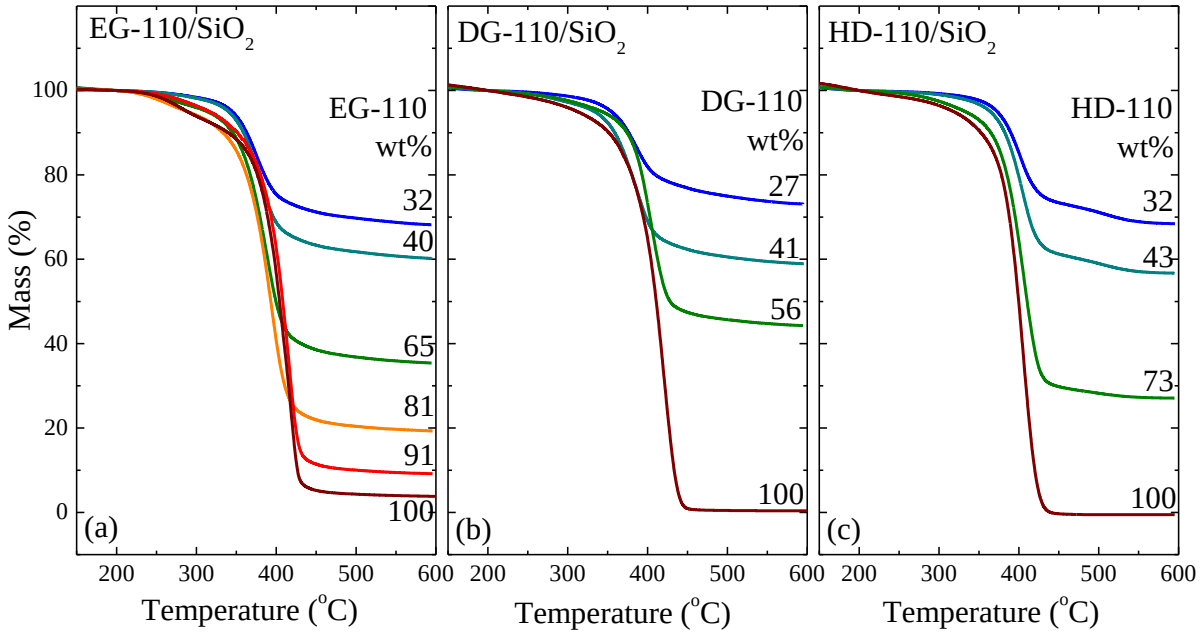

Figure 4.5: TGA measurements of EG-110 / SiO_2 (a), DG-110 / SiO_2 (b) and HD-110 / SiO_2 (c) nanohybrids.

The thermal properties of the polyesters in the nanohybrids were examined by DSC and the measurements expressed as specific heat, C_p, are shown in **Figure 4.6**, **Figure 4.7** and **Figure**

4.8. For the calculation of the heat capacity in the case of the hybrids, only the polymer mass is considered, since the contribution of the inorganic material to the C_p is an additive constant that would not influence thermal transitions.

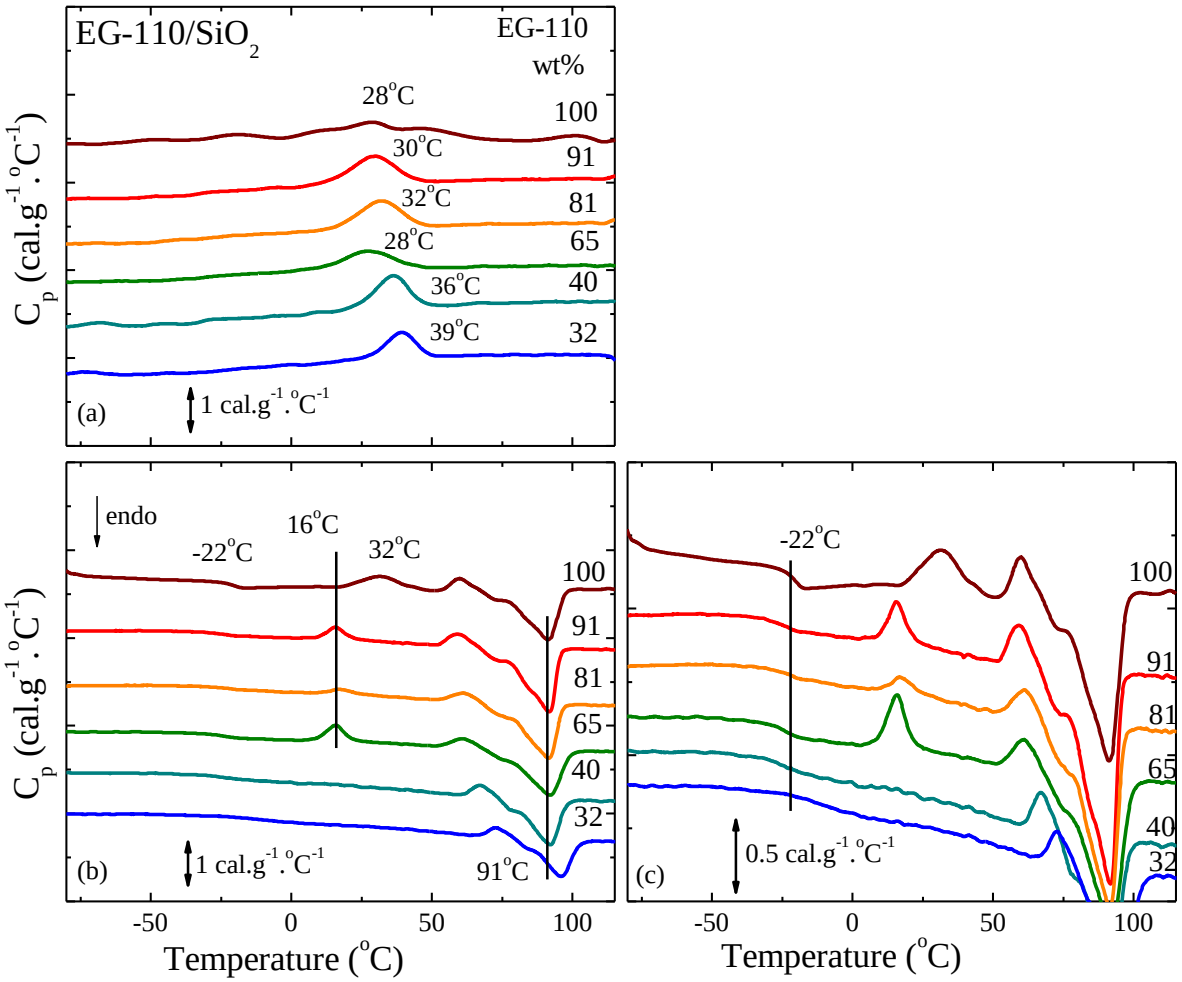

Figure 4.6: DSC measurements of EG-110 / SiO_2 nanohybrids during cooling (a) and heating (b). For clarity the heating is also presented in different scale (c) and the curves have been shifted vertically.

The bulk EG-110, discussed in Chapter3, crystallizes mainly through a cold crystallization mechanism during heating when the cooling rate is 10°C/min. In contrast to the pure polymer that shows a very weak crystallization exotherm at T_c = 28 °C, the nanocomposites show in general a more pronounced crystallization transition during cooling (**Figure 4.6**.a). The crystallization temperature is similar or higher than the respective of the bulk and reaches T_c = 39 °C for the nanohybrid with 32 wt % EG-110. This behavior is similar to the nanocomposites of the EG-110 with Na^+-MMT utilized as the additive, where the crystallization under cooling is enhanced in low loadings of the clay and will be also discussed in Chapter 6. [3]

During heating (**Figure 4.6**.c), the glass transition is observed at T_g = -22 °C for the pure polymer; this transition is observed in nanocomposites, as well, although it becomes very weak. The temperature where the glass transition appears for the nanohybrids is very similar to the bulk and the ΔC_p is reduced from 0.16 cal/g for the bulk EG-110 to 0.10-0.12 cal/g for the nanocomposites. Furthermore, for the lower polymer content nanocomposite, 32 wt %, the glass transition becomes too wide or very weak to be clearly discussed. Above the glass transition temperature, the main exothermic peak that is observed for the pure EG-110 at T_{c1} = 32 °C appears only above 65 wt % polymer content nanocomposites. The cold crystallization peak is weaker than the one in the bulk polymer and appears shifted at lower temperatures, T_{c1} =16 °C. This behavior indicates that the silica particles accelerate the crystallization of the polymer. In the bulk the heating rate of 10 °C / min is very high and the polymer does not have enough time to crystallize while by adding the silica nanoparticles, at the same heating rate, the majority of the chains are able to crystallize during cooling; there is only a small quantity of the polymer that crystallize during heating at T_{c1} = 16 °C, temperature lower than the bulk. The second weak exotherm that is observed for pure EG-110 at T_{c2} = 60 °C is noticed in all nanocomposites; the temperature T_{c2} shifts towards higher temperatures for the nanocomposites above 40 wt % and reaches the value of T_{c2} = 73 °C for the lower in polymer content nanocomposite, 32 wt % EG-110.

The main melting of the polymer in nanocomposites is observed at T_m = 91 °C, similarly to the bulk. It is only the 32 wt % in polymer content nanohybrid, that shows a higher melting temperature, at T_m = 97 °C. Nevertheless, the amplitude of the melting peak is clearly decreasing by increasing the amount of the additive in accordance to the XRD measurements, where the intensity of the crystalline peaks was also decreasing. This behavior could be attributed to the polymer chains adsorbed on the surfaces of the silica nanoparticles. Although the "free" polymer in the presence of the additive crystallizes faster than the bulk, the adsorbed polymer cannot crystallize.

The thermal behavior of the DG-110 / SiO_2 nanocomposites during heating with a rate of 10 °C/min expressed as specific heat, C_p, is shown in **Figure 4.7** together with the thermogram of the pure DG-110. As discussed in Chapter 3 this polymer is amorphous exhibiting a glass transition at T_g = -26 °C and ΔC_p= 0.32 cal/g. It is evident that the glass transition is weaker and broader for the nanocomposites with ΔC_p=0.20 cal/g, nevertheless, it is observed in all

concentrations. In all cases, the T_g for the nanohybrids is observed at a temperature T_g = -31 °C which is lower than the respective of the bulk.

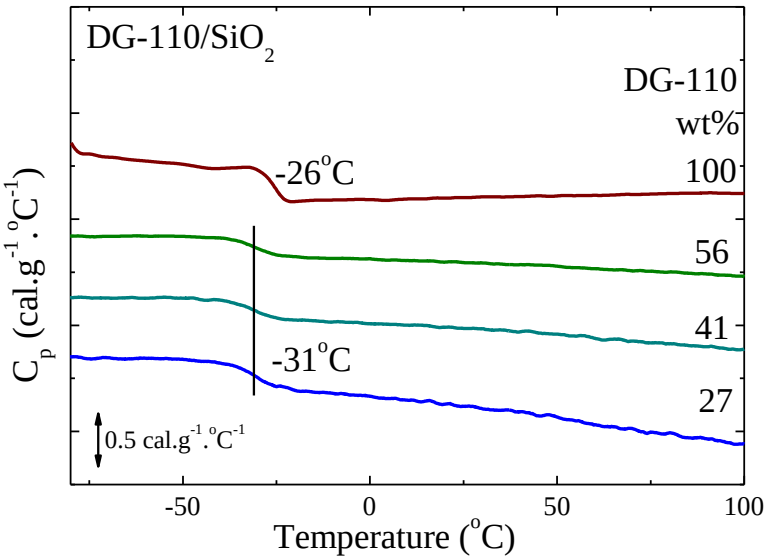

Figure 4.7: DSC measurements of DG-110 / SiO_2 nanohybrids during heating. The curves have been shifted vertically for clarity.

The DSC measurements of the nanohybrids composed of HD-110 and silica particles are shown in **Figure 4.8**. The pure polymer shows a very strong crystallization exotherm at T_c = 26 °C, whereas the nanocomposites show a weaker crystallization peak at similar temperatures, **Figure 4.8**.a.

During heating (**Figure 4.8**.b and **Figure 4.8**.c), the glass transition is observed at T_g = -45 °C for the pure polymer; this transition is completely suppressed for the nanocomposites. Above the glass transition temperature, the melting of the polymer is observed at temperatures similar to the bulk HD-110; the melting temperature does not show any dependence on the composition. On the other hand the heat of fusion is decreasing by increasing the amount of the additive at ΔH=17.78, 13.93 and 11.81 cal/g compared to the 23.44 cal/g of the bulk polymer.

The decrease of the thermal transitions with increasing the content of the additive in the nanocomposites is in agreement with the results of XRD measurements which showed that at the respective concentrations the crystalline diffraction peaks are very weak as well.

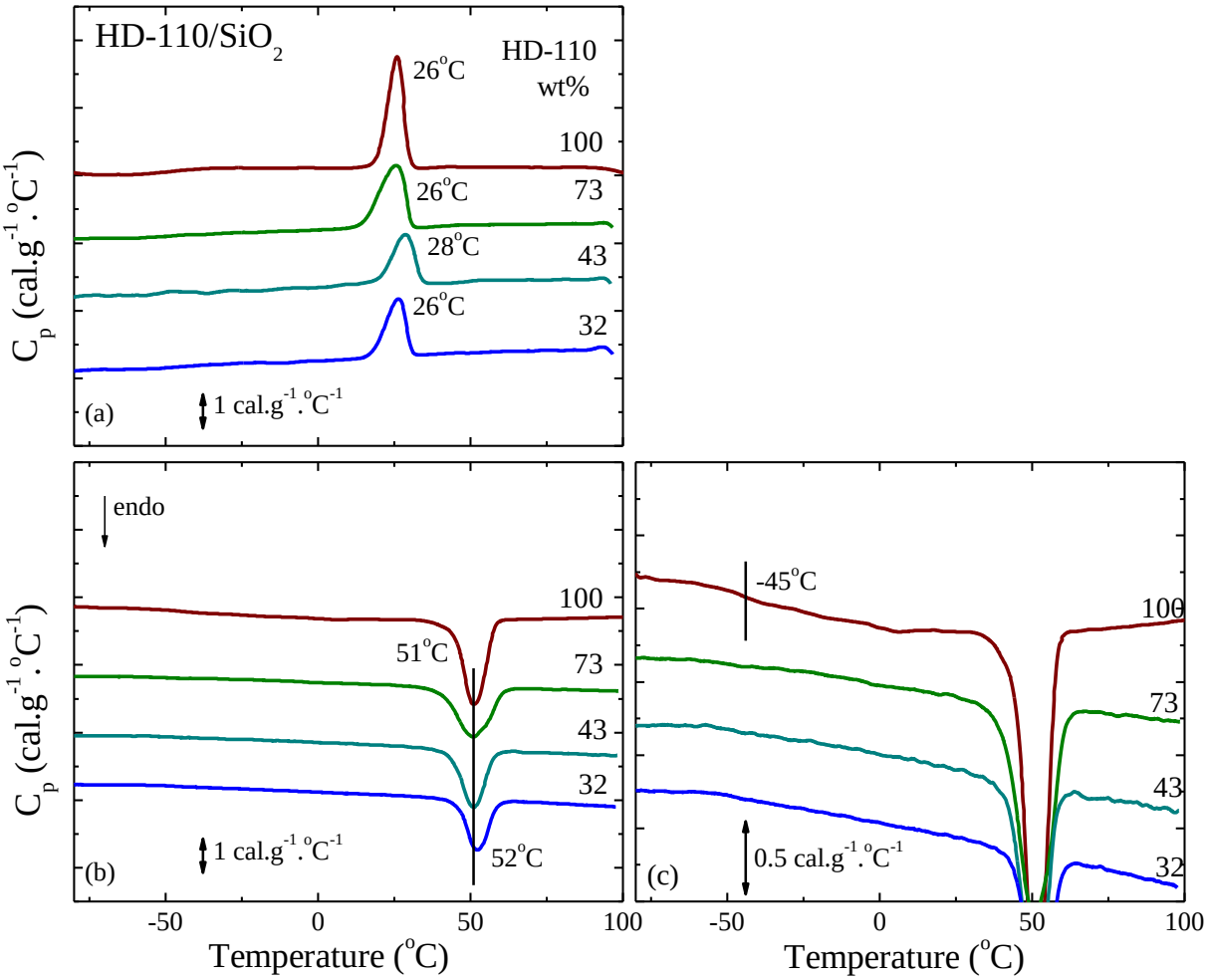

Figure 4.8: DSC measurements of HD-110 / SiO_2 nanohybrids during cooling (a) and heating (b). For clarity the heating is also presented in different scale (c) and the curves have been shifted vertically.

In another system of semi-crystalline polymer nanocomposites in which poly (ethylene oxide) was mixed with SiO_2, for nanocomposites with less than 35 wt % in polymer, DSC measurements showed double melting and crystallization peaks attributed to a different crystallization mechanism of the polymer close to the silica surfaces. [2] The HD-110 does not show similar behavior probably due to the different interactions between the polymer chains and the SiO_2 and/or to its lower molecular weight and thus smaller size compared to the radius of the nanoparticles.

Although the thermal transitions of the polyesters are not completely suppressed, the adsorption of the polymer chains on the surfaces can decrease the crystallinity and affect their properties (**Table 4.1**).

Table 4.1: Thermal characteristics of the neat polymers and of their nanocomposites.

Sample Polymer / SiO_2	T_g (°C)	T_c (°C)	T_{c1} (°C)	T_{c2} (°C)	T_m (°C)	Degradation Temperature (°C)
EG-110	-22	28	32	60	91	415
91wt% / 9wt%	-25	30	16	60	91	415
81wt% / 19wt%	-21	32	16	60	91	393
65wt% / 35wt%	-23	28	16	60	91	388
40wt% / 60wt%	-23	36	-	67	91	380
32wt% / 68wt%	-	39	-	73	96	375
DG-110	-26					420
56wt% / 44wt%	-31		No crystallization			403
41wt% / 59wt%	-31		No melting			386
27wt% / 73wt%	-31					385
HD-110	-45	26			51	405
73wt% / 27wt%	-	26	No cold		51	406
43wt% / 57wt%	-	28	crystallization		51	404
32wt% / 68wt%	-	26			52	401

4.3 Polymer Dynamics in Silica Nanocomposite Materials

In previous studies, the effect of the silica nanoparticles on polymer dynamics was investigated. [1], [4]–[6] The dynamic response of the polymer chains in the case of poly (ethylene oxide) showed that the nanocomposites could obtain similar of slightly faster dynamic behavior than that of the bulk polymer. [1], [5] Concerning another polyester, PLLA, faster dynamics were observed in silica nanocomposites, as well, both for the local and the segmental dynamics. [6] On the other hand the interfacial dynamics of the styrene-butadiene random copolymer with composition 27 wt % in styrene are slower when silica is added. [4]

In the present work polymer dynamics are investigated for the nanocomposites of two linear biobased polyesters, EG-110 and DG-110, in compositions where the majority of the polymer is in the vicinity on the additive surface. The dynamics in nanocomposites of ~30 wt % polymer are compared to the respective of the bulk presented in Chapter 3.

In the case of the linear biobased polyester nanocomposites, the powder was pressed to form disks of 12 mm in diameter and 0.3-0.6 mm in thickness. The pellets were annealed at 120 °C in vacuum for 24 hours and adhered between indium foils to improve the electrical contact with the electrodes.

Polymer dynamics are investigated in EG-110 / SiO_2 and DG-110 / SiO_2 nanocomposites at a broad temperature range and the imaginary part of the complex permittivity, ε'', as a function of frequency is presented in **Figure 4.9**. At low temperatures, relaxation processes can be observed, however, the spectra exhibit strong noise as well (**Figure 4.9**.a and c). At higher temperatures, close to the glass transition temperature of each polymer, another relaxation process is observed partially obscured by the conductivity (**Figure 4.9**.b and d). Further than the qualitative observations, a more quantitative analysis of the spectra is necessary in order to determine the relaxation processes and compare the findings.

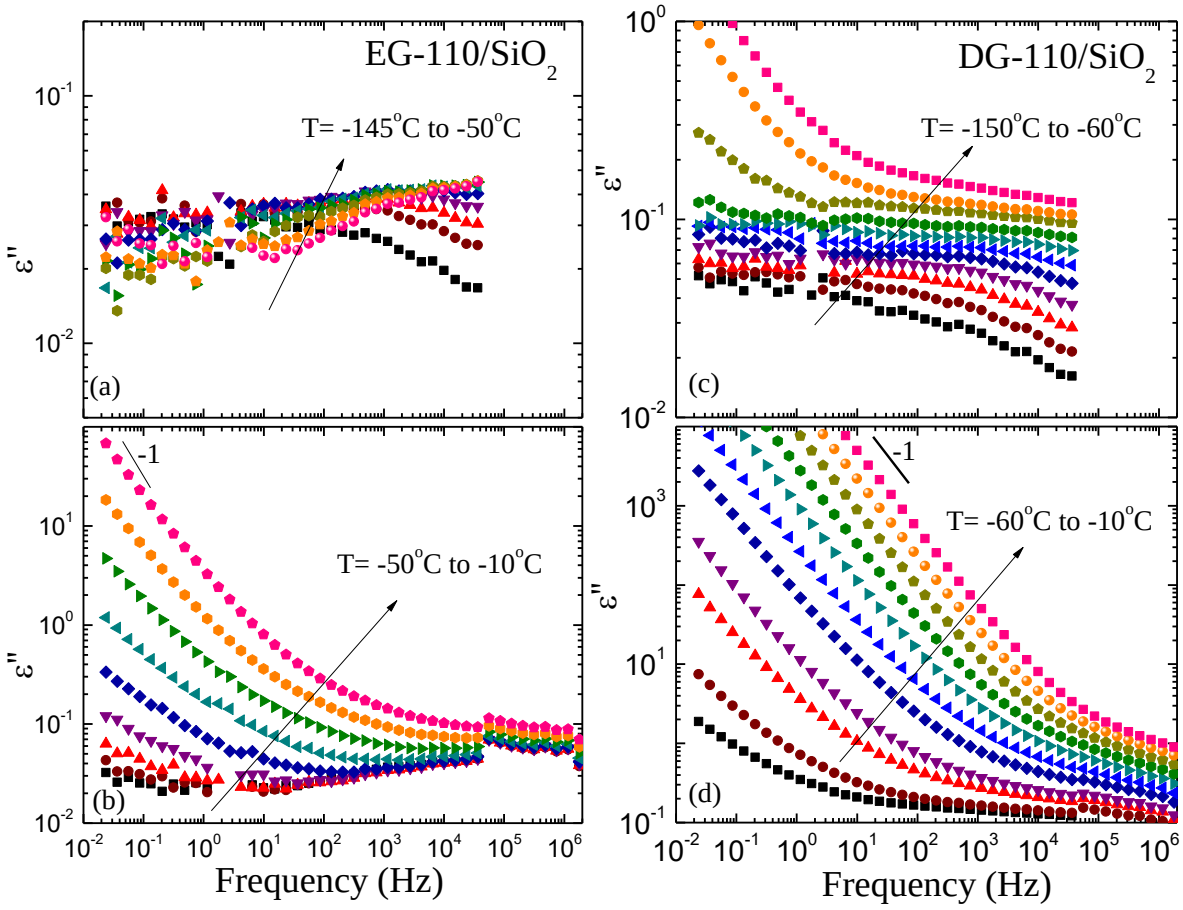

Figure 4.9: Imaginary part of the complex dielectric permittivity, ε'', of EG-110 / SiO_2 (a,b) and DG-110 / SiO_2 (c,d) nanocomposites as a function of frequency, for the low (a,c) and the high (b,d) temperature regime.

Figure 4.10 illustrates the quantitative analysis of the dielectric data at two different temperatures, for the EG-110 and DG-110 nanocomposites. The $\varepsilon^*(\omega)$ data were analyzed utilizing the empirical Havriliak - Negami (HN) functions whereas when necessary an ionic conductivity contribution was added. In spite of the noise in the data at low temperatures two sub-T_g processes are observed for both polyesters (Figure 4.10.a and c).

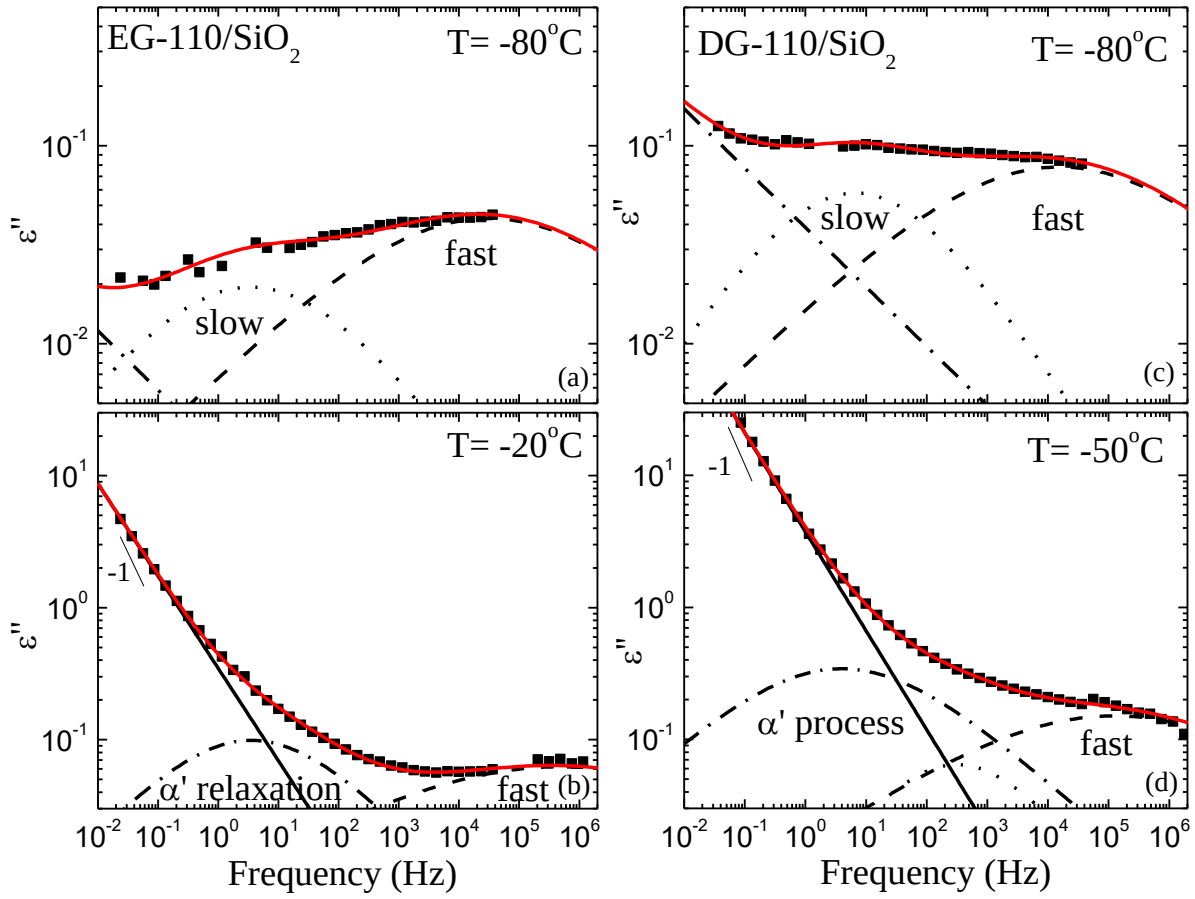

Figure 4.10: Imaginary part of the dielectric permittivity, ε'', of EG-110 / SiO_2 at (a) T= -80 °C and (b) T= -20 °C and of DG-110 / SiO_2 at (c) T= -80 °C and (d) T= -50 °C. The processes needed for the deconvolution of the spectra are shown with black lines, whereas the red lines are the summations of the processes.

For both the EG-110 and DG-110 nanocomposites, the shape parameter β of all three processes is fixed to 1.0. For the fast sub-T_g process the α parameter varies between 0.22 - 0.3 and the dielectric strength Δε increases with increasing temperature taking values 0.3 - 0.5 for the EG-110 and 0.45 – 2 for the DG-110. For the slower sub-T_g process the shape parameter α is similar for the two polymers and it is determined to be 0.27 - 0.45. For the EG-110 a relatively low relaxation strength of ~0.1 is obtained whereas for the DG-110 this process is stronger with a relaxation strength of Δε = 0.4 to 0.3. At higher temperatures, the

segmental relaxation process appears with shape parameter α around 0.35 - 0.55. The dielectric strength $\Delta\varepsilon$ decreases with temperature from 0.7 to 0.4 for the semi-crystalline EG-110 whereas for the amorphous DG-110 $\Delta\varepsilon$ takes higher values from 2.2 to 1.8. To differentiate the segmental relaxation process of the bulk polymer (α-process) to the respective of the nanocomposite, we will name the one of the nanocomposites with the same Greek letter followed by a prime apex (α'-process). It is noted that the contribution of the conductivity, for the nanocomposites of the EG-110 and DG-110, is denoted as a line with slope 0.7 and 0.75 respectively.

In **Table 4.2** the results for the three relaxation processes observed in EG-110 / SiO_2 and DG-110 / SiO_2 nanocomposites are presented.

Table 4.2: Parameters of the HN function for each relaxation process.

HN Parameters	Polymer / SiO_2 EG-110	Polymer / SiO_2 DG-110
Fast process		
β	1	1
α	0.23-0.3	0.22 - 0.3
Δε	0.3-0.5	0.45 - 2
Slow process		
β	1	1
α	0.3-0.42	0.27 - 0.45
Δε	0.1	0.4 to 0.3
α′-process – segmental motion		
β	1	1
α	0.4–0.55	0.35 - 0.52
Δε	0.70-0.40	2.2 to 1.8

Figure 4.11 shows the relaxation times of the EG-110 and DG-110 nanocomposites together with the respective ones for the relaxation processes observed in the bulk polymers, as solid lines. The three relaxation processes (two sub-T_g and the segmental) observed for the bulk polyesters are present in the nanocomposites as well; nevertheless their relaxation times

exhibit both similarities and differences in comparison with the corresponding dynamics of the polymers.

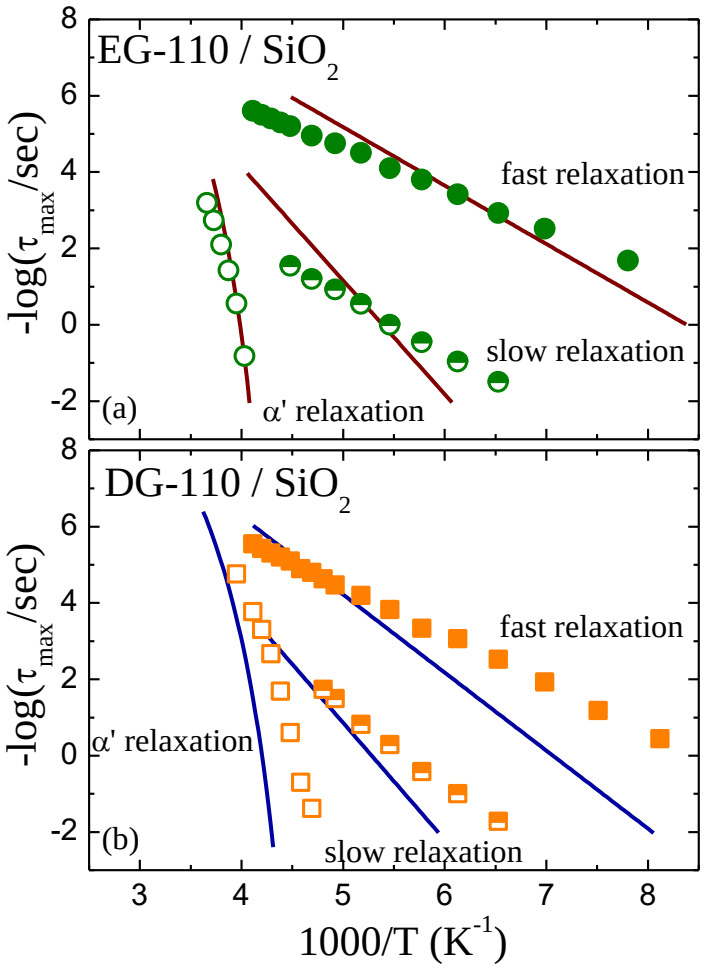

Figure 4.11: Arrhenius relaxation map of EG-110/ SiO_2 (a) and DG-110/ SiO_2 (b). The solid lines correspond to the relaxation processes of the pure polymer.

At low temperatures the two sub-T_g processes appear, following Arrhenius temperature dependencies. In both EG-110 / SiO_2 and DG-110 / SiO_2 nanocomposites due to the different dependencies of each of the sub-T_g processes in nanohybrids to the respective of the bulk, the relaxation times are crossing.

Both processes in the nanohybrids exhibit lower activation energies than those of the respective neat polymer. The activation energies of the fast processes are 20 ± 0.5 kJ/mol for the EG-110 / SiO_2 and 24 ± 1 kJ/mol for the DG-110 / SiO_2, whereas the slow processes obtain activation energy of 28 ± 2 kJ/mol for the EG-110 / SiO_2 and 36 ± 2 kJ/mol for the DG-110 / SiO_2, indicating that the motions become less restricted in nanocomposites. These results are summarized in **Table 4.3** together with the respective of the neat polymers.

For the EG-110 nanocomposite the obtained relaxation times of the segmental process are similar with the respective ones of the neat polymer following a VFT temperature dependence. On the other hand for the DG-110 nanocomposite the segmental relaxation is faster than the segmental of the bulk polymer and a VFT temperature dependence is observed as well. It is noted that for this nanohybrid the T_g was found at -30 °C, i. e., 4 °C lower than the bulk, by DSC.

To minimize the error in the fitting of the data with the VFT equation and to be consistent with the bulk, the value of $\tau_0 = 10^{-13}$ is kept fixed. The resulted parameters obtained by the fitting of the data with the VFT equation are B = 1830 ± 20 K and T_0 = 190.0 ± 2.0 K resulting in fragility parameter $D = B/T_0 \sim 9.6$ for the EG-110, and B = 1602 ± 30 K and T_0 = 167.0 ± 2.0 K resulting in $D = B/T_0 \sim 9.6$ for the DG-110, nanohybrids. It is noted that the fragility parameter of the respective polymers in the bulk is $D_{EG\text{-}110} = 6.2$ and $D_{DG\text{-}110} = 5.9$ as mentioned in Chapter 3. In **Table 4.3** the activation energies, the VFT equation parameters and the fragility parameters of both nanocomposites are summarized together with the respective of the bulk polymers.

The local motions appear to be more affected by the additive due to the interactions of the dipoles, in ester and hydroxyl groups, with the silica surface. However, the segmental dynamics remains similar to the bulk or faster with a more Arrhenius temperature dependence; this not significant effect on the segmental relaxation, has been observed for the poly (ethylene oxide) nanocomposites with high silica loadings as well. [1]

Table 4.3: Results of the relaxation processes for the linear polyesters in nanocomposites.

Material	Fast process E_a (kJ/mol)	Slow process E_a (kJ/mol)	α-relaxation	Fragility parameter
EG-110	30 ± 1	59 ± 1	B = 1286 ± 5 K T_0 = 208.0 ± 3 K	6.2
EG-110 / SiO_2	20 ± 0.5	28.0 ± 2.0	B = 1830 ± 20 K T_0 = 190 ± 2 K	9.6
DG-110	38 ± 1	60 ± 2	B = 1177 ± 5 K T_0 = 199.0 ± 1 K	5.9
DG-110 / SiO_2	24 ± 1	36 ± 2.0	B = 1602 ± 30 K T_0 = 167 ± 2 K	9.6

4.4 Effect of the Silica Nanoparticles on Polymer Properties

The three linear biobased polyesters EG-110, DG-110 and HD-110 were mixed with silica nanoparticles in order to investigate the effect of the additive on the structure, the thermal properties and the thermal stability of the polymer.

In the case of the semi-crystalline polymers EG-110 and HD-110, the crystallinity is decreased by increasing the content of the additive, as shown by both XRD and DSC. The crystallization and melting temperatures of the polymers in the nanocomposites are similar to the respective in the bulk. The semi-crystalline polymer, EG-110, in the bulk exhibits very slow kinetics, therefore a cold crystallization is evident; in the nanocomposites the crystallization is observed partially during cooling and partially during heating. This behavior can be attributed to the silica as a nucleating agent which enhances the crystallization kinetics when added in low loadings in the polymer matrix. On the other hand, in nanocomposites with high loadings of silica nanoparticles, the crystallinity is suppressed probably due to the adsorption of the polymer chains on the surfaces of the additive and / or due to chain confinement.

As far as the glass transition is concerned, the change in the heat capacity of the nanocomposites is lower than that of the bulk polymer both for the amorphous DG-110 and the semi-crystalline EG-110, whereas for the HD-110 nanohybrids the transition cannot be detected because it is either too wide or suppressed.

Finally the thermal degradation of the polymer in nanohybrids is observed at similar or lower temperatures to the respective in the bulk.

The dynamics of the semi-crystalline EG-110 and the amorphous DG-110 in the nanocomposites, investigated by dielectric relaxation spectroscopy, reveal the effect of the silica additive on both local and segmental dynamics. In both cases, the two sub-T_g local motions in the nanocomposites are less restricted possessing lower activation energies. Moreover, the segmental dynamics show differences in EG-110 and DG-110 nanocomposites, following the trend of the glass transition temperatures obtained by DSC for the nanocomposites, although for the specific nanohybrid, 32wt% EG-110/SiO_2, the T_g could not be clearly determined. In the case of the EG-110 nanocomposite the segmental dynamics are similar to the bulk, whereas for the DG-110 the relaxation times are faster. For both EG-110 and DG-110 nanocomposites the VFT temperature dependence is retained.

4.5 References

[1] H. Papananou, “Polymer structure and dynamics under confinement,” PhD Thesis, University of Crete, 2017.

[2] H. Papananou, E. Perivolari, K. Chrissopoulou, and S. H. Anastasiadis, “Tuning polymer crystallinity via the appropriate selection of inorganic nanoadditives,” *Polymer (Guildf).*, vol. 157, no. September, pp. 111–121, 2018.

[3] K. Androulaki, K. Chrissopoulou, D. Prevosto, M. Labardi, and S. H. Anastasiadis, “Structure and Dynamics of Biobased Polyester Nanocomposites,” *Biomacromolecules*, vol. 20, no. 1, pp. 164–176, 2019.

[4] L. T. Vo, S. H. Anastasiadis, and E. P. Giannelis, “Dielectric study of Poly(styrene- co -butadiene) Composites with Carbon Black, Silica, and Nanoclay,” *Macromolecules*, vol. 44, no. 15, pp. 6162–6171, 2011.

[5] S. Choudhary and R. J. Sengwa, “Dielectric dispersion and relaxation studies of melt compounded poly(ethylene oxide)/silicon dioxide nanocomposites,” *Polym. Bull.*, vol. 72, no. 10, pp. 2591–2604, 2015.

[6] P. Klonos and P. Pissis, “Effects of interfacial interactions and of crystallization on rigid amorphous fraction and molecular dynamics in polylactide / silica nanocomposites : A methodological approach,” *Polymer (Guildf).*, vol. 112, pp. 228–243, 2017.

5 Polymer / Graphite Oxide Nanocomposites

The three generations of the hyperbranched polyester polyols, Boltorn, as well as the hyperbranched poly (ester amide), Hybrane, studied in Chapter 3, were mixed with a hydrophilic graphite oxide in order to investigate the effect of the interfacial interactions and the confinement that the GO layers impose on the structure of the nanocomposites as well as on the polymer properties. The effect of the degree of branching of the Boltorn polyesters and the different functionality set by the amide group of the Hybrane in nanohybrids are discussed as well.

All nanocomposites, investigated by X-ray diffraction, reveal intercalated structure and suppressed thermal transitions compared to the respective of the polymers in the bulk. Polymer dynamics in graphite oxide nanocomposites, examined by Broadband Dielectric Spectroscopy, are compared with that of the respective bulk polymers; the local dynamics exhibit lower activation energies and the segmental relaxation in all cases show different temperature dependencies than in the bulk.

5.1 Graphite Oxide Characterization

The structure of the graphite oxide is examined by X-ray diffraction as illustrated in **Figure 5.1**. The measurement was performed after the GO was kept in vacuum for 24 hours in order to remove humidity. Its layered structure is confirmed by a strong peak at 2θ = 10.5° corresponding to an interlayer distance of 0.84 nm. GO was annealed at 120 °C overnight under vacuum in order to remove the water adsorbed on the surface of the layers and its main peak appears to be shifted in XRD at 2θ = 12.7 ° corresponding to 0.70 nm. Finally graphite oxide was thermally reduced at 200 °C overnight in vacuum; [1] following the reduction the layered structure of GO is destroyed and an exfoliated structure is obtained showing a broad halo. The thermal reduction of the GO does not result in a layered structure similar to the graphite with a sharp peak at 2θ = 26.7° despite the removal of the different oxygen groups. [2]

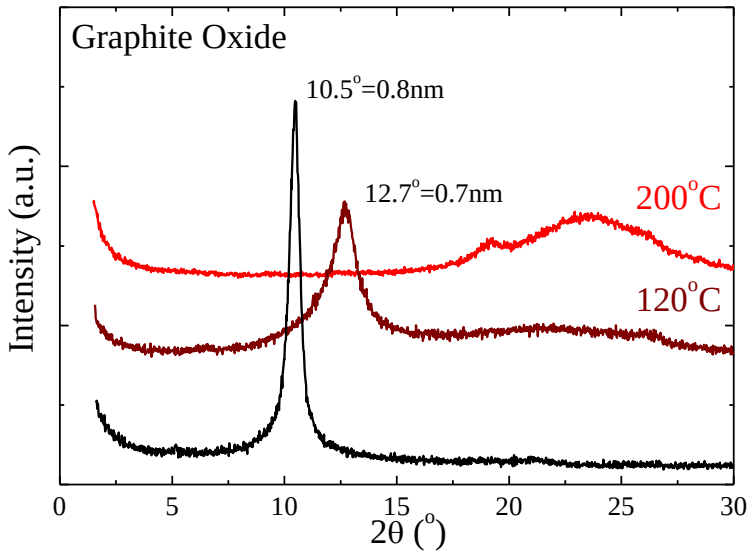

Figure 5.1: X-ray diffractograms of Graphite Oxide before and after thermal annealing at 120°C and thermal reduction at 200°C.

The thermal stability and the reduction of GO was investigated by TGA as shown in **Figure 5.2**. The humidity and the water adsorbed by the graphite oxide is removed up to 135 °C where the 17 wt % of the total mass is lost. Above 140 °C deoxygenation reactions occur in two steps probably due to the different functional groups (i.e. hydroxyl, ether, carbonyl oxygens) and at 600 °C there is only a residual of 41 wt % of the total mass. As shown is the inset, the thermal reduction happens at the most probable temperature of 205 °C. Above 600 °C (not shown) there is a further mass loss that corresponds to carbon combustion but is beyond the interest of this research. [3]

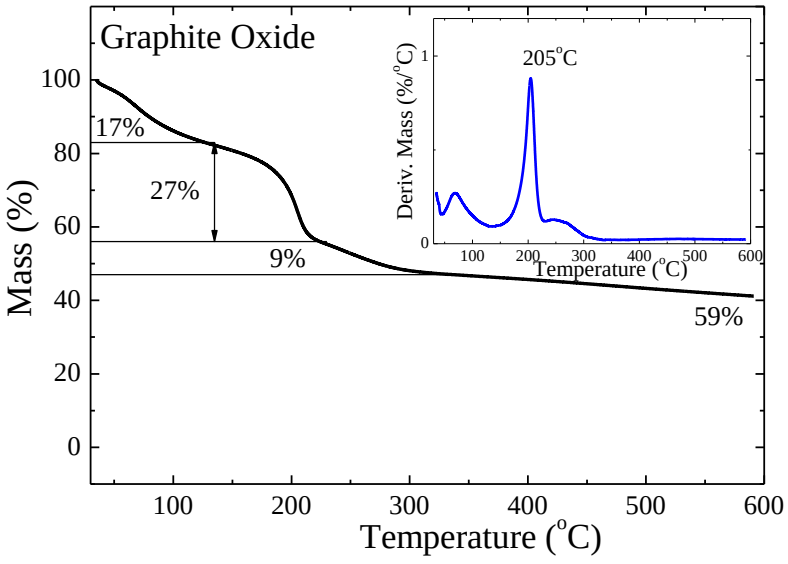

Figure 5.2: TGA measurement of Graphite Oxide. The first derivative is shown in the inset.

The thermal properties of the graphite oxide were investigated by DSC. The highly exothermic thermal deoxygenation of GO is illustrated in **Figure 5.3**. In accordance to the TGA measurement the GO is stable up to 140 °C where a small endothermic peak is observed before the main exotherm transition. As mentioned in the literature, the GO needs a small heat input before the thermal reduction which occurs around 200 °C. [3]

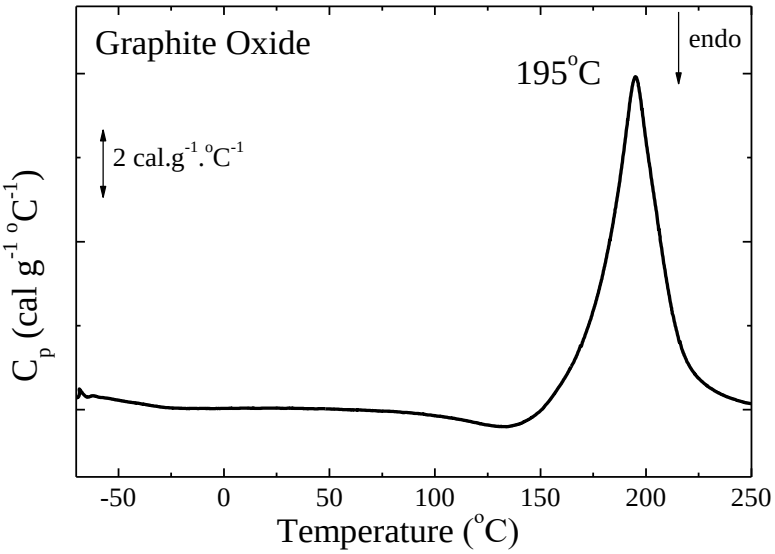

Figure 5.3: DSC measurement of Graphite Oxide.

The thermally reduced GO does not obtain the perfect structure of the graphene sheets;[4] on the other hand it is an easy way to obtain conductive materials with exfoliated structures. [5], [6]

5.2 Hyperbranched Polyesters / GO

Hyperbranched polymer / GO nanocomposites were prepared via a solution-intercalation method using deionized water as the solvent. The required amount of the polymer was first dissolved in water at room temperature, and, then, the respective amount of the graphite oxide was added under continuous stirring in order to ensure that the GO layers were well dispersed. Following the mixing, the suspension was transferred in a petri dish and the solvent was evaporated in a vacuum oven until it was completely dry. The samples were thermally annealed at 120 °C overnight under vacuum to erase any metastable structures formed during solvent evaporation and to achieve equilibrium. In order to examine the effect of the in-situ

thermal reduction of GO on the structure of the nanocomposites, all samples were thermally annealed at 200 °C overnight under vacuum.

5.2.1 Structural characterization of hyperbranched polyester/GO nanohybrids

Nanocomposites comprised of the hyperbranched polymers, Boltorn (H20, H30 and H40) and Hybrane, and graphite oxide, were prepared with 50 wt % polymer content. **Figure 5.4** shows XRD measurements of the hyperbranched polymers / GO nanocomposites after the thermal annealing at 120 °C, together with the diffractograms of the respective bulk polymers and the pure graphite oxide (black solid line in **Figure 5.4**.d).

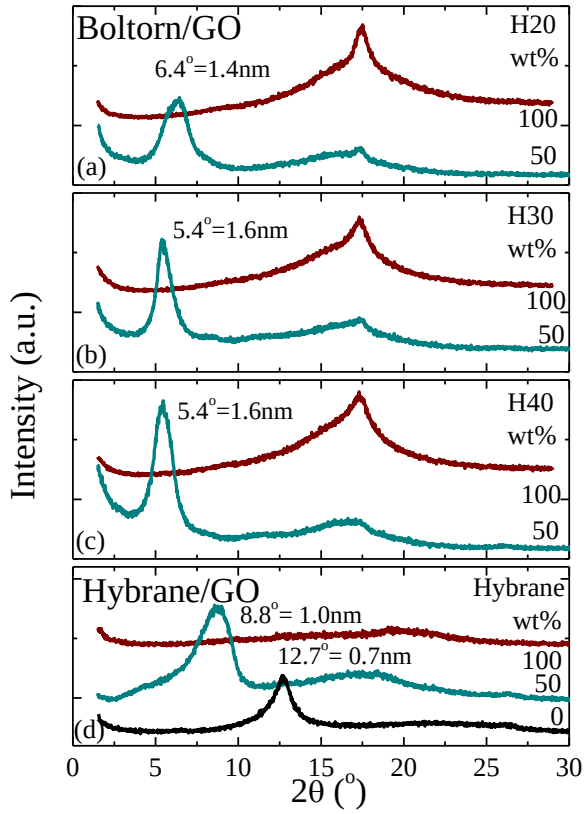

Figure 5.4: X-ray diffractograms of the annealed GO nanohybrids with H20 (a), H30 (b), H40 (c) and Hybrane (d).

For all nanocomposites intercalated structures were obtained, evident by the shift of the main peak of the graphite oxide towards lower angles. For the H20 / GO nanocomposite the peak is observed at 2θ = 6.4° corresponding at an interlayer distance d_{001} = 1.4nm, whereas for both H30 / GO and H40 / GO the interlayer distance is larger, at 1.6nm. For the Hybrane the peak appears at 2θ = 8.8° with d_{001} = 1.0nm, lower than the observed in Boltorn/GO nanocomposites.

The intercalated structures formed in the nanocomposites indicate favorable interactions between the polyesters and the graphite oxide. Taking into consideration the interlayer distance of the pure GO sheets, the thin polymer film formed between them obtains thickness of 0.7 to 0.9nm for the Boltorns, and lower for the Hybrane of 0.3nm. The great number of the hydroxyl and ester groups in the Boltorns could result in stronger interactions with the surfaces of the GO compared to the Hybrane, attributed to hydrogen bonding, so less amount of the Hybrane resides in the galleries of the additive.

5.2.2 Thermal properties of hyperbranched polyester/GO nanohybrids

The thermal properties of all polyesters in nanocomposites were investigated by differential scanning calorimetry (DSC). **Figure 5.5** shows the DSC thermograms of the neat H20, H30, H40, Hybrane and GO together with the respective hybrids of 50 wt % in polymer content. For the calculation of the heat capacity, in the case of the hybrids, only the polymer mass is considered.

The Boltorn/GO nanocomposites with 50 wt % polymer content exhibit no identifiable glass transition, as shown in **Figure 5.5**. At that polymer concentration all or most of the polymer chains are confined and/or reside on the GO surface, thus the absence of a T_g suggests that the transition is suppressed as a result of those interactions.

For the Hybrane / GO nanocomposite although the glass transition can be observed, it appears very wide and weak compared to the bulk. The glass transition temperature of the nanohybrid, is observed below the bulk polymer T_g and can be attributed to a small amount of the polymer which is not confined between the GO sheets but interacts with the additive. This behavior confirms the assumption that for the Hybrane / GO nanohybrids, less polymer chains are under confinement compared to the respective of the Boltorns.

In another example of a semi-crystalline polymer, poly (ethylene oxide) (PEO), in graphite oxide nanocomposites, where the polymer is intercalated into sub-nanometer graphite oxide layers, the thermal properties are suppressed and high-resolution inelastic neutron scattering shows that under these extreme confinement conditions, PEO adopts a planar zig-zag conformation. For these PEO / GO nanocomposites many chain-surface interactions occur the most important/ strong of which being the hydrogen bonds that are formed between the H of the hydroxyl groups of GO and the O of PEO. [7]–[9]

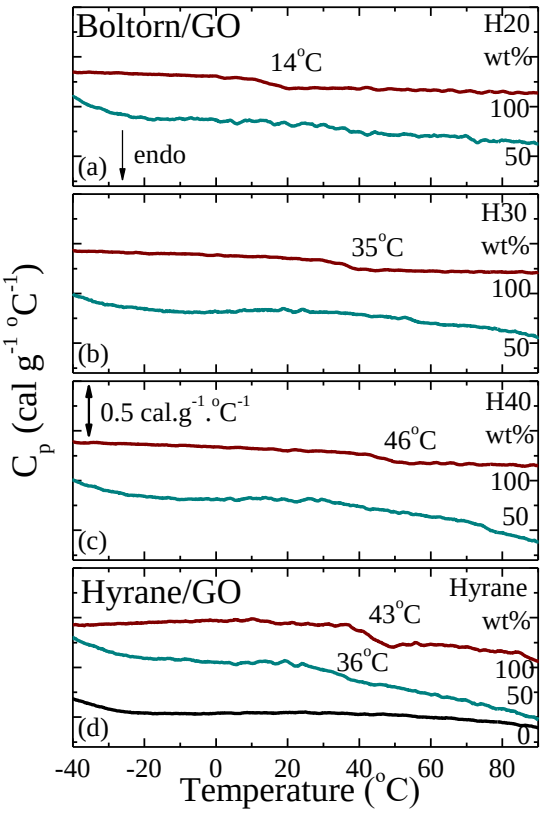

Figure 5.5: DSC measurements of GO nanohybrids with H20 (a), H30 (b), H40 (c) and Hybrane (d) during heating.

In **Figure 5.6** the thermal stability of the nanocomposites is shown measured by TGA. Concerning the thermal stability of the polymers in GO nanocomposites, it appears to be similar between the three generations of the Boltorns, with T_d=390 °C whereas for the Hybrane the main degradation peak is observed at much lower temperature, at T_d=270 °C. It is reminded that the neat Boltorn H20, H30 and H40 showed a main broad degradation step at 388, 380 and 423 °C respectively, which are close to the values observed in GO nanocomposites. The bulk Hybrane degrades mainly at 320 °C (a secondary degradation peak is observed at 435 °C), temperature much higher than in nanocomposites. It is noted that below 100 °C a small weight loss around 7-8 wt % is attributed to the water adsorbed by the nanocomposites and the pure GO.

The reduction of the GO in the Hybrane / GO nanocomposite found at 190 °C is reduced compared to the one of the pure GO that is shown at 205 °C, while for the Boltorn / GO nanocomposites it is found increased, at 230-237 °C. This transition is noted in **Figure 5.6**.a and b by the gray area. The thermal reduction of the graphite oxide results in enhanced thermal stability for the hyperbranched polyester polyols; nevertheless this is reduced for the

poly (ester amide). It is observed that the different functional groups of the polymer matrix affect the reduction temperature for the GO.

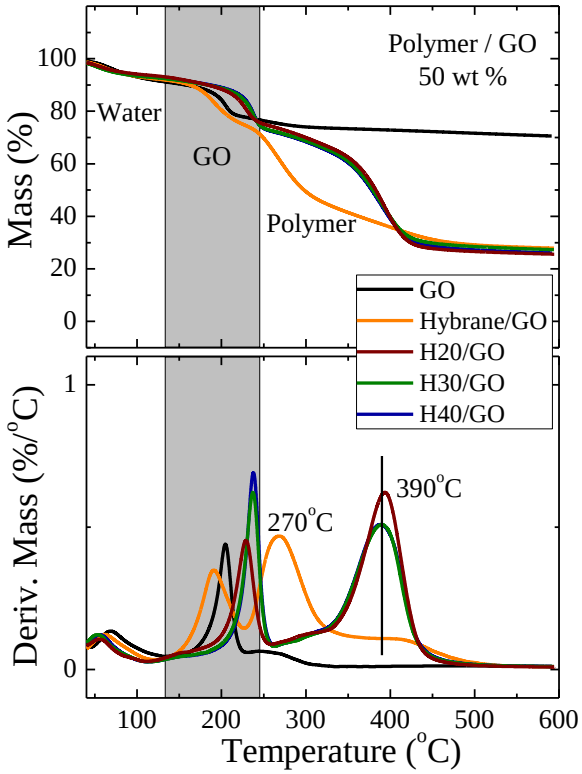

Figure 5.6: Thermal stability of the graphite oxide and the polymer/GO nanocomposites. TGA measurements (a) and the calculated derivative (b). The GO curve (black solid line) is normalized to the GO content of the nanocomposites.

In order to further investigate the exothermic reduction of the graphite oxide in nanocomposites DSC measurements were performed. In **Figure 5.7** the heat capacity of the hybrids, normalized by the mass of the graphite oxide, is presented. The exotherm of the Hybrane / GO nanocomposite is observed at 190 °C, a temperature that is lower than that of the neat GO, whereas the Boltorn nanohybrids exhibit significantly higher temperatures, 223-233 °C. By both TGA and DSC measurements it is confirmed that the thermal stability of the graphite oxide is enhanced by increasing the ester and hydroxyl groups in the polymer matrix, while the amide groups result in the opposite.

Furthermore for the hyperbranched polyester polyols, a difference is observed for the second generation of the Boltorns which obtains lower reduction temperature than the H30 and H40 nanocomposites. By increasing the branching (more hydroxyl groups) the reduction temperature of the GO is increased with an optimal number and no effect after that, indicated

by the same reduction temperature between the third and fourth generation. This behavior was observed by XRD as well.

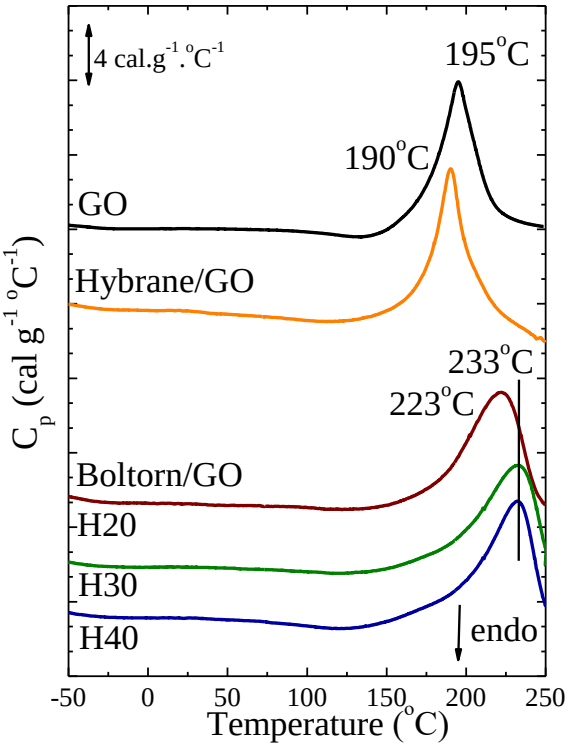

Figure 5.7: DSC measurements of the thermal reduction of Graphite Oxide in nanohybrids during heating.

Recently the effect of the polymer / graphite oxide interactions on the extent of the reduction of GO and on its reduction temperature has attracted the scientific interest. The investigation of thermal properties by Glover et al. shows that the thermal reduction of pure GO is affected during the in situ reduction in nanocomposites with poly (vinyl pyrrolidone) (PVP), poly (vinyl acetate) (PVAc) and poly (vinyl pyrrolidone / vinyl acetate) copolymer as the different polymer matrices, resulting in better thermal stability for the GO by increasing the PVP content against the PVAc. [10] In that case, by increasing the number of ester groups the reduction temperature of the GO is reduced, while in our case the opposite is observed.

Interestingly, it has been observed by Ye et al. that both polar and aromatic polymers can decrease the reduction temperature of GO but non-polar polymers cannot. It is assumed that the change in the reduction temperature of GO is associated with the favorable interactions between the polymers and the GO sheets. [11] Moreover Barroso-Bujans et al. reported lower reduction temperatures of the GO for nanocomposites with hydrophilic polymers such as poly

(ethylene oxide) (PEO), poly (vinyl methyl ether) (PVME), poly (vinyl alcohol) (PVA), poly (vinyl pyrrolidone) (PVP) and poly (acrylic acid) (PAA), forming polymer-adsorbed GO structures. [12]

Although in those studies it was concluded that more favorable interactions of the polymer to the GO sheets result in lower reduction temperatures, there is no clear mechanism for this assumption. We could conclude that the different polymer matrices with different functional groups obtain various mechanisms resulting in either enhanced or reduced thermal stability for the GO.

In the present study the hyperbranched polymers provide increasing number of hydroxyl groups by increasing the generation; it is noted that Hybrane has 8 secondary hydroxyl groups whereas H20, H30 and H40 16, 32 and 64 primary hydroxyl groups respectively. More favorable interactions with the GO are indicated by increasing the OH number in the macromolecule, and higher reduction temperatures are obtained. The polymer with the larger number of OH groups in this case could stabilize the functional groups of the graphite oxide, upon heating.

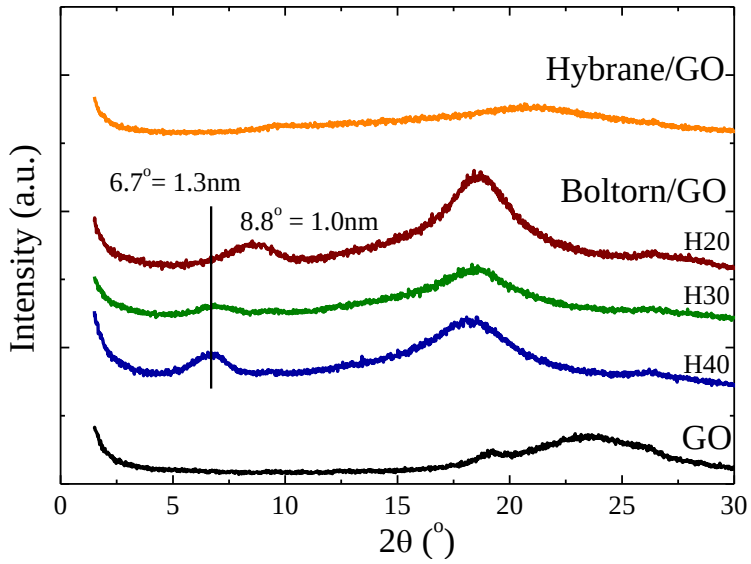

Figure 5.8: X-ray diffractograms of GO nanohybrids together with the pure GO (black line) after thermal annealing at 200°C.

In order to examine the structure of the nanohybrids after the thermal reduction of the graphite oxide, all samples were thermally annealed at 200 °C overnight in vacuum and the X-ray diffractograms obtained are shown in **Figure 5.8**. For the Boltorn nanocomposites, a significant reduction of the coherence of the nanohybrid structure is obtained, since only a very weak peak is observed that corresponds at 1.0 - 1.3 nm interlayer distance. Those values

correspond to polymer thickness similar to the nanocomposites of the smaller molecules, i.e. Hybrane and H20, before the annealing. On the other hand the Hybrane / GO nanohybrid exhibits no peak indicating a completely disordered structure. It is referred that the thermal reduction of the GO results in exfoliated structures due to the removal of the internal oxygens of the layers. In the case of the nanocomposites the graphite oxide obtains a layered structure due to the favorable interactions with the polymer and after the annealing the reduced GO layers are either less coherent or even dispersed in the polymer matrix.

5.3 Polymer Dynamics in Graphite Oxide Nanocomposites

In previous studies of polymer dynamics in PEO / GO nanocomposites the effect of the confinement was examined on the local and segmental dynamics, both experimentally and by computational methods. Polymer intercalation into sub-nanometer graphite oxide layers leads to the complete suppression of crystallization phenomena and segmental relaxation, as well as a slow-down of the local motions. [7]–[9]

The dynamics of the hyperbranched polymers utilized in the current work, was investigated by molecular dynamic simulations upon addition of graphene sheets. A significant slowing down is detected both in the local and in the overall polymer dynamics in the composite systems. The strong dynamic slowing down is accompanied by the occurrence of a glass-like transition at a considerably higher temperature compared to that characterizing the respective pristine polymer systems. [13]

In the present work, polymer dynamics under confinement was investigated for the 50 wt % nanocomposites of the hyperbranched polymers (the polyester polyols, Boltorn, and the poly (ester amide) Hybrane). It is reminded that in these polymer / graphite oxide nanocomposites very thin polymer films are formed between the sheets of the additive resulting in suppressed thermal properties. The dynamics was probed by dielectric relaxation spectroscopy in a wide range of frequencies and temperatures, both above and below the glass transition temperature, T_g, of the respective bulk polymers. The results obtained for the polymer dynamics under confinement are compared to the respective ones of the bulk polymer, presented in Chapter 3. When graphite oxide is used as the additive, a strong conductivity is evident in all cases.

Moreover, dielectric measurements were performed for the hyperbranched polymer / GO nanocomposites that were annealed at 200 °C and in which a less coherent structure was obtained, as well. All samples were conductive due to the reduction of the GO and the formation of a graphene-like material, as discussed in Chapter 1. [4] The GO content of the nanocomposites is very high (50 wt %) thus the percolation of the sheets, results in a conductive material. The results obtained are not further discussed in the present dissertation.

In the case of the hyperbranched polyester nanocomposites, the powder was pressed to form disks of 12 mm in diameter and 0.3 - 0.6 mm in thickness. The pellets were annealed at 120 °C in vacuum and adhered between indium foils to improve the electrical contact with the electrodes.

Boltorn/GO

Dielectric relaxation spectroscopy measurements were performed for the three nanocomposites H20/GO, H30/GO and H40/GO, comprising 50 wt % polymer and 50 wt % graphite oxide.

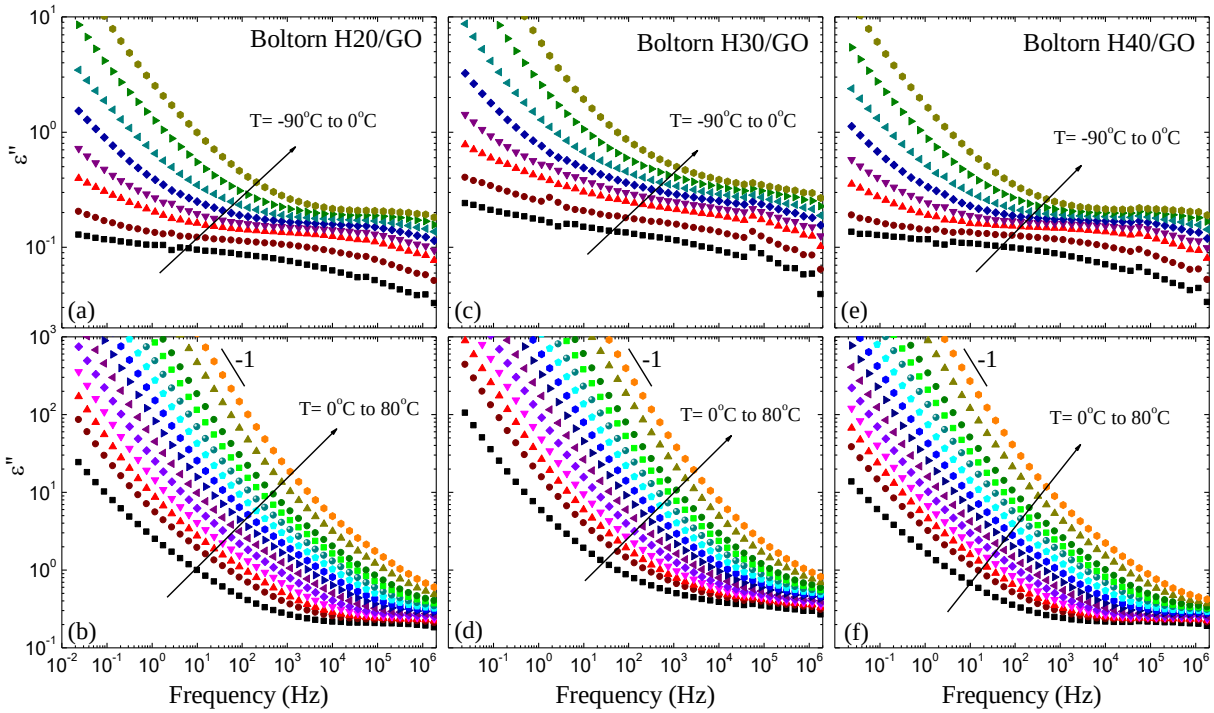

Figure 5.9: Imaginary part of the complex dielectric permittivity, ε'', as a function of frequency, for the low (a, b, c) and the high (d, e, f) temperature regime, of H20/GO (a, b), H30/GO (c, d) and H40/GO (e, f).

Figure 5.9 shows the imaginary part of the complex dielectric permittivity for the three nanocomposites in a very broad temperature range. The spectra of the nanohybrids are similar for the three generations at both low and high temperature regimes. At low temperatures, the spectra have a very broad peak probably due to multiple relaxation processes of low dielectric strength (**Figure 5.9**.a, c and e). At higher temperatures, the presence of an additional process becomes evident but it is partly obscured by the MWS effect and the conductivity that follows. The origin of the Maxwell-Wagner-Sillars polarization effect (MWS) is the presence of the surfaces as discussed in Chapter 1.

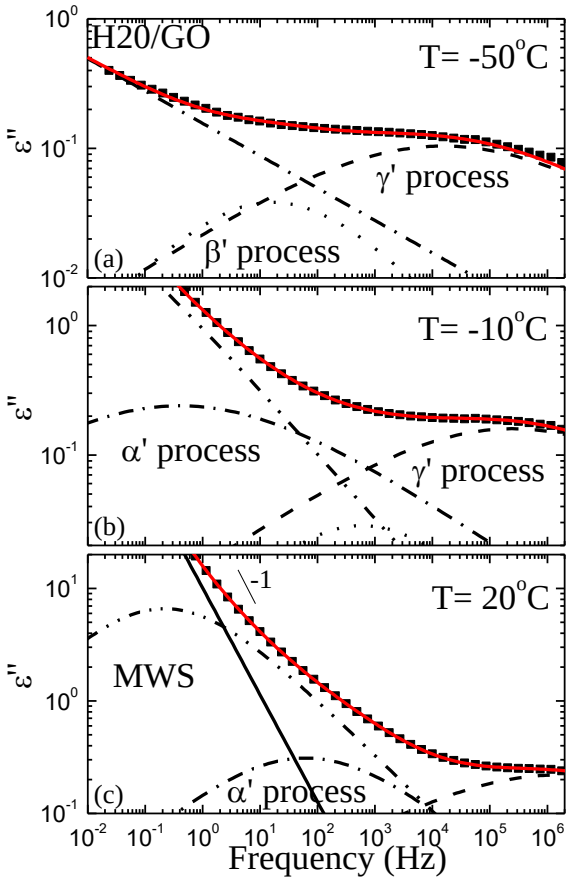

Figure 5.10: Representative analysis of Boltorn H20/GO. Imaginary part of the dielectric permittivity, ε'', at T= -50°C far below the bulk polymer T_g (a), T= -10°C (b) and T=20°C above the T_g (c). The processes needed for the deconvolution of the spectra are shown with black lines, whereas the red lines are the total fits.

In **Figure 5.10** the representative analysis of the spectra of the second generation Boltorn H20 nanocomposite is shown for three temperatures, two below and one above the T_g of the bulk polymer. The ε*(ω) data were analyzed utilizing the empirical Havriliak - Negami (HN) functions and an additional ionic conductivity contribution at low-frequencies and high temperatures.

The spectra analysis shows that in all cases, multiple relaxation processes are necessary to obtain a good fit to the data. The behavior is qualitatively very similar between the three nanohybrids and all relaxation processes are evident in all nanocomposites. To differentiate the processes of the nanocomposites than those in the bulk, they will be named by the same Greek letter followed by a prime apex (α′, β′,γ′). All parameters of the fitting for the Boltorn / GO nanohybrids are summarized in **Table 5.1**.

Table 5.1: Parameters of the HN function for each relaxation process in Boltorn / GO nanocomposites.

Parameters	Boltorn / GO
γ′-process – local motions of free –OH groups	
β	1
α	0.23 - 0.30
Δε	0.7 - 2.7
β′-process – local motions of ester groups	
β	1
α	0.41 - 0.45
Δε	0.2 - 0.6
α′-process – segmental motion	
β	1
α	0.26 - 0.56
Δε	5.0 - 2.7

For the three Boltorn / GO nanocomposites, two sub-T_g relaxation processes are observed, the γ'- and β'- process; at low temperatures the shape and relaxation strength parameters are determined. In all cases the β parameter is fixed to 1.0. For the γ'-process the temperature dependent α parameter takes values between 0.23 − 0.3 and Δε between 0.7 − 2.7. The β'-process obtains α parameter around 0.41 - 0.45 and a quite low dielectric strength, Δε ∼ 0.2 - 0.6, for all three generations.

At higher temperatures, below the bulk polymer T_g, the α'-process appears and, at even higher temperatures, the slow MWS process becomes evident. The α parameter of the α'-process for all three nanocomposites is around 0.26 − 0.56 and Δε decreases from 5 to 2.7; for the slow

process, α is around 0.5. At low frequencies and high temperatures, the addition of a contribution due to ionic conductivity is necessary as a line with a slope of ~0.95 – 0.98.

In **Figure 5.11** the results of the above analysis concerning the relaxation times of all the three Boltorn nanocomposites are illustrated in an Arrhenius representation. The relaxation times of the two sub-T_g relaxation processes are very similar for the three generations. For the fastest γ'-process, the activation energies that result from the temperature dependence of the relaxation times take values $E_{\gamma',H20}$ = 36 ± 1.5 kJ/mol, $E_{\gamma',H30}$ = 31 ± 1.0 kJ/mol, and $E_{\gamma',H40}$ = 30 ± 1.0 kJ/mol. This process is attributed to the motion of the polar hydroxyl groups of the confined chains. The second sub-T_g process, β', shows similar temperature dependence to the γ'-process. It is attributed to the carbonyl reorientation and the activation energies for this process are $E_{\beta',H20}$ = 33.5 ± 2.0 kJ/mol, $E_{\beta',H30}$ = 35 ± 2 kJ/ mol, and $E_{\beta',H40}$ = 28 ± 2 kJ/mol.

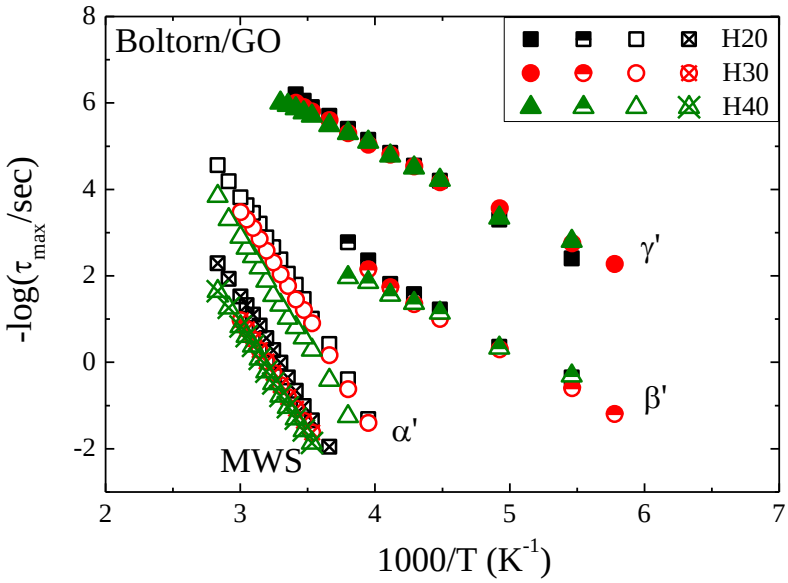

Figure 5.11: Arrhenius relaxation map of H20/GO, H30/GO and H40/GO.

The dielectric strength of the α'-process decreases with increasing temperature that is a dependence typical of the segmental relaxation. Moreover, the activation energy of the process suggests that it is not related to the motion of a single subunit. In fact, the values which are very similar for the three confined polymers $E_{\alpha',H20}$ = 99.5 ± 5.0 kJ/mol, $E_{\alpha',H30}$ = 98 ± 3.0 kJ/mol, and $E_{\alpha',H40}$ = 97 ± 2.0 kJ/mol, are very high . The segmental α'-relaxation exhibits a more Arrhenius-like temperature dependence. Its relaxation times are quite similar between the generations, however a dependence is evident with slower segmental dynamics when increasing the generation. As mentioned above, it appears in the frequency window at slightly

higher temperatures by increasing the generation (from -20 to -10 °C). It is noted that DSC did not show any thermal transitions for the hybrids with 50 wt % polymer content.

The relaxation times of the H20, H30 and H40 nanocomposites are presented in **Figure 5.12**a, b and c respectively, together with the relaxation processes of the respective bulk polymer (solid lines).

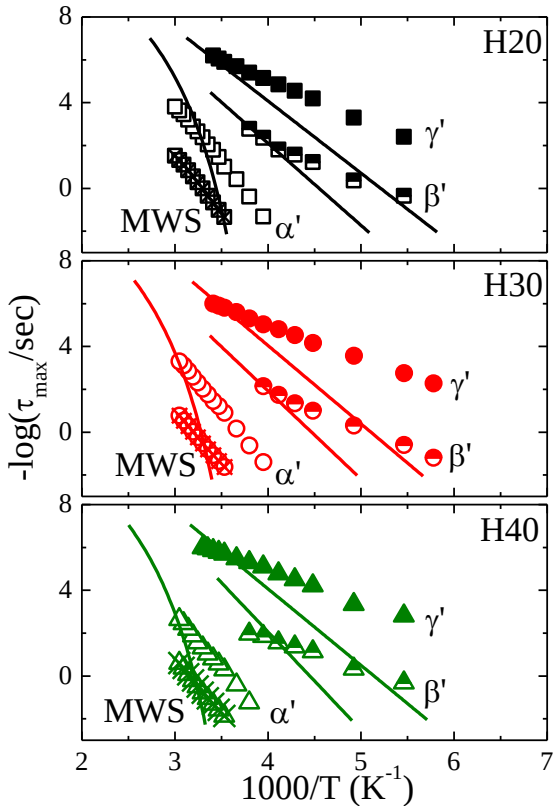

Figure 5.12: Arrhenius relaxation map of H20/GO, H30/GO and H40/GO. Solid lines correspond to the relaxation processes for the pure H20, H30 and H40 respectively.

The motions of the sub-T_g processes are faster than the respective ones of the neat polymers and more importantly with much weaker Arrhenius temperature dependencies. Comparison of the activation energies of the β′- and γ′-processes to the respective ones of the pure polymers are shown in **Table 5.2**.

This result can be understood considering that in Boltorn / GO nanocomposites, under confinement, spatial restrictions do not allow the formation of an extended network of hydrogen bonds, similar to the one formed in the pure polymers, causing the activation energy for the respective motions to be lower than the one of the bulk. Thus, both the hydroxyl motions and the carbonyl reorientation become easier.

At higher temperatures, even more significant deviations in the segmental relaxation between the pure polymer and the nanohybrids appear. For the Boltorn nanocomposites, the α'-process appears at lower temperatures to be faster than the one of the neat polymers having an Arrhenius and not a VFT temperature dependence. Due to this different temperature dependence of the segmental process, at higher temperatures, the α'-process tends to cross the α-process of the bulk polymer. This crossing is more clearly observed for the H20 / GO nanocomposite because the dependence of the relaxation time of the α' relaxation on generation (at the same temperature) is weaker than the difference between the glass transition temperatures in the bulk polymers.

Finally, at even higher temperatures, the slow MWS process appears, for all confined systems, due to interfacial polarization because of the large number of interfaces that exist in the nanocomposites and the ions trapped in their proximity. This process shows an Arrhenius temperature dependence and similar relaxation times for all three generations.

Table 5.2: Results of the relaxation processes for the Boltorns in nanocomposites.

Boltorn	γ- process E_a (kJ/mol)	β- process E_a (kJ/mol)	α-process
H20	65.0 ± 1.5	70.0 ± 3.0	VFT
H30	69.5 ± 1.0	81.0 ± 9.0	
H40	66.5 ± 1.5	86.0 ± 2.0	
Boltorn / GO	**γ'- process E_a (kJ/mol)**	**β'- process E_a (kJ/mol)**	**α'- process E_a (kJ/mol)**
H20 / GO	36.0 ± 1.5	33.5 ± 2.0	99.5 ± 5.0
H30 / GO	31.0 ± 1.0	35.0 ± 2.0	98.0 ± 3.0
H40 / GO	30.0 ± 1.0	28.0 ± 2.0	97.0 ± 2.0

We can assume that the interactions of the polymer with the additive and the different conformations of the chains due to the severe confinement result in easier local motions due to less hydrogen bonding and in a different segmental relaxation mechanism for the confined polymer in Boltorn / GO nanocomposites compared to the bulk. The Arrhenius behavior of the segmental relaxation under confinement observed below the glass transition temperature of

the bulk polymer discussed here for the hyperbranched polyester polyols, has been reported for the PEO / Na^+-MMT nanocomposite as well. [14] Moreover, polymer dynamics in Boltorn / GO appears very similar to the Boltorn / Na^+-MMT nanocomposites in both low and high temperature regime that will be discussed in Chapter 6. [15]

Hybrane/GO

Figure 5.13 shows the imaginary part of the complex dielectric permittivity for the Hybrane / GO 50 wt % nanocomposite. At the low temperature regime one strong relaxation process can be clearly observed while at few very low temperatures a shift of the data could be attributed to a fast relaxation process with very low dielectric strength. By increasing the temperature, but still below the glass transition temperature of the bulk polymer (T_g = 43 °C), another relaxation process is observed, partly obscured by strong MWS polarization effect and the conductivity.

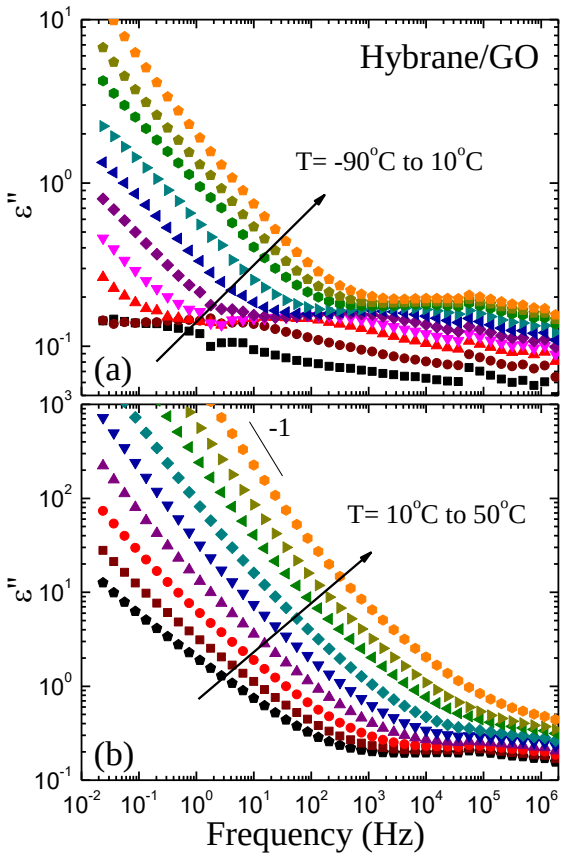

Figure 5.13: Imaginary part of the complex dielectric permittivity, ε", as a function of frequency, for the low (a) and the high (b) temperature regime, of Hybrane/GO.

The analysis of the dielectric spectra at three different temperatures, two below and one above the T_g of the bulk polymer, is presented in **Figure 5.14**. The spectra at very low

temperatures show two sub-T_g processes, the fast of low dielectric strength that can be observed in very few temperatures and the slow which is stronger and becomes dominant in all the low temperature regime. The shape and relaxation strength parameters for this slow process are determined. The β parameter is fixed to 0.68, the α parameter is increasing with temperature from 0.29 to 0.45 and Δε ranges between 1.1 to 1.4. The segmental α′-process is observed only at few temperatures below the glass transition temperature with the α parameter around 0.5 and Δε decreasing from 3 to 1.8. It is noted that DSC shows a weak glass transition, for the hybrid with 50 wt % polymer content, at temperatures lower than the T_g of the bulk polymer. For the slow MWS process, α is around 0.5 and the ionic conductivity is denoted as a line with a slope of ~0.93.

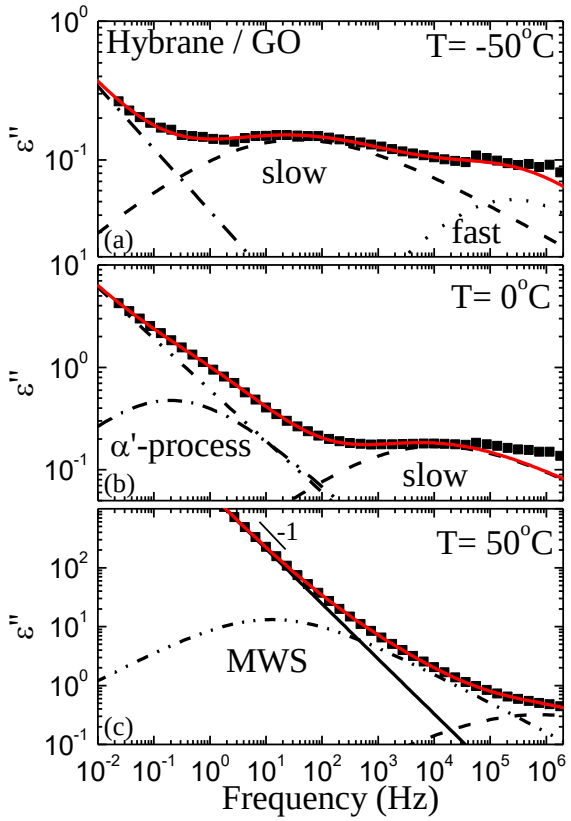

Figure 5.14: Analysis of Hybrane/GO. Imaginary part of the dielectric permittivity, ε", at T= -50°C far below the bulk polymer T_g (a), T= 0°C below the T_g (b) and T= 50°C above the T_g (c). The processes needed for the deconvolution of the spectra are shown with black lines, whereas the red lines are the summations of the processes.

In **Figure 5.15**, the relaxation times of the Hybrane / GO nanocomposite are illustrated in an Arrhenius representation together with the relaxation times of the bulk Hybrane, the slow process of the hyperbranched H30 and of the linear DG-110, discussed in Chapter 3. The fast sub-T_g relaxation process is observed at very few temperatures with relaxation times faster

than the bulk, whereas the slow process appears slower than the respective of the bulk polymer. Additionally in the bulk polymer the fast process is dominant but in the case of the Hybrane / GO nanocomposite the slow process is stronger.

The activation energies of the two sub-T_g relaxation processes are 25 ± 2.0 kJ/mol for the fast process and 58 ± 1.0 kJ/mol for the slow. Those values are very similar to the corresponding ones for the free and the restricted motion of the hydroxyl groups with 33 ± 2.0 kJ/mol and 60 ± 4.0 kJ/mol respectively, in the bulk polymer. According to the literature neither of the sub-T_g relaxations could be related to the dynamics of the graphite oxide or to water molecules adsorbed on the GO sheets. [16]

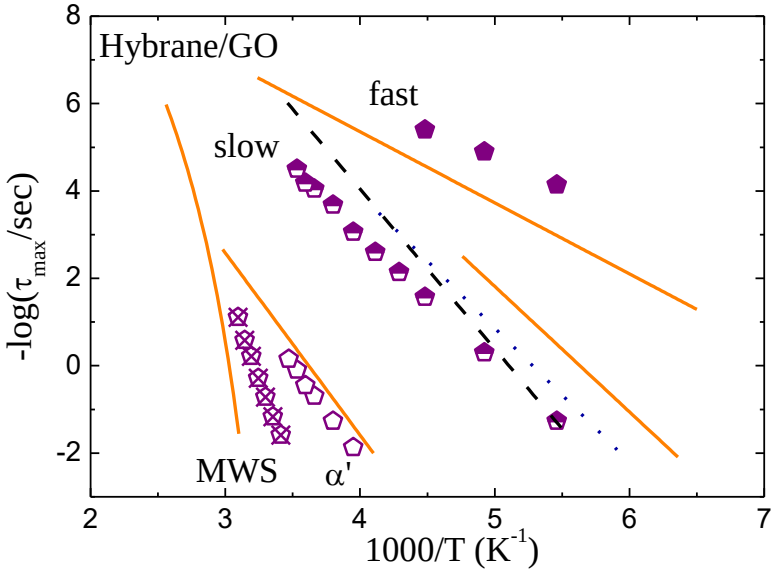

Figure 5.15: Arrhenius relaxation map of Hybrane/GO. Solid orange lines correspond to the relaxation processes for the pure Hybrane.

The α′-process, evident at temperatures below the bulk polymer T_g, obtains an Arrhenius temperature dependence (E_a = 80 ±5 kJ/mol) and very similar relaxation times to the intermediate process of the bulk Hybrane; however above 20 °C it cannot be analyzed because of the strong conductivity and MWS process. The peculiar but interesting characteristic of this process resides on its dielectric strength which is much higher compared to the bulk; from 0.05 for the intermediate process in the bulk the dielectric strength in the nanocomposite is 3 to 1.8. Moreover, the dielectric strength decreases with increasing temperature, property typical for the α-process in the bulk and the α'-process under confinement respectively. Although the relaxation times of the α′ process are very similar to the intermediate process

of the bulk polymer, its characteristics indicate a segmental relaxation process. Nevertheless, the intermediate process attributed to the motion of the branch discussed in Chapter 3, could contribute to the dielectric strength of the aforementioned process.

We can assume that the interactions of the polymer with the additive result in faster segmental dynamics, behavior similar to the Boltorn / GO nanocomposites. Furthermore the segmental dynamics under confinement appears with an Arrhenius temperature dependence and the α'-process tends to cross the segmental in both, Boltorn and Hybrane.

5.4 Graphite Oxide as an Additive in Polymer Nanocomposite Materials

The three generations of the hyperbranched polyester polyols, Boltorn (H20, H30 and H40), were mixed with graphite oxide, GO, in order to investigate the effect of the additive on the polymer structure, properties and dynamics. Additionally, the hyperbranched poly (ester amide), Hybrane, obtaining similar architecture and functional groups to the Boltorn, with an extra amide group in its repeating unit, is mixed with the GO as well.

In all cases intercalated structures are obtained revealing favorable interactions between the polymers and the surfaces of GO. Boltorn nanocomposites obtain higher interlayer distances than the one with Hybrane (i.e. thicker polymer film and larger amount under confinement). After thermal annealing at 200 °C that causes thermal reduction of GO, the coherence of the structure in all nanocomposites is significantly reduced; in the case of the Hybrane nanocomposite the peak of the intercalated structure is completely vanished.

All hyperbranched polymers are amorphous with a dependence of the glass transition temperature, T_g, on the generation; Hybrane exhibits T_g close to the respective temperature of the fourth generation Boltorn. For the Boltorn nanocomposites in 50 wt %, where the polymer is intercalated between the GO layers, no thermal transition is evident. At the same concentration, for the Hybrane / GO nanocomposite, although the glass transition can be observed, it is at lower temperature and of decreased amplitude of the heat capacity step compared to the bulk. This behavior leads to the conclusion that the amount of the polymer under confinement does not contribute to the transition, thus the origin of the observed T_g is the excess polymer which is not intercalated but interacts with the additive. The thermal

properties investigated for the Boltorn and Hybrane nanocomposites, reveal stronger interactions in Boltorn / GO.

The thermal reduction of graphite oxide shows that the different functional groups of the polymer matrix affects the reduction temperature of GO. Enhanced thermal stability was obtained for the hyperbranched polyester polyols, whereas it is reduced for the poly (ester amide). The thermal degradation of the polymer in GO nanohybrids appears at similar or lower temperatures to the respective in the bulk.

Polymer dynamics in the Boltorn / GO nanocomposites, investigated by dielectric relaxation spectroscopy, reveals a significant effect of the additive on both local and segmental dynamics and great similarities between the three generations. The local motions of the hydroxyl and carbonyl groups observed in the bulk polymers, obtain lower activation energies in the nanocomposites due to the decreased hydrogen bonding under confinement. Interestingly the segmental dynamics appears at temperatures lower than the T_g of the bulk polymer and shows an Arrhenius temperature dependence, suggesting a different relaxation mechanism. By increasing the generation, slower segmental dynamics is observed, nevertheless the slowdown of the dynamics is smaller than the change in the T_g of the neat polymers. It is noted again, that under confinement no thermal transition is observed in the nanocomposites at the temperature range of the glass transition.

For the Hybrane / GO nanocomposite only sub-T_g dynamics can be analyzed due to the strong polarization effect and the conductivity which becomes dominant at high temperatures. Local dynamics greatly differs than the respective in the bulk, with one strong sub-T_g process, attributed to the restricted motion of the hydroxyl groups; this process is slower than both sub-T_g processes of the neat Hybrane. At temperatures close and below the bulk polymer T_g another process appears with relaxation times similar to the intermediate process of the bulk polymer but with increased dielectric strength and similarities to the segmental relaxation. This process is attributed to the segmental relaxation under confinement which shows a different relaxation mechanism through an Arrhenius temperature dependence, similar with the one observed in the Boltorn / GO nanocomposites.

5.5 References

[1] S. Eigler, S. Grimm, M. Enzelberger-heim, P. Mu, and A. Hirsch, "Graphene oxide : efficiency of reducing agents," *Chem Commun*, vol. 49, pp. 7391–7393, 2013.

[2] M. Jin, H. Jeong, T. Kim, and K. P. So, "Synthesis and systematic characterization of functionalized graphene sheets generated by thermal exfoliation at low temperature," *J. Phys. D. Appl. Phys.*, vol. 43, p. 275402, 2010.

[3] D. Krishnan *et al.*, "Energetic graphene oxide : Challenges and opportunities," *Nano Today*, vol. 7, no. 2, pp. 137–152, 2012.

[4] B. K. Erickson, R. Erni, Z. Lee, N. Alem, W. Gannett, and A. Zettl, "Determination of the Local Chemical Structure of Graphene Oxide and Reduced Graphene Oxide," *Adv. Mater.*, vol. 22, pp. 4467–4472, 2010.

[5] I. Jung, D. A. Dikin, R. D. Piner, and R. S. Ruoff, "Tunable Electrical Conductivity of Individual Graphene Oxide Sheets Reduced at ' Low ' Temperatures," *Nano Lett.*, vol. 8, no. 12, pp. 4283–4287, 2008.

[6] Q. Du *et al.*, "Preparation of functionalized graphene sheets by a low-temperature thermal exfoliation approach and their electrochemical supercapacitive behaviors," *Electrochim. Acta*, vol. 55, no. 12, pp. 3897–3903, 2010.

[7] F. Barroso-Bujans, F. Fernandez-Alonso, S. Cerveny, S. F. Parker, A. Alegría, and J. Colmenero, "Polymers under extreme two-dimensional confinement: Poly(ethylene oxide) in graphite oxide," *Soft Matter*, vol. 7, no. 16, pp. 7173–7176, 2011.

[8] F. Barroso-Bujans *et al.*, "Chain length effects on the dynamics of poly(ethylene oxide) confined in graphite oxide: A broadband dielectric spectroscopy study," *Macromolecules*, vol. 46, pp. 7932–7939, 2013.

[9] I. Garcia-Yoldi, F. Álvarez, and J. Colmenero, "On the interactions between poly(ethylene oxide) and graphite oxide: a comparative study by different computational methods.," *J. Chem. Phys.*, vol. 138, no. 9, p. 094308, 2013.

[10] A. J. Glover, M. Cai, K. R. Overdeep, D. E. Kranbuehl, and H. C. Schniepp, "In situ reduction of graphene oxide in polymers," *Macromolecules*, vol. 44, no. 24, pp. 9821–9829, 2011.

[11] S. Ye and J. Feng, "A new insight into the in situ thermal reduction of graphene oxide dispersed in a polymer matrix," *Polym. Chem.*, vol. 4, no. 6, pp. 1765–1768, 2013.

[12] F. Barroso-bujans, A. Alegria, J. A. Pomposo, and J. Colmenero, "Thermal Stability of Polymers Confined in Graphite Oxide," *Macromolecules*, vol. 46, pp. 1890–1898, 2013.

[13] K. Karatasos, "Graphene/hyperbranched polymer Nanocomposites: Insight from molecular dynamics simulations," *Macromolecules*, vol. 47, no. 24, pp. 8833–8845, 2014.

[14] M. M. Elmahdy, K. Chrissopoulou, A. Afratis, G. Floudas, and S. H. Anastasiadis, "Effect of confinement on polymer segmental motion and ion mobility in PEO/layered silicate nanocomposites," *Macromolecules*, vol. 39, no. 16, pp. 5170–5173, 2006.

[15] K. Androulaki, K. Chrissopoulou, D. Prevosto, M. Labardi, and S. H. Anastasiadis, "Dynamics of Hyperbranched Polymers under Confinement: A Dielectric Relaxation

Study," *ACS Appl. Mater. Interfaces*, vol. 7, no. 23, pp. 12387–12398, 2015.

[16] S. Cerveny, F. Barroso-Bujans, Á. Alegría, and J. Colmenero, "Dynamics of water intercalated in graphite oxide," *J. Phys. Chem. C*, vol. 114, no. 6, pp. 2604–2612, 2010.

6 Polymer / Clay Nanocomposites

In the current Chapter two series of polymers with different architecture, the linear biobased polyesters and the hyperbranched polymers discussed in Chapter 3, are utilized for the development of polymer / clay nanocomposites. The effect of polymer / surface interactions as well as the severe confinement, inside the nanometric galleries of the clay, on the polymer structure, the thermal properties and the polymer dynamics, for both local and segmental motions, are investigated.

In all cases the interactions of the polymer with the surface of the clay are favorable and intercalated structures are obtained. In nanocomposites with low polymer content, where all the polymer chains are under confinement, thermal transitions are suppressed for both crystalline and amorphous polymers, examined by DSC.

Polymers dynamics under confinement was examined in a wide temperature range by Broadband Dielectric Spectroscopy. The local dynamics of all polymers shows many similarities whereas differences are observed in the segmental dynamics between polymers of different architecture. Although DSC indicates suppressed thermal transitions under confinement, Dielectric Spectroscopy probes the segmental relaxation which is found slower than the respective in the bulk for the linear polyesters, whereas for the hyperbranched polymers obtains a different relaxation mechanism.

6.1 Sodium Montmorillonite Characterization

The structure of the pure clay, natural hydrophilic sodium montmorillonite, Na^+-MMT, is presented in **Figure 6.1** before and after thermal annealing at 200 °C for 24 hours. Montmorillonite exhibits diffraction peaks at $2\theta = 19.7°$, 21.9° and 27.8° which correspond to characteristic distances within the clay layers. The interlayer spacing of the clay, when water molecules are adsorbed inside the galleries, is 1.1nm whereas the interlayer spacing of the dry clay is 1nm.

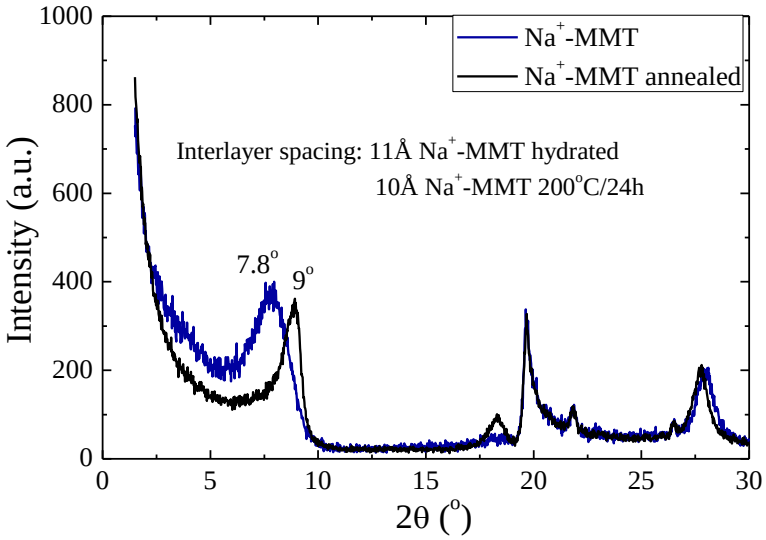

Figure 6.1: X-ray diffractograms of Na^+-MMT before and after thermal annealing.

In **Figure 6.2** the thermogravimetric measurement of the neat sodium montmorillonite is presented together with the calculated derivative which is shown in the inset. The water adsorbed in the galleries of the clay is the 6.5 wt % of the total mass and is completely removed up to 120 °C. The clay is stable in the investigated temperature range.

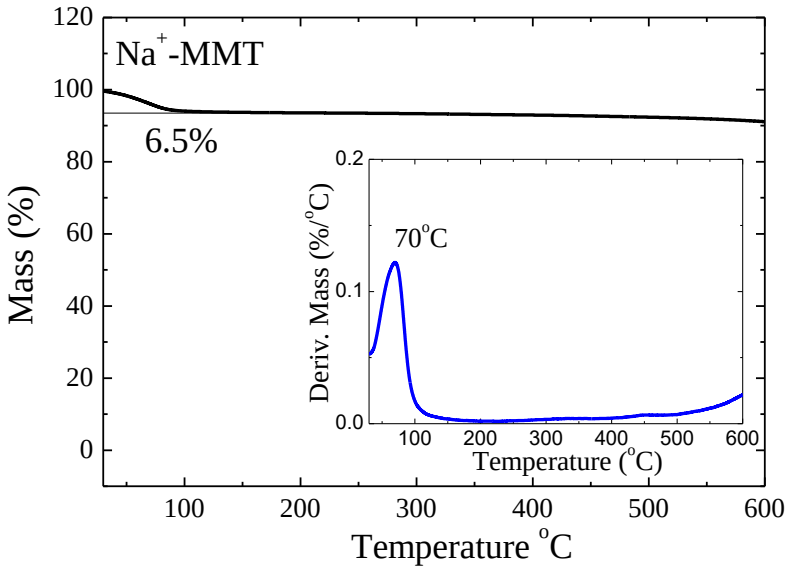

Figure 6.2: TGA measurement of sodium montmorillonite, Na^+-MMT. The first derivative is shown in the inset.

6.2 Biobased Linear Polyesters / Na^+-MMT

The linear polyesters EG-110, DG-110 and HD-110 were mixed with Na^+-MMT to prepare hybrids over a broad range of compositions, via a solution-intercalation method using deionized water as the solvent.

The required amount of polyesters was first dissolved in water at room temperature, and, then, the respective amount of clay was added under continuous stirring in order to ensure that the individual clay layers were well dispersed. Following mixing, the solvent evaporated initially in ambient conditions until a concentrated slurry was obtained, which was, then, transferred to a vacuum oven to completely dry. Finally, all samples were thermally annealed at 130 °C overnight under vacuum to erase any metastable structures formed during solvent evaporation and to achieve equilibrium. [1]

6.2.1 Structural characterization of polyester / Na^+-MMT nanohybrids

Figure 6.3 shows XRD measurements of all the nanocomposites after the thermal annealing, together with the diffractograms of the pure polymer and the clay. In all cases intercalated structures are obtained, evident by the shift of the main peak of the inorganic material towards lower angles. Upon addition of low amount of polymer (e.g., ~15wt %) the original peak of the inorganic material has disappeared and a new one at $2\theta = 6.7°$ for EG-110 (**Figure 6.3**a) and at $2\theta = 6.4°$ for DG-110 (**Figure 6.3**.b) appears corresponding to interlayer distances $d_{001} = 1.3$ nm and $d_{001} = 1.4$ nm, respectively.

Upon further addition of polymer (i.e., for hybrid with ~30wt % polymer), the existence of a double peak is evident with different relative intensity; the one is at the same diffraction angle as before whereas the second one appears at even lower angles i.e., at $2\theta = 5.2°$ corresponding to interlayer distance of $d_{001} = 1.7$nm for both EG-110 and DG-110. The picture is very similar for HD-110 in which the two peaks are at $2\theta = 6.4°$ and $2\theta = 5.0°$ ($d_{001} = 1.4$nm and $d_{001} = 1.8$nm respectively (**Figure 6.3**.c)).

With further increase of the polymer content, it is the peak at the lower diffraction angle that prevails, always at the same angle independently of the composition. The appearance of these peaks indicates that the polymer chains intercalate between the inorganic layers, forming mono- and bi-layers within the interlayer galleries and at the end a structure with alternating inorganic layers / polymer bi-layers, is formed. It is noted that the observed intercalated

structures have a significant coherence, which becomes evident by the existence of the third and in certain cases even the fourth order diffraction peaks. A similar mechanism of chain intercalation with mono- and bilayers of polymer chains inside the galleries of hydrophilic layered silicates has been observed before for semi-crystalline poly (ethylene oxide) both experimentally [2], [3] and computationally [4].

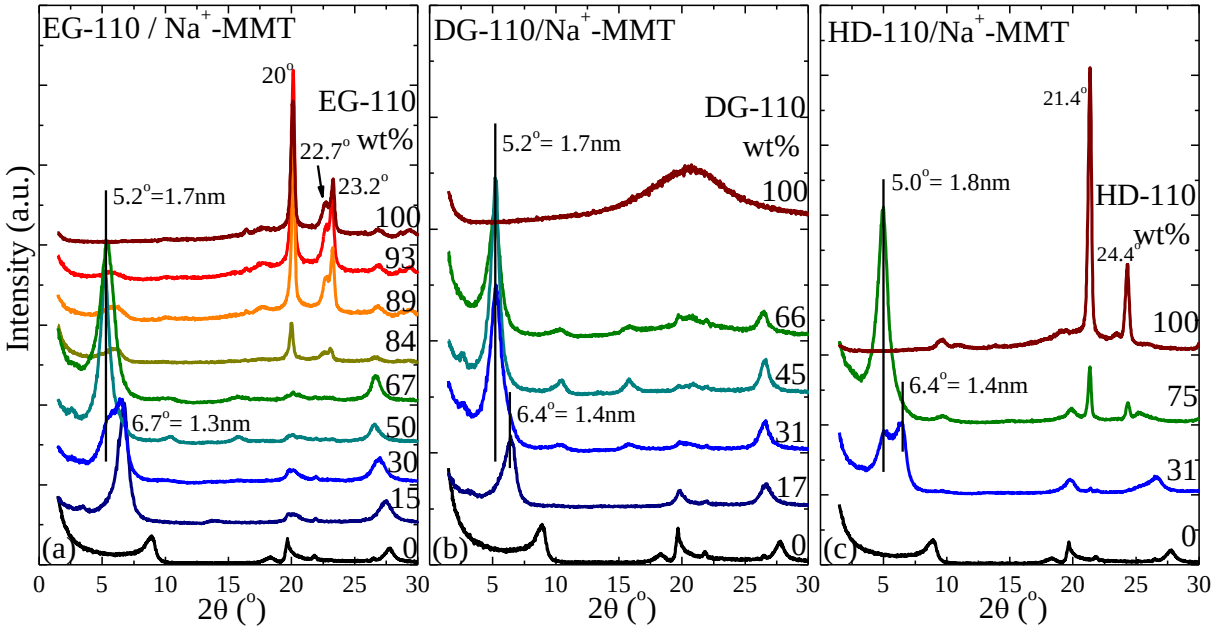

Figure 6.3: X-ray diffractograms of EG-110 / Na^+-MMT (a), DG-110 / Na^+-MMT (b) and HD-110 / Na^+-MMT (c) nanohybrids after thermal annealing.

Equally important is the observation that, in the case of the semi-crystalline polymers, EG-110 and HD-110, the crystalline peaks of the polymer exist only for nanohybrids with very high polymer content (equal or higher than 75 wt % in polymer), indicating that not only the intercalated polymer but the polymer close to the stacks of the inorganic particles is completely amorphous and it is only the excess chains that are far away from the inorganic surfaces that are able to crystallize. When the crystalline peaks are observed, they are at the same positions with the respective ones of pure polymer suggesting that the presence of the inorganic material did not alter the crystalline structure. [5]

6.2.2 Thermal properties of polyester / Na^+-MMT nanohybrids

The thermal stability of the polymer in clay nanocomposites is investigated and the thermogravimetric measurements of all nanohybrids are presented in **Figure 6.4**. All nanocomposites exhibit one main degradation step, attributed to the degradation of the

polymer chain; the decomposition temperature is found decreased compared to the bulk polymer. Moreover, the hybrids of EG-110 and DG-110 with high polymer quantity, obtain a small weight loss at lower temperatures attributed to the volatile molecules of low molecular weight, as discussed in Chapter 3.

The thermal stability of all the three polymers in nanocomposites for the whole composition range compared to the respective bulk polymer are presented in **Table 6.1**. The most probable decomposition temperature for the EG-110 nanocomposites is determined at 415, 412, 415, 406, 396, 382, 375 and 369 °C for 100, 93, 89, 84, 67, 50, 30 and 15 wt % in polymer respectively. For the DG-110 nanohybrids the degradation temperatures are at 420, 401, 389, 384 and 375 °C for 100, 66, 45, 31 and 17 wt % respectively and for the HD-110 nanocomposites at 405, 401 and 371 °C for 100, 75 and 31wt % respectively.

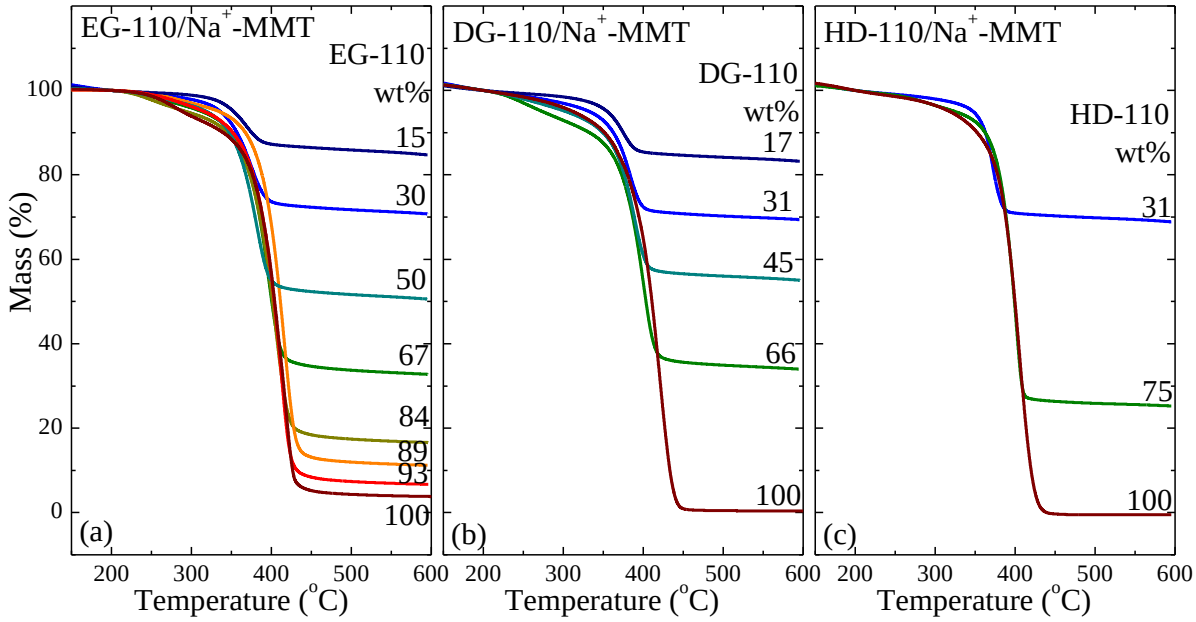

Figure 6.4: TGA measurements of EG-110 / Na^+-MMT (a), DG-110 / Na^+-MMT (b) and HD-110 / Na^+-MMT (c) nanohybrids.

The thermal properties examined by DSC for the linear polyesters in nanocomposites expressed as specific heat, C_p, are illustrated in **Figure 6.5**, **Figure 6.6** and **Figure 6.7** for the EG-110, DG-110 and HD-110 respectively. For the calculation of the heat capacity in the case of the hybrids, only the polymer mass is considered, since the contribution of the inorganic material to the C_p is an additive constant that would not influence thermal transitions.

In contrast to the pure polymer that shows a very weak crystallization exotherm during cooling at T_c = 28 °C, the EG-110 nanocomposites show in general a more pronounced transition, the amplitude of which shows a non-monotonic behavior (**Figure 6.5**a); it increases in amplitude and becomes sharper with increasing the concentration of the additive and becomes broader again for the lowest polymer content where it is observed. Irrespectively of the strength of the transition, the crystallization temperature shifts clearly toward higher temperatures with increasing additive concentration and reaches T_c = 49 °C for the 50wt % EG-110 nanohybrid. For the nanocomposite with the lowest polymer content, no crystallization exotherm is observed since all polymer is intercalated and it is impossible to crystallize within the ~1nm galleries of the inorganic material.

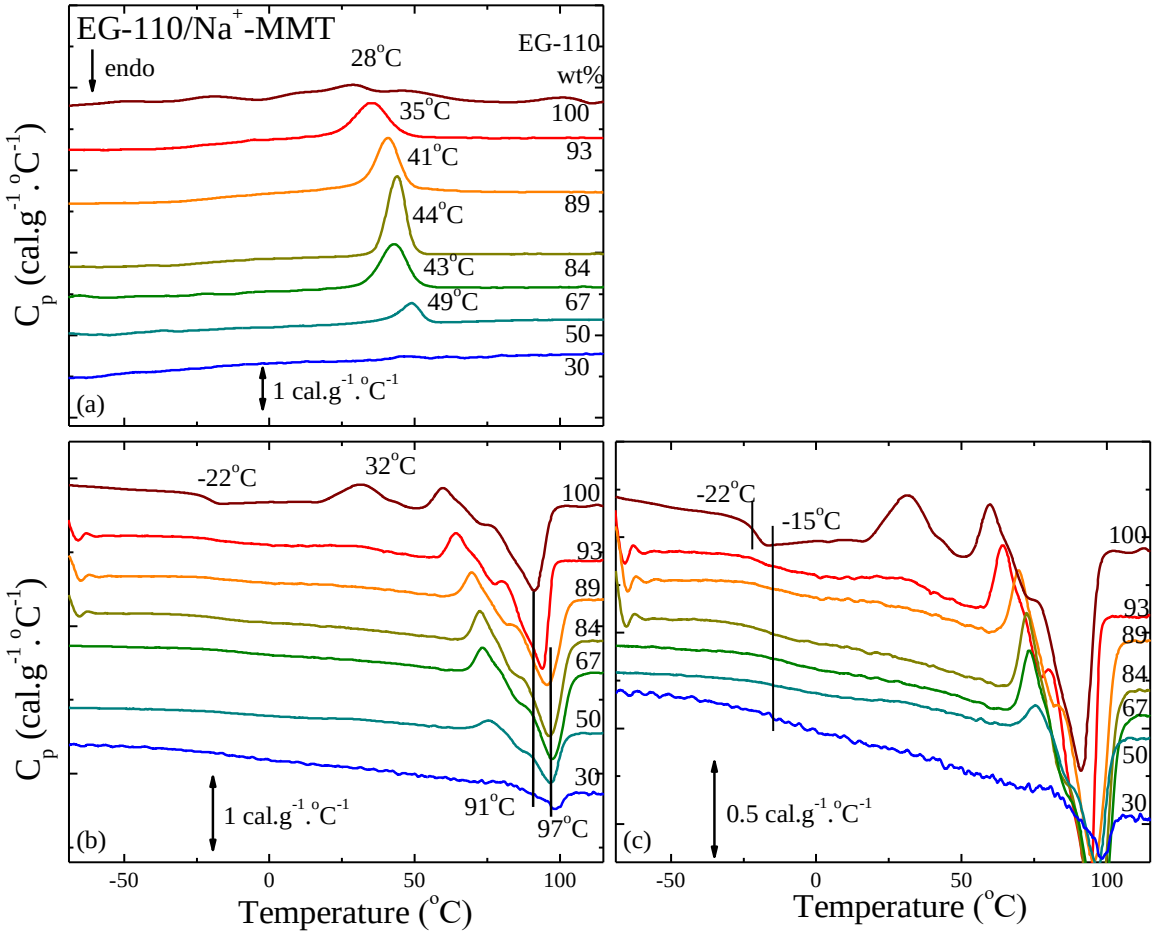

Figure 6.5: DSC measurements of EG-110 / Na^+-MMT nanohybrids during cooling (a) and heating (b). For clarity the heating is also presented in different scale (c) and the curves have been shifted vertically.

During heating (**Figure 6.5**b), the glass transition is observed at T_g = -22 °C for the pure polymer; this transition shifts to higher temperatures and becomes extremely weak for the

hybrids with polymer content higher than ~80wt %. When a glass transition is observed, its temperature is T_g ~ -15 °C.

Above the glass transition temperature, the main exothermic peak that is observed for pure EG-110 at T_{c1} = 32 °C, is not observed in any of the EG-110 nanocomposites. This means that the chains that had crystallized with a cold crystallization in the pure polymer have already crystallized during cooling in the case of the nanocomposites. The second weak exotherm that is observed for pure EG-110 at T_{c2} = 60 °C is observed in most of the nanocomposites; nevertheless, the temperature T_{c2} shifts significantly towards higher temperatures and reaches the value of T_{c2} = 76 °C for the nanocomposite with 50wt % EG-110.

The final melting of the polymer, is observed at a higher temperature, T_m = 97 ±1 °C than that of the bulk EG-110; nevertheless, this temperature does not show any dependence on composition. It is noted that, whereas DSC shows crystallization and melting peaks for almost all hybrid compositions, crystalline diffraction peaks are not observed in the XRD measurements for compositions below 67wt % in EG-110 indicating that the structures lack the coherence necessary for a diffraction peak to appear.[5]

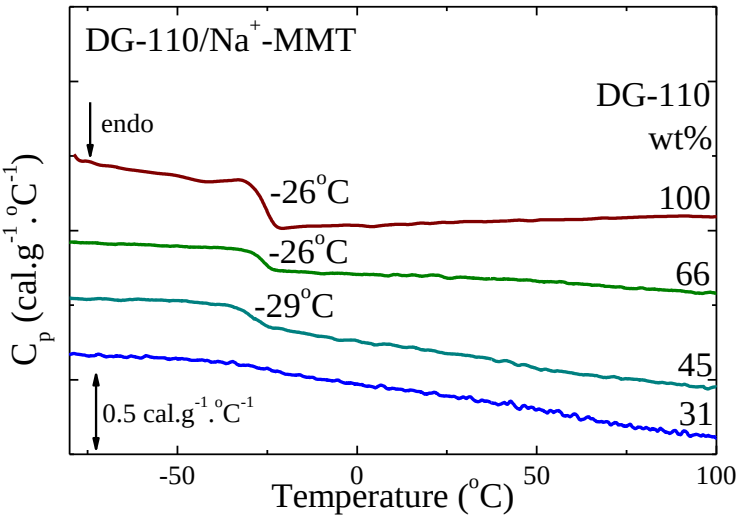

Figure 6.6: DSC measurements of DG-110 / Na^+-MMT nanohybrids during heating.

The thermal behavior of the DG-110 nanocomposites during heating with a rate of 10 °C/min is shown in **Figure 6.6** expressed as specific heat, C_p, together with the thermogram of the pure polymer. DG-110 is amorphous exhibiting a glass transition at T_g = -26 °C and ΔC_p= 0.32 cal/g while in nanocomposites the glass transition is observed only at a relatively high polymer

content, where the polymer is in excess outside the filled galleries. When a glass transition is observed, the glass transition temperature is very similar to the one of the pure polymer.

In composition below ~30wt % in polymer, no transition is observed either because it is too weak to be detected or because it is suppressed when the polymer is confined in the very small dimensions of the interlayer galleries of the inorganic material. ΔC_p decreases as the polymer content decreases (ΔC_p= 0.15 cal/g for both the 66 and 45 wt % nanocomposites) and goes to zero for polymer concentration lower than 30 wt %.

An explanation that has been proposed for similar hydrophilic systems suggests that for the low polymer content (here less than ~30 wt %), the majority of chains are intercalated within the inorganic layers and, thus, confinement causes a suppression of the transition. [1] Similar thermal behavior has been observed in glassy polystyrene/organoclay nanohybrids as well, where there was no trace of the glass transition in the composites in which the polymer chains were intercalated within the inorganic layers. [6]

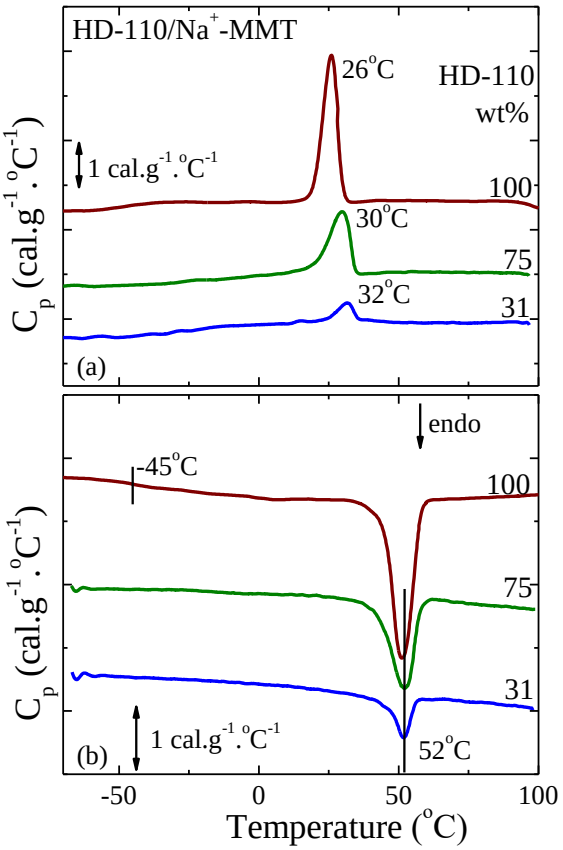

Figure 6.7: DSC measurements of HD-110 / Na^+-MMT nanohybrids during cooling (a) and heating (b).

The DSC measurements of the nanohybrids composed of HD-110 are shown in **Figure 6.7**. In this case the pure polymer shows a very strong crystallization exotherm at T_c = 26 °C, while the nanocomposites show a transition of decreasing amplitude by increasing additive concentration (**Figure 6.7**a). Moreover the crystallization temperature for the nanohybrids, shifts toward higher temperatures.

Table 6.1: Thermal characteristics of the neat polymers and of their nanocomposites.

Sample Polymer/Na^+-MMT	T_g (°C)	T_c (°C)	T_{c1} (°C)	T_{c2} (°C)	T_m (°C)	Degradation Temperature (°C)
EG-110	-22	28	32	60	91	415
93wt% / 7wt%	-15	35	-	64	94	412
89wt% / 11wt%	-15	41	-	70	96	415
84wt% / 16wt%	-	44	-	73	97	406
67wt% / 33wt%	-	43	-	73	97	396
50wt% / 50wt%	-	49	-	-	97	382
30wt% / 70wt%	-	-	-	-	98	375
15wt% / 85wt%	-	-	-	-	-	369
DG-110	-26	No crystallization No melting				420
66wt% / 34wt%	-26					401
45wt% / 55wt%	-29					389
31wt% / 69wt%	-					384
17wt% / 83wt%	-					375
HD-110	-45	26	No cold crystallization		51	405
75wt% / 25wt%	-	30			52	401
31wt% / 69wt%	-	32			52	371

During heating (**Figure 6.7**b), the glass transition is observed at T_g = -45 °C for the pure polymer; this transition is completely suppressed for the nanocomposites. Above the glass transition temperature, the melting of the polymer is observed at similar temperature, T_m = 52 °C, to the bulk HD-110; nevertheless, this temperature does not show any dependence on composition. The heat of fusion decreases from 23.44 cal/g for the bulk HD-110, to 15.37 and

6.13 cal/g for the 75 and 31 wt % in polymer content nanocomposites respectively, since almost all polymer quantity is intercalated and does not crystallize.

It is noted that for the low polymer content nanocomposite (31 wt %), DSC shows very weak crystallization and melting peaks in contrast to the XRD measurements where crystalline diffraction peaks are not observed, indicating that only a very small polymer quantity lacking significant coherence is able to crystallize.

The temperatures of the thermal transitions and the polymer degradation for the three linear polyesters in clay nanocomposites are summarized in **Table 6.1** and compared to the respective in the bulk.

6.3 Structural and Thermal Characterization of Hyperbranched Polyesters / Na^+-MMT

The hyperbranched polyesters Boltorn H20, H30 and H40 and the hyperbranched poly (ester amide) Hybrane S1200, studied in Chapter 3, were also blended with the hydrophilic sodium montmorillonite, Na^+-MMT to form nanocomposites. The synthesis, the structural and thermal properties of the Boltorn nanocomposites were performed by K. Androulaki and were extensively discussed in the respective master thesis, while the Hybrane nanocomposites were investigated by Dr. Fotiadou. [1], [7]

These results will be summarized in this thesis as well so that the obtained structure and properties can be correlated with the polymer dynamics under confinement that are investigated in the current work by Dielectric Spectroscopy and which will be discussed in detail on the current Chapter.

The nanocomposites were prepared via a solution-intercalation method using deionized water as the solvent medium. The polymers were mixed with Na^+-MMT, in water, to synthesize a broad range of compositions covering the complete range between pure polymer and pure clay. Following solvent evaporation, all samples were triturated and thermally annealed at 200 °C for 24 h, to erase any metastable structure formed and to achieve equilibrium. [8], [9]

The XRD measurements of all the hybrids synthesized utilizing H20, H30 and H40 together with the diffractograms of the neat polymer and the pure inorganic material are illustrated in Figure 6.8.a, b and c respectively. The bulk Boltorns are amorphous and they exhibit just a weak amorphous halo. The inorganic material shows a diffraction peak at 2θ = 9°. Addition of polymer (5 wt %) results in a shift of the peak of the clay toward lower angles, verifying the intercalation of the polymer chains inside the inorganic galleries that causes an increase of the interlayer distance. Nevertheless, this peak is broad with a shoulder at the interlayer distance of the Na^+-MMT, indicating still the presence of empty galleries. Upon further addition of polymer the shoulder corresponding to the empty galleries disappears. At low polymer content there is a peak at 2θ = 5.7° corresponding to an interlayer spacing of d_{001} = 1.55 nm with no dependence on the generation, whereas above 50wt % the peak jumps at 2θ = 4.5° for the H20, 2θ = 4.3° for the H30 and 2θ = 4.1° for the H40, corresponding to an interlayer spacing of 1.95, 2.05 and 2.15 nm respectively and thus indicating the formation of bi-layers of polymer inside the galleries.

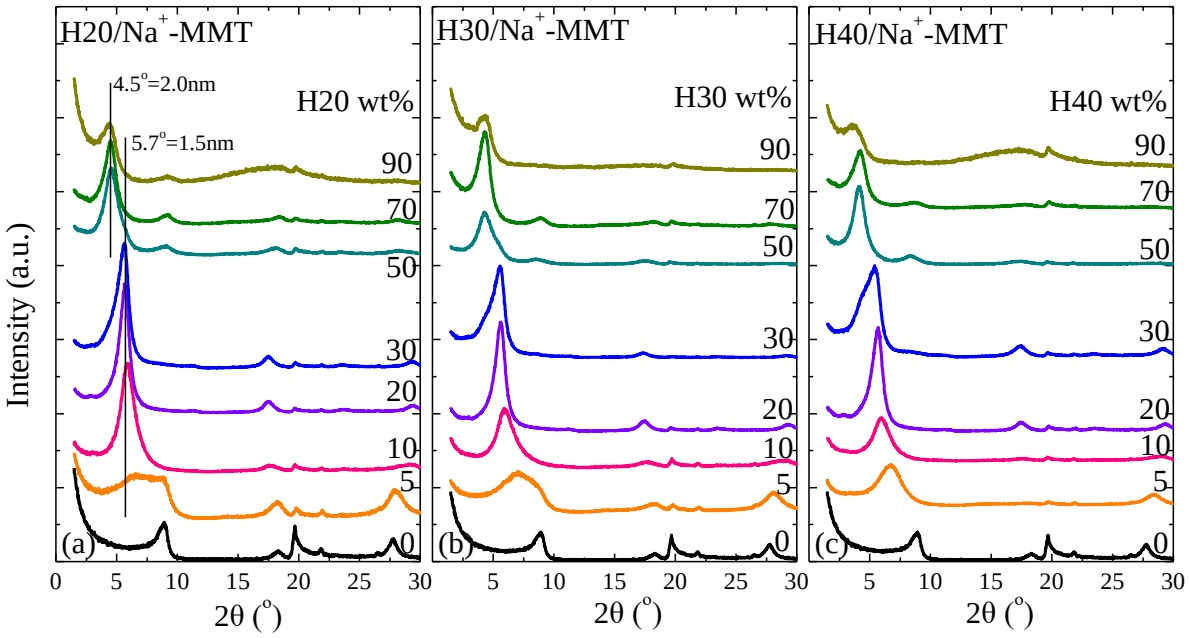

Figure 6.8: X-ray diffractograms of Boltorn / Na^+-MMT nanohybrids.

Taking into consideration the interlayer spacing of the pure montmorillonite, a thin polymer film of ~0.55 nm and of ~1.00 nm thickness can be assumed for the mono- and bi-layers respectively, for all hybrids. In the case of completely full galleries, a second-order diffraction peak can be observed because of the coherence of the structure. The macromolecules exist in flatten conformations inside the galleries; atomistic molecular dynamics simulations [10]

calculated the radii of gyration, R_g, of these systems as $R_{g,H20} \approx 0.8$ nm and $R_{g,H30} \approx 1.05$ nm (at ambient temperature), i.e., similar to the measured changes in the thicknesses in the intercalated films. [9]

Similar results are obtained for the Hybrane nanocomposites; the results of the XRD measurements are shown in **Figure 6.10**.a, with intercalated structures formed for all polymer compositions. Nanohybrids with mono and bi-layers of polymer chains with increasing polymer content are observed in this case as well whereas for completely filled galleries, i.e., above 50 wt % in polymer content, the polymer chains can form an additional layer inside the galleries reaching total thickness of 1.30 nm. [8]

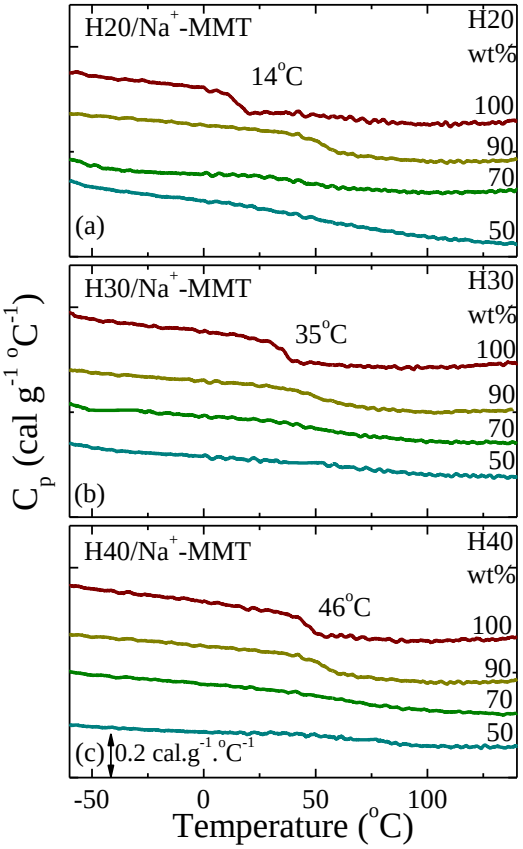

Figure 6.9: DSC measurements of (a) H20 / Na^+-MMT, (b) H30 / Na^+-MMT and (c) H40 / Na^+-MMT nanohybrids during heating.

Figure 6.9 shows the DSC thermograms of H20, H30, and H40 and of the respective hybrids with 50, 70, and 90 wt % in polymer. The Boltorn / Na^+-MMT nanocomposites with 50 and 70 wt % polymer content exhibit no identifiable glass transition (the same holds for all hybrids with lower polymer content). At these polymer concentrations all or most of the polymer chains are confined and the absence of a T_g suggests that the transition is either suppressed

because of confinement or too weak or too broad to be detected by DSC. For all three kind of nanocomposites, only the hybrids with 90 wt % polymer content exhibit a clear glass transition. In all cases, the transition is broader than the respective one of the neat polymer and it is found at higher temperatures, similar between the three generations. Since at lower concentrations no transition is evident, we attribute the one at 90 wt % to excess polymer chains outside the filled galleries that, nevertheless, interact with the inorganic surfaces causing an increase of the T_g. [9]

For Hybrane nanocomposites, presented in **Figure 6.10**.b, the glass transition is observed only in the nanocomposites with the higher polymer concentrations (>50 wt %). Hybrids with lower polymer concentrations do not show any step suggesting that the transition is suppressed.

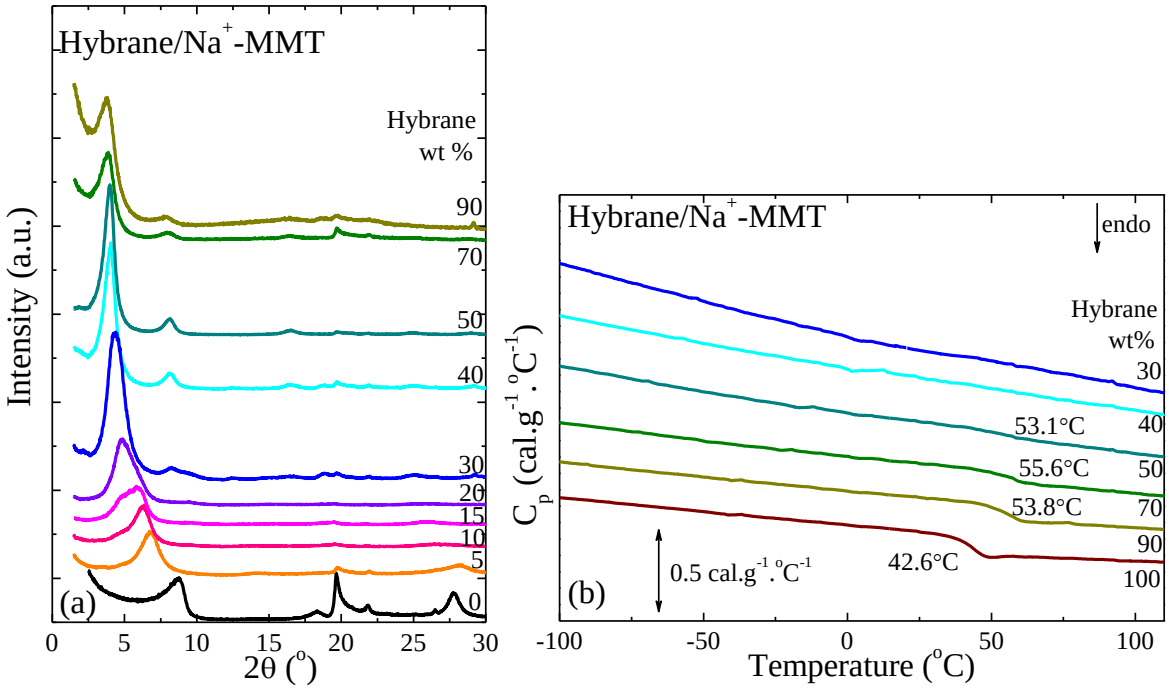

Figure 6.10: Hybrane / Na^+-MMT nanohybrids structure (a) and thermal properties (b). [8]

Furthermore, the T_g of excess Hybrane (for the composites with high polymer content) is by almost 10 °C higher than that of the pure polymer, indicating that the transition of the non-intercalated chains is affected by the presence of the inorganic surfaces, similarly to the hyperbranched polyesters. [8]

Particularly for hyperbranched polymers, it has been found that the glass transition depends strongly on the mobility of their terminal groups. [11] Their partial immobilization due to the interaction with the inorganic surface would, therefore, result to a shift of the apparent glass

transition to higher temperatures, in line with the experimental findings. This increase of the polymer T_g in the presence of the inorganic galleries has been observed before in other hydrophilic polymer / Na^+-MMT nanocomposites. [1]

In **Table 6.2** the glass transition temperatures of the hyperbranched polymers in all nanocomposites with high polymer content, above 50 wt %, are summarized and compared to the respective bulk polymers. As discussed above in all cases the glass transition is suppressed under confinement and the excess polymer obtains higher T_g.

Table 6.2: Thermal characteristics of the neat polymers and of their nanocomposites.

Sample Polymer / Na^+-MMT	T_g (°C)	Sample Polymer / Na^+-MMT	T_g (°C)
H20	14	H40	46
90wt% / 10wt%	54	90wt% / 10wt%	54
70wt% / 30wt%	55	70wt% / 30wt%	66
50wt% / 50wt%	-	50wt% / 50wt%	-
H30	35	Hybrane	43
90wt% / 10wt%	51	90wt% / 10wt%	54
70wt% / 30wt%	59	70wt% / 30wt%	56
50wt% / 50wt%	-	50wt% / 50wt%	53

6.4 Polymer Dynamics under Confinement

In previous works, the dynamics of different polymers has been studied under confinement, in intercalated polymer / layered silicate nanocomposites and their relaxation times were compared to the ones of the bulk polymers. Faster, similar or even slower segmental dynamics was observed depending on the system and the specific polymer / surface interactions that may speed up or slow down the relaxation times in conjunction with the geometrical confinement effect that speeds up the dynamics since it restricts the size of the cooperatively rearranging regions. [1], [3], [12]–[15] However, a common finding of those studies was that in almost all cases, the temperature dependence of the segmental dynamics changed from a VFT to an Arrhenius one indicating that the confined system appears to be a stronger glass.

In the present work polymer dynamics under severe confinement is investigated. In polymer / layered silicate nanocomposites very thin polymer films of ~1nm thickness are formed inside the galleries of the clay making them ideal systems in order to investigate polymer properties under sever confinement. Polymer dynamics is investigated for the nanocomposites of the two linear biobased polyesters EG-110 and DG-110, and for the nanocomposites obtained by all hyperbranched polymers, i.e., the polyester polyols, Boltorn, and the poly (ester amide), Hybrane. The effect of the confinement on polymer dynamics is probed for all polymers by comparing the relaxation times of the intercalated polymers to the respective in the bulk.

6.4.1 Linear polyesters / Na^+-MMT

The linear biobased polyesters mixed with the hydrophilic sodium montmorillonite, Na^+-MMT, provide nanocomposites with intercalated structures as already discussed previously in the present chapter. Dielectric Relaxation Spectroscopy measurements were performed for the two polyesters under confinement, one of which, DG-110, is amorphous, and the other, EG-110, semi-crystalline utilizing 30 wt % polymer nanohybrids, where all polymer chains are intercalated within the complete filled galleries of the inorganic material. The obtained relaxation modes are investigated and compared to the respective of the bulk polymer, presented in Chapter 3.

In the case of the linear polymer / clay nanocomposites, the powder was pressed to form disks of 12 mm in diameter and 0.3-0.6 mm in thickness. The pellets were annealed at 120 °C in vacuum for 24 hours and adhered between indium foils to improve the electrical contact with the electrodes. All samples were cooled to the lowest starting temperature with a cooling rate of 10 °C/min and were thermally equilibrated at successively increasing temperatures before the isothermal data collection.

Figure 6.11 shows the imaginary part of the complex permittivity, ε'', as a function of frequency, for the two nanocomposites with 30 wt % EG- 110 and 30 wt % DG-110, at a broad temperature range. At low temperatures, multiple relaxation processes are observed for both nanocomposites with lower dielectric strength for the DG-110 (**Figure 6.11**.a and c), while above the glass transition temperatures of the neat polymers, another relaxation process is observed, partially obscured by the interfacial polarization effect, MWS, (**Figure 6.11**.b) and

the conductivity (Figure 6.11.d). In all cases, analysis of the spectra is necessary to quantitatively compare the findings.

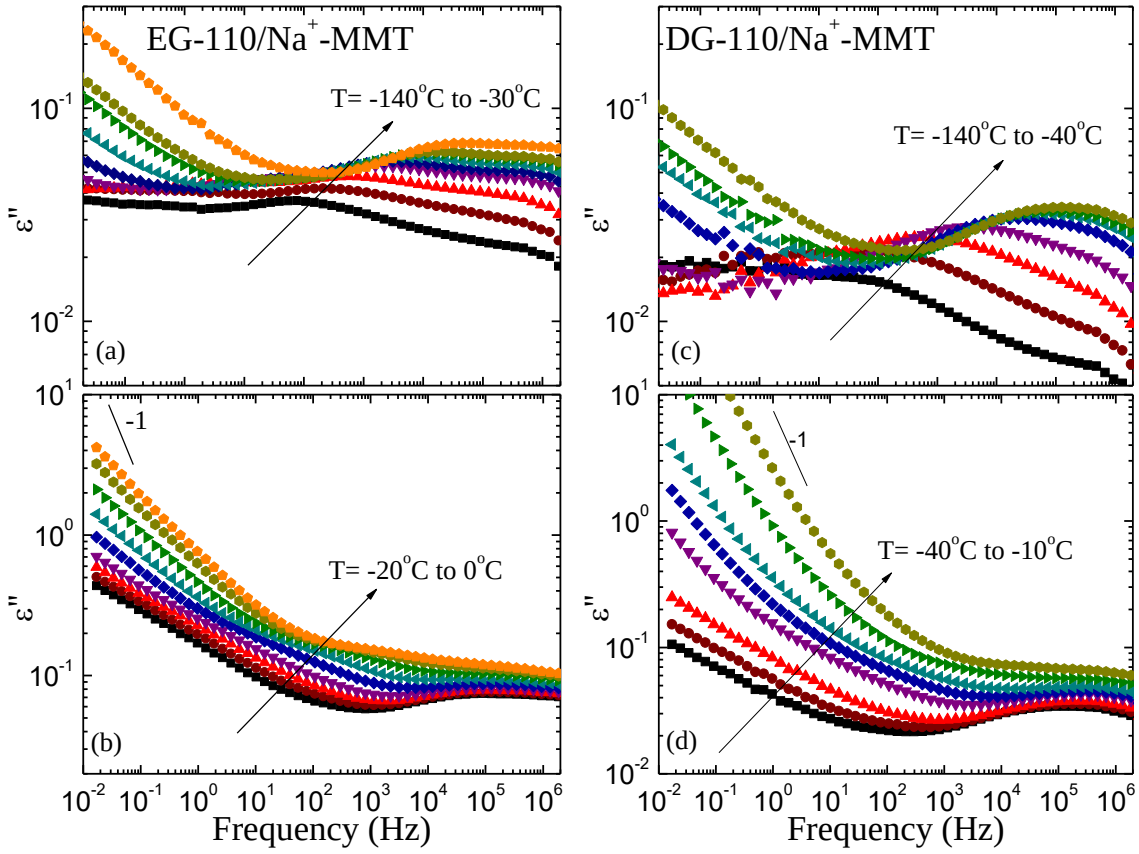

Figure 6.11: Imaginary part of the complex dielectric permittivity, ε", for EG-110 / Na^+-MMT (a,b) and DG-110 / Na^+-MMT (c,d) as a function of frequency, for the low (a,c) and the high (b,d) temperature regime.

Figure 6.12 illustrates the quantitative analysis of the dielectric data at two different temperatures for the EG-110 and DG-110 nanocomposites together with the bulk polymer analysis at the same temperatures. The $\varepsilon^*(\omega)$ data were analyzed utilizing the empirical Havriliak - Negami (HN) functions. An additional ionic conductivity contribution at low-frequencies and high temperatures is included.

At the low temperature regime two relaxation processes are observed due to the local motions of the polymers, similarly to the pure polymers; however, the spectra exhibit different shape and possess lower dielectric strength (Figure 6.12.a and c). Above the glass transition temperature of the respective bulk polymers (it is noted that for the specific nanocomposites no glass transition could be observed by DSC), another process appears

attributed to the segmental relaxation but slower than the α-process of the bulk EG-110 and DG-110.

For the nanocomposites of the present investigation, the β parameter of all three processes and for both systems is fixed to 1.0. For the fast sub-T_g process the α parameter varies between 0.25 and 0.34 and the dielectric strength Δε is 0.15−0.3 and 0.3−0.5 for DG-110 and EG-110, respectively, and increases with increasing temperature in both cases. For the slower sub-T_g process a relatively low relaxation strength of ~0.1 is obtained for both nanocomposites, whereas the α parameter is determined to be 0.32−0.45 and 0.4−0.65 for DG-110 and EG-110, respectively.

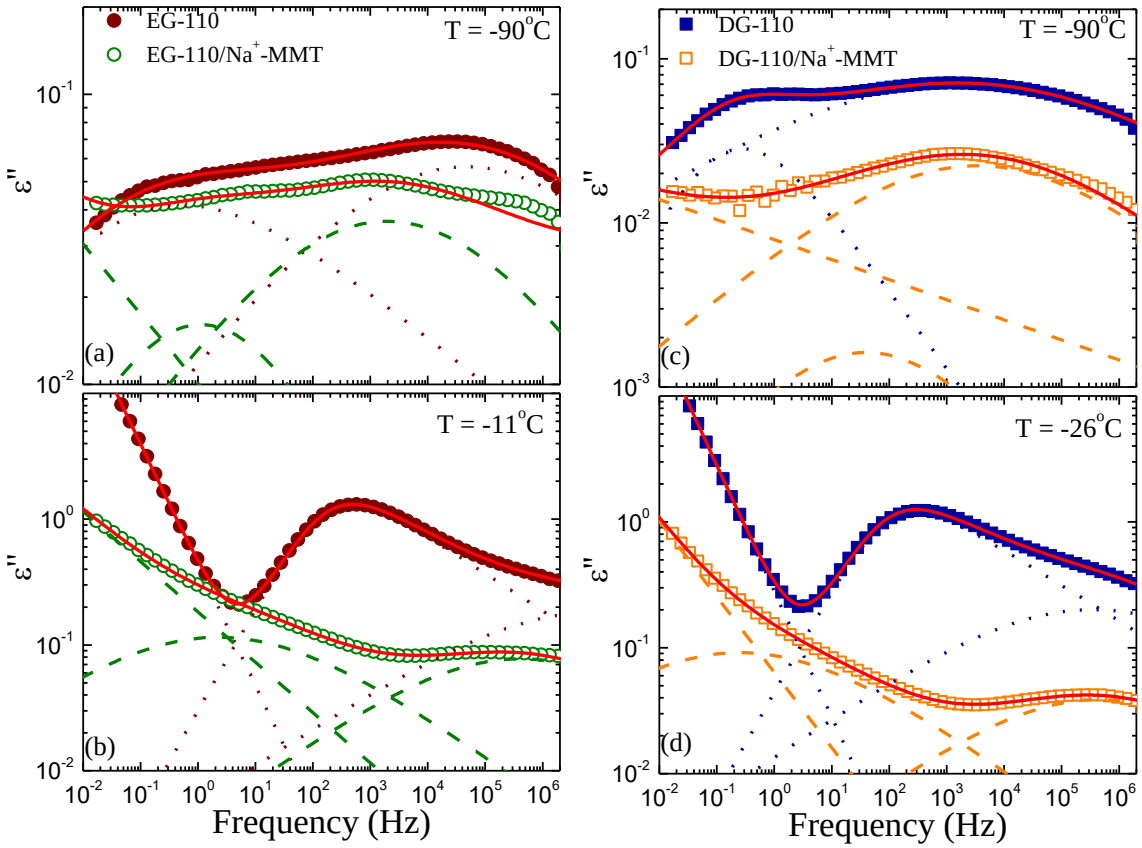

Figure 6.12: Imaginary part of the dielectric permittivity, ε'', for EG-110 and 30 wt % EG-110 / Na^+-MMT nanocomposite at -90 °C (a) and at -11 °C (b) and for DG-110 and 30 wt % DG-110 / Na^+-MMT nanohybrid at -90 °C (c) and at -26 °C (d). The red solid lines are the total fit, whereas the dotted and dashed lines are the deconvoluted relaxation processes for the neat polymers and for the nanocomposites, respectively.

At higher temperatures, the segmental relaxation process appears slower than the respective process of the bulk polymers with shape parameter α around 0.3−0.5 for both nanocomposites, whereas the dielectric strength Δε decreases from 1.4 to 0.35. It is noted

that, for the nanocomposites, the influence of conductivity to the spectra is significantly lower but there is a strong interfacial polarization effect, the contribution of which is denoted as a line with slope 0.4−0.6.

Figure 6.13 shows the relaxation times of the two nanocomposites with 30 wt % EG-110 and 30 wt % DG-110 together with the relaxation processes observed in the bulk polymer, as solid lines. The three relaxation processes of the bulk polymers are also present in nanocomposites; their relaxation times exhibit both similarities and differences in comparison with the corresponding dynamics of the neat polymers. The two sub-T_g processes of the confined polymers appear at similar relaxation times with the ones of the bulk DG-110 and EG-110 with both of them following Arrhenius temperature dependencies; both processes in the nanohybrids exhibit lower activation energies than those of the neat polymers.

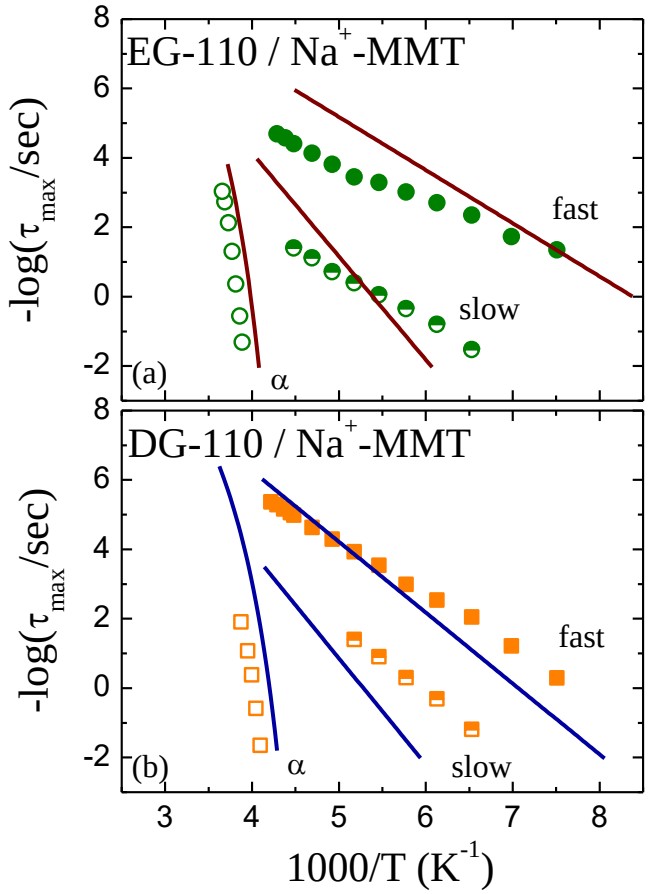

Figure 6.13: Arrhenius relaxation map of EG-110 / Na^+-MMT. Solid lines correspond to the relaxation processes for the pure EG-110.

It is reminded that for the bulk polymers the two sub-T_g processes, the fast and the slow, are attributed to the free and restricted rotation of the hydroxyl groups with their activation

energies shown in **Table 6.3**. In nanocomposites the activation energy of the fast process is 19.6 ± 0.4 kJ/mol for the EG-110 and 28.5 ± 0.5 kJ/mol for the DG-110, whereas for the slow process is 26.0 ± 0.5 kJ/mol for the EG-110 and 36 ± 1 kJ/mol for the DG-110 indicating that the motions become even less restricted than in the bulk.

For the nanocomposites the obtained relaxation times for the segmental process are slower than the respective ones of the neat polymer following a VFT temperature dependence as well. The parameters obtained by the fit are B = 1165 ±20 K and T_0 = 222.0±2.0 K for the EG-110 and B = 1418 ± 25 K and T_0 = 204.0 ± 3.0 K for the DG-110 nanohybrid, resulting in fragility parameter D = B/T_0 ~ 5.2 lower than the one of the bulk EG-110 and D = B/T_0 ~ 7.0, higher that the respective of the bulk DG-110.

Table 6.3: Results of the relaxation processes for the linear polyesters in nanocomposites.

Material	Fast process E_a (kJ/mol)	Slow process E_a (kJ/mol)	α- process	Fragility parameter
EG-110	30 ± 1	59 ± 1	B = 1286 ± 5 K T_0 = 208.0 ± 3 K	6.2
EG-110 / Na^+-MMT	19.6 ± 0.4	26.0 ± 0.5	B = 1165 ± 20 K T_0 = 222.0 ± 2 K	5.2
DG-110	38 ± 1	60 ± 2	B = 1177 ± 5 K T_0 = 199.0 ± 1 K	5.9
DG-110 / Na^+-MMT	28.5 ± 0.5	36 ± 1.0	B = 1418 ± 25 K T_0 = 204.0 ± 3 K	7.0

According to previous studies on polymer dynamics in polymer / layered silicate nanocomposites the temperature dependence of the segmental relaxation changed from a VFT to an Arrhenius one, indicating that the confined system appears to be a stronger glass. [3], [11] Similar behavior is observed in hyperbranched polyesters under confinement as well, and will be discussed in the following paragraph. [8] In the current case of the linear polyesters, the VFT temperature dependence of the segmental relaxation times is retained. This may be attributed to the small size of the polymers in this study, which may be

comparable to the size of the interlayer distance and, thus, does not result in a significant confinement. [5]

6.4.2 Hyperbranched polyesters / Na^+-MMT

The dynamics of the three Boltorn hyperbranched polyesters was investigated in the bulk and under severe confinement; nanohybrids of ~ 50 wt % Boltorn / Na^+-MMT were utilized because the structural characterization indicated that in these compositions all polymer chains are intercalated inside filled galleries. For the Hybrane nanohybrids, it is the 30 wt % Hybrane / Na^+-MMT nanocomposite where all the amount of polymer appears to be under confinement. Dynamics was probed by dielectric relaxation spectroscopy in a wide range of frequencies and temperatures, both above and below the glass transition temperature, T_g, of the bulk polymers. The results obtained for the polymer dynamics in nanocomposites are compared to the respective of the bulk polymer, presented in Chapter 3.

For all hyperbranched nanocomposites, the powder of the material was pressed to form disks 12 mm in diameter and 0.3–0.6 mm in thickness. The pellets were annealed at 140 °C in vacuum for 24 h and adhered between indium foils to improve the electrical contact with the electrodes. All samples were kept at the highest starting temperatures for 30 min prior to the measurements and were thermally equilibrated at successively decreasing temperatures before the isothermal data collection.

Boltron / Na^+-MMT

Figure 6.14 shows the imaginary part of the complex dielectric permittivity for the three Boltorn / Na^+-MMT nanocomposites in a very broad temperature range. The spectra of the hybrids compared between the three generations of the Boltorn, both below as well as above the T_g of the respective polymer, are very similar. At low temperatures, multiple relaxation processes are observed while at higher temperatures, but still below the glass transition temperature of neat polymer (no calorimetric T_g has been observed by DSC for the specific hybrids), the presence of an additional process becomes evident which is observable even above T_g. For even higher temperatures (above 30 °C), an additional process appears in all nanocomposites attributed to the Maxwell-Wagner-Sillars polarization effect (MWS), due to the presence of the surfaces.

The behavior is clearly different than the dynamics of the bulk H20, H30, and H40 where two sub-T_g relaxation processes of different shape, higher dielectric strength and significantly slower relaxation times, and the segmental relaxation above the T_g, were observed. To differentiate the processes in nanocomposites are named with the same Greek letter as in the bulk, followed by a prime apex (α', β', γ').

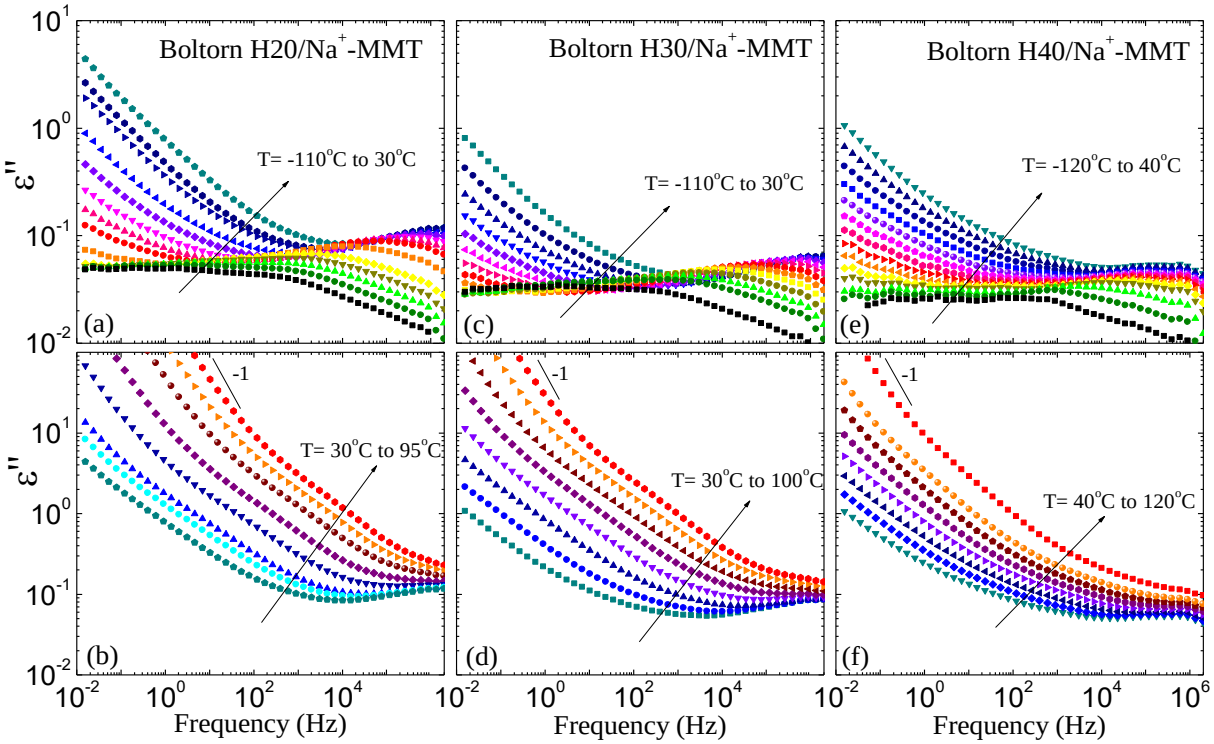

Figure 6.14: Imaginary part of the complex dielectric permittivity, ε'', as a function of frequency, for the low (a, c, e) and the high (b, d, f) temperature regime, of H20 / Na^+-MMT (a, b), H30 / Na^+-MMT (c, d) and H40 / Na^+-MMT (e, f).

Quantitative comparison on the relaxation processes and their characteristic times was performed both between the three different generations of the polymers and between the polymers in the bulk and under confinement in the nanohybrids. The ε*(ω) data were analyzed utilizing the empirical Havriliak-Negami (HN) functions and an additional ionic conductivity contribution at low-frequencies and high temperatures.

Figure 6.15 demonstrates the representative analysis of the spectra of the second generation 50 wt % Boltorn H20 nanocomposite, for three temperatures, below, slightly above and much above the T_g of the bulk polymer. From the spectra at low temperatures, the shape and relaxation strength parameters are determined for the γ'- and β'-processes of the nanocomposites. For all the three generation nanocomposites, the β parameter of the γ'-

process is fixed to 1.0; temperature dependent α parameter (0.23 − 0.31) and Δε (0.2 − 0.87) values were utilized with the dependencies derived from the low temperature spectra. The β'-process can be resolved only in a limited range of temperatures; for all the three generations the β parameter is fixed to 1.0, the α parameter takes values around 0.3 − 0.4 and the dielectric strength, Δε ∼ 0.1, is quite low in all cases.

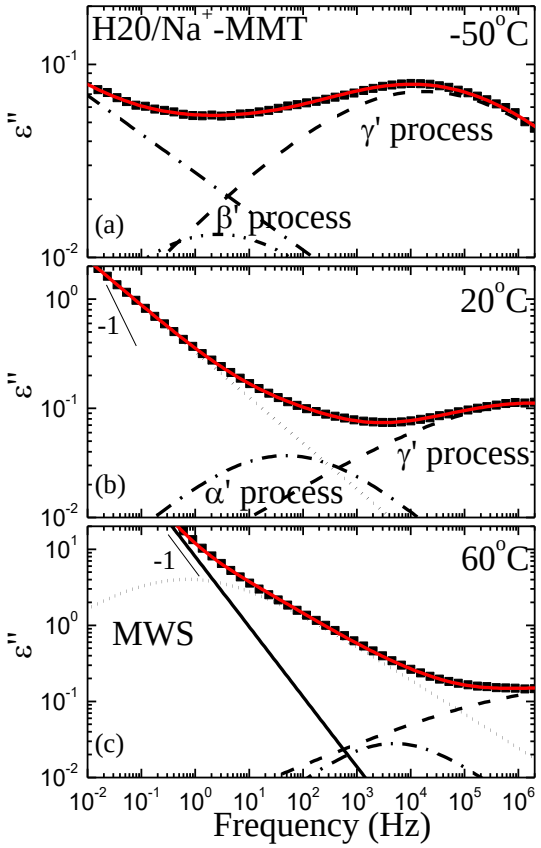

Figure 6.15: Representative analysis of Boltorn H20 / Na^+-MMT. Imaginary part of the dielectric permittivity, ε'', at T=-50°C below the bulk H20 T_g (a), T=20°C above the T_g (b) and T=60°C well above the T_g (c). The processes needed for the deconvolution of the spectra are shown with black lines, whereas the red lines are the summation of the processes.

At higher temperatures, below the bulk polymer T_g, the intermediate α'-process appears and, at even higher temperatures, the slow MWS process becomes evident. For both the intermediate and the slow process the β parameter is fixed at 1.0. The α parameter of the α'-process for all three nanocomposites is around 0.26−0.5 and Δε decreases from 0.7 to 0.12; for the slow process, α is around 0.45−0.53. All the fitting parameters are summarized in **Table 6.5**. At low frequencies and high temperatures, the addition of a contribution due to ionic conductivity is necessary as a line with a slope of ∼0.92−0.98, it is noted that conductivity can obtain values lower that 1 for composite materials. [16]

Figure 6.16 shows the results of the above analysis concerning the relaxation times for all three Boltorn nanocomposites in an Arrhenius representation. The two sub-T_g relaxation processes observed obtain very similar relaxation times for the three generations. The intermediate, α'-process, exhibits an Arrhenius temperature dependence and relaxation times that become slower by increasing the generation is attributed to the segmental relaxation under confinement that substitutes the well-known α-process. According to recent studies on linear polymers, such as poly (ethylene oxide), confined within the galleries of layered silicate, the segmental relaxation (α'- process) was observed below the bulk polymer T_g, with an almost Arrhenius temperature dependence. [3] This Arrhenius like behavior of the α'- process, was also observed in previous studies of PMPS under confinement. [12] Similar findings were observed for other glass formers in nanopores, as well. [17]–[19]

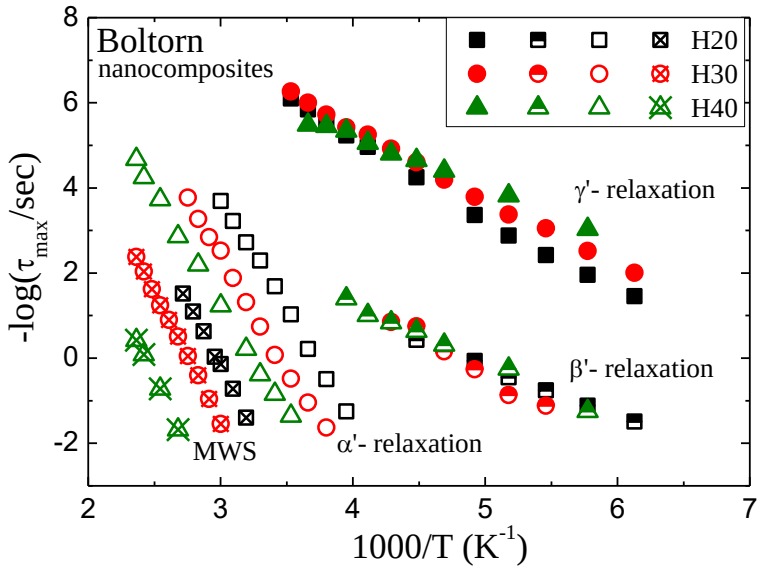

Figure 6.16: Arrhenius relaxation map for the H20 / Na^+-MMT, H30 / Na^+-MMT and H40 / Na^+-MMT nanocomposites.

For the fastest, γ'-process, the activation energies that result from the temperature dependence of the relaxation times have values $E_{\gamma',H20}$ = 32.5 ± 2.5 kJ/mol, $E_{\gamma',H30}$ = 31 ± 2 kJ/mol, and $E_{\gamma',H40}$ = 23 ± 1 kJ/mol (Table 6.4). This process is identified as the motion of the polar hydroxyl groups of the confined chains. These values are very similar to the activation energy obtained for the sub-T_g process for a linear poly (ethylene oxide) (neat and confined), the dynamics of which was measured with DRS. [3] As discussed in Chapter 3, higher activation energies were obtained for the bulk Boltorn polymers which were attributed to the hindrance in the motion imposed by the formed hydrogen bond network. Under confinement, the

flattened conformation that the polymers assume because of the spatial restrictions is not appropriate for the hydrogen bonds to form, causing the activation energy for the respective motion to be lower than the one of the bulk, and to approach the value obtained for a non-hydrogen bonded system.

The second sub-T_g process, called β', shows similar temperature dependence to the γ'-process. The activation energies for this process are $E_{\beta',H20}$ = 23.5 ± 1.0 kJ/mol, $E_{\beta',H30}$ = 32.5 ± 2.5 kJ/mol, and $E_{\beta',H40}$ = 26 ± 1 kJ/mol. This motion is attributed to the carbonyl reorientation and is less restricted motion under confinement due to the fewer hydrogen bonds as well. Thus, the relaxation times for the two sub-T_g processes are much faster than the respective ones of the neat polymers and with much weaker Arrhenius temperature dependencies; for comparison reasons the activation energies for the Boltorn polymers, in the bulk and in nanocomposites, are summarized in **Table 6.4**. The lower activation energy observed, for the sub-T_g processes under confinement, is a behavior similar to the linear polyesters.

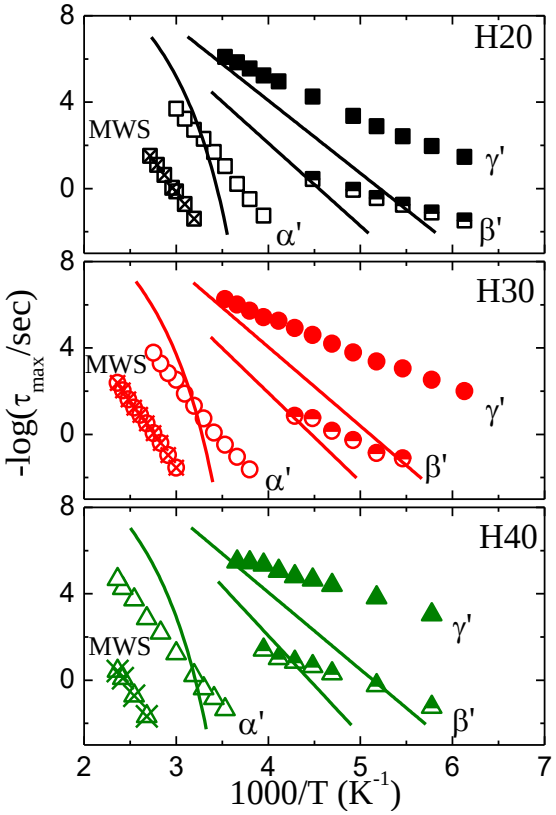

Figure 6.17: Arrhenius relaxation map of Boltorn / Na^+-MMT nanocomposites. Solid lines correspond to the relaxation processes for the respective pure polymer.

The relaxation times of the H20, H30 and H40 nanocomposites are presented in **Figure 6.17**.a, b and c respectively, together with the relaxation processes of the respective bulk polymer

(solid lines). In the case of the Boltorn polymers, the α'-process is much faster than the one of the neat polymer for lower temperatures or in the proximity of the glass transition temperature but, at higher temperatures, it appears to cross the α-process of the bulk polymer becoming much slower. The dielectric strength of the α' process decreases with increasing temperature that is a property typical of the segmental relaxation. Also the activation energy of the process suggests that it is not related to the motion of a single subunit. In fact, their values are very high: $E_{\alpha',H20}$ = 99.4 ± 2.0 kJ/mol, $E_{\alpha',H30}$ = 100.7 ± 2.0 kJ/mol, and $E_{\alpha',H40}$ = 99.2 ± 2.0 kJ/mol, whereas they are very similar for the three confined polymers (**Table 6.4**). Nevertheless, it appears in the frequency window at higher temperatures with increasing the generation (−30, −10, and 10 °C). Additionally, the difference between the bulk T_g and the temperature at which the α'-process appears, seems to be rather similar for the three generations (H20, 44 °C; H30, 45 °C; and H40, 36 °C). It is noted once more that DSC did not show any thermal transitions for the hybrids with 50 wt % polymer content, whereas, for higher compositions, where a transition was indeed observed its temperature was higher that the respective of the pure polymers. [9]

Table 6.4: Results of the relaxation processes for the Boltorns in nanocomposites.

Boltorn	γ- process E_a (kJ/mol)	β- process E_a (kJ/mol)	α- process
H20	65.0 ± 1.5	70.0 ± 3.0	VFT
H30	69.5 ± 1.0	81.0 ± 9.0	
H40	66.5 ± 1.5	86.0 ± 2.0	
Boltorn / Na^+-MMT	**γ′- process E_a (kJ/mol)**	**β′- process E_a (kJ/mol)**	**α′- process E_a (kJ/mol)**
H20 / Na^+-MMT	32.5 ± 2.5	23.5 ± 1.0	99.4 ± 2.0
H30 / Na^+-MMT	31.0 ± 2.0	32.5 ± 2.5	100.7 ± 2.0
H40 / Na^+-MMT	23.0 ± 1.0	26.0 ± 1.0	99.2 ± 2.0

Finally, at even higher temperatures, the slow MWS process appears, for all confined systems, due to interfacial polarization because of the large number of interfaces constituting the

nanocomposites and the ions trapped in their proximity. This process shows an Arrhenius temperature dependence and a significant effect on the generation as well.

Hybrane / Na⁺-MMT

Figure 6.18 shows the imaginary part of the complex dielectric permittivity for the Hybrane/Na⁺-MMT nanocomposite in a very broad temperature range. At low temperatures, the spectra seem to have two relaxation processes like in the case of the pure polymer; nevertheless, all curves have a very different shape (very narrow) with lower dielectric strength.

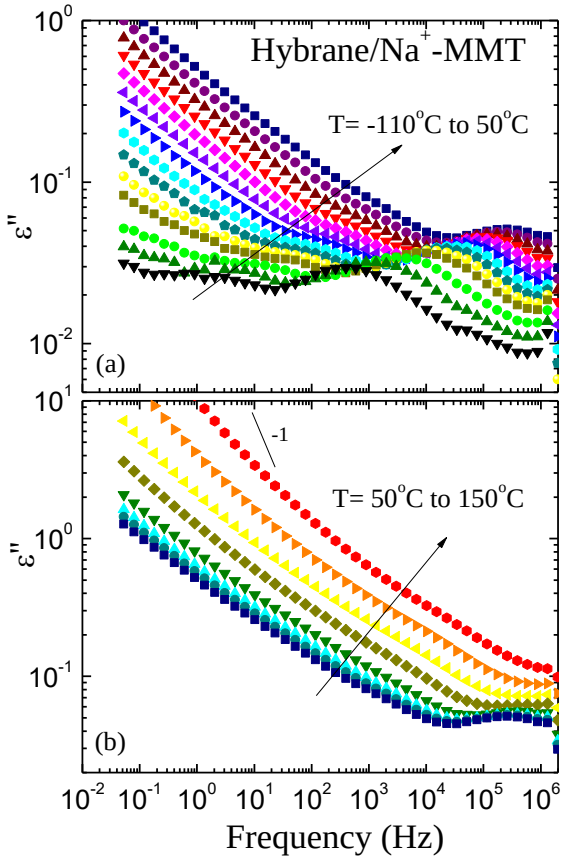

Figure 6.18: Imaginary part of the complex dielectric permittivity, ε", of Hybrane/Na⁺-MMT as a function of frequency, for the low (a) and the high (b) temperature regime.

At higher temperatures, around the T_g of the bulk polymer, no relaxation processes are observed; only a strong interfacial polarization effect is present. It is only at even higher temperatures, 90 °C (dark yellow diamonds) to 150 °C (red circles) where another process is evident due to a peculiar increasing of the dielectric strength in the data, as shown in **Figure 6.18**.b.

Figure 6.19 demonstrates the representative analysis of the spectra of the Hybrane nanocomposite, for three temperatures, below, slightly above and much above the T_g of the bulk polymer. From the analysis, it appears that in all cases, multiple relaxation processes are necessary to obtain a good fit to the data. From the spectra at low temperatures, the shape and relaxation strength parameters are determined for both the fast and the slow sub-T_g processes of the nanocomposites.

The fast process is asymmetric and quite narrow, with the α parameter increasing from 0.55 to 0.67 by increasing the temperature and $\Delta\varepsilon \sim 0.15$. The slow process exhibits very low dielectric strength, $\Delta\varepsilon \sim 0.1$ which decreases by increasing temperature to $\Delta\varepsilon \sim 0.03$ at 50 °C whereas the β parameter is fixed to 1.0 and the α parameter takes values around 0.46 − 0.74.

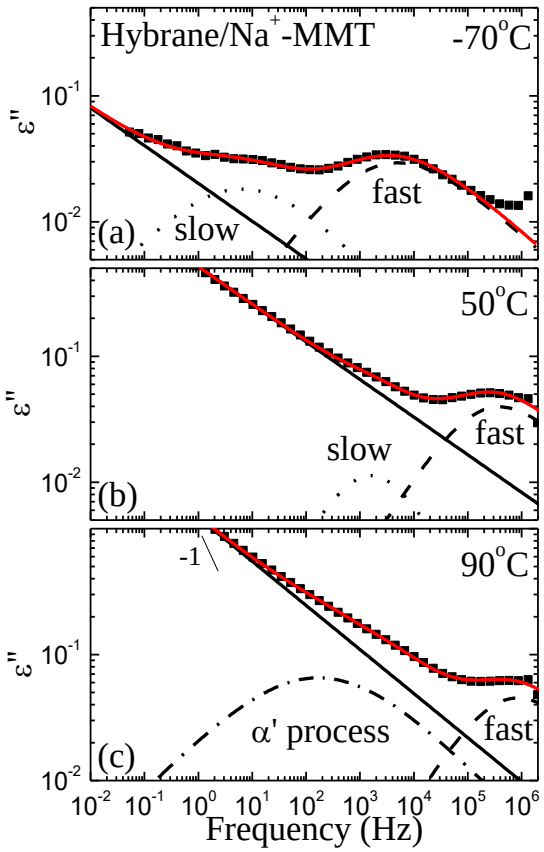

Figure 6.19: Imaginary part of the dielectric permittivity, ε'', of Hybrane/Na^+-MMT at T=-70°C below the bulk polymer T_g (a), T=50°C above but close to the T_g (b), and T=90°C well above the T_g (c). The processes needed for the deconvolution of the spectra are shown with black lines, whereas the red lines are the convolution of the processes.

At temperatures well above the bulk polymer T_g, the α'-process appears. The β parameter of the α'-process is fixed at 1.0; the α parameter is around 0.44 - 0.6 and Δε decreases from 0.36 to 0.15. At low frequencies and high temperatures, the addition of a contribution due to MWS

polarization is necessary as a line with a slope of ~0.3 – 0.35; it is noted that the conductivity is observed only at few high temperatures. All the fitting parameters obtained by the analysis of both linear and hyperbranched polymers in clay nanocomposites are presented together in the following **Table 6.5**.

Table 6.5: Parameters of the HN function for each relaxation process in polymer/Na^+-MMT nanocomposites.

HN parameters	Polymer / Na^+-MMT			
	EG-110	DG-110	BOLTORN	HYBRANE
Fast / γ΄- process – local motions of free –OH groups				
β	1		1	<1
α	0.25-0.34		0.46-0.74	0.55-0.67
Δε	0.30-0.50	0.15-0.30	0.20-0.87	0.15
Slow process – local motions of constrained –OH groups				
β	1		No process	1
α	0.40-0.65	0.32-0.45		0.46-0.74
Δε	0.10			0.10-0.03
β΄-process – local motions of ester groups				
β	No process		1	No process
α			0.30-0.40	
Δε			0.10	
α΄-process				
β	1		1	1
α	0.30-0.50		0.26-0.50	0.44-0.60
Δε	1.40-0.35		0.70-0.12	0.36-0.15

Figure 6.20 shows the relaxation times of the Hybrane nanocomposite in an Arrhenius representation together with the relaxation processes of the bulk Hybrane presented in Chapter 3. The two sub-T_g relaxation processes are observed with weaker Arrhenius dependence compared to the bulk polymer; the intermediate and segmental relaxation are not observed, however at much higher temperatures the α'-relaxation is evident.

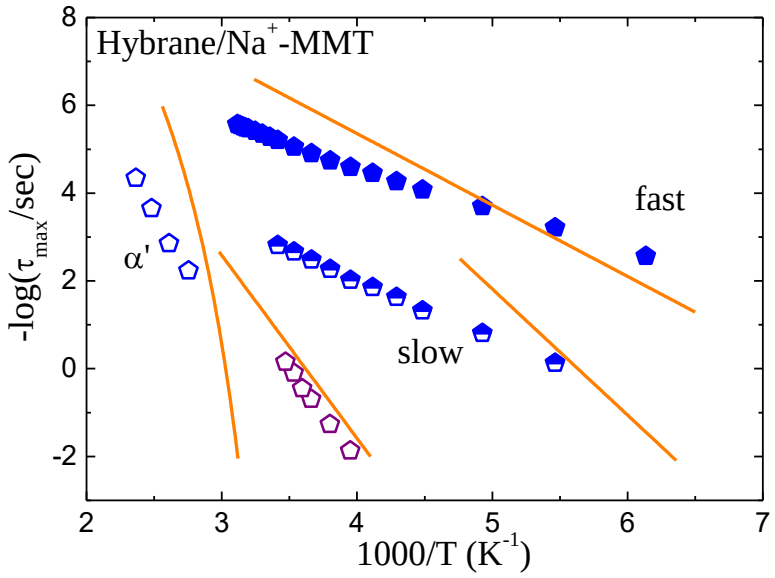

Figure 6.20: Arrhenius relaxation map of Hybrane / Na^+-MMT. Solid lines correspond to the relaxation processes for the pure Hybrane and the purple open pentagons to the α′-process of the Hybrane / GO.

For the sub-T_g relaxation processes, the activation energies that result from the temperature dependence of the relaxation times are 19.0 ± 1 kJ/mol for the fast and 25.5 ± 0.5 kJ/mol for the slow process. As mentioned above both relaxations obtain lower activation energies than the bulk (33.0 ± 2 kJ/mol for the fast and 60 ± 4 kJ/mol for the slow), behavior similar to the Boltorn nanocomposites. However, in this case the relaxation times of the fast process are close to the respective in the bulk at low temperatures and cross by increasing temperature resulting in slower relaxation times. This fast process is attributed to the rotation of the hydroxyl groups that becomes less restricted in nanocomposites. Probably this fast process is the one observed by quasielastic neutron scattering measurements, as well, performed on the same hyperbranched poly (ester amide) Hybrane showing that the very local sub-T_g dynamics exhibits similar behavior in the bulk and under confinement. In that work the sub-T_g process was attributed to a methyl and/or hydroxyl group rotation which could be coupled and also affected by both intra and intermolecular hydrogen bonds that are formed in these hyperbranched systems. [8]

As far as the α'-process is concerned, it can be observed only at very few temperatures, well above the T_g of the bulk Hybrane, with relaxation times slower than the respective of the bulk polymer; this process resembles the behavior of the relaxation times observed for the α'-process of the Boltorn nanocomposites at high temperatures. From its relaxation times,

although only few points can be obtained, an Arrhenius temperature dependence is evident with significantly high activation energy, 101 ± 5 kJ/mol. This process could be a continuation of the α′-process observed at lower temperatures for the Hybrane / GO nanocomposite (Chapter 5) illustrated in **Figure 6.20** as purple open pentagons; it is noted that the activation energy of this process is very high, 80 ±5 kJ/mol, as well.

6.5 Polymers of Different Architecture under Confinement

Nanocomposite materials with the natural hydrophilic clay, sodium montmorillonite and various polymers were synthesized. The polymers utilized were three linear biobased polyesters with differences in their repeating unit and four hyperbranched polymers, three polyester polyols with different degree of branching, Boltorn, and a poly (ester amide), Hybrane, of similar architecture. The nanohybrids were prepared by solution mixing in water over a broad range of compositions and thermal annealing was applied following solvent evaporation to ensure equilibrium.

The structure of the clay nanocomposites as well as the morphology of both the linear and the hyperbranched polymers under confinement were studied by X-ray diffraction. In all cases intercalated structures were obtained and a layer by layer structure was formed inside the galleries of the clay, depending on the polymer content.

A thin polymer film was formed within the galleries of the inorganic material with mono-layer thickness ∼0.35nm for the linear polyesters, ∼0.40nm for the hyperbranched Hybrane and ∼0.50nm for the Boltorn nanocomposites of low polymer content. For hybrids obtaining polymer content higher than 50 wt %, only filled galleries are formed with bilayers of ∼0.7nm and ∼1.0nm thickness for both the linear and hyperbranched polyesters respectively; while for the poly (ester amide) an extra layer is formed of total thickness 1.3nm. The structural differences of the nanocomposites could be attributed to the different interactions between the polymer (containing different functional groups) and the clay surface as well as to the polymer architecture.

The polymers show different thermal properties as discussed in Chapter 3; all the hyperbranched polymers and the linear DG-110 are amorphous, whereas the other two linear polyesters, EG-110 and HD-110, are semi-crystalline with different crystallization behavior. In

the presence of the additive, the thermal properties of all polymers are strongly affected; the thermal transitions under confinement, where all the polymer is inside the galleries, are completely suppressed and only the excess polymer shows thermal transitions with differences compared to the bulk.

In polymer / layered silicate nanocomposites it is not only the confined polymer which is affected, but it is also the polymer quantity outside of the galleries that shows differences in the thermal properties. The glass transition, whenever it can be resolved, appears insensitive to the presence of the inorganic material for the linear polymers, whereas it appears shifted at higher temperatures for the hyperbranched ones. For the semi-crystalline polymer, EG-110, nanohybrids in contrast to the pure polymer, the crystallization occurs during cooling and the cold crystallization observed in the neat EG-110 is not evident. In both EG-110 and HD-110 the crystallization and melting temperatures are similar or higher than the respective ones of the bulk polymer.

The composition of the nanohybrids where all the thermal transitions are suppressed is 50 wt % for the hyperbranched Boltorn nanocomposites and 30 wt % in polymer content for the linear polyesters and the hyperbranched Hybrane.

Finally the thermal stability of the polymer in the nanohybrids is similar to the one observed in the bulk of nanocomposites with low additive loading and gradually deteriorates by increasing the content of the clay.

Polymer dynamics was studied utilizing dielectric relaxation spectroscopy for the nanocomposites where all the polymer is anticipated to more-or-less reside within the completely filled galleries of the clay; the relaxation processes under confinement were investigated and compared to the respective in the bulk.

In all cases, the nanocomposites show two sub-T_g processes and the segmental relaxation. The fast and slow local relaxations obtain lower activation energies compared to the respective of the bulk in both linear and hyperbranched polyesters, indicating that the two motions are less restricted. Due to the spatial restrictions under confinement the polymer obtains a flatten conformation which does not favor the formation of the hydrogen bonds. The relaxation times

of the two sub-T_g processes are very similar between three generations of the hyperbranched polyesters, Boltorn, in polymer/clay nanohybrids.

The segmental relaxation exhibits significant differences between the linear and the hyperbranched polyesters. In the case of the segmental dynamics under confinement for the linear polymers, the α′-process becomes slower for both polymers retaining, however, the VFT temperature dependence. This behavior could be attributed to their low molecular weight and thus small size, which may be comparable to the size of the interlayer distance. Therefore in this case polymer chains are not significantly confined.

On the other hand, the segmental relaxations under confinement for the hyperbranched polyester polyols reveal an Arrhenius temperature dependence; the α′-process emerges, below the T_g of the respective bulk polymer, with Arrhenius temperature dependence and a significant dependence on the generation. Similar Arrhenius behavior is observed for the segmental hyperbranched poly (ester amide) under confinement, nevertheless the α′-process is evident only at high temperatures.

6.6 References

[1] S. Fotiadou, K. Chrissopoulou, B. Frick, and S. H. Anastasiadis, "Structure and Dynamics of Polymer Chains in Hydrophilic Nanocomposites," *J. Polym. Sci. Part B Polym. Phys.*, vol. 48, pp. 1658–1667, 2010.

[2] K. Chrissopoulou *et al.*, "Crystallinity and Chain Conformation in PEO / Layered Silicate Nanocomposites," *Macromolecules*, vol. 44, pp. 9710–9722, 2011.

[3] M. M. Elmahdy, K. Chrissopoulou, A. Afratis, G. Floudas, and S. H. Anastasiadis, "Effect of confinement on polymer segmental motion and ion mobility in PEO/layered silicate nanocomposites," *Macromolecules*, vol. 39, no. 16, pp. 5170–5173, 2006.

[4] E. Hackett, E. Manias, and E. P. Giannelis, "Computer Simulation Studies of PEO / Layer Silicate," *Chem. Mater.*, vol. 12, pp. 2161–2167, 2000.

[5] K. Androulaki, K. Chrissopoulou, D. Prevosto, M. Labardi, and S. H. Anastasiadis, "Structure and Dynamics of Biobased Polyester Nanocomposites," *Biomacromolecules*, vol. 20, no. 1, pp. 164–176, 2019.

[6] R. A. Vaia, H. Ishii, and E. P. Giannelis, "Synthesis and Properties of Two-Dimensional Nanostructures by Direct Intercalation of Polymer Melts in Layered Silicates," *Chem. Mater.*, vol. 5, no. 12, pp. 1694–1696, 1993.

[7] K. Androulaki, "Structure and dynamics in hyperbranched polymer / layered silicate nanocomposites," University of Crete, Master Thesis, 2013.

[8] S. Fotiadou *et al.*, "Structure and Dynamics of Hyperbranched Polymer / Layered Silicate Nanocomposites," *Macromolecules*, vol. 46, pp. 2842–2855, 2013.

[9] K. Androulaki, K. Chrissopoulou, D. Prevosto, M. Labardi, and S. H. Anastasiadis, "Dynamics of Hyperbranched Polymers under Confinement: A Dielectric Relaxation Study," *ACS Appl. Mater. Interfaces*, vol. 7, no. 23, pp. 12387–12398, 2015.

[10] I. Tanis, K. Karatasos, A. N. Assimopoulou, and V. P. Papageorgiou, "Modeling of hyperbranched polyesters as hosts for the multifunctional bioactive agent shikonin," *Phys. Chem. Chem. Phys.*, vol. 13, no. 22, pp. 10808–10817, 2011.

[11] K. Karatasos, "Glass transition in dendrimers," *Macromolecules*, vol. 39, no. 13, pp. 4619–4626, 2006.

[12] S. H. Anastasiadis, K. Karatasos, and G. Vlachos, "Nanoscopic-Confinement Effects on Local Dynamics," *Phys. Rev. Lett.*, vol. 84, no. 5, pp. 915–918, 2000.

[13] K. Chrissopoulou, S. H. Anastasiadis, E. P. Giannelis, and B. Frick, "Quasielastic neutron scattering of poly (methyl phenyl siloxane) in the bulk and under severe confinement," *J. Chem. Physicshysics*, vol. 127, p. 144910, 2007.

[14] L. T. Vo, S. H. Anastasiadis, and E. P. Giannelis, "Dielectric study of Poly(styrene- co -butadiene) Composites with Carbon Black, Silica, and Nanoclay," *Macromolecules*, vol. 44, no. 15, pp. 6162–6171, 2011.

[15] K. Chrissopoulou and S. H. Anastasiadis, "Effects of nanoscopic-confinement on polymer dynamics," *Soft Matter*, vol. 11, no. 19, pp. 3746–3766, 2015.

[16] F. Kremer and A. Schönhals, *Broadband Dielectric Spectroscopy*. Berlin: Springer, 2003.

[17] A. Schönhals, H. Goering, and C. Schick, “Segmental and chain dynamics of polymers: From the bulk to the confined state,” *J. Non. Cryst. Solids*, vol. 305, no. 1–3, pp. 140–149, 2002.

[18] A. Schönhals, H. Goering, C. Schick, B. Frick, and R. Zorn, “Polymers in nanoconfinement: What can be learned from relaxation and scattering experiments?,” *J. Non. Cryst. Solids*, vol. 351, no. 33-36 SPEC. ISS., pp. 2668–2677, 2005.

[19] A. R. Brás, I. M. Fonseca, M. Dionísio, A. Schönhals, F. Affouard, and N. T. Correia, “Influence of nanoscale confinement on the molecular mobility of ibuprofen,” *J. Phys. Chem. C*, vol. 118, no. 25, pp. 13857–13868, 2014.

7 Conclusions

In the present thesis polymer dynamics was investigated in nanocomposites comprising of polymers with different architecture and various additives. Those results were compared to the respective of the bulk polymer in order to comprehend the structure to properties relationship in nanohybrids by altering the additive geometry and the polymer-additive interactions.

The polymers utilized were three linear polyesters (EG-110, DG-110 and HD-110), with hydroxyl end groups and different repeating units, three hyperbranched polyester polyols of different generations (Boltorn H20, H30 and H40) and the hyperbranched poly (ester amide), Hybrane. Nanocomposites based on three different additives, silica nanoparticles of spherical geometry as well as a multi-layer graphite oxide and a layered silicate, sodium montmorillonite, were prepared by solution mixing.

The structural investigation of the nanocomposites shows homogeneous systems with well dispersed additives in the polymer matrix with intercalated structures formed for the layered silicates and the GO, indicating favorable interactions with the polymers. A multi-layer polymer structure is identified inside the filled galleries affected by the interactions of each system. Interestingly, stronger affinity is observed for the polyester amide with the clay and for the polyester polyols with the GO.

The thermal characterization showed that the hyperbranched polymers are amorphous and the linear polyesters are either semi-crystalline or amorphous depending on their repeating unit. By increasing the concentration of the additive in all nanocomposites the thermal properties of the polymer are gradually suppressed as a result of a thin polymer layer formed close to the interface of the additive. Although in nanocomposites with high loadings of silica the transitions are not completely suppressed, unlikely the case of the clay nanocomposites in the same polymer content, the crystallinity is significantly reduced; this is attributed to the much stronger confinement effect in the hybrids of layered silicates.

Polymer dynamics investigated by Broadband Dielectric Spectroscopy, in a wide temperature regime, reveals multiple relaxation processes observed in both the bulk polymer and the nanocomposites. Nevertheless, significant differences are observed which originate by the polymer-additive interactions which can be very different between the different systems. In

the bulk, the local dynamics are attributed to the rotation of hydroxyls and the reorientation of carbonyl groups, while the segmental relaxation is observed above each polymer's T_g, as expected. The same processes are identified in nanocomposites with different characteristics due to the interactions with the additive and the effect of confinement.

The local motions are found possessing lower activation energy in most of the cases, because they are less constrained due to the reduced hydrogen bonding in nanohybrids. It is noted that in the bulk, mostly identified in hyperbranched polyester polyols, an extended network of hydrogen bonds is formed.

For the linear polyesters the segmental relaxation in nanocomposites retains its VFT temperature dependence whereas for the hyperbranched polymer nanocomposites, the segmental relaxation appears far below the glass transition temperature of the respective bulk polymer with an Arrhenius temperature dependence. The confinement affects strongly the segmental dynamics of the hyperbranched polymers in both GO and clay nanocomposites. On the contrary, the segmental dynamics for the linear polyesters is similar to the bulk, not only in silica nanohybrids of lower confinement but in clay nanocomposites as well, due to their low molecular weight.

In the current work, by altering polymer architecture and additive geometry, we reveal the effect of the different polymer-additive interactions on polymer dynamics, which result in either faster or slower segmental dynamics but do not alter the strong or fragile glass behavior of the polymer. Moreover, under severe confinement an Arrhenius-like segmental relaxation and strong glass behavior is obtained, while lower hydrogen bonding in nanocomposites results in easier local dynamics.

Future work

In the future it would be interesting to investigate polymer dynamics under confinement in similar systems, utilizing polyesters of various molecular weights to understand the transition from a VFT to an Arrhenius temperature dependence of the segmental relaxation time. By increasing the polymer chain length a more restricted environment could occur, probably resulting in a more Arrhenius behavior. It would be an intriguing study to identify the critical molecular weight in which this behavior would be achieved or if this different behavior will be obtained gradually.

The additive geometry causes different confinement effect, and the spherical silica nanoparticles due to their curvature and the space left between the particles do not provide a very restricted environment to the polymer. Investigating polymer dynamics in hyperbranched polymer / silica nanocomposites would reveal the effect of the interfacial interactions on the segmental relaxation in a less confined system.

Finally, biodegradable polymer nanocomposites are developed in order to improve the thermal and mechanical properties of the pristine polymers while they retain their biodegradability. Thus, a possible future study could be the investigation of the effect of the nanofillers on the viscoelastic behavior of the nanohybrids in conjunction to their effect on the aliphatic polyesters biodegradation, since in the literature different and sometimes contradictory results have been reported.